Design, synthesis, and characterization of biomimetic oligomers

Laursen, Jonas Striegler

Publication date:
2014

Document Version
Peer reviewed version

Design, synthesis, and characterization of biomimetic oligomers

PhD Thesis

Jonas Striegler Laursen

January 2014

Department of Chemistry

Technical University of Denmark

Preface

The work presented in this thesis is the result of a Ph.D. study following the Ph.D. programme at the Technical University of Denmark. The Ph.D. study has been carried out at the Department of Chemisty from October 2010 to January 2014, under the supervision of Prof. Christian A. Olsen. During my Ph.D. I spend six month in the group of Prof. Kent Kirshenbaum at the Department of Chemistry, New York University, U. S. A.

The work presented in this thesis consist of two parts. The first part describes the design, synthesis and evaluation of monomeric and oligomeric β-peptoid-systems, made to investigate the foldameric properties of β-peptoids. The second part describes further studies of the binding interaction of α-peptide/β-peptoid hybrid oligomers and lipid monolayers.

First and foremost I would like to thank Christian A. Olsen for his guidance and engagement throughout this work, and for providing an excellent and inspiring research environment. I would also like to thank the CAO group, for providing a great working environment and for making the past three years an amazing experience.

Assoc. Prof. Peter Fristrup is acknowledged for carrying out computational studies. For the crystallographic studies performed during the work Assoc. Prof. Pernille Harris is acknowledged. Prof. Lone Gram and Dr. Line Hein-Kristensen are acknowledged for performing the biological evaluation of synthesized compounds. The laboratory of Prof. David Gidalevitz are acknowledged for carrying out X-ray reflection studies of synthesized compounds.

A special thank to Prof. Kent Kirshenbuam for housing me during my external stay, and to the rest of his group for showing me a good time while I was there.

Finally I would like to thank my family and friends for their moral support throughout these three years. Especially I would like to thank my girlfriend Julie for her encouragement and for always being there for me.

Abstract

Peptides and proteins made from the 20 canonical amino acids are responsible for many processes necessary for organisms to function. Beside their composition, proteins obtain their activity and unique selectivity through an ability to display functionalities accurately in the three-dimensional space. These properties are highly sought after in pharmaceutical agents, where the interest in this class of compounds is increasing. However, due to susceptibility to proteolytic degradation in cellular environments and often poor cell-penetrating properties, this class of compounds has traditionally been considered unsuitable for drug discovery. Circumventing the inherent stability problems, non-natural peptide analogues have shown significant potential for the development of new materials and pharmacologically active ligands.

Mimics of natural amino acids have received considerable attention, for their ability to mimic the structural elements seen in proteins. Two prominent peptidomimetics are β-peptides and α-peptoids (*N*-alkylglycines), which have been shown to fold into helical and sheet-like arrangements. To expand the chemical space available for mimicking protein structure their features have been combined to give the β-peptoids, which has found use in biologically active compounds but has been sparsely studied with respect to folding propensity. Thus, an aim of this Ph.D. project has been to investigate the effect of structural variations, including side chain substitution, introduction of thioamides, and trifluoroacetylation, on the *cis*–*trans* amide bond rotamer equilibria in monomer model systems. The latter systems revealed an increase in the preference for *cis*-amides as compared to their parent compounds and thus provide novel strategies for affecting the folding of peptoid constructs. Using NMR spectroscopy, X-ray crystallographic analysis, and density functional theory (DFT) calculations, we found evidence for the presence of thioamide–aromatic interactions through C_{sp^2}–H···S_{amide} hydrogen bonding. Based on these studies we designed a β-peptoid oligomer from residues prone to fit a helical arrangement found by DFT calculations. The designed oligomer indeed proved the existence of a β-peptoid helical conformation by X-ray. Further studies of these compounds indicated a structured display in solution. These helices thus definitively show that the β-peptoids should be considered a valid addition to the already existing ensemble of foldamer designs.

Sequences of alternating α-peptides and β-peptoids, containing basic α-amino acid residues have been shown to possess antimicrobial activity. Using X-ray surface scattering techniques the interaction of two oligomers, containing different basic moieties, and model lipid membranes of Gram-positive and Gram-negative bacteria, respectively, were investigated. We also synthesized fluorophore labeled analogues of the hybrid oligomers, which during a preliminary biological screening, showed cases of enhanced antimicrobial activity. The X-ray scattering studies confirmed earlier findings, showing that the guanidino-group binds more deeply into the membranes of Gram-positive bacteria, and that the nitrobenzoxadiazole-fluorophore enhanced this interaction.

Resume

Peptider og proteiner, bestående af de 20 naturligt forekommende aminosyrer, udfører mange processer, som er nødvendige for organismers funktioner. Udover deres sammensætning opnår proteiner deres aktivitet og unikke selektivitet ved at være i stand til at placere deres funktionaliteter præcist i rummet. Disse egenskaber er eftertragtede i forbindelse med udviklingen af nye typer medicin, hvor interessen for denne type stoffer er stigende. Desværre bliver disse forbindelser nedbrudt af proteaser, og er ofte dårlige til at trænge ind i celler, hvorfor man har anset denne type stoffer som uegnede til udvikling af nye lægemidler. Unaturlige analoger af peptider har vist sig at være proteasestabile, og besidde egenskaber som gør dem interessante i forbindelse med udvikling af nye materialer og lægemidler. Især analoger af de naturlige aminosyrer har tiltrukket sig særlig meget opmærksomhed da de er i stand til at efterligne stukturelementer fra proteiner. To af de mest prominente analoger er *β*-peptider og *α*-peptoider (*N*-alkylglyciner), som har vist sig at kunne danne både heliske og *β*-sheet-lignende strukturer. For at udvide mængden af stoffer som kan danne analoger af proteinstrukturer, har man kombineret egenskaberne for *β*-peptider og peptoider og derved udviklet *β*-peptoider. Forbindelserne er blevet brugt i biologisk aktive systemer, men kun undersøgt for foldnings egenskaber i et begrænset omfang. Det har således det været et mål for dette Ph.D. project, at undersøge hvordan *cis–trans* ligevægten for amidbindingen påvirkes i monomere modelsystemer efter hhv. ændring af sidekæder, introduktion af thioamider, samt trifluoracetylering af *N*-terminalen. De sidst nævnte systemer udviste en øget præference for *cis*-konformationen, sammenlignet med de oprindelige forbindelser, hvilket giver nye muligheder for at påvirke foldningen i peptoid systemer. Ved at anvende NMR-spektroskopi, røntgenkrystallografisk analyse samt "density functional theory" (DFT)-beregninger, fandt vi frem til en vekselvirkning mellem et thioamid og et aromatisk system gennem en C_{sp^2}–H···S_{amid} hydrogenbinding. Ud fra vores studier designede vi en oligomer indeholdende enheder, med stor tilbøjelighed til at antage en konformation, som ifølge DFT beregningerne skulle føre til en helisk struktur. Ved røntgenkrystallografi udviste denne oligomer en helisk struktur. Yderligere studier af denne helix indikerede tilstedeværelsen af en ordnet struktur i opløsning. Med denne heliske struktur kan man definitivt tilføje *β*-peptoiderne til de allerede eksisterende foldamer designs.

Sekvenser bestående af skiftevis *α*-peptid- og *β*-peptoid enheder, indeholdende basiske *α*-aminosyrer har udvist antimikrobielle egenskaber. Ved at bruge teknikker baseret på røntgenstrålers spredning ved refleksion fra overflader, har vi undersøgt vekselvirkningen mellem to hybrid oligomerer og modelmembraner af Gram positive og Gram negative bakterier. Vi har også syntetiseret fluorophor-mærkede analoger af hybrid oligomererne, som ved en indledende biologisk screening viste øget aktivitet. De førnævnte røntgenstudier bekræftede de tidligere resultater, og viste at guanidino-grupper binder dybere i membraner fra Gram positive bakterier, samt at nitrobenzoxadiazol-fluorophoren forstærker denne vekselvirkning.

Abbreviations

aa	Amino acid
Ala	Alanine
Alloc	Allyloxycarbonyl
AMP	Antimicrobial peptide
Arg	Arginine
bn	Benzyl
bnz	Benzhydryl
Boc	*Tert*-butoxycarbonyl
C. albic	*Candida albicans*
Cbz	Carboxybenzyl
CD	Circular dichroism
CF	5(6)-Carboxyfluorescein
CL	Cardiolipin
DBU	1,8-Diazabicycloundec-7-ene
DCC	Dicyclohexylcarbodiimid
Dde	1-(4,4-dimethyl-2,6-dioxacyclohexylidene)ethyl
DFT	Density functional theory
DIC	Diisopropylcarbodiimid
DMF	Dimethyl formamide
DMSO	Dimethylsulfoxide
DNA	Deoxyribonucleic acid
DPPG	1,2-Dipalmitoyl-sn-glycero-3-phosphatidylglycerol
E. coli	*Eschericia coli*
Fmoc	9-Fluorenylmethoxycarbonyl
GIXD	Grazing incidence X-ray diffraction
HATU	1-[Bis(dimethylamino)methylene]-1*H*-1,2,3-triazolo[4,5-b] pyridinium 3-oxid hexafluorophosphate
HBTU	*N*,*N*,*N'*,*N'*-Tetramethyl-*O*-(1*H*-benzotriazol-1-yl)uronium hexafluorophosphate
HIV	Human immunodeficiency virus
HOAt	1-Hydroxy-7-azabenzotriazol
HOBT	1-Hydroxy-1*H*-benzotriazol
hRBCs	human red blood cells
IC	Inhibitory concentration
kcal	Kilo calories
kJ	Kilo Joule
LG	Leaving group
LPS	Lipopolysaccharide
LS	Lung surfactant
Lys	Lysine
M	Molar
MIC	Minimum inhibitory concentration

MRSA	Methicillin-resistant *Staphylococcus aureus*
NBD	Nitrobenzoxadiazole
NBO	Natural bond order
nm	Nanometer
NMR	Nuclear magnetic resonance
npm	1-Naphthylmetyl
P. aureg	*Pseudomonas aureginosa*
PC	Phosphatidylcholine
PE	Phosphatidylethanolamine
PEG	Polyethylene glycol
PG	Phosphatidylglycerol
ph	Phenyl
phe	Phenyl alanine
Pro	Proline
PS	Phosphatidylserine
PyBOP	(Benzotriazol-1-yloxy)tripyrrolidinophosphonium hexafluorophosphate
RNA	Ribonucleic acid
rpe	(Rac)-1-phenylethyl
S1npe	(*S*)-1-(1-naphthyl)ethyl
sbu	(*S*)-*Sec*. butyl
sce	(*S*)-1-cyclohexylethyl
SM	Sphingomyelin
spe	(*S*)-Phenylethyl
SPS	Solid-phase synthesis
Tat	Transcription-transactivating
TBDMS	*tert*-butyldimethylsilyl
^{t}Bu	*Tert*-butyl
TFA	Trifluoroacetic acid
TFE	Trifluoroethanol
THF	Tetrahydrofurane
VRE	Vancomycin-resistant Enterococus facium
XR	X-ray reflectivity
Å	Angstrom

Table of contents

1 Introduction

Proteins and peptides constitute a major class of biological polymers, which Nature rely on to carry out a broad variety of sophisticated chemical operations, such as catalysis, tight and specific binding, transport and storage of nutrients and metabolites and signaling. These biomolecules are polymers built from a single type of monomer, namely the 20 canonical amino acids, which are connected by amide linkages (peptide bonds), allowing for great variation of the sequence. The diversity of the polymer arises from variations in the chain length and identity of the side chain of each residue along the sequence.[1] For most proteins the specific function arises from the ability to obtain a well-defined three-dimensional structure, which is encoded by the sequence of amino acids. These structures are governed by a series of non-covalent interactions such as hydrogen bonding, hydrophobic interactions, van der Waals- and electrostatic interactions and covalently by disulfide bonds.[2] A vast amount of research has been performed to obtain a fundamental understanding of the relationship between amino acid sequence, folding, and functions of proteins.[3] Traditionally this class of compounds has not been considered suitable for drug design due to the high cost of production, susceptibility to proteolytic degradation in cellular environments, and often poor cell-penetrating properties.[4] Nevertheless, the interest in this type of compounds has been increasing in the pharmaceutical industry after the development and marketing of recombinant protein therapeutics.[5] For this reason, research in unnatural oligomers capable of mimicking the folding patterns of proteins have received considerable attention.[6,7] In these efforts a number of backbone constructs have been identified that adopt rather stable secondary structures. Unnatural analogues of peptides that contain the same functionality, with a similar or complementing three-dimensional display might retain the interactions with an intended target.[7-9] Given their unnatural origin, peptidomimetics are thought to exhibit improved stability towards enzymatic degradation and hence have improved bioavailability. The field of research in unnatural compounds displaying the ability to fold in a similar manner to peptides and proteins were coined ”foldamers” by Gellman in the late 1990’s.[10] This field of research contains two important goals, one is exploring the properties of folding behavior in unnatural backbones which also helps the understanding of the sequence–folding relationship of natural oligomers. Second, this field of research holds the possibility to provide protein-like functions in synthetic compounds that overcome the limitations of the natural oligomers as therapeutic agents. Recently numerous accounts of foldameric compounds capable of interrupting protein-protein interactions have been reported, showing this class of compounds to be promising candidates for drug-development.[7,9] The research in foldameric compounds has also resulted in a number of oligomeric compounds capable of adopting stable structures. These compounds can be divided into two classes, foldamers closely resembling peptides (peptidomimetic foldamers), and compounds having none or very little similarity to peptides (non-peptidomimetic foldamers). Though the latter class may not share much similarity with the natural peptides, members have shown the ability to display similar folding patterns.

Compounds of this type have provided a basic understanding of factors that dictate the folding propensities of oligomers of a given residue type, extending the ensemble of methods for obtaining folded structures. The peptidomimetic foldamers are built on backbones resembling that of the natural peptides, to which minor alterations are made. Through the development of such molecules it has been shown that even minor alterations may greatly affect the folding propensity and bioactivity of the compound.

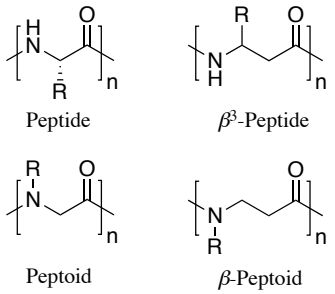

Figure 1.1. Generic structure for peptides and peptidomimetic backbones.

The aim of this project has been to obtain fundamental understanding of the folding propensities of *β*-peptoids, a combination of two well-studied peptidomimetic foldamers, the *β*-peptides and peptoids (Figure 1.1). *β*-Peptoids have been combined with *α*-amino acids, giving hybrid oligomers that display some interesting bioactive properties, but thus far studies of their folding propensity have been sparse.[11-13]
The following chapter will provide a brief overview of the fundamental research in understanding the folding propensity of peptides and their synthesis. A discussion of foldamers will provide examples of how folding has been obtained in both peptidomimetic and non-peptidomimetic oligomers. Being the parent compounds of *β*-peptoids, a special focus will be given to *β*-peptides and peptoids. Also oligomers based on combinations of these residues will be discussed, as they have proved to be valuable additions.

1.1 Peptide folding

Proteins are macromolecules build up from the 20 canonical amino acids, which are connected by amide linkages, or peptide bonds. By varying the positioning and number of residues, these 20 building blocks allow for an almost infinite variation of the sequence (primary structure). However, proteins realize their high potential and diversity by folding the backbone into well-defined arrangements, displaying the functionalities appropriately in the three dimensional space (secondary structure). The patterns in which the protein display its functionalities give rise to active sites, in which residues spaced far apart in the backbone sequence can be placed in close proximity. These displays are achieved using a relatively small number of secondary structure elements, predominantly helices, *β*-sheets (strands), and turns (Figure 1.2). These elements will also have very well defined orientations in the globular protein (tertiary structure).

Figure 1.2. Cartoon representations of secondary structure types.[14]

The specific folding of a given sequence of α-amino acid residues is stabilized by a series of weak non-covalent interactions, such as hydrophobic interactions, hydrogen bonding, van der Waals- and electrostatic interaction and covalently by disulfide bonds.[2] By disrupting these interactions the protein loses its secondary structure and thereby its activity.[15,16] In the beginning of the 20th century it was realized that the unfolding of a protein is a reversible process, and that the refolding of some proteins can take place *in vitro*, in the absence of the cellular machinery.[17] This also makes it possible to design and synthesize folded proteins in the laboratory which, given their complexity, is an extremely challenging task. To achieve this goal the propensity of smaller fragments, or peptides, to form discrete folds have been studied intensely.[1]

1.1.1 Helices

The existence of both the helix and β-sheet were discovered by Pauling and Corey in 1951.[18,19] Helices are the most abundant type of secondary structure, it is estimated that a third of all residues in proteins participate in a helical motif.[20] Helices are stabilized by hydrogen bonding, and it is the bonding partners that determine the identity of the helix (Figure 1.3). The identity of a helix is defined by the number of residues and atoms needed to complete a full turn.

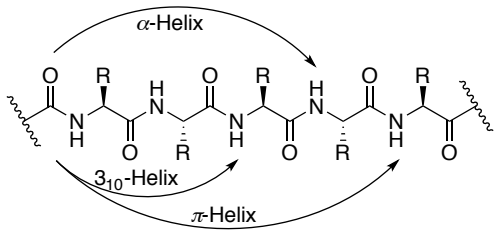

Figure 1.3. Hydrogen bonding pattern for various peptide helices.

Amongst the helices the most common is known as the α-helix, which has a hydrogen bond between the carbonyl oxygen of the *i*th residue and the amide hydrogen of the (*i*+4th) residue. This gives a helix with 3.6 residues per turn, and a pitch of 5.4 Å. When the α-helix is the most abundant helix it is because this geometry places the backbone and side chains in such a way that steric interactions are avoided (Figure 1.4). As indicated in figure 1.3 other helices are possible, the 3_{10} helix is slightly

narrower and rises with a pitch of 6.0 Å, which places the side chains to experience some steric interactions.[21]

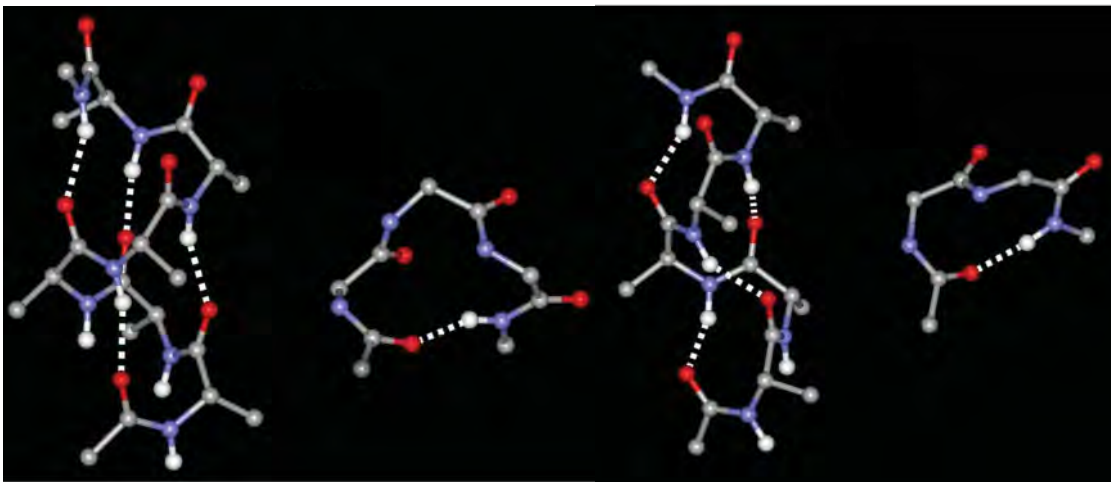

Figure 1.4. Left: The α-helix, and the building block constituting one turn (α-turn). right: The 3_{10} helix and the sequence of one turn (type III β-turn).[22]

The π-helix is rarely observed, probably due to its wider and more flat conformation as compared to the two mentioned helices. This allows for an axial hole inside the helix, which is too narrow to fit a water molecule yet too wide to allow for van der Waals association across the axis which greatly reduces stability.[23]

1.1.2 β-Sheets

β-sheets consist of extended segments of a peptide chain (strands) that are interconnected by hydrogen bonds. When the β-sheet was first proposed, by Pauling and Corey, they where thought to be flat.[19] Since then X-ray crystallography has shown a number of different variations in the structure of β-sheets.[24] These variations are caused by the fact that the chain is composed from chiral L-amino acids. The chiral subunits tend to assume minimum energy conformations that twist the sheet away from planarity.[25] Twisting of the strands results in the introduction of energetically unfavorable distortions to the interchain hydrogen bonds. The final conformation is hence a result of an energetic compromise of optimizing conformational energy of the strand while preserving the interchain hydrogen bonds.

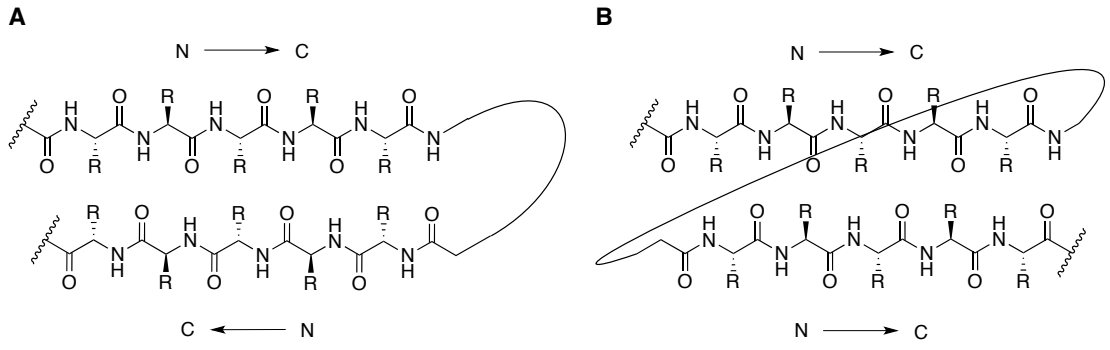

Figure 1.5. The hydrogen bonding pattern of antiparallel (A) and parallel (B) β-sheets.

As the β-sheet motif is composed from two segments of the chain, they do not necessarily have the same directionality. β-sheets are either parallel or antiparallel, meaning that the interconnected strands have the same *N*- to *C*-terminus direction or the opposite, respectively (Figure 1.5). Whether the β-sheet is parallel or antiparallel results in a slightly different overall conformation.

1.1.3 Turns

The direction of a peptide sequence can be changed, and if this happens in a well defined manner through hydrogen bonding this motif is known as a turn.[26] Turns are characterized according to the number of residues in the hydrogen bonded ring: γ-turns (three residues), β-turns (four residues), α-turns (five residues), and π-turns (six residues).[27] Turns, unlike helices and β-sheets, do not represent a certain set of torsion angles, which allows for some variation within each class of turn (Figure 1.6). These variations are referred to as the type of a specific turn-class, for instance eight types of β-turns have been identified.[26]

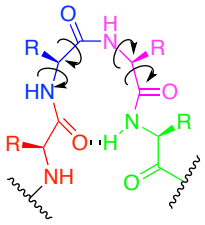

Figure 1.6. Turn-structure with hydrogen bond between position *i* and *i* + 3 (β-turn). The arrows indicate flexible torsion angles.

As shown in figure 1.4 these motifs make up the individual turns of helices, e.g. the torsion angles of a type III β-turn are the same as those of an α-helix.

1.2 Peptide synthesis

The synthesis of peptides is a valuable tool in biology, drug discovery, and many other areas. As peptides are oligomers of amino acids, even the synthesis of relatively short peptide chains require a large number of operations, many of which are purifications, when using conventional synthetic methodologies. To efficiently produce peptides and proteins different technologies are available e.g. extraction from natural sources, production by recombinant DNA technology or by chemical synthesis.[28] The size of the desired peptide determines which of the technologies are best suited for production. For large peptides recombinant DNA technology has proven useful, as illustrated by the production of insulin and hormones.[28] Macromolecules that, due to their size and complexity, have only been obtained by natural means are referred to as biologics. Given the advantages in synthetic methods, such as solid-phase synthesis (SPS)[29] and chemical ligation,[30] the amount of biologics is decreasing. However, many molecules relevant to research regarding structure,

function or activity are of a substantially smaller size and of less complexity, and since the introduction of SPS this has been the method of choice for peptide production in research laboratories. This method deviates from conventional synthesis by growing the peptide on an insoluble polymer material. In this manner many purification steps can be avoided by simply washing the solid-bound product. As we have applied this method to the synthesis of foldameric compounds, a brief introduction to the principle and factors involved in SPS will be given.

1.2.1 Solid-phase synthesis

The basic principle of SPS is to grow oligomeric compounds on an insoluble support (Figure 1.7). This is achieved by adding the first residue to the support through the *C*-terminal, while the *N*-terminus remains protected. After attaching the residue, excess reagents and solvent can be removed by filtration, leaving only the coupled compound and the solid support. In the next step the *N*-terminal protecting group is removed, and the next residue attached, resulting in elongation of the oligomer. This procedure is then repeated until an oligomer of the desired length is achieved, at which time it can be cleaved from the support.

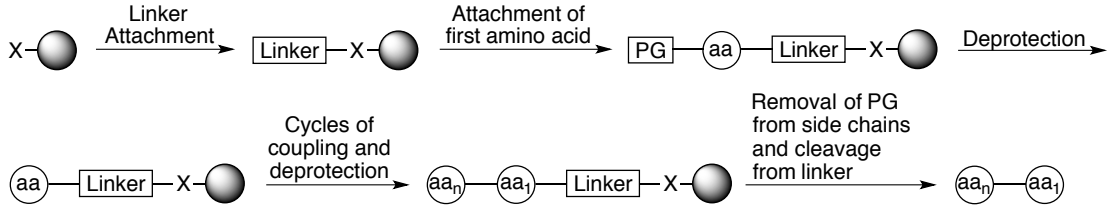

Figure 1.7. Illustration of the principle of solid-phase peptide synthesis.

By being able to simply filter of any excess reagents, and wash the compound on the resin, vast amounts of time can be saved using SPS compared to conventional solution-phase chemistry. This method also has its limitations, given that incomplete reactions will lead to by-products which are highly similar to the desired product, and are hence difficult to remove.

For a successful solid supported synthesis a number of factors are in play. Starting with the choice of solid support, the handle attaching the oligomer is to the support, the activating agent, the protecting groups and finally the cleaving conditions.

1.2.2 Solid supports

A variety of solid supports are in existence, and in the process of selecting one that fits the conditions and reactants of the synthesis is important.[31] When solid-phase peptide synthesis was first described by Merrifield, beads of polystyrene with 2% cross-linked divinylbenzene was employed as solid support (Figure 1.8 A).[29] This resin is still widely used today, however, a serious drawback of this type of resins are their incompatibility with polar solvents. If exposed to polar solvents the apolar nature of the resin will make the beads contract leaving the reactive sites inaccessible for the

incoming reagents. To improve the properties of this resin Albericio and co-workers developed a resin combining polystyrene and polyethylene glycol (PEG), an example of this type of resin is PEG-polystyrene (Figure 1.8B).[32] This combination enhanced the swelling properties of the solid support in both polar and non-polar solvents. Also a pure PEG resin has been designed by cote, named ChemMatrix (Figure 1.8C).[33] The cross-linked PEG makes the resin amphiphilic, providing good swelling properties in most solvents. This resin has been shown to be better than polystyrene-based resins for the synthesis of complicated and highly basic peptide sequences.[34]

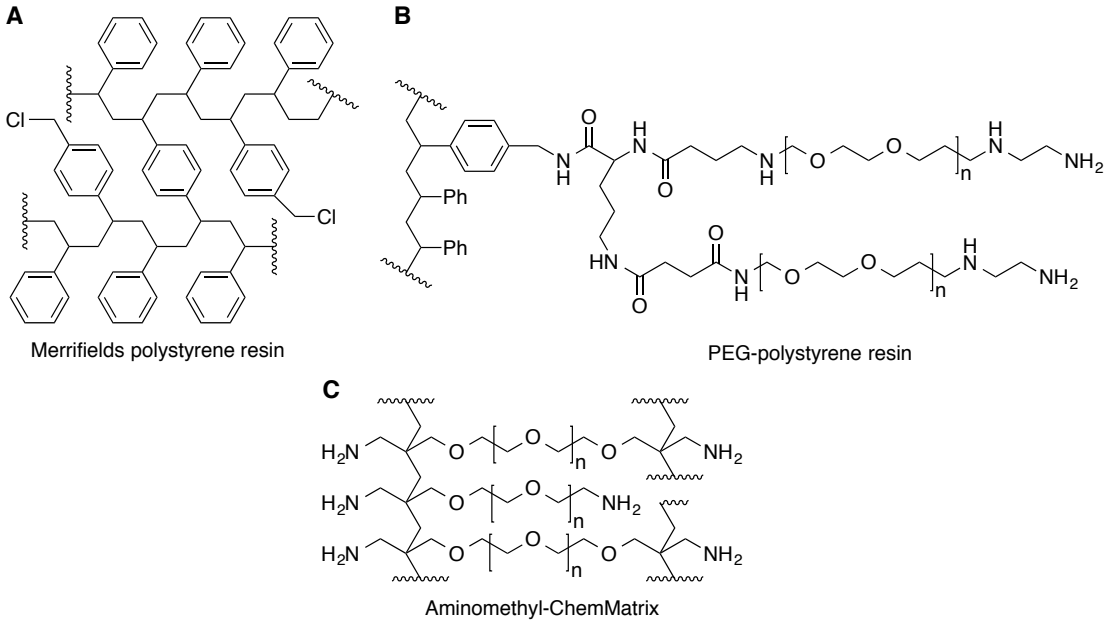

Figure 1.8. Structures of selected solid supports.

1.2.3 Handles/linkers

As can be seen from figure 1.8 most of the resins have amino functionalities to which compounds can be attached. If a peptide was directly attached to the resin through a peptide bond it would be impossible to cleave it from the resin without breaking any further peptide bonds. Therefore linkers, or handles, have been developed to enable cleavage of the synthesized compounds without degradation. Also for this class of compounds a broad variety of alternatives exist, depending on the desired *C*-terminal functionality and desired cleaving conditions.

One of the most used type of handles for making peptide acids is based on trityl (**1**).[35] The trityl group is also known as a side chain rotecting group, thus, it allows for simultaneous cleavage from the resin and deprotection. Since it is a very acid labile handle it is also possible to cleave the peptide from the resin without deprotecting the side chains.[36] It has been showed that substitutions at the 2-postion of the trityl group can enhance the sensitivity to acids.[35] A peptide linked to trityl (**1**, X = H) can be cleaved using pure acetic acid, when using 2-chlorotrityl (**1**, X = Cl) 20% acetic acid in CH_2Cl_2 is sufficient. This also serves as an example of how small changes to the structure of handles have a large effect on their properties.

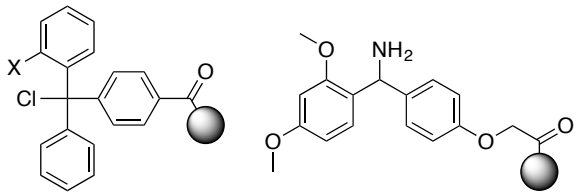

Figure 1.9. Structure of two linkers commonly used in solid-phase chemistry.

Another widely used family of handles are based on a benzhydryl-skeleton, and results in *C*-terminal amides upon cleavage using trifluoroacetic acid (TFA). One of the most prominent members of this group is the rink amide handle (**2**).[37] The linkers mentioned here are both acid-labile and compatible with Fmoc-solid-phase chemistry, which will be discussed below. Linkers displaying base-lability[38] or photo-lability[39] are also available. Furthermore, linkers connecting the backbone to the resin have been developed.[40]

1.2.4 Coupling reagents

When creating peptides the ability to form amide bonds, by linking a carboxylic acid of one amino acid and the amine of another, is crucial. This reaction does not occur spontaneously, but requires heating to >200 °C[41] or some other kind of activation[42]. Heating to these temperatures is seldom optimal for the substrates, and activation by coupling reagents is used instead. These reagents are used to convert the acid OH into a better leaving group (LG), before the amino substrate is added (Figure 1.10).

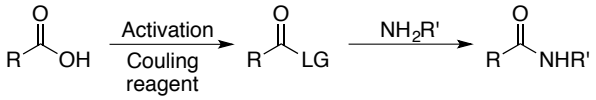

Scheme 1.1. Principle of the activation process for amide-bond formation.

One of the first, and still widely used, types of coupling reagents are carbodiimides. Within this class one of the first coupling reagents to be used in synthesis was dicyclohexylcarbodiimide (DCC), which was first used in 1955 (Figure 1.10).[43] The reactivity of the carbodiimides can be tuned by variation of the end-groups. This has yielded in a large variety of this kind of coupling reagents. One of the best known members of this family is diisopropylcarbodiimid (DIC). The activating mechanism of this class of coupling reagents is shown in scheme 1.2.

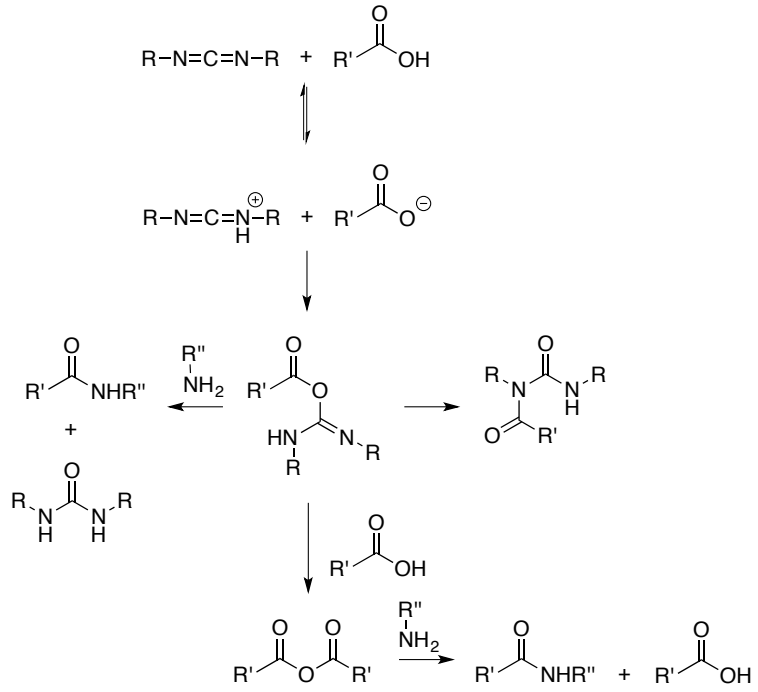

Scheme 1.2. Coupling using carbodiimid-based activating agents.

As can be seen from scheme 1.2 the first step of the activation is coupling of the acid to the carbodiimide forming an *O*-acylurea. From here the reaction can follow three different pathways, where only two leads to the desired product. The first is direct addition of the amine to the formed *O*-acylurea yielding the desired amide. The next path is a rearrangement forming an *N*-acylurea by-product. Finally, adding another acid resulting in an anhydride, which can subsequently be attacked by an amine, also giving the desired amide. One problem that can occur when using carbodiimides is the possible formation of oxazolone-compounds from the *O*-acylurea, which leads to epimerization of the amino acid.[44] To reduce epimerization additives have been introduced.[45] These additives react with the *O*-acylurea forming an intermediate, termed activated ester, which has an enhanced reactivity towards amines. The lower degree of epimerization and the better reactivity of the activated esters are most likely coursed by hydrogen-bonding between the OXt ester and the amine.[42] The most common additives are 1-hydroxy-1*H*-benzotriazol (HOBt) and 1-hydroxy-7-azabenzotriazol (HOAt) (Scheme 1.3).

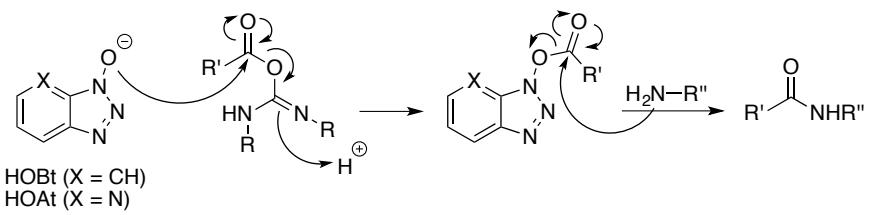

Scheme 1.3. Coupling using OXt additives. HOBt = 1-hydroxy-1*H*-benzotriazol, HOAt = 1-hydroxy-7-azabenzotriazol

The 1*H*-benzotriazol additive has also been used to develop another class of coupling reagents. This class consists of salts of 1*H*-benzotriazoles associated with uronium/aminium, phosphonium or immonium and a counter ion.

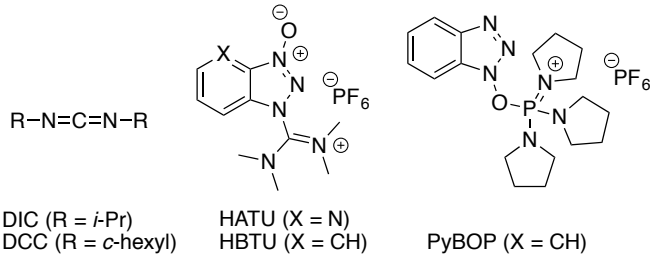

Figure 1.10. Examples of coupling reagents. DIC = diisopropylcarbodiimid, DCC = dicyclohexylcarbodiimid, HATU = 1-[Bis(dimethylamino)methylene]-1*H*-1,2,3-triazolo[4,5-b] pyridinium 3-oxid hexafluorophosphate, HBTU = *N,N,N′,N′*-Tetramethyl-*O*-(1*H*-benzotriazol-1-yl)uronium hexafluorophosphate, PyBOP = (Benzotriazol-1-yloxy)tripyrrolidinophosphonium hexafluorophosphate.

Figure 1.10 shows a small selection of the many variants of these salts available. Also the counterion can be varied, however, no effect on reactivity has been observed. These compounds react directly with the carboxylic acid, forming an activated ester, which will subsequently react with the amine (Scheme 1.4). When using uronium or aminium salts the timing of addition of the different species is crucial. If the amine is added before the activated ester is formed, it can react with the coupling reagent yielding guanidinium by-products.[46] To avoid the formation of guanidinium by-products, phosphonium salts can be used instead. Another important consideration when using these salts is that base is added to deprotonate the amino acid prior to activation. This puts some restraints on the protecting groups that can be used during synthesis.

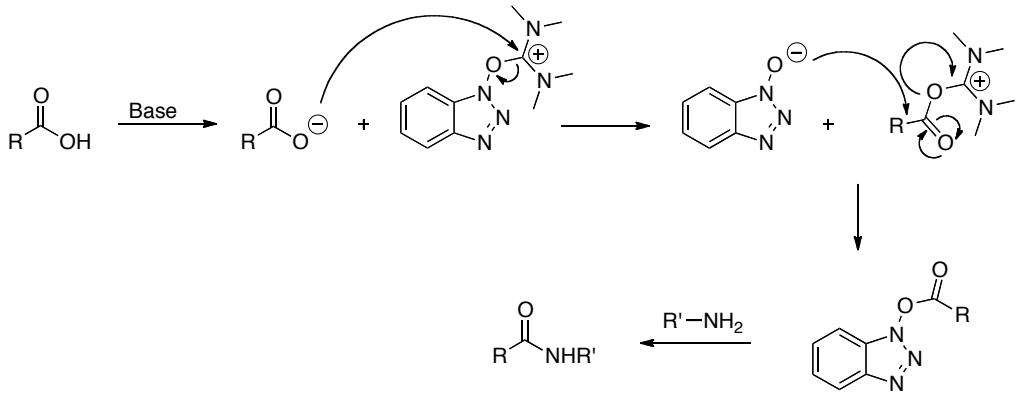

Scheme 1.4. Coupling using ammonium/uranium type coupling reagents.

Also a broad variety of coupling reagents involving different reaction pathways exist. What is described here are some of the most common classes, which can be applied on a large selection of substrates.[42]

1.2.5 Protecting group strategies

When synthesizing peptides two main strategies exist: the Fmoc strategy[47,48] and the Boc-strategy[49]. Both these strategies rely on the orthogonal removal of the *N*-terminal protecting group over the side chain protecting group, allowing for the addition of the next residue. The Boc protecting group is removed using TFA, whereas the Fmoc group is removed upon treatment with 20% piperidine or 2% 1,8-diazabicycloundec-7-ene (DBU) in dimethyl formamide (DMF). Therefore, stability towards the chosen conditions will be crucial for the side chain protecting groups. When the peptide is connected to the solid support by a handle, the protecting groups must either be stable to the cleaving procedure or designed for removal upon cleavage. If one wishes to modify the side chain while the peptide is bound to the solid support, three degrees of orthogonality is required. That is, the side chain protecting group can be cleaved without cleaving the peptide from the support or removing the terminal nor any other protecting group in the peptide. As the amino acids have different side chain functionalities, they need different protecting groups, figure 1.11 shows a few of the commonly used.[50]

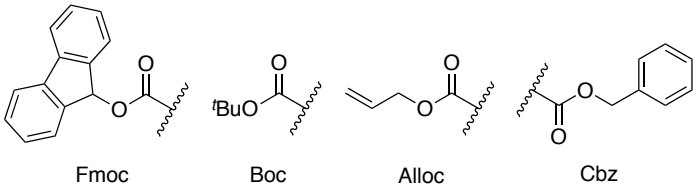

Figure 1.11. Selection of some commonly used protecting groups. Fmoc = 9-Fluorenyl methoxycarbonyl, Boc = *tert*-butoxycarbonyl, Alloc = Allyloxycarbonyl, Cbz = Carboxybenzyl.

1.3 Foldamers

The ability of oligomers to display an ordered arrangement of sub-units is not exclusive to the proteins and peptides. Various chemotypes capable of adopting stabilized three-dimensional structures have been identified and been named "foldamers".[10] The term has been further specified by Moore, who defined foldamers as "Oligomers that fold into a conformationally ordered state in solution, the structures of which are stabilized by a collection of non-covalent interactions between nonadjacent monomer units".[8] Within this class of compounds a wide variety of un-natural backbones have been developed and studied.[7,8,51] However, these definitions also holds limitations as it is not sufficient to display a stable structure, the molecule must also be in equilibrium with an unfolded state. Compounds that adopts helical structures, but are locked by covalent constraints predetermining the backbone conformation are hence excluded from this category (Figure 1.12).[8]

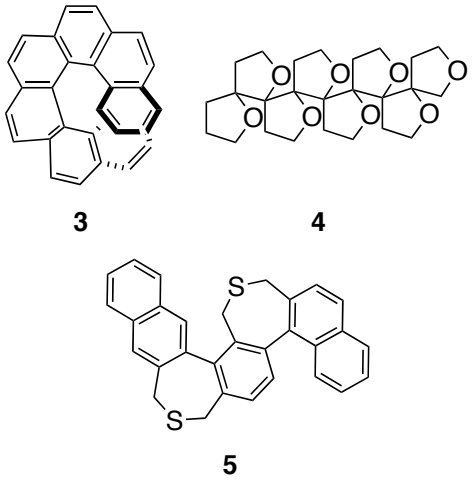

Figure 1.12. Examples of molecules not classified as foldamers: Helicenes (**3**),[52] Polyoxapolyspiroalkanones (**4**),[53] and "geländer" helices (**5**).[54]

As peptides are themselves foldamers, it is not surprising that many of the interactions utilized in the stabilization of these natural compounds are also prevalent in the unnatural systems. However, as the ensemble of backbones and side chains are much broader, other types of interactions can play a key role in structure determination.[51]

1.3.1 Non-peptidomimetic foldamers

Any stabilized structure can be described by the torsion angles of the backbone, or from a design point of view, any structure can be achieved through control over these angles. This implies that the difficulties designing a molecule that adopt a predictable fold are increasing with the amount of rotatable bonds in each residue. An effective way to restrict rotation around single bonds is by introduction of π-conjugation, as this will favor the two sp^2-hybridized systems to be co-planar, which gives only two favorable conformations. The structures of these molecules can be further affected by the introduction of non-covalent bonding partners, which can only interact in one of the two conformations (Figure 1.13).

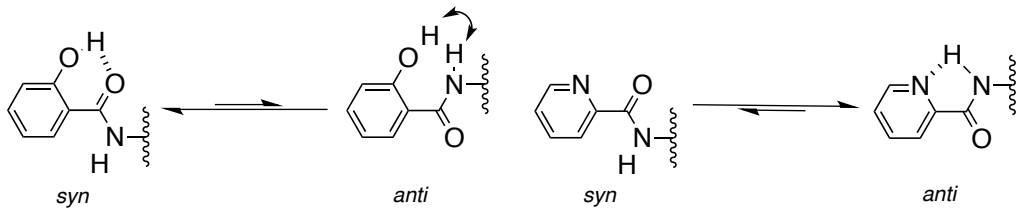

Figure 1.13. Examples of monomers on which local conformational control is exerted. Attractive interactions are marked as hashed lines and repulsive as arrows.

By connecting units of the type shown in figure 1.13 a variety of folded structures can be obtained (Figure 1.14).[55-58] Depending on the substitution pattern of the aromatic system, and the preferred interactions both helical (**6** and **7**), Straight (**8**), and curved (**9**) structures can be obtained. As most of these monomer molecules are flat, the

number of possible secondary structure motifs of a specific oligomer is limited, and the prediction of their folding is much easier than for the natural peptides.

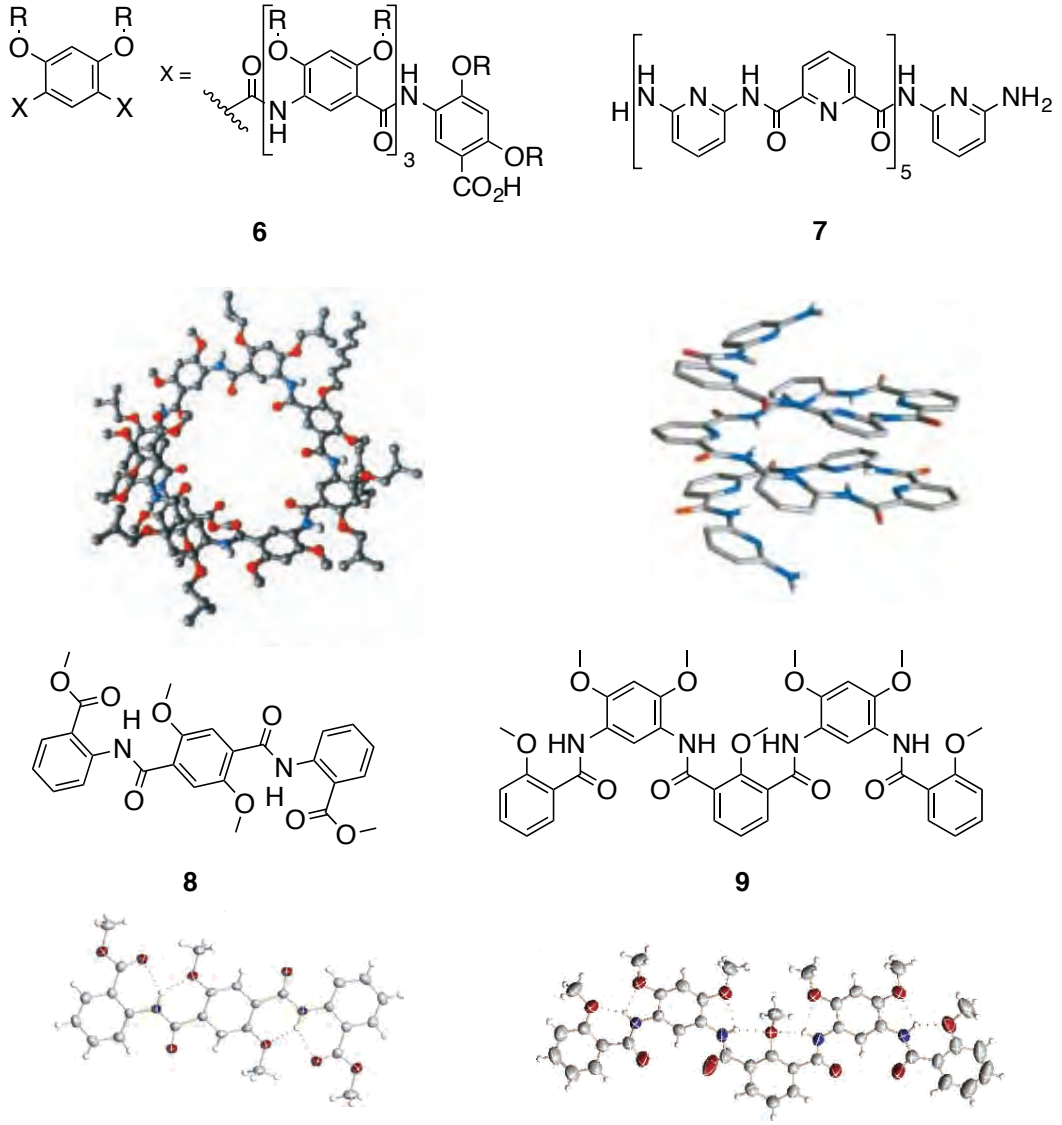

Figure 1.14. Examples of secondary structures from arylamide type building blocks.

The examples shown in figure 1.14 all use secondary amide bonds to connect the aromatic residues, and hydrogen bonds to control the rotation. Another way to control the rotation around an amide bond is the introduction of a tertiary amide, between an aromatic acid and an aromatic amine, in which case the two aryl groups are projected to the same side (*trans* amide bond) (Scheme 1.5).[59]

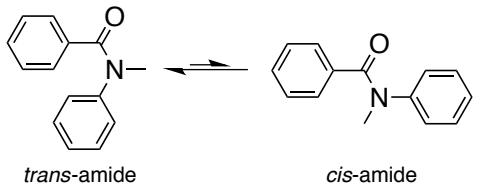

Scheme 1.5. *cis–trans* equilibrium for aromatic amides

Although no clear preference for the rotation around the aryl–NCO or aryl–CON bonds are defined, it is affected by sterics and weak electrostatic interactions between the aryl groups. Especially when molecules carrying this motif is dissolved in protic solvents the interactions of the aryl groups are reinforced by a solvophobic effect. This pattern has been used to furnish foldameric oligomers of e.g. guanidines and ureas connecting aromatic rings (Figure 1.15).[60,61] When interconnecting two aromatic moieties in this way they can be arranged to allow for an almost perfect face-to-face stacking interaction.

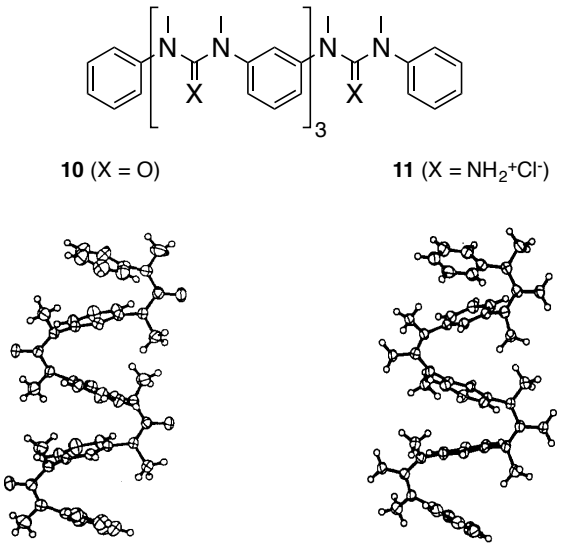

Figure 1.15. Examples of secondary structure of aromatic urea and guanidine-compounds.

The tertiary amide is also known from the naturally occurring amino acid proline. Despite an inability to form hydrogen bonds, polyprolines have been shown to adopt helices of all *cis*- or *trans*-amide bonds, referred to as polyproline helix type I and II, respectively (Figure 1.16).[22]

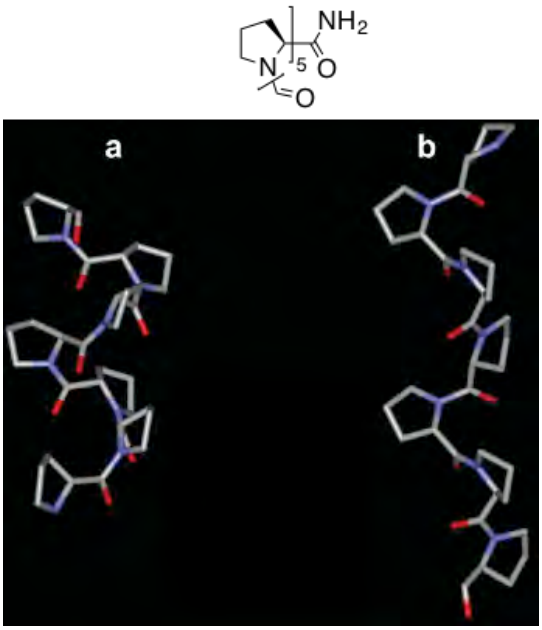

Figure 1.16. The two types of helices formed by polyproline. a) type I (all *cis*) b) Type II (all *trans*).[22]

The examples of this section have utilized the control over the conformation of a relatively small number of bonds, and in these efforts exploited local interactions of a single residue or by non-covalent interactions with a neighboring residue to construct folded molecules. Most of these monomer building blocks have little resemblance to the naturally folded amino acid sequences found in nature, although they use some of the same interactions to stabilize secondary structure. One of the major differences from the natural oligomers to those of this section is the ability to engage in interactions with more distant residues than the neighbors.

1.3.2 Peptidomimetic foldamers

In traditional medicinal chemistry, peptidic compounds have not been considered suitable for drug development. This is due to their susceptibility to proteolytic degradation in cellular environments and often poor cell penetrating properties. To circumvent the inherent stability issues, extensive research in mimicking peptide structure and function has been undertaken. Compounds able to mimic or complement the three-dimensional folding of peptides and proteins have been further classified as peptidomimetic foldamers. Most strategies for the preparation of molecules that fold like oligomers of α-amino acids contain only minor modifications to the natural amino acids.[8] Concerning foldamers, alterations to the backbone, e.g. positioning of the side chains or the addition of fragments, are the most studied. If a methylene unit is added to the backbone of an α-amino acid, the corresponding β-amino acid is formed, if yet another methylene is added the product is a γ-amino acid and so forth. Even though these molecules have more rotatable bonds than the natural α-amino acids, their oligomers have been shown to form stable helices, resembling those of α-peptides (Figure 1.17).[62,63]

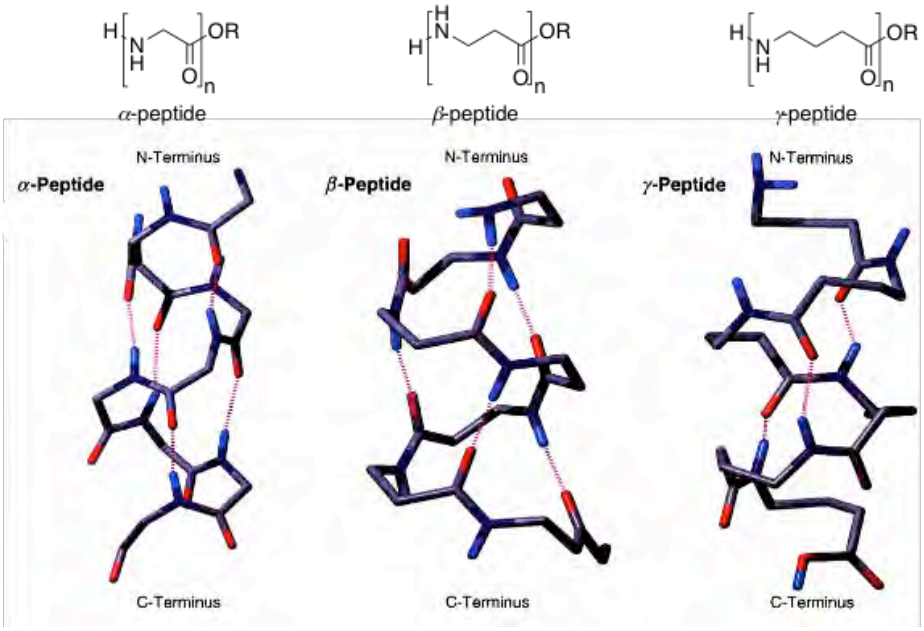

Figure 1.17. Structures of the helices from α-, β- and γ-peptides.[62]

Given their close relation to the α-amino acids, it is not surprising that the β-amino acids have received considerably more attention than further elongated analogues. As can be seen from figure 1.17, when the backbone is elongated additional carbons capable of carrying a side chain are present. This is a major difference from natural peptides, and a major factor in the determination of which secondary structures can be formed by these molecules (Section 1.4). The introduction of additional backbone carbon atoms has also made substitution of individual backbone atoms possible, while retaining the side chain on a carbon. This kind of substitution is also possible for α-amino acids where the $C\alpha$ has been substituted with a nitrogen to give azapeptides[64] and azatides[65] (Figure 1.18A). The conformation of azapeptides is rigidified due to the planarity of the urea, and repulsion between the lone pairs of the two covalently linked nitrogens. This gives azapeptides a tendency to adopt torsion angles corresponding to those of a peptide turn, which has been shown both in solution[66] and by X-ray crystallography[67]. A β-peptide analogue of the azatides has also been made, termed an aza-β-peptide.[68] For this family the aza-β^3-peptides have been shown to form an eight membered turn called a hydrazino-turn.[69] This turn structure is stabilized by hydrogen bonds from "amide" hydrogen to both the hydrazine-group and the carbonyl oxygen of the adjacent residue (**12**). This motif has also been demonstrated in the solid state for a hexamer compound, consisting of three such turns (**13**).[70]

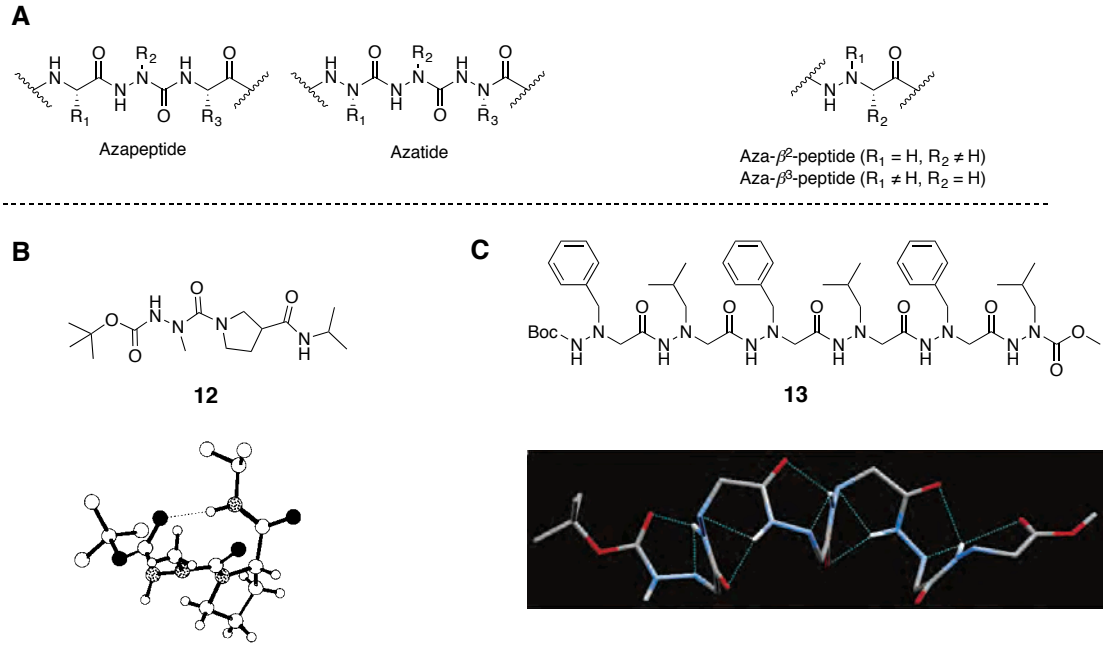

Figure 1.18. A) Structures of aza-β- and aza-peptides. B) Crystal structure of an azapeptide turn.[67] C) Crystal structure of a hexameric aza-β^3-peptide.[70]

As shown in figure 1.15 aryl-ureas have been used to furnish create foldamers from aromatic residues, but also aliphatic ureas have shown foldameric properties. Being aza-analogues of γ^4-peptides, they form well-defined helical structures, stabilized by three-centered hydrogen bonds (Figure 1.19).[71]

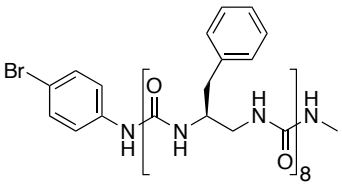

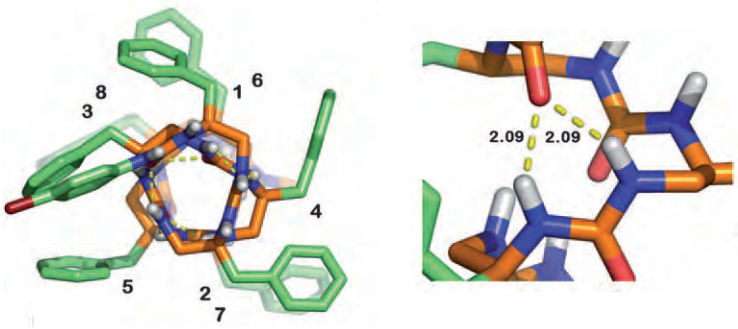

Figure 1.19. Right) Top view of an oligourea-helix. Left) Stabilizing three-centered hydrogen bond.[71]

Versions of the aza-β-peptides carrying an oxygen rather than a nitrogen in the backbone have also been proposed as foldamers and are called α-aminoxy peptides.[72]

In a similar way to the *N–N* bond, the repulsion of lone pairs in the *N–O* bond are thought to rigidify the backbone. The foldameric properties of these molecules have been shown in both solution and in the solid state, where it was shown that monomer model systems formed turn like structures. These structures are stabilized through hydrogen bonding interactions from the amide hydrogen to the carbonyl oxygen of the adjacent residue (Figure 1.20A).[73,74] Oligomers as short as dimers of these compounds have been shown to fold into helical arrangements (Figure 1.20B).[75] Analogues of the α-aminoxy peptides carrying one (β-aminoxy) or two additional methylenes (γ-aminoxy) in the backbone have also been prepared, and exhibits the same tendency to form turns between adjacent residues and helices in oligomers based on the same interactions.[75] In addition to this the β-aminoxy residues have been shown to engage in three-centered hydrogen bonding pattern including the amide hydrogen and the adjacent carbonyl carbon, but also the backbone oxygen (Figure 1.20C).[76] This structure can be further stabilized by the introduction of a cyclic constraint in the backbone (**17**).

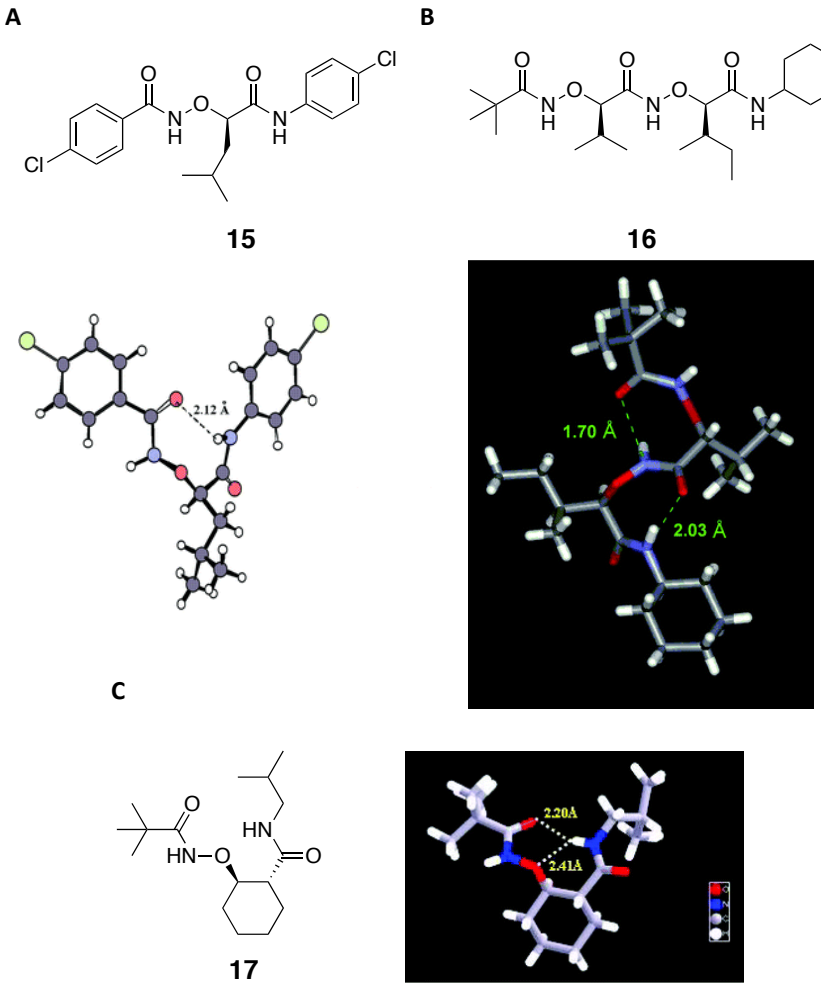

Figure 1.20. X-ray crystal structures of A) α-Aminooxy *N-O* turn.[74] B) Helix of an α-aminoxy dimer.[75] C) β-Aminoxy *N-O* turn of cyclically constrained monomer.[76]

1.4 β-Peptides

Like the α-peptides described above, the β-peptides consist of amino acid building blocks. The amino acids of β-peptides represent a minimal step away from the α-amino acid backbone, by the introduction of an additional methylene. Hence, these compounds are especially appealing for investigations into the field of folded non-biological polymers. β-amino acids are found in nature, displaying far greater diversity than the proteinogenic amino acids.[63] Amongst the most common β-amino acids are β-alanine, an essential component of pantotheic acid (vitamin B_5), which is a part of coenzyme A (Figure 1.21).[77]

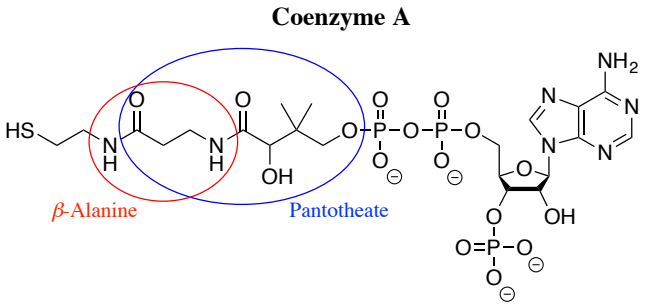

Figure 1.21. Structure of coenzyme A.

Although being present in natural compounds, no pure β-peptidic sequences from natural sources are known.[63] Early investigations of polymeric β-peptides indicated that they are capable of adopting stable helical structures, although the precise geometries of their secondary structure was challenging to determine.[78,79,80,81] Even though adding a single methylene unit to each residue in the backbone may seem as a small alteration, it introduces a cascade of conformational and chemoselective possibilities.

1.4.1 Conformational properties of β-peptides

The conformations of β-amino acids, as monomer building blocks or in a peptide strand are described by the torsion angles, ω, ϕ, θ, ψ of the backbone (Figure 1.22).[82]

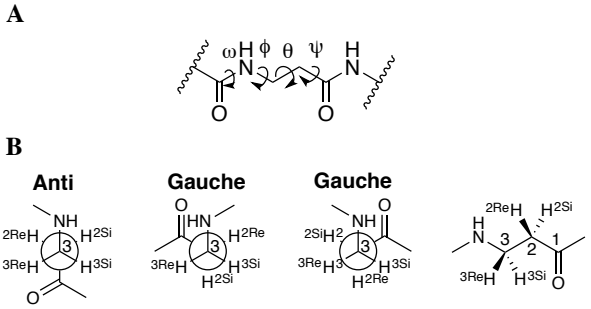

Figure 1.22. A) Definition of torsion angles in β-peptides. B) Rotamers of β-alanine regarding the θ angle.

In this convention a *cis* amide bond will have an ω angle of 0°, and the *trans* 180°, and the θ angle will be ±60° for the gauche conformation and 180° for the anti. Like

the α-peptides, the torsion angles providing the lowest energy conformation of a β-peptide falls within a certain region.[82] Compared to the α-amino acids, a few additional components such as the number of side chains, and their stereo- and regiochemistry, determines which set of torsion angles will provide the most stable conformation.[83] The conformational preference of β-amino acids can be described by the rotation around the C^2–C^3 bond, also given as the torsion angle θ (Figure 1.22B). If no substituents are present in the backbone the residue will have a high degree of flexibility. In both cases of having a single substituent at either C^2 (β^2-amino acid) or C^3 (β^3-amino acid) a gauche conformation is favored (Figure 1.23).[84] If a β-amino acid has substituents on both backbone methylenes ($\beta^{2,3}$amino acid), it is the stereochemical relationship between the side chains that determines the most stable backbone conformation. If the two substituents have the same stereochemistry the residue will strongly favor a gauche configuration, and if they have the opposite stereochemistry the anti conformation will be strongly favored.[84]

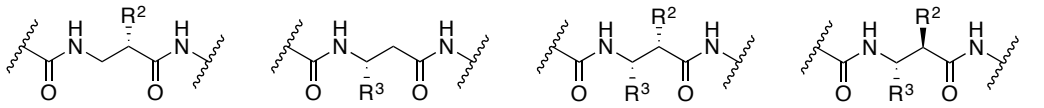

β^2-Residue favours a gauche conformation

β^3-Residue favours a gauche conformation

$\beta^{2,3}$-Residue syn configuration strongly favours a gauche conformation

$\beta^{2,3}$-Residue anti configuration strongly favours an anti conformation

Figure 1.23. Preferred conformation of substituted β-amino acids.

In the case of $\beta^{2,3}$ residues the side chains can be connected, this type of compounds show an even greater preference for the gauche conformation.[85] The torsion angles for the cyclically constrained residues can be fine-tuned by changing the size of the ring.[86] The prefered conformation of the β-amino acids in a sequence determines what secondary structures can be adopted. Helical and turn-like structures require gauche conformations, whereas an anti conformation will lead to extended structures.[87,88,89]

1.4.2 Helices of β-peptides

Oligomers of β-amino acids that are most stable in a gauche conformation are known to adopt helical conformations.[79,85,90] As for the α-peptides, β-peptides can also adopt a number of different helical structures.[83,91] The helical structure displayed by an oligomer is determined by the precise θ angles of the oligomer. Referring to a β-amino acid having a gauche conformation does not refer to an exact θ value, but merely the directionality of the side chains. The factors described in the last paragraph can be used to manipulate the dihedral angles more precisely. It is the exact torsion angles that will further define what kind of helix is the most stable.

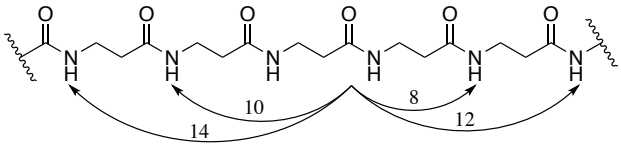

Figure 1.24. Possible helices of β-peptides.

This far five distinct helices have been identified for oligomeric β-peptides: a 14,[84,92,93,94] a 12-,[95] a 10-,[96,97] an 8-[98] and a mixed 10/12-helix[87] (Figure 1.24). These helices are named according to the number of bonds in their hydrogen bonded rings making up a full turn of the helix.[85]

1.4.3 The 14-helix

The most studied secondary structure motif amongst β-peptides is the 14-helix.[91] The 14 membered ring that makes up one full turn of the helix consist of three residues, connected by a hydrogen bond between an *N–H* (*i*) and *C=O* (*i* + 2) (Figure 1.25). Somewhat surprising, these helices are quite stable compared to α-helical displays of α-peptides.[83] The stability of this helix type is affected by the substitution pattern of the backbone, as it has been shown that β^2-oligomers form less stable helical displays as compared to β^3-oligomers, with the same side chains.[84] Further, the helices of β^3-peptides display right handed helices, whereas the helices of β^2–residues are left-handed.[91] Also, as the *C=O* bonds of both the α-helix and the 14-helix is directed along the helical axis a macro-dipole is created, which in the natural α-helix runs in the *N*- to *C*-terminal direction, but in the 14-helix is reversed.

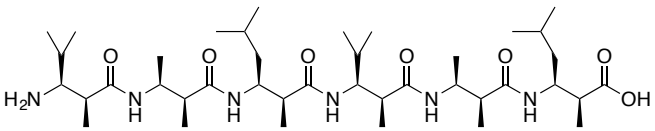

18

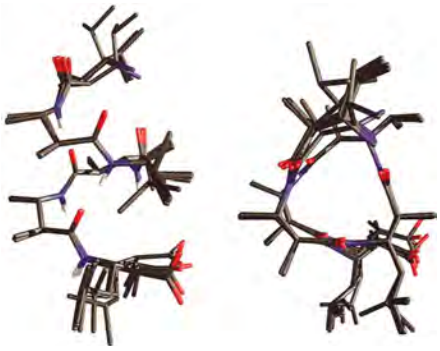

Figure 1.25. NMR structure of a $\beta^{2,3}$-hexapeptide in MeOD.[84]

It should also be noted that in the patterns formed, two kinds of positions are available for substitution, the axial and the lateral, and for any other substituents than fluorine

and hydroxide, the substituents must occupy lateral positions in order to form helical displays.[99]

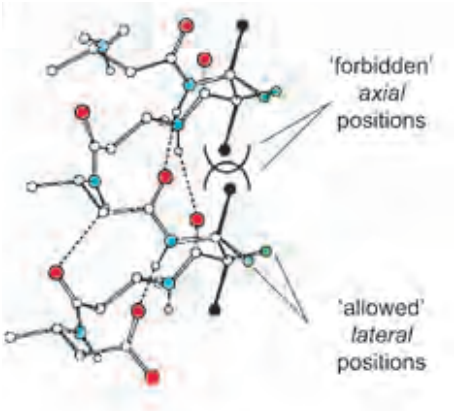

Figure 1.26. Structure of 14-helix with axial substituents.[99]

The formation of helices in α-peptides require 10-12 residues whereas the 14-helix can be formed from six residues.[90] To further stabilize helical displays, a cyclic constraint has been introduced into the backbone of β-peptides. As few as four of these residues have been shown to display a helical conformation.[100]

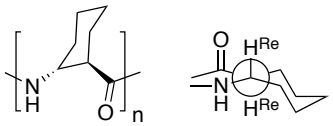

Figure 1.27. Structure of *trans*-2-aminocyclohexanecarboxylic acid.

If a *trans*-cyclohexane is used as constraint, the θ torsion angle will be near 55°, which specifically stabilizes the 14-helix (Figure 1.27).[85] Oligomers of *trans*-2-aminocyclohexanecarboxylic acid, has been shown to adopt very stable 14-helices by NMR and X-ray crystallography (Figure 1.29).[85,101]

The collection of side chains allowed in the 14-helix has been shown to posses great diversity.[84,90,93,102,103] However, initial studies of the 14-helix found it difficult to achieve both helix stabilization and great diversity of side chains within the same molecule.[101] The most stabilizing residues found were the cyclically constrained, but these were found hard to further functionalize.[104] To overcome these issues Gellman and co-workers synthesized a sequence of combined β^3- and cyclically constrained β-amino acid residues (**21**).[93] This β-peptide was a further development of two β-peptides designed by Seebach and co-workers (**19**)[105] and DeGrado and co-workers (**20**)[106], respectively, to deal with the generally low propensity to form helical structures in water.[107] The two latter mentioned β-peptides were designed to allow ionic interactions of the side chains, which stabilizes the helical display near neutral pH, but unfolding occurs at either basic or acidic conditions.

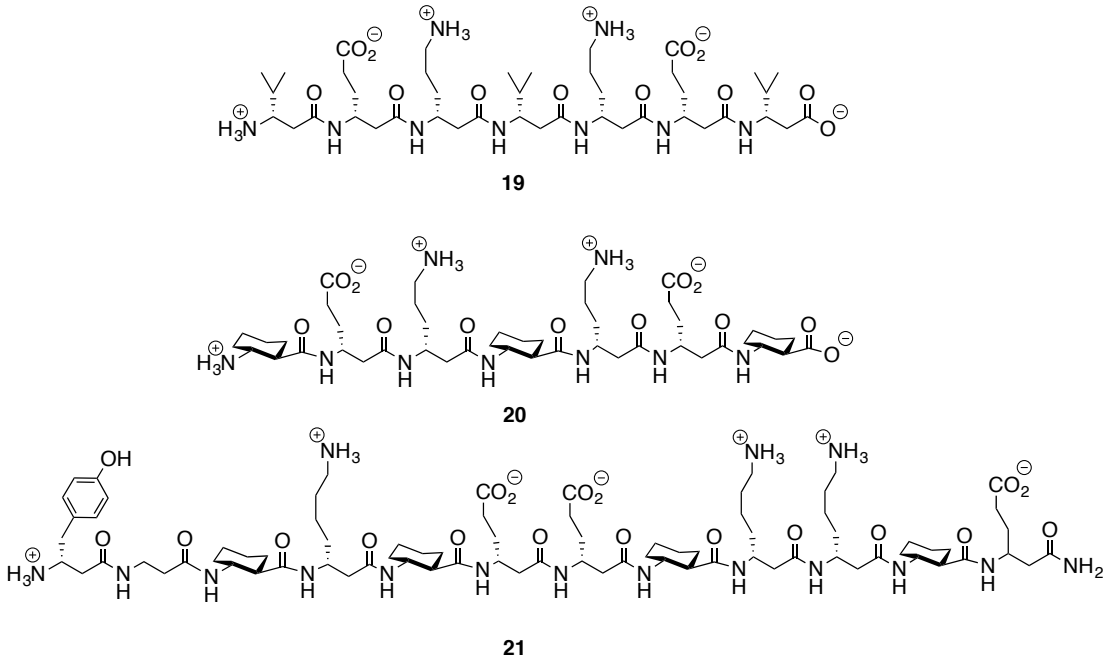

Figure 1.28. Sequences designed to increase helix stability in water, and to improve the diversity of side chains within a helix.

The sequence designed by Gellman contained a lower percentage of preorganized residues, as well as residues not able to engage in ionic interactions, but still the circular dichroism-spectre showed retention of the helical conformation, even at extreme pH conditions (pH 2 and 12).[93] It was hence concluded that the introduction of les than 50% pre-organized residues were sufficient to stabilize the formation of 14-helical displays.

1.4.4 The 12-helix

When the size of the cyclic backbone constrain is decreased to a *trans* substituted pentane ring, the dihedral angles are restricted in a way that does not allow the 14-helix. For the *trans*-2-cyclopentane carboxylic acid residues the θ torsion angle is found to be above 85°, and oligomers composed from these residues fold into 12-helices (Figure 1.29).[95] The secondary structure is stabilized by hydrogen bonds between *N–H* (*i*) and *C=O* (*i* + 3), which gives approximately 2.5 residues per turn.

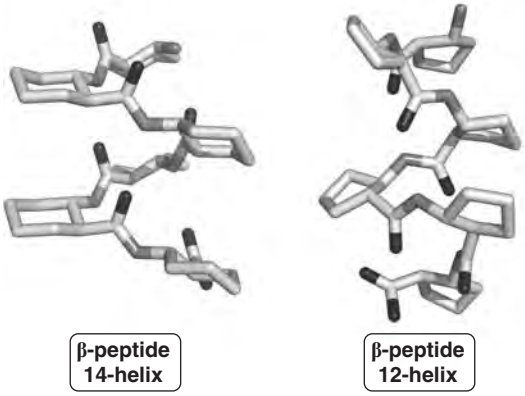

Figure 1.29. Crystal structures of: Left) The 14-helix of β-peptides containing the cyclohexyl backbone constraint.[85] Right) The 12-helix of cyclopenthyl-constrained β-peptides[86].

The ability to switch between two different helix-types by making relatively modest modifications, reveals a significant difference to the α-peptides. Using β-amino acid building blocks a far greater control over the secondary structure can be exerted than for the α-amino acids. β-peptides made from these residues tend to be poorly soluble in water, therefore an analogue carrying a pyrrolidine-constraint in an alternating fashion was designed (Figure 1.30). These positively charged oligomers were shown to retain the 12-helical display of the parent oligomer.[108]

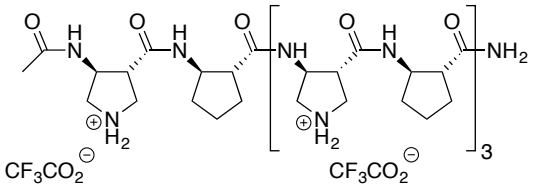

22

Figure 1.30. Pyrrolidinyl containing oligomer.

The amino functionality of the pyrrolidine-constraint has also been used to incorporate side chains.[109] This was achieved through sulfonylation of the amine, incorporating a selection of proteinogenic side chains e.g. **23** and **24**.

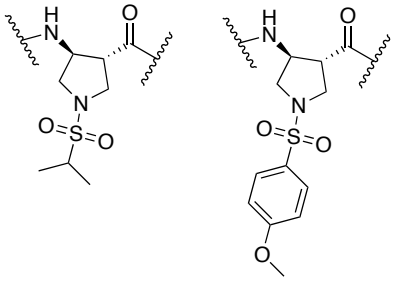

23 **24**

Figure 1.31. Structure of sulfonylated cyclically constrained residues.

It was also noted that upon incorporation of these residues, into sequences otherwise consisting of purely cyclopentane- or pyrrolidine constrained residues, the oligomers retained both their solubility and structural display.

1.4.5 The 10-helix

Only a few examples of this helix type have been reported, one of which is the terminally unprotected tetramer of *trans*-2-cyclohexane carboxylic acid.[96] In this case both the penta- and hexamer were found to adopt the 14-helix, like the protected tetra-, penta-, and hexamer. Oligomers of β-amino acids containing an oxetane ring have also been shown to adopt this conformation (**25**).[97]

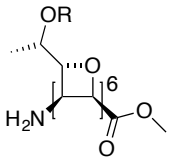

25

R = TBDMS or Bn

Figure 1.31. Structure of oxetane oligomer.

Interestingly, in this case the amino group and carboxylic acid are *cis* on the four membered ring, as opposed to the *trans* configuration of cyclopentane- and cyclohexane-constrained residues discussed above.

1.4.6 The 8-helix

This kind of helix has never been observed experimentally. However, crystal structures of short oligomers of 1-(aminomethyl) cyclopropanecarboxylic acid residues revealed a propensity to form eight-membered ring hydrogen bonds.[98]

1.4.7 The 10/12-helix

When a β-peptide sequence consist of alternating β^2- and β^3 residues, the resulting helix has a mix of 10- and 12 membered rings.[87] In this helix amides surrounded by methylenes interact with one another (i, i + 2) forming 10 membered rings, while the 12 membered rings are formed by amides surrounded by side chains (i, i + 3).

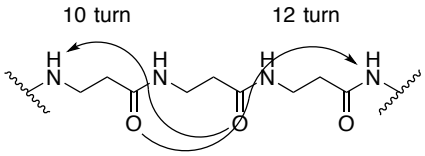

Figure 1.33. Hydrogen bonding in 10/12-helices.

In contrast to the uniform alignment of the *C=O* bonds of the 12- and 14-helices, the carbonyls in the 10/12-helix are oriented differently. The amide bonds of the 10-ring has the *C=O* bond perpendicular to the helical axis, whereas the *C=O* bonds of the 12-ring are directed along the helical axis.

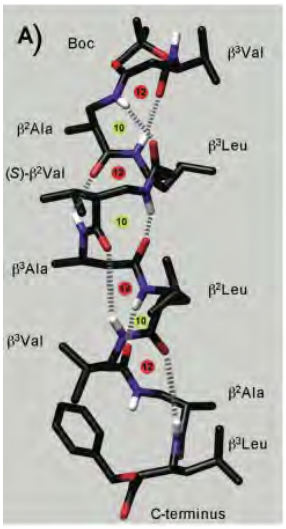

Figure 1.34. NMR-solution structure of a 10/12-helix in MeOH.[91]

This helical type is special as no naturally occurring peptides consist of two different types of turns. This strengthen the ability to manipulate the display of side chains further, again by relatively modest means.

1.4.8 Sheets

Sheets of β-peptides can, in principle, be assembled in two ways, one with an anti configuration of the C^2-C^3 bond, and one with a gauche conformation.[89] Sheets formed by anti-configured β-amino acids will display a net dipole, as all the carbonyl oxygens are oriented in the same direction, and the amide protons opposite. In contrast, the α-peptidic β-sheet display no dipole, due to the alternating direction of the carbonyls. Backbones of gauche-type β-amino acids would lack a dipole for the same reason.

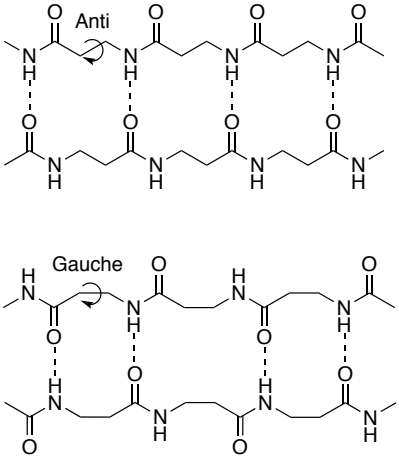

Figure 1.35. Hydrogen bonding pattern in sheet-structures of β-peptides.

From the studies of helices it was shown that β-peptides containing (2*R*,3*S*)-$\beta^{2\text{-}3}$ amino acids could not possibly fold into a helical conformation, as this substitution pattern puts both substituents in the "forbidden" axial position (Figure 1.35).[63] These

residues form fully extended conformations, with all carbonyl oxygens pointing in one direction, the amide protons in the opposite, and the side chains oriented approximately perpendicular to the amide planes, which is ideal for sheets. Sheets of this type was demonstrated by Seebach and co-workers (**26**).[110] This study also showed that by incorporating a flexible residue into the strand a turn could be introduced (**27**).

A

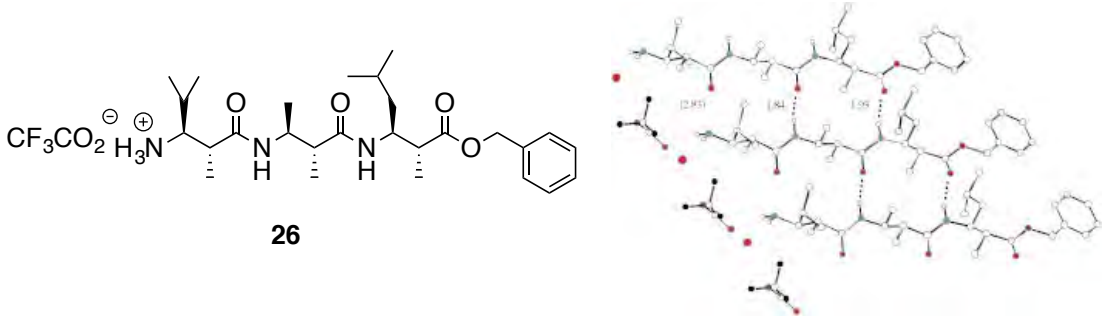

26

B

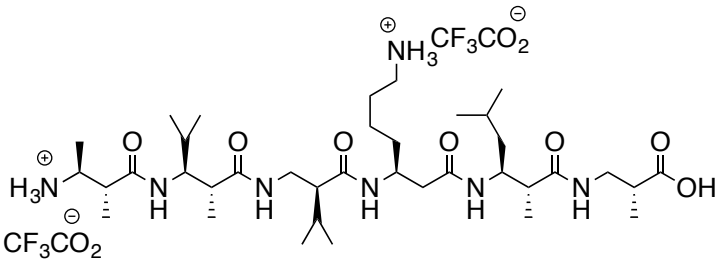

27

Figure 1.36. A) X-ray crystal structure of a β-peptide trimer packing in a β-sheet like arrangement. B) NMR-structure of a β-peptide hexamer displaying a turn motif.[110]

1.4.9 Non-hydrogen bonded structures

Different analogues of the α-amino acid proline have been prepared.[111,112] It has been shown that although unable to form hydrogen bonds, oligomers of these residues form secondary structures in solution. From the crystal structure of $(\beta^3 h\text{Pro})_{2,3}$-derivatives a higher oligomer was modeled, which pointed to a helical conformation.[112]

1.5 Bioactivity of β-peptides

Compounds exhibiting bioactivity consisting of either pure β-peptides, or peptidic compounds with a single or several mimetic residues have been synthesized. From the structural control that can be exerted on foldamers a number of useful compounds have been made. The simple separation of cationic and lipophilic side chains has been

used to furnish potent antimicrobials,[113,114] cell penetrating compounds[115-117] and the ability to form further helical displays have furnished compounds capable of biomolecular recognition.[118]

After having established that β-peptides are stable to proteases *in vitro*, a number of *in vivo* tests were performed to determine how this type of compound would be distributed.[119-121] It was found that only half the amount of a nonapeptide consisting of three (β^3-hAla–β^3hLys–β^3Phe) repeats was degraded during 7 days from injection into rats.[121] A second β-peptide of four residues, were tested in a similar manner, and showed to be distributed to different organs from the nonamer.[120] It was shown to cross the blood-brain barrier, intervene in the regulation of a number of genes and displayed no inflammatory effect, while retaining the same metabolic stability of the nonamer. This enhanced proteolytic stability presents a great advantage over the natural proteins and peptides with regard to designing a successful drug.

1.5.1 β-peptide inhibitors of protein interactions

The interaction of proteins control many cellular processes, and is therefore an emerging target for the development of a range of therapeutics. Proteins usually interact by making intermolecular contacts over a large binding domain, which is often a non-polar cleft. Designing synthetic molecules with a high affinity for one domain over another is challenging. As the domains are often large and do not differ much, they are nearly impossible to target selectively using conventional "small-molecule"-drugs. In the endeavor to create more selective therapeutic compounds the foldamers offer many attractive scaffolds.

Seebach and co-workers designed an amphiphilic β-peptide with a 14-helical structure (**28**), mimicking the α-helices of human apolipoproteins, which are involved in lipid uptake and transport.[118] Since amphipathic α-helical peptides are able to inhibit the lipid uptake process it was thought that β-peptides with an appropriate display of side chains might also be potent inhibitors. It was indeed shown that amphipathic β-peptides inhibited the process, while a series of unstructured β-peptides could not. It is also noteworthy that these compounds are only half the size of the natural peptides of which they are analogues.

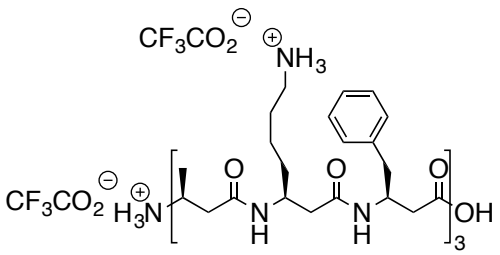

28

Figure 1.37. β-Peptide shown to inhibit fat uptake.

The fusion of enveloped HIV virion with a host cell is mediated by the viral protein gp41.[122] α-Peptides derived from gp41 (e.g. **29**) can act as potent anti HIV agents by binding to pre-fusion states of gp41, thereby disrupting the fusion mechanism, involving the formation of a six-helix bundle. Schepartz and co-workers reported a decamer β-peptide designed to inhibit cell-fusion, by the same mechanism.[123] The design was based on the observation that three residues, two tryptophans and an isoleucine, of the natural sequence contributed especially to the binding.[124] In a later paper the same group showed that the distribution of these residues could be optimized giving a potency in cell-fusion assays in the low-micromolar range (**30**).[125] It was later suggested that the sites responsible for the high binding affinity in the fusion process of gp41 were more spatially delocalized.[126] Gellman and co-workers have designed extended sequences of mixed α- and β-residues, arranged in repeats of $\beta\alpha\alpha\alpha\beta\alpha\alpha$, forming a helix that binds more efficiently to the surface of the central trimeric coiled coil of gp41.[127] The longer α/β-peptide analogue **31** exhibited low nanomolar potency protection against infection by primary HIV-isolates in a cell-based assay. From this study it is worth noting that the foldamers are equipotent to the parent α-peptides in cell-fusion inhibition assays and in inhibition of HIV-1 infectivity. Even though the sequence only contained two β-peptide residues it showed a highly improved proteolytic stability. Crystallographic data confirmed a six-helix bundle of three helices of **31** and the gp41 fragment (Figure 1.38).[126] This strategy is attractive as six-helix bundle fusion mechanism is common to many vira and thus represents an important target for drug development.

A

29: Ac-TTWEAWDRAIAEYAARIEALIRAAQEQQEKNEAALREL-NH_2

30: H-β^3O-β^3V-β^3I-β^3E-β^3V-β^3W-β^3O-β^3V-β^3W-β^3E-OH

31: *Ac*-β^3T-TWE-β^3X-WD-β^3Z-AIA-β^3E-YA-β^3X-RIE-β^3X-LI-β^3Z-AAQ-β^3E-QQ-β^3E-KNE-β^3X-AL-β^3Z-EL-NH_2

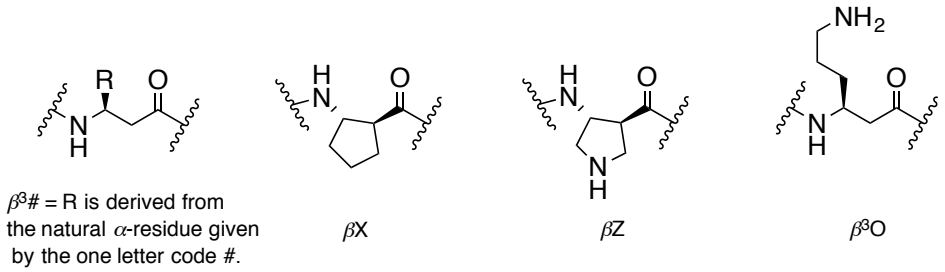

β^3# = R is derived from the natural α-residue given by the one letter code #.

βX

βZ

β^3O

B **C**

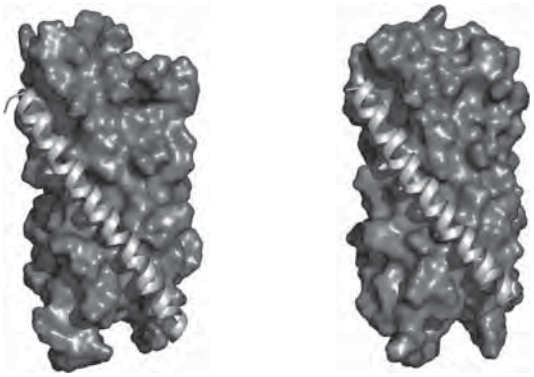

Figure 1.38. A) Sequence of gp41 derived peptide and foldamer mimics. B) **29** bound to gp41.[127] C) **31** bound to gp41.[126]

The protein p53 is a transcription factor controlling the survival of cells, by upregulating the expression of gene products that promote cell-cycle arrest or induce apoptosis.[128] The human oncogene protein product double minute 2 (hDM2) negatively regulates p53 by binding to the p53 transcription domain and targeting the protein for degradation by the proteasome. In many cancers hDM2 is overexpressed, why inhibitors of the p53/hDM2 interaction holds potential as chemotherapeutic agents.[129] The binding interaction of p53 and hDM2 has been localized to a short α-helical domain in p53 (**32**), that binds to a hydrophobic cleft on the surface of hDM2.[130] Based on this sequence Schepartz and co-workers developed a β-peptide analogue (**33**) mimicking the p53 activation domain, displaying three key hydrophobic residues, found in p53 binding-studies, on the same face of a 14-helix.[131] Through combinatorial screenings[132] and docking studies *in silico*[133] the sequence was optimized yielding **34** which exhibits a low nanomolar affinity for hDM2. The interaction of p53 and hDM2 happens inside cells, making cell penetration an important factor. The Schepartz group reported on two strategies to improve on the

cellular uptake; the modifications of the sequence to promote cell uptake[134] and by the introduction of alkene side chain cross links to stabilize the folding[135]. These studies showed that attachment of cationic residues did indeed promote cellular uptake, but at the same time diminished the affinity for hDM2.[134] On the other hand, the introduction of a hydrocarbon bridge stabilized the secondary structure and thereby the affinity, but had a decreasing effect on the cellular uptake.[135]

A

32: H-SQETFSDLWKLLPEN-OH

B

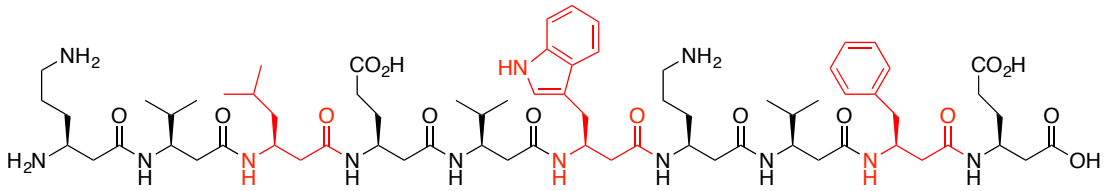

33

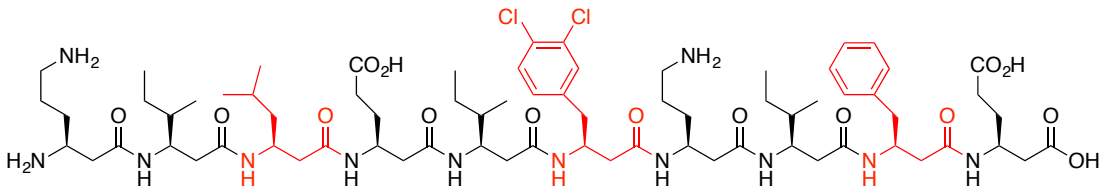

34

Figure 1.39. A) Residues 15–29 of the α-helical binding domain of p53, the residues responsible for the binding interaction are marked in red. B) Structures of two β^3-peptide mimics of peptide **32**.

B-cell lymphoma protein 2 (Bcl-2) family of proteins also play a crucial role in the life and death of cells. This balance is controlled by a complex network of binding interactions between pro-survival and pro-apoptotic Bcl-2 family members, the misregulation of this balance is implicated in many cancers.[136] Despite the complexity of signaling, the structural features of the binding interaction are very well conserved within this family. It has been shown that an α-helical BH3 domain from a pro-apoptotic member binds into a hydrophobic cleft of a pro-survival counterpart.[137] Hence mimics of the proapoptotic BH3 domains of Bcl-2 would be useful in cancer treatment. Gellman and co-workers designed a series of mimics that binds tightly to the BH3 recognition site of pro-survival Bcl-2 family members.[138,139] The designs were based on a BH3 peptide from the protein Bak (**35**). After screening ~300 sequences, of β- or α/β- known to adopt helical structures, a lead compound consisting of an alternating 1:1 mixture of α- and β-residues were found (**36**), which displayed low micromolar binding affinity for Bcl-x_L. A modification to this sequence having a foldamer *N*-terminal region and an α-peptidic *C*-terminal region (**37**) increased the binding affinity by 1000-fold.[140] However, despite extensive efforts improvement of the proteolytic stability has been unsuccessful.[141,142] In a later study

with mimics composed of different mixtures of α- and β-residues carrying identical side chains to the natural BH3 domain of the protein Puma (**38**), a sequence with low nanomolar binding affinity for Bcl-x_L was identified (**39**).[143] Using a similar distribution of α- and β-residues to the HIV-inhibiting β-peptides ($\alpha\alpha\beta\alpha\alpha\alpha\beta$), sequences of both high binding affinity and improved proteolysis resistance have been furnished. Further, it was shown that the bound state of a helix, formed by a related α/β-peptide mimic (**40**), is almost identical to the α-peptidic prototype (Figure 1.40D).[144]

A

35 H-GQVGRQLAIIGDDINR-NH_2

36 Ac-βZ-A-βX-R-βX-L-βX-K-β^3B-A-β^3D-A-β^3F-A-βZ-*NH*

37 Ac-βZ-A-βX-R-βX-L-βX-K-β^3L-GDAFNR-NH_2

38 Ac-EEQWAREIGAQLRRMADDLNAQYERR-NH_2

39 Ac-EEQ-β^3W-AR-β^3E-IGAβ^3Q-LR-β^3R-MAD-β^3D-LN-β^3AQYEβ^3R-R-NH_2

40 Ac -EEQ-β^3W-AR-β^3E -IGAβ^3Q-LR-β^3R-MAD-β^3D-LN- β^3A QYE–NH_2

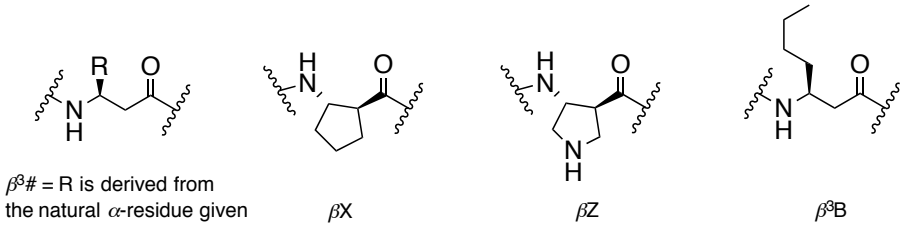

B **C** **D**

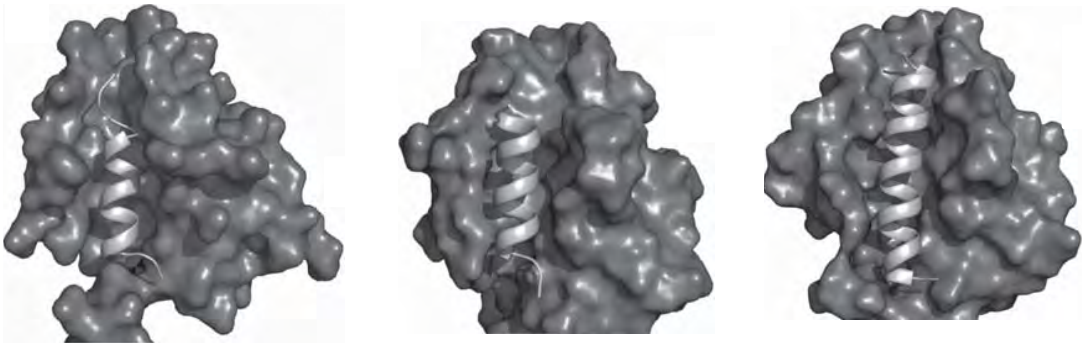

Figure 1.40. A) Sequences natural peptides and their mimics. B) NMR structure of peptide #1 bound to Bcl-x_L.[137] C) Crystal structure of hybrid #3 bound to Bcl-x_L.[140] D) Crystal structure of hybrid #6 bound to Bcl-x_L.[144]

1.5.2 Antimicrobial activity of β-peptides

Helicity and amphipathicity are prevalent amongst natural antimicrobial peptides, which are important components of the innate immune system and toxins of a variety of different vertebrate and invertebrate species, including human.[145] These peptides are assumed to have more than one possible mechanism of action in killing bacterial cells. The nature of antimicrobial peptides, their mechanism of action and cell selectivity will be elaborated upon in chapter 4. A common feature of all mechanisms is the ability of the peptide to interact with bacterial cell surfaces, which are distinct from mammalian cell surfaces as they are charged.[146,147] Mimicry of the amphipathic α-helicity of these peptides has led to a large number of potent antimicrobial β-peptidic compounds, designed as both 14-[114] (**28** and **41**–**43**) and 12-helices (**44**),[148] which show low IC_{50} values as well as selectivity towards bacterial cells rather than mammalian.

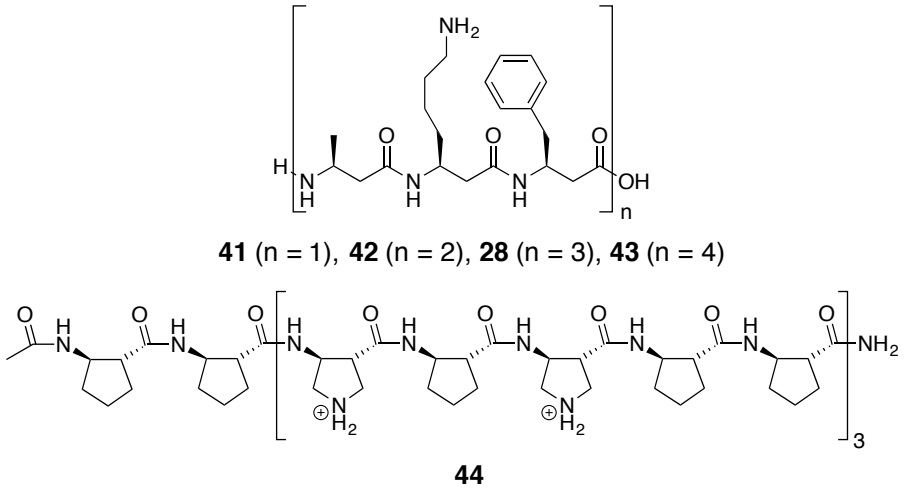

Figure 1.41. Antimicrobial β-peptides designed to display 14-helicity (**28** and **41**–**43**) and 12-helicity (**44**).

1.5.3 Cell-penetrating β-peptides

Peptides and proteins usually have rather poor cell penetrating properties, an exception being the naturally occurring cell-penetrating peptides. An example is the transcription-transactivating (Tat)-protein of human immunodeficiency virus.[149] The cell-penetrating properties of Tat, and related proteins, have been ascribed to short 10–20 residue sequences. These peptide fragments are highly cationic, and often rich in arginine. The attachment of these fragments to other cargo molecules have been shown to impart cell-penetrating properties in species otherwise incapable of crossing membranes.[150] Such abilities make this class of compounds useful as drug delivery vehicles, and have motivated efforts towards protease stable foldamer analogues. Raines and Gellman synthesized an analogue of Tat in which each α-amino acid residue was substituted for a β^3-residue, the resulting β-peptide was capable of crossing human cell membranes with an efficiency resembling that of the natural analogue.[116] The ability of amphipathic versus unordered polycationic sequences to

cross membranes has been studied by Seebach and Co-workers, who showed that a seven-residue β^3-homoarginine was the most efficient.[117] These two classes of compounds, ordered and unordered, have been shown to exhibit different cell penetrating mechanisms, [151,152] and later studies have shown that the efficiency and mechanism of penetration are dependent on the folding behavior of the β-peptide.[153,154]

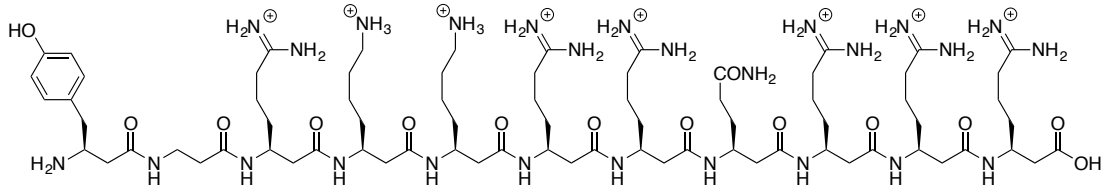

45

Figure 1.42. β^3-Peptide derived from the naturally occurring Tat peptide (residues 47–57).

1.6 Peptoids

Oligomers of *N*-subtituted glycines, called peptoids (or α-peptoids), were initially investigated as lead compounds for drug development.[155] Peptoids are described as peptide mimics where the side chain has been shifted to the nitrogen rather than the α-carbon. Oligomers of this kind present an attractive scaffold as they can be generated using a straight forward sub-monomer based synthesis, that allows for the incorporation of a broad variety of side chain functionalities (Figure 1.43).[156,157]

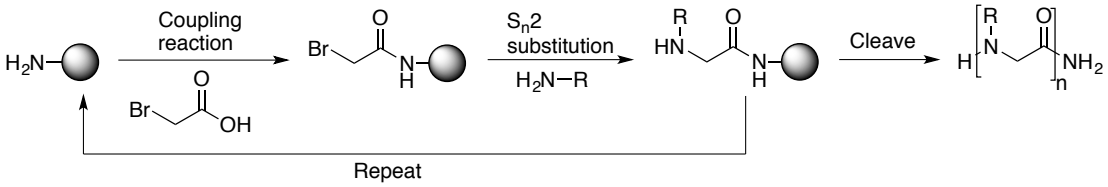

Figure 1.43. Illustration of the principle of sub-monomer peptoid synthesis.

The submonomer synthesis involves the addition of a primary amine to an α-bromo acetylated compound, in this way all primary amines can potentially be utilized in the synthesis of peptoids. The ease of synthesis and diversity of sequence, makes this class of compounds highly amenable for high throughput screening.[158,159] Peptoids are believed to hold great value as therapeutics due to their enhanced proteolytic stability[160] and increased cell-penetrating properties, as compared to α-peptides.[161] The early peptoid research was mostly based on the generation of large oligomer libraries, which could be screened for novel functions. However, biologically active peptoids have also been discovered through rational design.[162,163] The use of peptoids as drug delivery agents has also been explored, by conjugation of known bioactive agents to peptoid oligomers.[164,165] Many applications of peptoids require a certain well defined display of functionalities. Therefore the propensity of peptoids to adopt specific secondary structures has been studied intensively.

1.6.1 Peptoid structure

By moving the side chain from the α-carbon to the nitrogen the backbone chirality and the ability to form hydrogen bonds are lost. The tertiary amide nitrogens of peptoids yield a lower energy barrier of rotation, around the amide bond, than the secondary amides of peptides. The greater stability of *trans* peptide bonds in α-amino acids is assumed to solely arise from steric effects of *C*-α substituents in the *cis* conformation.[166] Hence the isomerization between *cis* and *trans* conformations happens far more readily in peptoids than in the secondary amides of α-peptides (Figure 1.44).

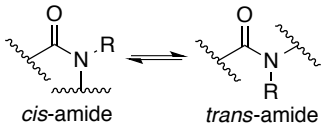

Figure 1.44. Equilibrium of *cis*- and *trans*-amides.

The lack of hydrogen bonding capabilities present a challenge in stabilizing secondary structures, as the amide bond rotation becomes a major stabilizing factor. These characteristics make peptoid oligomers highly flexible, which also complicates the *de novo* design of well defined structures. However, early research in peptoid secondary structure revealed that peptoids had a propensity to form helical structures analogous to the polyproline I helix in solution, which consist of all *cis* amides.[167] This structure was later confirmed in the solid state (Figure 1.45).[168] It was shown that helix formation was promoted if the sequence consisted of at least 50% *N*-α-chiral side chains, or if every third residue (*i, i*+3 positions) is α-chiral and aromatic and the *C*-terminus has an α-chiral side chain.[169,170] Circular dichroism-investigations of the length dependence of helix formation also revealed that at the nonamer length the signal was inconsistent with helicity otherwise observed for sequences up to 20 residues.[169]

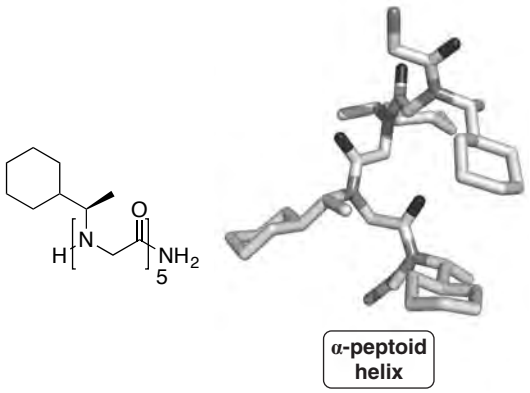

Figure 1.45. X-ray crystal structure of a peptoid oligomer.

It was found that at exactly this length the *C*- and *N*-terminal was connected by hydrogen bonding, creating a loop conformation consisting of both *cis* and *trans* amides.[171]

In an effort to obtain high-resolution structures of peptoids, covalent constraints have been introduced. Head-to-tail cyclizations of peptoids have resulted in a number of crystal structures, giving information on the distribution of *cis* and *trans* isomers in turn-like displays.[172] Similar approaches of covalently connecting two side chains to stabilize helical displays have been reported (Figure 1.46).[173,174]

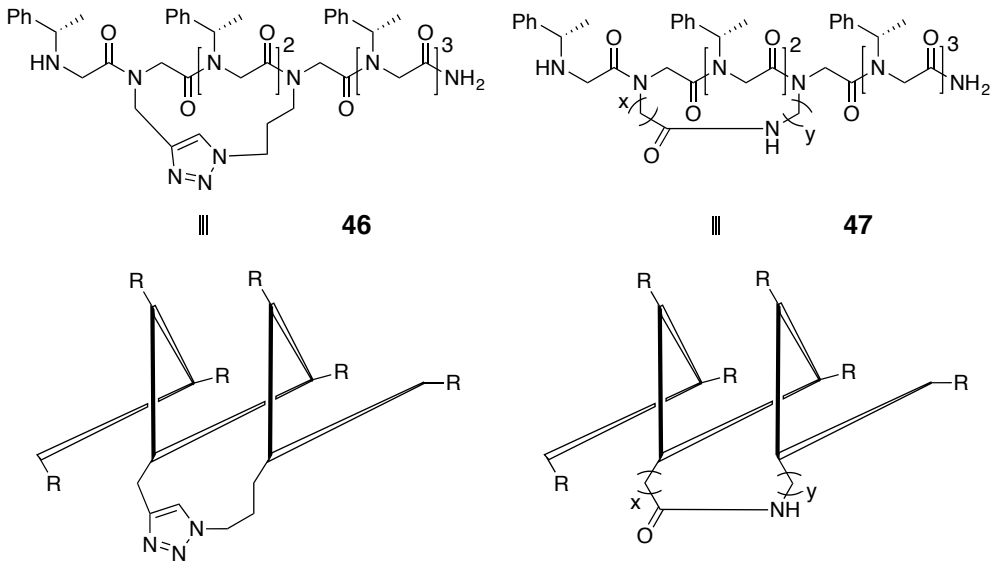

Figure 1.46. Examples of side chain constrained peptoids.

These efforts showed that upon introduction of side chain "bridges" the amount of α-chiral aromatic side chains could be reduced to 33% in organic solvents and 50% in water.

The investigations of peptoid oligomers have indeed shown that peptoids are capable of forming secondary structures, and that control over the isomerization of the amide bond is important for the rational design of folded peptoids. As peptoid compounds are devoid of hydrogen bonding capabilities, a number of other non-covalent interactions have been proposed to stabilize the secondary structure of peptoids. To gain insight into the factors governing the conformational preferences a series of monomer model-systems have been investigated.[175,176] Determination of the amide bond *cis*/*trans* ratio, by NMR, upon changing the size and electronic properties of the side chains, revealed that the conformational preference at a local residue can be tuned (Table 1.1).[177] In general, it was shown that branched and unbranched alkanes (**48a**) gave rise to a preference for the *trans* conformation.[176] However, it was shown that by attaching a secondary carbon to the backbone (**48b**) the *trans* conformation became less favored. A later report has shown that by going from a secondary carbon to a *tert*-butyl group (**48c**) the amides exclusively populate the *cis*-conformation.[178] This implies that the sterics around the amide can be used to manipulate the

population distrubituion of *cis*- and *trans*-conformations. When incorporating benzylic side chains (**48d**) the preference was comparable to that of an unbranched alkane.[176] Further, it was shown that incorporation of both α-chirality and aromaticity (**48e**) gave a slight preference for the *cis*-conformation in polar solvents, and a slightly higher $K_{cis/trans}$ in apolar solvents as compared to the achiral aromatic side chain. It was also shown that by using electron poor aromatic systems (**48f** and **48g**) the preference for the *cis*-conformation was further enhanced, and was exclusively populated when using triazolium-type side chains (**48h**).[176,179] Also the incorporation of a naphthyl group in combination with α-chirality gave a strong preference for the *cis*-conformation, however, as the naphthyl group had to be installed through the 1-position (**48i**) this effect has been argued to arise from steric effects, as a naphthyl group attached through the 2-position (**48j**) behaves like the phenylethyl-peptoid (**48e**).

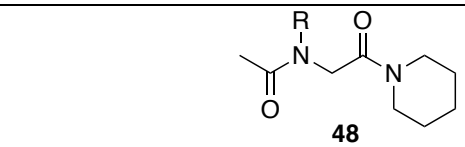

48

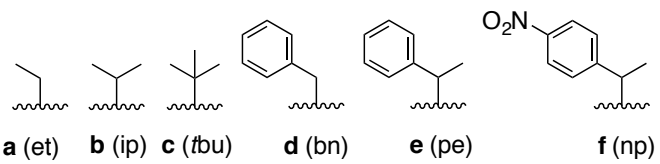

a (et) **b** (ip) **c** (*t*bu) **d** (bn) **e** (pe) **f** (np)

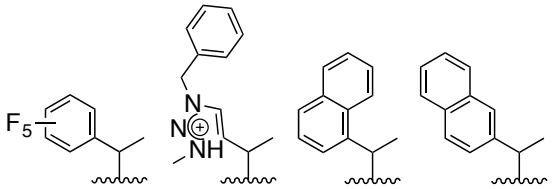

g (fe) **h** (bte) **i** (2npe) **j** (1npe)

		CD_3OD	CD_3CN	$CDCl_3$
Comp.	Side chain	$K_{cis/trans}$	$K_{cis/trans}$	$K_{cis/trans}$
48a[a]	et	0.5	0.7	0.2
48b[a]	ip	0.6	1.1	0.4
48c[b]	tBu	>19.0	>19.0	>19.0
48d[a]	bn	0.6	1.2	0.2
48e[a]	pe	1.3	2	0.7
48f[a]	np	1.8	3.4	1.5
48g[a]	fe	2.5	3.8	1.6
48h[c]	bte	11.1	11.8	>19.0
48i[a]	2npe	1.6	2.2	0.9
46j[a]	1npe	4.6	6.3	2.6

Table 1.1. *cis–trans* equilibrium constants of different peptoids, determined by NMR. [a] From ref 176. [b] From ref 178. [c] From ref 179.

These findings suggest that the lone pair (*n*) of the amide oxygen can interact with the aromatic moiety attached to the α-carbon of the side chain. This kind of interaction has been observed in other systems, and is referred to as $n \rightarrow \pi^*_{Ar}$ interactions.[180,181] This sort of interaction is known from the literature, through both calculations and experimental data.[181,182] The data from table 1.1, suggest that the population of the *cis*-conformation is increased upon introduction of electron poor aromatic rings, which correlates with this kind of interaction.[176,177] Contrary, when using aniline type side chains *trans* is the only conformation found.[175] This preference was investigated prior to their use as peptoids, in *N*-methyl acetanilide, where it was argued that the electron rich center of the aromatic ring would repel the amide oxygen in the *cis*-conformation.[183] It was also found that when changing the *C*-terminal from an ester to an amide the *trans* became more populated, indicating that the electronic properties of the termini has some importance. It was thus postulated that the *N*-terminal amide oxygen might interact with the *C*-terminal carbonyl carbon. This kind of interaction has also been investigated in proline-systems and helices of collagen-like peptides, which led to the suggestion of an interaction similar to a hydrogen bond, but rather than delocalizing the oxygen lone pair (*n*) to a σ^* orbital of a hydrogen, it is delocalized to an empty π^* orbital of a carbonyl carbon ($n \rightarrow \pi^*_{C=O}$).[184,185] Due to the positioning of the π^* orbitals, the strength of the interaction is optimized when the incoming lone pair "attacks" along the Burgi-Dunitz trajectory,[186] similar to a nucleophilic attack.[187] The requirements for this kind of interaction are met by the backbones of peptoids, where this interaction have been proposed as a stabilizing factor.[177] Further, it has been shown that the interaction can be used to manipulate the *cis–trans* isomeric distribution of proline systems upon changing the electronic properties of the involved donor-acceptor system (Scheme 1.6).[187] It was shown that by substituting a carbonyl oxygen for sulfur, which increases the nucleophilicity of the donor, the conformation allowing the $n \rightarrow \pi^*$ overlap was more favored. If the $n \rightarrow \pi^*_{C=O}$ effect is present in peptoids or β-peptoids, it should be possible to change or enhance the preferred conformations by altering the electronic properties of the backbone.

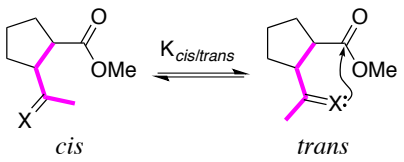

Scheme 1.6. Proline system used to explore $n \rightarrow \pi^*$ interactions.

Recently a paper, by Gorske and co-workers, describing another mode of $n \rightarrow \pi^*_{aryl}$ was published. Herein it is argued that the direct interaction between the lone pair and the aromatic moiety is only present when the aromatic system is severely electron deficient.[188] In electron rich, neutral and slightly electron deficient systems a "bridged" interaction was proposed (bridged $n \rightarrow \pi^*$). In this interaction the transfer of electron density is facilitated by an intermediary *N*-α-*C*-*H* σ^* orbital (Figure 1.47).

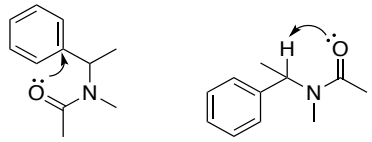

Figure 1.47. Representation of an $n \rightarrow \pi^*$ (left), and a "bridged" $n \rightarrow \pi^*$ interaction (right).

The understanding of how these factors dictate the conformations of the individual peptoids has been crucial in understanding the fundamental folding propensities of peptoids.[189] The understanding of peptoid folding was tested by solving the structures of two linear trimers and a cyclic nonamer by X-ray crystallography, and simultaneously doing a blind prediction *in silico*.[190] The predicted structures from this study were in close agreement with the experimentally determined X-ray structure (Figure 1.47).

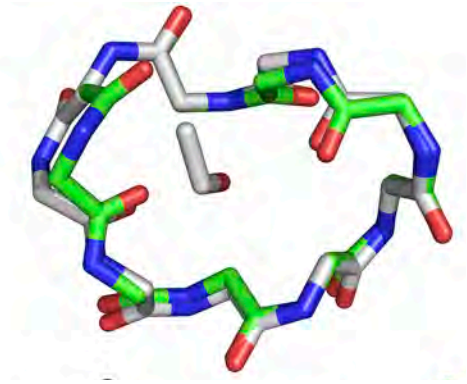

Figure 1.47. Comparison of structures found by X-ray crystallography (gray) and by molecular modeling (green).[190]

By taking some of the most uniform residues, it has been possible to rationally design certain motifs. A homo-oligomer composed of (*S*)-*N*-(1-naphthylethyl)glycine has been shown to fold into a rather robust helix, with approximately three residues per turn and a helical pitch of 6.0 Å (Figure 1.48).[191] The use of alternating *cis* and *trans* promoting residues has also provided compounds with a well-defined secondary structure. In these cases either *tert*-butyl[178] or naphthylethyl[192] was used as *cis*-promoters, whereas *N*-aryl was used as *trans*-promoting side chains in both accounts.

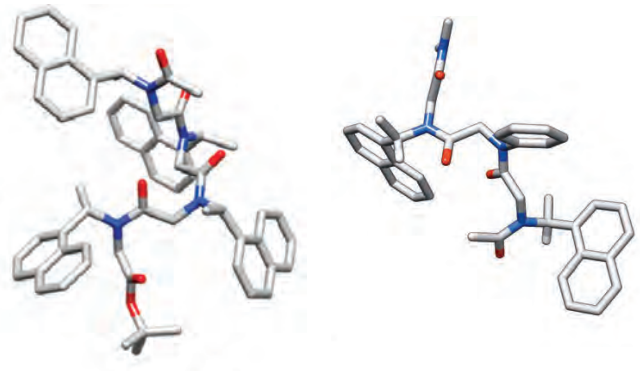

Figure 1.48. X-ray crystal structure of a peptoid helix with (*S*)-1-(1-naphthyl)ethyl side chains.[191]

1.6.2 Bioactivity of Peptoids

Like β-peptides, peptoids have shown superior stability towards protease degradation as compared to the natural proteins and peptides. Given their foldameric properties, these residues have also attracted attention for their potential as pharmaceuticals. As peptoids were originally thought as a way to fast and efficiently synthesize large libraries from which lead compounds could be found through high throughput screenings, many bioactive peptoids have been identified this way. As the focus of this thesis is the structure and function of foldameric compounds, the following examples of bioactive peptoids have been chosen as they describe efforts to realize activity through a structure based design.

1.6.3 Peptoids as antimicrobials and cell penetrating compounds

Like β-peptides the peptoids are stable to proteolytic enzymes found in cellular environments. As for natural peptides, a limiting factor in testing and marketing a β-peptide drug is the tedious synthesis, which is also associated with high cost of production. As the side chains are shifted to the nitrogen in the peptoidic backbones the chirality is eliminated making the synthesis of peptoids far more straight forward than both α- and β-peptide oligomer synthesis.

Peptoids have been investigated with regard to many of the same functions as the β-peptides, since these studies were based on rather simple systems displaying only a single type of secondary structure. As one of the first secondary structures found in peptoids were helical, an effort to design antimicrobial peptoids were undertaken. Some of the first examples of antimicrobial peptoids, made by Goodson and co-workers, were di- and trimers effective against both Gram positive and Gram negative bacteria with minimum inhibitory concentration (MIC) values of 5–40 μM.[193] However, these short peptoids also displayed a modest hemolytic activity at low concentrations. Barron and co-workers synthesized analogues of the naturally occurring magainin-2,[194] which later underwent further scrutiny resulting in some general guidelines for the synthesis of peptoid antimicrobials, which are further discussed in section 4.5.1.[162]

Kodadek and co-workers evaluated the ability to cross mammalian cells of peptoids versus their corresponding α-peptide sequences (e.g. **49**).[161] In this study it was found that the peptoids displayed a 3- to 30-fold increase in cell-penetrating properties over the peptides. The authors suggested that this increase was due to the lack of backbone amide hydrogens increasing the overall lipophilicity of the molecule. Following this investigation a more thorough study of 350 peptoid- and their corresponding peptide tetramers were tested to generate structure–activity relationship.[195] It was found that generally the cell penetrating ability of peptoids was twice that of the corresponding peptides, with the peptoids being slightly more lipophilic given lower polarity of the backbone. It was also noted that the peptides and peptoids with the highest cell

permeabilities shared common side chain compositions of one-third hydrophobic and two-thirds hydrophilic residues.

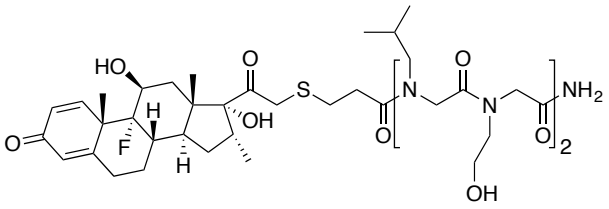

49

Figure 1.49. Example of a cell-penetrating peptoid.

Like for the β-peptides, the ability of peptoids to cross membranes has led to research in their ability to transport cargo. Bräse and co-workers evaluated some simple fluorophore conjugated peptoid hexamers, (*N*Lys)$_6$ (**50**) and (*N*Arg)$_6$ (**51**), for their ability to cross membranes.[196] For these peptoids it was concluded that the guanidino-groups were responsible for a more rapid uptake. The same research group made an effort to characterize the secondary structure of a rhodamine-labeled hexa-*N*Lys (**52**), and found it to display a helix-like structure.[197]

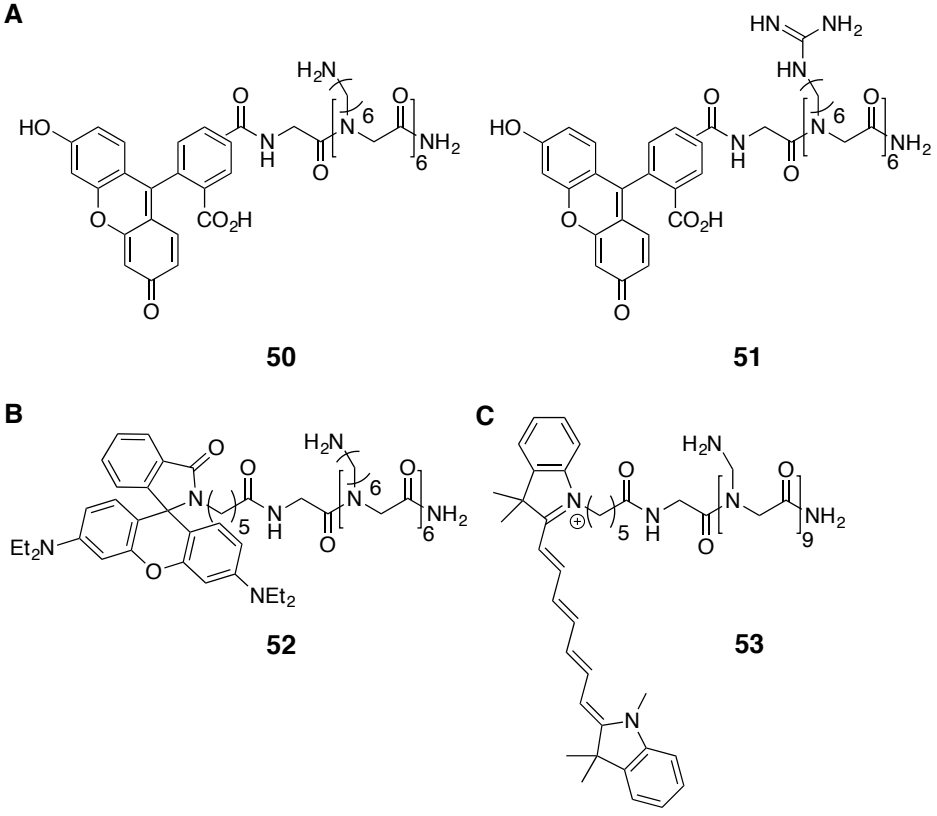

50 **51**

52 **53**

Figure 1.50. Cell-penetrating peptoids used to explore transport across membranes.

Bradley and co-workers found that a fluorescein-labeled peptoid nonamer [(*N*Lys)$_9$] (**53**) displayed remarkable delivery properties in being able to label a variety of cell lines within minutes.[198] Due to the proteolytic stability of these peptoidic fluorescent

probes they have recently been utilized to track primary phagocytes over several days *in vivo*.[199]

1.6.4 Lung surfactant mimics

Lung surfactant (LS) is a naturally occurring material essential for proper respiration in humans. It is composed of lipids and proteins that regulate the surface tension at the air-liqiud interface in the lungs.[200] A deficiency of functional LS leads to respiratory distress syndrome, a leading cause of mortality in premature infants and respiratory impairment in adults. Treatment with synthetic LS formulations is less effective than the naturally occurring LS, and animal LS have been shown to cause an immune response. Barron and co-workers have designed peptoid mimics of the helical hydrophobic surfactant protein SP-B.[201] The peptoid was designed to mimic the *N*-terminal segment of SP-B (residues 1 to 25) having a hydrophobic insertion region (residues 1 to 9) and an amphipathic helix containing arginine and lysine. The SP-B mimics had α-chiral (*S*)-phenylethyl (*N*spe) or (*S*)-*sec*-butyl (*N*sbu) as hydrophobic side chains and to promote helicity, and *N*Arg or *N*Lys as cationic residues.

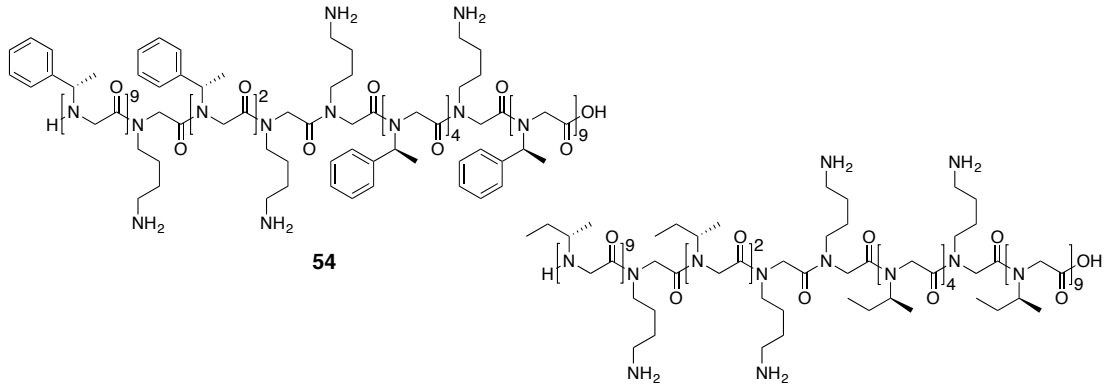

Figure 1.51. Examples of lung surfactant peptide mimics.

The helicity was examined using CD-spectroscopy, and as expected it was found that oligomers with a high content of *N*spe displayed more stable helices. When tested for their surface activity, it was shown that the aliphatic containing peptoids were better at interacting with lipid mixtures. This shows that varying the stability of the secondary display is possible and can in some cases be beneficial. The study also concluded that the substitution of lysine-like for arginine-like side chains had no effect on the surface activity.

1.6.5 Peptoid-peptide interactions

Appella designed a helical peptoid (**56**), designed to mimic the binding sequence of the protein p53, responsible for binding to the human double minute 2 protein, as explained earlier.[202] The peptoid was designed to display three key hydrophobic side

chains on a helical peptoid. It was found that using a rigid helical peptoid scaffold did not lead to effective mimicry of p53. However, when using a less structured peptoid lacking helix inducing residues reasonable binding affinities in the low micromolar range could be obtained, without loss of cell-penetrating ability.

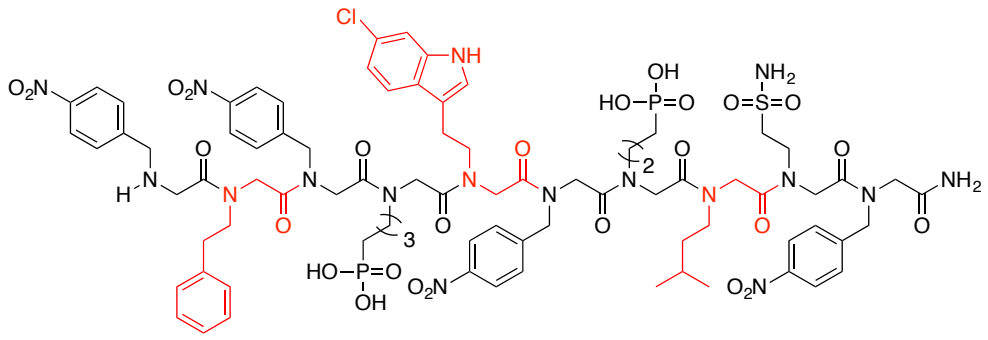

56

Figure 1.52. Structure of peptoid used to inhibit the interaction of p53 and hDM2, residues important for binding are shown in red.

The ability to interact with proteins without well-defined structures has also been used as an asset to break fibril formation. Liskamp and co-workers designed a peptoid (**57**) mimicking the core region of amylin (residues 20 to 29), a protein known to aggregate and form amyloid fibrils (β-sheets) in insulin producing β-cells.[203] It was found that peptoids could break up the hydrogen bonding patterns of the β-sheets without displaying a well-defined structure, and thereby terminate aggregation.

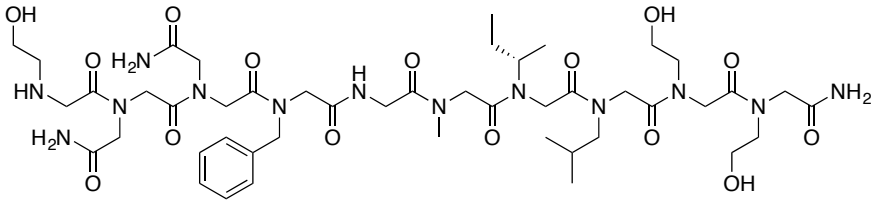

57

Figure 1.53. β-Sheet breaking peptoid.

Also a number of peptoids have been identified that binds to specific proteins and inhibit their function.[204] These peptoid oligomers have been identified through library synthesis and subsequent high-throughput screening. The positive hits have most often been modified to optimize certain capabilities e.g. cell-penetration. As these bioactive, and in a therapeutic context highly relevant, compounds have not been investigated and optimized with regards to their secondary structure they have not been discussed here.

2 β-Peptoids

2.1 Secondary structure of β-peptoids

β-Peptoids contains the modifications of both the β-peptides and peptoids, an extra methylene in the backbone and the side chain attached to the nitrogen.[205] As these compounds are also devoid of hydrogen bonding capabilities, one must expect that the factors governing secondary structure formation for oligomers of β-peptoids are more similar to peptoids than β-peptides. The secondary structure of β-peptoids is not as well explored as for the two parent compounds. Given the lack of hydrogen bonding capability, and the additional backbone methylene, these compounds should be very flexible. The first investigation of the secondary structure in β-peptoid oligomers, was inspired by the early investigations of peptoid oligomers.[206] By looking at CD-spectra of growing oligomers, of the type (β-*N*-(*S*)-phenylethyl)$_n$-OH (β*N*spe), it was concluded that these compounds did not form any regular structure in MeOH, Trifluoroethanol (TFE) or MeCN solution. However, a similar study performed on *N*-terminally acetylated oligomers of the type (β-*N*spe)$_n$-NH_2 showed that the CD-signal was both dependent on the length of the oligomer and the temperature of the solution.[207] These findings suggest that β-peptoids longer than four residues fold into some kind of ordered structure. The first high resolution structure of a β-peptoid oligomer was determined for a cyclized homo-tetramer with propargyl side chains (**58**).[208] This constrained structure displayed all the amide bonds in the *cis*-conformation.

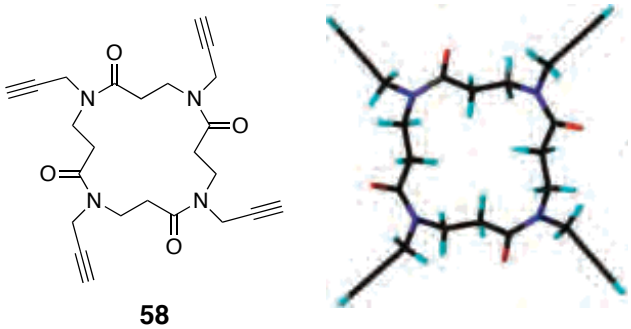

58

Figure 2.1. X-ray crystal structure of cyclic tetramer **58**.[208]

To get a better understanding of the folding propensities, and to develop new scaffolds for multivalent display, a series of linear and cyclic alternating α/β-peptoids were synthesized.[209] NMR-spectroscopy of the linear compounds revealed quite heterogeneous mixtures of *cis*- and *trans*-conformations. The CD spectra, on the other hand, indicated that the compounds have at least one ordered conformation, which is dependent on the solvent. The cyclically constrained compounds exhibited the same CD-spectral shape, but with a more intense trace, implying some stabilization of the secondary structure. The octamer was later used to determine the importance of the amount of α-chiral side chains and their pattern.[210] Here it was shown that increasing

the amount of α-chiral side chains from 50% to 75% did not have a pronounced effect of the conformational preference. However, when the pattern of the side chains where shifted so that the α-chiral side chains resided on the peptoid residue (**60**) rather than the β-peptoid (**59**), the NMR-spectrum revealed a more homogeneous distribution of the *cis*- and *trans*-conformations (Figure 2.2).

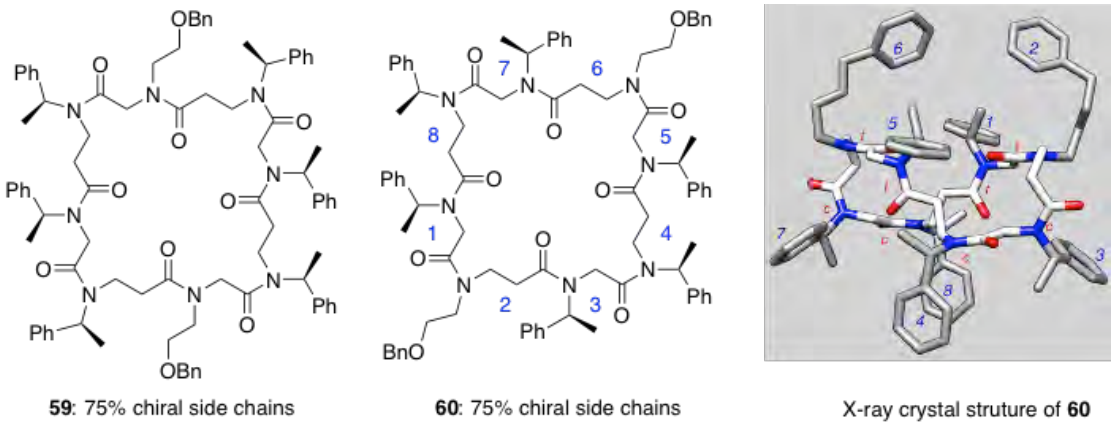

Figure 2.2. Structures of cyclic α-/β-hybrid peptoids with different side chain distributions, and X-ray crystal structure of **60**.[210]

Further, the X-ray crystal structure was solved for this compound revealing four *cis*-amides and four *trans*-amides. These are distributed in pairs, giving rise to a twisted rectangular shape of the backbone, with the *cis*-amide pairs located at the corners. The β-peptoid with propargyl side chains has also been used in cyclic scaffolds of mixed α– and β-peptoids.[211] An X-ray crystal structure of a tetramer, with a sequence of alternating α- and β-peptoid residues, revealed all β-peptoids to be in a *cis*-conformation while the α-peptoids where in the *trans*-conformation.

The existing literature on linear oligomers of β-peptoids or β-peptoid-hybrids shows ambiguities concerning their foldameric properties. To obtain experimental data regarding the folding propensities of β-peptoids, we designed a series of monomers, inspired by the studies of peptoids. These monomers were designed to test the influence of steric bulk and stereo-electronic effects on the *cis–trans* ratio. Ultimately we hope that knowledge on how the individual residues behave, would result in guidelines to rationally design oligomers with defined structures.

2.2 Design and synthesis of monomeric β-peptoid model systems

First it was decided that all model compounds should be based on acetylated β-peptoid model. This design was chosen as it was thought to mimic the local interactions encountered in an oligomer structure. In this way the effect of the side chains can be investigated with regard to steric bulk and stereoelectronic properties. Since a study has shown that the capping of these compounds are influencing on the CD-spectrum of oligomers, we decided to prepare series of both *C*-terminal *tert*-butyl

esters and morpholino amides (Figure 2.3).[212] The *tert*-butyl ester was chosen as these can also be readily deprotected, which allows for further coupling. The tertiary amide of the morpholino compounds were chosen as they are closer to the actual properties of the backbone of a β-peptoid oligomer.

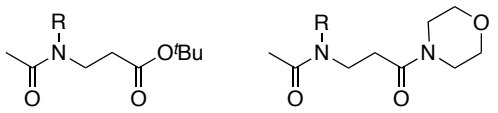

Figure 2.3. Structure of β-peptoid backbones.

Our preliminary study was designed to investigate a diverse set of *N*-alkyl side chains regarding the steric bulk, α-branching, aromatic vs. saturated substituents and direct attachment of aromatic compounds (*N*-aryl substituents). A set of eight side chains (**a**–**i**) were installed in monomer model systems (Scheme 2.1). To probe the effects of the various side chains on the *cis–trans* rotamer preference, the monomers were acetylated to generate a *N*-terminal tertiary amide. As the rotation around the amide bond is sufficiently slow, the population of the *cis*- and *trans*-conformation can be determined by integration of the ^{1}H NMR peaks assigned to each rotamer, analogous to the studies of α-peptoids.[176,177,179]

Syntheses of the β-peptoid monomers were achieved by aza-Michael addition of a primary amine to either *tert*-butyl-acrylat (**61**) or acryloylmorpholine (**62**), giving the monomer series **63a–i** and **64a–i** (Scheme 2.1). This reaction was carried out in MeOH, which has turned out to be superior to earlier suggested mixtures of tetrahydrofurane (THF) and water[206] or the originally proposed mimethylsulfoxide (DMSO).[205] The Michael addition was followed by acetylation to give the desired *N*-terminally capped monomers **65a–i** and **66a–i** for NMR evaluation.

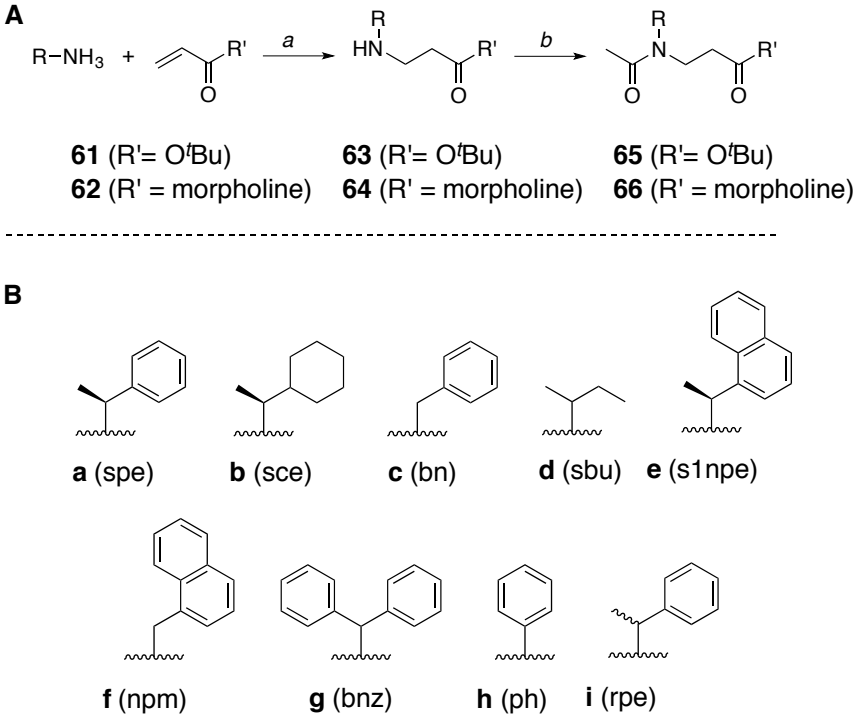

Scheme 2.1. A) Acetylated monomers **65a**-**h** and **66a**-**h**. Reagents and conditions: (a) MeOH, 50 °C, 16h; (b) (i) for esters Ac_2O (2 equiv), pyridine (2 equiv), DMF, 0 °C → rt, 4h or (ii) for amides AcCl (2 equiv), pyridine (2 equiv), CH_2Cl_2, 0 °C, 1h. B) Abbreviations for *N*-alkyl side chains used: spe = (*S*)-1-phenylethyl, sce = (*S*)-1-cyclohexylethyl, bn = benzyl, sbu = sec-butyl, s1npe = (*S*)-1-(1-naphthyl)ethyl, npm = 1-naphthylmetyl, bnz = benzhydryl, ph = phenyl, rpe = (rac)-1-phenylethyl.

In addition to the *N*-alkyl side chains and *C*-terminal capping group, model systems designed to probe local $n \rightarrow \pi^*$ interactions were prepared. The concept of these designs was to alter the electronic properties of the backbone, thereby altering the strength of the interactions. In case of an $n \rightarrow \pi^*$ interaction being present, one of the conformations should be further stabilized. The *N*-terminal amides was modified by the introduction of a trifluoroacetyl group, which was installed by treating **63a**, **63e**, **63f, 64a**, **64e** and **64f** with trifluoroacetic anhydride (Scheme 2.2). Due to the electron withdrawing effect of fluorine, this modification was made to enhance the acceptor capabilities of the amide carbonyl carbon.

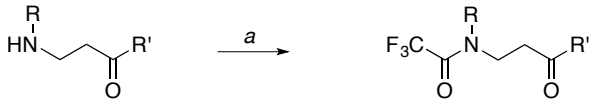

Scheme 2.2. Synthesis of a series of backbone modified monomer models: a) trifluoroacetic anhydride (2 equiv), pyridine (2 equiv), CH_2Cl_2, 0 °C, 1h.

The carbonyl oxygens were also substituted with sulfur, creating minimal peptide bond surrogates with altered electronic properties.[187] Sulfur has an electronegativity close to that of carbon, as a result the *C=S* bond should be less polarized than a *C=O* bond.[213] We reasoned that this substitution would enhance an $n \rightarrow \pi^*$ delocalization as sulfur is a softer base than oxygen, and thus a better electron pair donor. This

substitution was done selectively at both amide groups of compounds **66a**, **e**, **f** using Lawesson's reagent (**69**).[214,215] This reagent is a mild thionating agent for ketones, esters and amides, that allows preparation of the thio analogue of the parent compound. In solution Lawesson's reagent is in equilibrium with a more reactive dithiophosphonium ylide (**70**) (Scheme 2.3). This ylide can react with a carbonyl group to give a thiooxaphophetane (**71**) intermediate, which collapses to give the thiocabonyl-analogue (**72**) (Scheme 2.3). The driving force of this reaction is the formation of a very stable *P=O* bond.

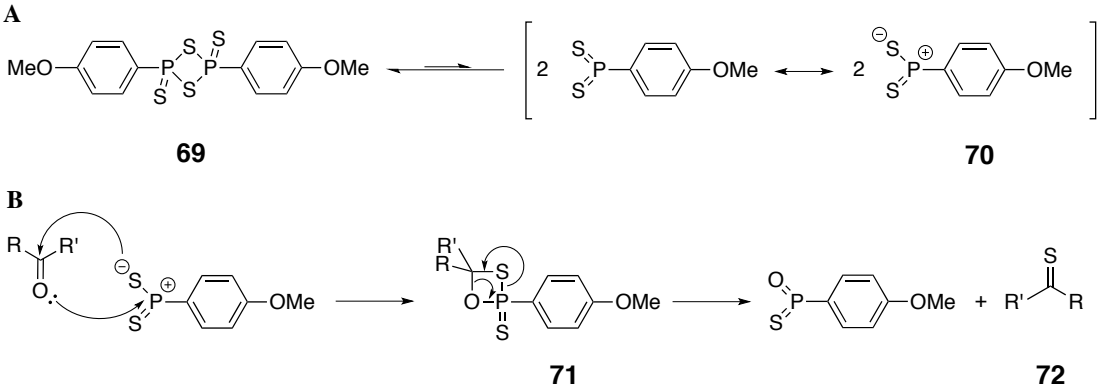

Scheme 2.3. Reaction mechanism for thionation using Lawessons reagent.

Lawessons reagent has been used to replace amide bonds in biologically active peptides with thioamides, in an effort to furnish more potent and selective compounds. These studies have shown that Lawessons reagent will convert amides to thioamides in the presence of esters, without formation of thioesters.[216] This selectivity can also be used to selectively install the thioamide at either end of the *β*-peptoids (Scheme 2.4).

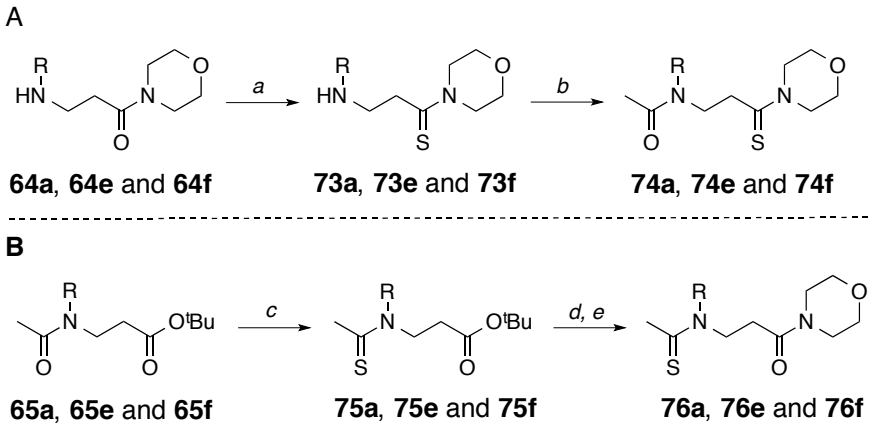

Scheme 2.4. Synthesis of thioamide-containing monomeric model compounds. Reagents and conditions: (a) Lawesson's reagent (1.5 equiv), toluene, 110 °C, 3 h; (b) AcCl (2 equiv), *i*-Pr_2NEt (2 equiv), CH_2Cl_2, 0 °C, 3 h; (c) Lawesson's reagent (0.6 equiv), toluene, 110 °C, 1 h; (d) 1M $LiOH_{aq}$–DMF 1:1, rt, 16 h; (h) morpholine (2 equiv), HBTU (2 equiv), *i*-Pr_2Net (2 equiv), CH_2Cl_2, rt, 16 h.

By applying Lawessons reagent to **64a**, **64e**, **64f**, the *C*-terminal thioamide containing monomers **73a**, **73e** and **73f** can be obtained. The monomers can subsequently be acetylated giving the thionated monomeric model systems **74a**, **74e** and **74f** (Scheme 2.4A). If Lawessonss reagent is applied to the acetylated monomers **75a**, **75e**, **75f** in equimolar amounts, only the *N*-terminal amides are transformed to thioamides giving **75a**, **75e** and **75f**. The obtained compounds can then be deprotected and the desired *C*-terminal capping group can be installed by a coupling reaction. For our purpose we chose to install morpholine capping groups yielding the *N*-terminally thionated compounds **76a**, **76e** and **76f** (Scheme 2.4B).

2.3 Synthesis of monomeric peptoid model systems[a]

As fluorination and thionation of peptoid backbones of any length had not been described prior to our investigation, we decided to prepare peptoid analogues as well. For these compounds we chose a single scaffold, which we thought most likely to engage in any of the interactions we were investigating. As the peptoids present a shorter and less flexible backbone, we thought it relevant to investigate if the introduction of these groups would have comparable effects in this system.

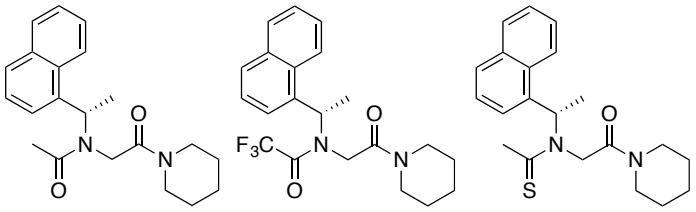

Figure 2.4. Synthesized peptoid model systems.

The preparation of the monomeric model systems were achieved by applying published methods for solution-phase peptoid synthesis[209] in combination with the protocols described in section 2.3 for β-peptoids, giving compounds **77, 78** and **79** (Figure 2.4).

2.4 Methods to evaluate monomeric model systems

Because the isomerization of the tertiary amide bond is slow on the NMR timescale, two sets of signals appear. Though most of these signals exist as multiplets and overlap with those of the isomer, it was possible for all the systems investigated to isolate a pair of corresponding signals. The ratio of the integrals of the signal for each isomer gives the $K_{cis/trans}$ of the amide bond directly. In all model systems containing an α-chiral side chain, the methine proton was used to determine the isomeric ratio

[a] The syntheses of the monomeric peptoid model systems were performed by fellow Ph.D student Jens Engel-Andreasen.

(Figure 2.5). For the systems without chiral side chains the methyl of the acetyl group could be used to determine the ratio.

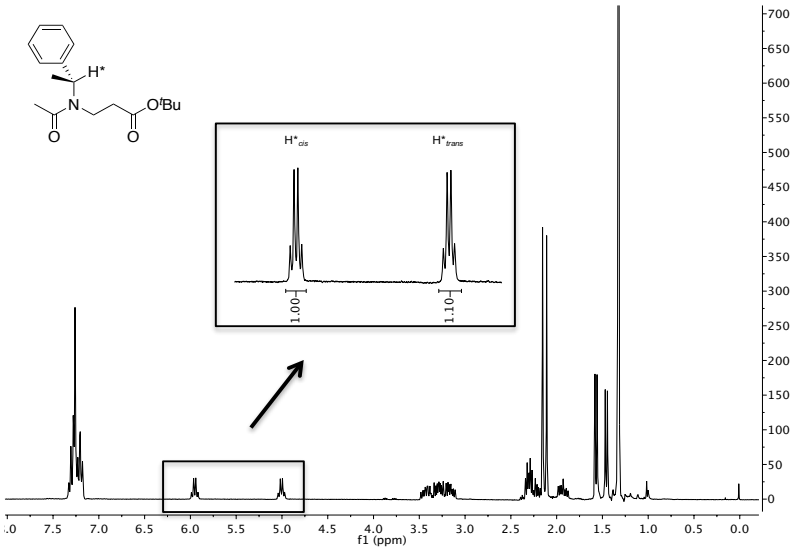

Figure 2.5. ^{1}H NMR-spectrum highlighting the signal utilized for determination of $K_{cis/trans}$.

This method has been used in earlier studies where it was determined that the signal with the most downfield chemical shift corresponds to the *cis* conformation.[217] To assess if our system displayed the same trend, we performed rotating frame Overhauser effect spectroscopy (ROESY). The highlighted signals correspond to correlations **a**–**c** involving the methine proton as shown in figure 2.6.

In the *trans*-conformation, the methine proton (quartet) has correlations to the side chain CH_3 protons (**b**) as well as the *N*-acetyl CH_3 protons (**c**). The further downfield shifted quartet only has an ROE correlation to the side chain CH_3 protons (**a**). Thus, the *N*-acetyl CH_3 group from the conformation with upfield shifted signal is in closer proximity to the methine proton, which confirms the assignment of this spin system as originating from the *trans*-conformation.

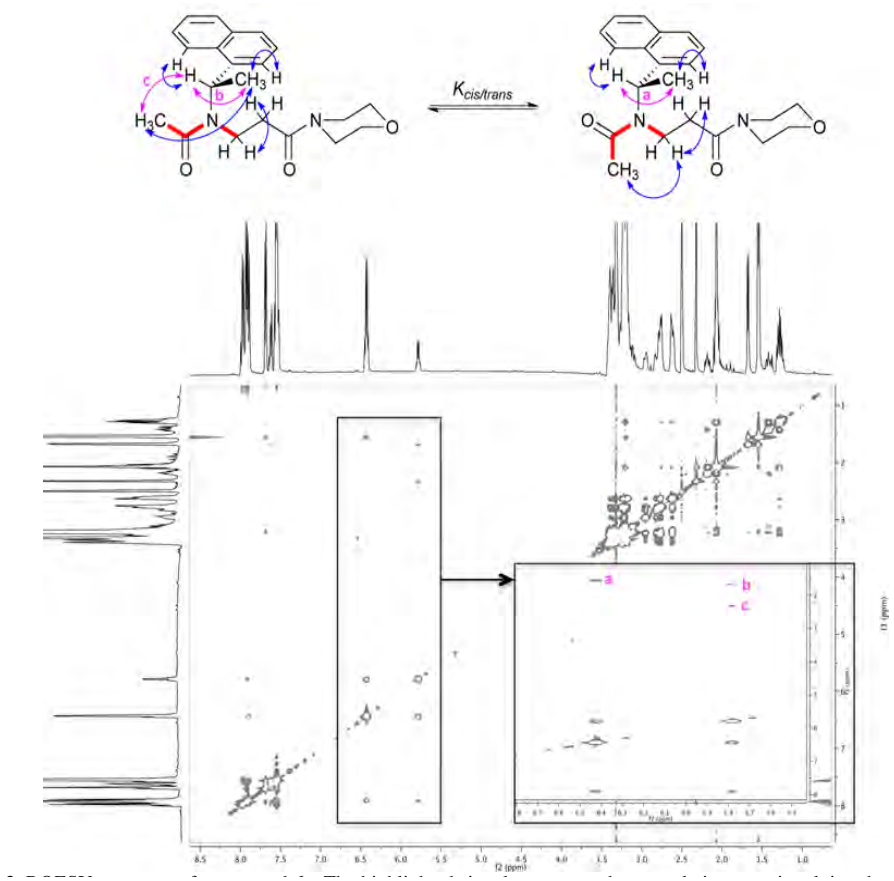

Figure 2.6. ROESY spectrum used for assigning the signals to the *cis*- and *trans*-conformations respectively.

We also evaluated if using chiral vs. achiral side chains had any effect on the *cis–trans* ratio. For this we chose to use a monomer with an spe side chain, as this side chain has been shown to determine the handedness of helices in peptoid oligomers.[169]

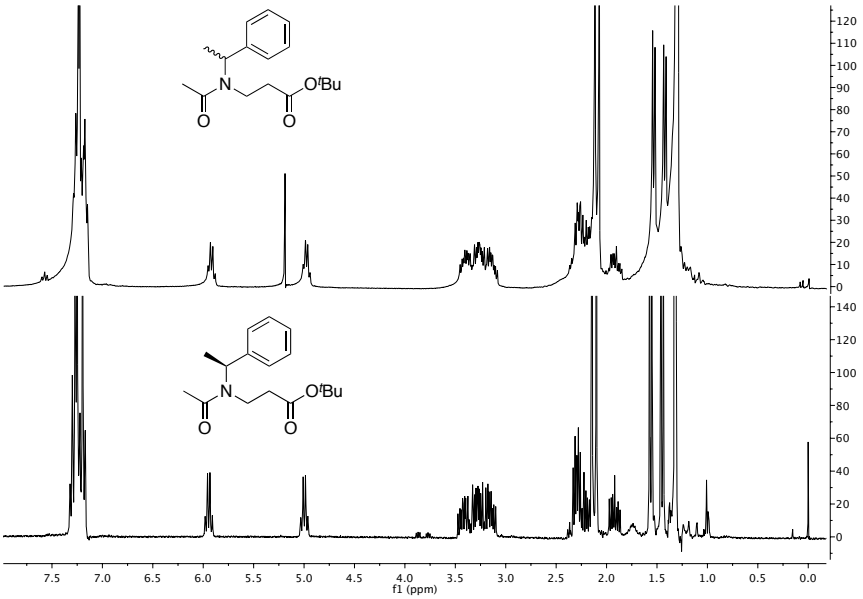

Figure 2.7. ^{1}H NMR spectra of the racemic mixture **75i** (top), and the enantio-pure **75a** (bottom).

^{1}H NMR of **75a** and **75i** revealed identical spectra, confirming that the chirality does not influence the *cis–trans* ratio ($K_{cis/trans}$) (Figure 2.7).
To ensure that any observed effects were intramolecular, we recorded a series of NMR-spectra at increasing concentrations from 6–200 mM (Figure 2.8). This series showed no change in the observed $K_{cis/trans}$.

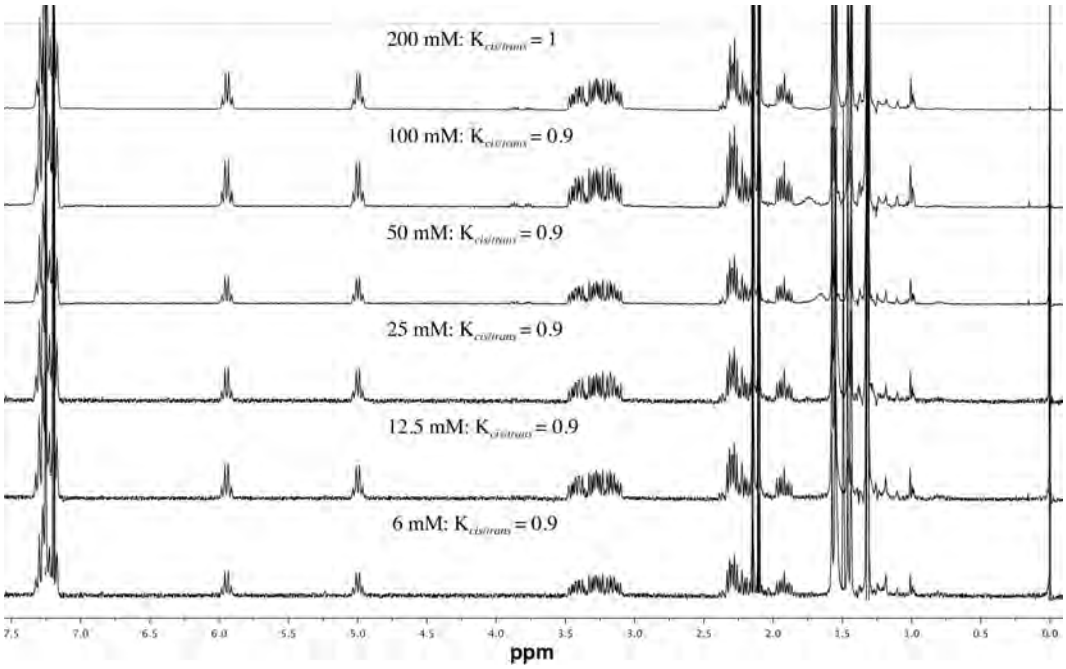

Figure 2.8. Concentration dependence on $K_{cis/trans}$ for compound **75a** in $CDCl_3$ at 298 K.

2.5 Conformational investigation of β-peptoid monomers

As mentioned, sterics play a crucial role in the formation of most secondary structures, and as we are installing an additional methylene in the backbone, we are also changing the available space for the side chains to occupy. We therefore made a series of compounds, inspired by earlier investigations of peptoid monomer behavior. For the investigation of our monomer model-systems, we first installed the spe side chain (**65a**). This side chain was chosen as it is one of the most studied side chains, with regard to peptoid folding and we thought this as an ideal reference point, as it is both α-chiral and contains an aromatic moiety. This side chain gave rise to a slight preference for the *trans*-configuration of the *N*-terminal amide bond (Table 2.1). Next we installed the (*S*)-1-cyclohexylethyl (sce) side chain (**65b**) to remove the aromatic moiety, but retaining the steric bulk. This substitution resulted in a drop in $K_{cis/trans}$, as also seen for the peptoid analogues. As the cyclohexyl ring contains five additional hydrogen atoms and deviates from planarity, it is thought to be more sterically demanding than a phenyl ring. Following the investigations of peptoids, this should give rise to an increase in the *cis–trans* ratio. We interpret the drop as our system having enough room to accommodate the additional bulk, and that an interaction involving a carbonyl oxygen and the aromatic moiety are present. We next sought to decrease the steric congestion of the side chain while retaining the aromaticity, this

was achieved by introduction of a benzyl (bz) group (**65c**). This gave comparable *cis*–*trans* ratios to compound **65a.**

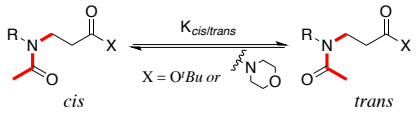

		D_2O		DMSO-D_6		CD_3OD		CD_3CN		$CDCl_3$		C_6D_6	
Comp.	Side chain	$K_{cis/trans}$ [a]	ΔG [b]	$K_{cis/trans}$ [a]	ΔG [b]	$K_{cis/trans}$ [a]	ΔG [b]	$K_{cis/trans}$ [a]	ΔG [b]	$K_{cis/trans}$ [a]	ΔG [b]	$K_{cis/trans}$ [a]	ΔG [b]
						C-terminal esters							
65a	spe	0.8	0.5	0.8	0.5	0.7	0.9	0.8	0.5	0.9	0.3	0.8	0.5
65b	sce	0.5	1.7	0.6	1.2	0.4	2.2	0.5	1.7	0.4	2.2	0.5	1.7
65c	bn	1	0	0.9	0.3	0.9	0.3	0.9	0.3	0.7	0.9	0.7	0.9
65d	sbu	0.5	1.7	0.5	1.7	0.4	2.2	0.4	2.2	0.5	1.7	0.4	2.2
65e	s1npe	n.s.[c]	-	3.6	–3.1	5.6	-4.2	3.6	–3.1	5.3	–4.1	6.3	–4.5
65f	npm	n.s.[c]	-	0.7	0.9	0.9	0.3	0.7	0.9	0.9	0.3	0.9	0.3
65g	bnz	n.s.[c]	-	0.9	0.3	0.6	1.2	0.9	0.3	0.7	0.9	0.5	1.7
65h	ph	0.2	3.9	All *trans*	-	All *trans*	-	All *trans*	-	All *trans*	-	All *trans*	-
						C-terminal amides							
66a	spe	0.7	0.9	0.8	0.5	0.5	1.7	0.8	0.5	0.4	2.2	0.4	2.2
66b	sce	0.3	2.9	0.5	1.7	0.3	2.9	0.4	2.2	0.4	2.2	0.3	2.9
66c	bn	1	0	0.5	0.3	0.7	0.9	0.9	0.3	0.3	2.9	0.3	2.9
66d	sbu	0.2	3.9	0.7	1.7	0.2	3.9	0.4	2.2	0.1	5.6	0.1	5.6
66e	s1npe	2.9	–2.6	3	–2.7	3	–2.7	3.1	–2.8	2.9	–2.6	3.5	–3.1
66f	npm	0.9	0.3	0.6	1.2	0.9	0.3	0.8	0.5	0.4	2.2	0.5	1.7
66g	bnz	0.8	0.5	0.9	0.3	0.5	1.7	0.9	0.3	0.4	2.2	0.5	1.7
66h	ph	n.s.[c]	-	All *trans*	-	All *trans*	-	All *trans*	-	All *trans*	-	All *trans*	-

Table 2.1. Rotamer equilibrium constants ($K_{cis/trans}$) for acetylated β-peptoid monomers in various solvents and their corresponding differences in free energy (ΔG, given in kJ/mol). [a] Determined by integration of ^1H NMR spectra of 12 mM solutions at ambient temperature.
[b] $\Delta G = -RT \times \ln (K_{cis/trans})$. [c] Not soluble.

This indicates that the α-branching of the side chains is less important than seen for peptoids, where the introduction of α-branching gives rise to an approximately 2-fold increase in $K_{cis/trans}$. Both the aromaticity and the majority of the bulk were removed by installation of a *sec*-butyl side chain (**65d**). This gave $K_{cis/trans}$ values comparable to **65b**, which is consistent with peptoid findings. When the bulk of the aromatic moiety was increased, by introduction of the (*S*)-1-(1-naphthyl)ethyl (S1npe) side chain (**65e**), the $K_{cis/trans}$ showed a preference for the *cis*-conformation. To assess if the increased bulk alone was responsible for the shift in preference, we removed the α-branching using 1-naphthylmethyl (npm) as side chain (**65f**). Unlike for the two less bulky spe and bn side chains, the removal of the methyl group highly influences $K_{cis/trans}$. The npm side chain gives comparable values to **65a** and **75c**, meaning that a more bulky aromatic group and additional α-branching is required to induce preference for the *cis*-conformation. In an attempt to determine whether some of the bulk can be moved, we installed a benzhydryl (bnz) side chain (**65g**). Surprisingly, the introduction of additional bulk in this position has no effect as compared to the spe side chain, which will be elaborated upon in section 2.6. Finally we attached the phenyl (ph) moiety directly to the amide nitrogen (**65h**), which gave rise to a single set of NMR signals corresponding to the *trans*-conformation. This observation is consistent with peptoid investigations of a variety of substituted aromatic moieties.

We also evaluated the same series carrying a *C*-terminal amide rather than the *tert*-butyl ester. The results are shown in the lower panel of table 2.1, and upon inspection these compounds show the same trends as the esters. This is interpreted as an indication that this terminus does not engage in $n \rightarrow \pi^*$ interactions.
Although our reference system (**65a**) has a slightly different *cis–trans* ratio than observed for the peptoid analogue, the alterations of side chains exhibit the same trends as observed for peptoids.

2.5.1 Trifluoroacetylated analogues

As we found the *β*-peptoids to display the same behavior as peptoids upon side chain substitution, we turned our attention to backbone modifications. We first sought to investigate if $n \rightarrow \pi^*_{\text{amide}}$ interactions were a determining factor for the observed conformational preferences. Although interactions of this kind would not be expected to have a pronounced effect on *β*-peptoid structure due to unfavorable geometry.[218] First, we reasoned that upon changing the *C*-terminal capping group from the *tert*-butyl ester to the morpholine amide, we also changed the acceptor capabilities of the carbonyl carbon. As the oxygen of the ester is electron withdrawing and the amide nitrogen is electron-donating, the carbonyl of the ester will be most electrophilic, and hence be most prone to engage in an $n \rightarrow \pi^*$ interaction. We interpreted the lack of change in the observed *cis–trans* ratios upon this change as an absence of an $n \rightarrow \pi^*$ interaction in the $N \rightarrow C$-terminal direction. To determine if an interaction in the opposite direction was present we installed a trifluoroacetyl group in the *N*-terminal of a selection of compounds. We reasoned that this substitution would significantly alter the electronic properties of the carbonyl group due to the inductive electron-withdrawing effect of the fluorines. This should decrease the electronegativity of the *N*-terminal carbonyl, rendering this position a weaker donor of a lone pair from oxygen, while the carbonyl carbon atom would become a stronger acceptor. Upon inspection of the $K_{cis/trans}$ values, we were surprised to find opposing effects in **67a** vs. **65a** and **67e** vs. **65e** which decreased and increased, respectively, while the last compound **67f** behaved like **65f** (Table 2.2).

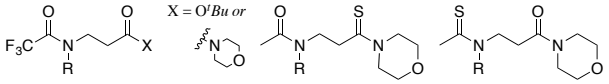

		D_2O		DMSO-D_6		CD_3OD		CD_3CN		$CDCl_3$		C_6D_6	
Comp.	Side chain	$K_{cis/trans}$[a]	ΔG[b]	$K_{cis/trans}$[a]	ΔG[b]	$K_{cis/trans}$[a]	ΔG[b]	$K_{cis/trans}$[a]	ΔG[b]	$K_{cis/trans}$[a]	ΔG[b]	$K_{cis/trans}$[a]	ΔG[b]
Trifluoroacetylated C-terminal esters													
67a	spe	n.s.[c]	-	0.4	2.2	0.3	2.9	0.4	2.2	0.3	2.9	0.3	2.9
67e	s1npe	n.s.[c]	-	6.8	–4.2	6.3	–4.3	6.6	–4.6	6.3	–4.3	6.3	–4.3
67f	npm	n.s.[c]	-	0.8	0.5	0.8	0.5	0.8	0.5	0.9	0.3	1.0	0.0
Trifluoroacetylated C-terminal amides													
68a	spe	0.4	2.2	0.4	2.2	0.3	2.9	0.4	2.2	0.2	3.9	0.2	3.9
68e	s1npe	n.s.[c]	-	5.6	–4.2	5.0	–3.9	5.5	–4.1	4.8	–3.8	4.5	–3.7
68f	npm	n.s.[c]	-	0.8	0.5	1.0	0.0	0.8	0.5	0.7	0.9	0.6	1.2
C-terminal thioamides													
74a	spe	0.9	2.2	0.5	1.7	0.5	1.7	0.5	1.7	0.2	3.9	0.2	3.9
74e	s1npe	n.s.[c]	-	2.0	–1.7	3.4	–3.0	2.8	–2.5	2.2	–1.9	2.6	–2.3
74f	npm	n.s.[c]	-	0.9	0.3	0.8	0.5	0.9	0.3	0.3	2.9	0.3	2.9
N-terminal thioamides													
76a	spe	0.4	0.9	0.9	0.3	0.4	2.2	0.7	0.9	0.5	1.7	0.5	1.7
76e	s1npe	n.s.[c]	-	5.4	–4.1	4.7	–3.8	4.5	–3.7	3.3	–2.9	5.2	–4.0
76f	npm	n.s.[c]	-	1.0	0.0	0.6	1.2	0.9	0.3	0.3	0.3	0.3	2.9

Table 2.2. Rotamer equilibrium constants ($K_{cis/trans}$) for trifluoro-acetylated and thioamide containing β-peptoid monomers in various solvents and their corresponding differences in free energy (ΔG, given in kJ/mol). [a] Determined by integration of ^1H NMR spectra of 12 mM solutionsat ambient temperature. [b] $\Delta G = -RT \times \ln(K_{cis/trans})$. [c] Not soluble.

As the effects are opposite or non-existing, another explanation than $n \rightarrow \pi^*$ interactions is most likely causing the changes. The most obvious of the effects is seen in **67e**, where we have a congested amide to which we add a further bulk. By being in the *cis*-conformation the two sterically demanding groups, the side chain and the trifluoroacetyl group, are placed to avoid clashing. On the other hand, in the case of **65e**, the decrease may be explained by a weakened $n \rightarrow \pi^*_{aryl}$ interaction. In support of this hypothesis, it has been shown that the rotamer equilibrium of a trifluoroacetylated proline derivative was governed by sterics, while the mono- and difluoroacetylated analogues were affected by the electron-withdrawing inductive effect of fluorine.[219] Further, it was suggested that fluorine could act as a doner of a lone pair to a π^* orbital of the adjacent carbonyl carbon, this would give rise to stabilization of the opposite of the anticipated conformation. Indeed, this kind of interaction is precedented in literature, for example by using molecular torsion balances. We also tested the morpholine anlogues, which showed the same $K_{cis/trans}$ values as the *tert*-butyl esters. This renders it very unlikely that an interaction of the *C*-terminal carbonyl group is involved in conformational stabilization.

2.5.2 Thioamide analogues

We next investigated the carbonyl donor capabilities by evaluating the thioamide analogues. This substitution has been shown to enhance the $n \rightarrow \pi^*$ interaction in proline systems.[187] If any carbonyl–carbonyl interactions were to be playing a role in the conformational preference of β-peptoids, the enhanced "nucleophilicity" of sulfur should give rise to differences in the $K_{cis/trans}$ as compared to the oxygen-analogues. In

substituting both *C*- and *N*-terminal carbonyl oxygens, it is possible to probe if the $n \rightarrow \pi^*$ interaction is in the $C \rightarrow N$ or $N \rightarrow C$ direction. We first installed the thioamide in the *C*-terminal of the compounds **74a**, **74e** and **74f.** We discovered that these compounds have the same selectivity as observed in the amide analogues. However, it is noticeable that the $K_{cis/trans}$ for compound **74a** is somewhat lower than for the parent oxoamide. If an $n \rightarrow \pi^*$ interaction between the two carbonyl groups in the $C \rightarrow N$ direction were present, it would stabilize the *cis*-conformation. Therefore the interaction might involve the aromatic ring. An interaction from this carbonyl oxygen to a side chain moiety has not been described in the peptoid-literature. As the oxygen is placed further away in our *β*-peptoid system, it might be likely that a conformation allowing an $n \rightarrow \pi^*_{aryl}$ interaction is possible. We next synthesized the *N*-terminal thioamides **76a**, **76e** and **76f,** which again followed the same trend as the parent oxoamides. In this series the compound containing s1npe (**76e**) displayed an increased $K_{cis/trans}$, which is the opposite of the expected if an $n \rightarrow \pi^*$ interaction is present in the $N \rightarrow C$ direction. This change in the $K_{cis/trans}$ value would indicate an interaction with the aromatic ring rather than the *C*-terminal carbonyl carbon, as it has been described in conventional peptoids and thiopeptoids.[176,177,188]

2.5.3 Peptoid monomer model systems

We prepared compounds **77–79** to address if the effects of trifluoroacetylation and thioamideintroduction were also present in peptoids. Compound **77** has previously been investigated,[176] and exhibited the same $K_{cis/trans}$ values as reported in CD_3CN and $CDCl_3$ and an intermediate value in DMSO-d_6, suggesting the presence of a solvent effect. For compound **78**, an even higher $K_{cis/trans}$ was observed, which was much less affected by the solvent polarity. Like for the *β*-peptoid (**68e**) this equilibrium is most likely primarily dictated by sterics. Finally, we saw higher $K_{cis/trans}$ values for the thiopeptoid (**79**), than for the oxoamide analogue in polar solvents. This again suggest the presence of an $n \rightarrow \pi^*_{aryl}$ interaction between the sulfur and the aromatic side chain.

2.6 X-ray crystallography of monomeric model systems[b]

Diffraction quality crystals of **65g** and **68e** were obtained by slow evaporation from chloroform solutions, as well as the peptoid **79** by slow evaporation from ethyl acetate. Thus, the solid state crystal structures were solved by X-ray structure determination. The structure of **65g** revealed a fully extended backbone conformation, with *trans*-amide configuration (Figure 2.9), which is consistent with the observed $K_{cis/trans}$ of 0.7 in $CDCl_3$.

[b] X-ray crystal structures were solved by Associate Professor Pernille Harris

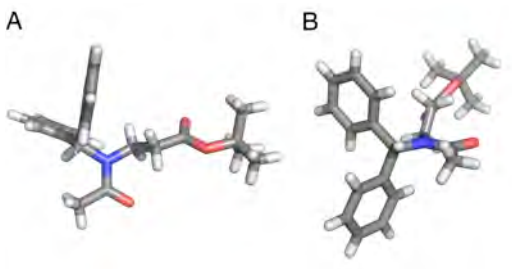

Figure 2.9. X-ray crystal structure of compound **65g**.

It is worth noting the periplanar relationship of the two phenyl groups, which are also pointed away from the acetyl CH_3 group (Figure 2.9B). This relationship may help explain the high *trans*-amide ratio observed in solution despite a significant steric bulk.

Compound **68e** crystallized in the *cis*-conformation, as would be expected from the observed $K_{cis/trans}$ values (Figure 2.10A). Although we suspected that the electron lone pair donating capabilities of the *N*-terminal carbonyl in the trifluoroacetylated compounds would be diminished, it appears to engage in an interaction like those described for peptoids by Gorske and co-workers.[188] It is also noteworthy that one of the naphthyl hydrogens is in close proximity to the carbonyl oxygen, which could also be interacting. The X-ray crystal structure revealed a rather dense packing, with two monomer molecules aligned with the backbones in an antiparallel manner. As this arrangement gives rise to an edge to face aromatic π–π interaction, the presence of other interactions in solution involving the aromatic moiety cannot be definitively excluded.

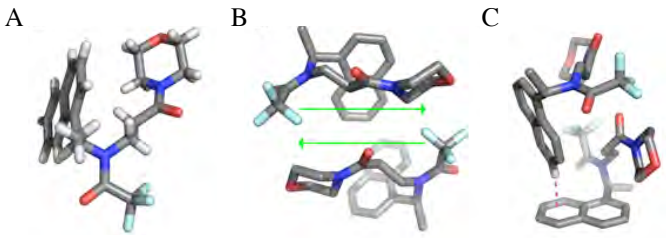

Figure 2.10. X-ray crystal structure of compound **68e**.

The X-ray crystal structure of thiopeptoid **79** also revealed the presence of a *cis*-amide configuration. The distances from the *C*-terminal carbonyl oxygen to the *N*-terminal carbonyl carbon is fully consistent with the presence of an $n \rightarrow \pi^*_{amide}$ interaction.[184,220] As was also the case for compound **68e**, the distance to the side chain methine-hydrogen is indicative of an indirect interaction.[188]

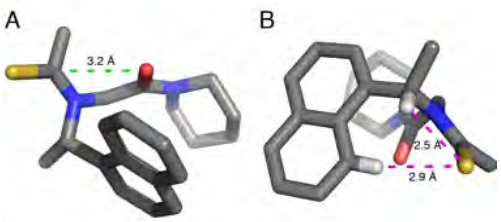

Figure 2.11. X-ray crystal structure of compound **79**.

Interestingly, the distance between the sulfur and the same naphthyl hydrogen as described for **68e** is in close proximity, consistent with an overlap of their orbitals, which would give rise to a *C–H*···S_{amide}. This could offer an alternative explanation to the stabilization of the *cis*-conformation upon introduction of a thioamide functionality.

2.7 Evidence for aromatic *C–H*···S_{amide} interactions[c]

In order to explore the identity of the putative non-covalent carbonyl–aryl interaction in this system, density functional theory (DFT) calculations were performed. The computational study was carried out in order to gain further insight to the molecular features responsible for the *CH*···S_{amide} interaction, and its effect on the observed preference for the *cis*-amide configuration in the presence of the s1npe side chain. Initially the molecules **66e** and **76e** was built in both *cis*- and *trans*-conformation, and a conformational search was performed. This search showed the *cis*-amide configuration to have the lowest energy for both systems, which is in agreement with the experimentally determined $K_{cis/trans}$ ratios. When visualizing the ensemble of conformations within 21 kJ/mol (Figure 2.12), a more homogeneous distribution is observed for the thioamide containing system. This difference in distribution indicates that there might be a stabilizing interaction between sulfur and the naphthyl group. This geometry is also consistent with the X-ray crystal structure for **79**, revealing close proximity of the naphthyl *H*-8 and the sulfur.

[c] The computational investigation of the monomer model systems were preformed by Associate Professor Peter Fristrup.

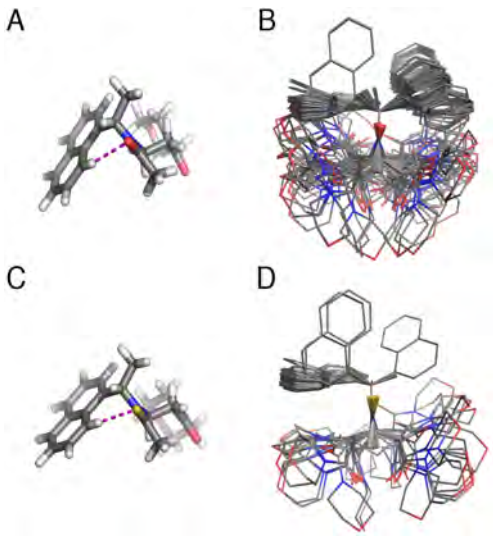

Figure 2.12. Calculated structures of **66e** (A and B) and **76e** (C and D). B and D shows all structures within 21 kJ/mol of the global minimum super imposed.

To further investigate the electronic properties responsible for the observed *cis*-amide preference in the *N*-terminal thioamide analogues, a natural bond order (NBO) analysis was carried out. By including the trifluoroacetylated compounds **68e** and **78** we were able to pinpoint the effect of this substitution in both peptoid and *β*-peptoid backbones. First we compared the *cis*-conformations of **66e** and **76e** it is notable that although the longer *C*=*S* bond compared to the *C*=*O* bond (1.7 Å vs. 1.2 Å) caused the distance to the hydrogen of the naphthyl to increase from 2.9 Å to 3.2 Å, the NBO analysis clearly showed that the interaction was strongest in the thioamide case. We found that the natural charge of the naphthyl hydrogen in the thioamide was lower than in the oxoamide analogue (0.2436 au or **76e** vs. 0.2455 au for **66e**), although both hydrogens are more electron-deficient than their neighboring hydrogens which does not have such intramolecular interactions (0.2503 au for **76e** and 0.2487 au for **66e**). In addition, second order perturbation analysis of **76e** and **66e** revealed a calculated stabilizing energy of 0.84 kcal/mol for this interaction in the thioamide, while the interaction in the oxoamide gives a stabilization of less than the 0.5 kcal/mol threshold.

In the trifluoroacetylated compound **68e,** the amide oxygen is less negatively charged than its acetylated parent compound **66e** (–0.657 au in **68e** and –0.716 au in **66e**). As a consequence, the electrostatic interaction with the naphthyl hydrogen is expected to be much smaller than for **66e**, and is indeed found to be below the 0.5 kcal/mol threshold. This suggest that the increased *cis–trans* ratio is most likely caused by the increased steric congestion upon introduction of a trifluoroacetyl group rather than an increase in the electrophilicity of the carbonyl carbon. Finally it should be noted that the investigated *trans*-configured molecules showed a fully extended backbone, with neither $n \rightarrow \pi^*_{\text{aryl}}$ nor $n \rightarrow \pi^*_{\text{amide}}$ interactions.

We next investigated the peptoid series, where the closer proximity of the *C*-terminal carbonyl group may allow for the possibility of $n \rightarrow \pi^*$ interactions in addition to the

$CH^{\cdots}S_{amide}$ interaction. For all the peptoid compounds an interaction of the carbonyl group and the naphthyl hydrogen was present in the second order perturbation of the NBO analysis. In the peptoid system the interaction is only slightly stronger for the thioamide containing analogue **79** (0.63 kcal/mol) as compared to the oxoamide **77** (0.58 kcal/mol). Surprisingly the value for the trifluoroacetylated analogue **78** is even higher at 0.65 kcal/mol, it should be noted that with the small energies involved, these differences are within the accuracy of this method.

To experimentally probe the existence of an interaction between the sulfur and the hydrogen in the eight position of the naphthyl group, we turned our attention back to the NMR-spectra. Indeed, a comparison of the chemical shifts assigned to the naphthyl hydrogen in the *cis*-amide conformation of compounds with altered electronic properties of the carbonyl support the existence of the proposed interaction in solution as well. The decrease in electron density of the carbonyl oxygen by introduction of fluorine should render the hydrogen less shielded which should be causing an upfield shift of the ^{1}H NMR signal, which was indeed observed (Figure 2.13, **66e** vs. **68e**).

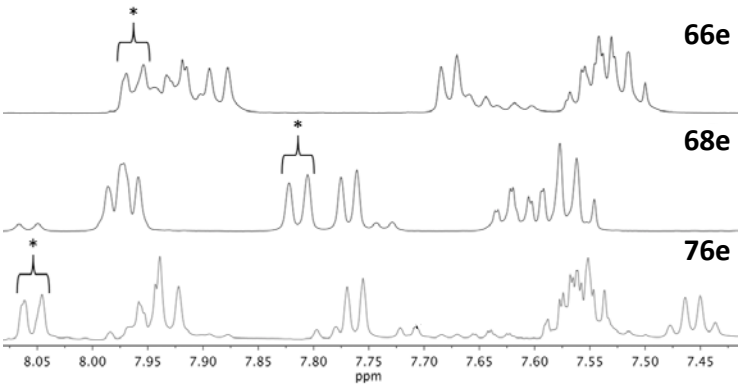

Figure 2.13. Aromatic region of the ^{1}H-NMR spectra of **66e**, **68e** and **76e** recorded in CD_3CN. The asterisk denotes the signal assigned to the proton in the eight position in the naphthyl group.

Substitution of oxygen with sulfur (**66e** vs. **76e**) should in principle affect this interaction in the same manner. However, the opposite was observed, with a downfield shift of the signal, which is consistent with the calculated ensembles and the observed $K_{cis/trans}$ values that indicate a stronger interaction for sulfur. Although hydrogen bonds to oxoamides should be stronger than those to thioamides, we speculate that the geometric restraint required for formation of the eight membered ring in our system does not allow for optimal hydrogen bonding distance, and therefore the larger radius of sulfur enables a higher degree of orbital overlap than the oxygen. This is also supported by the NBO analysis as mentioned.

2.8 Concluding remarks

To obtain fundamental knowledge of the amide bond isomerization in β-peptoids, several series of monomer model systems including varying steric demand and stereoelectronic properties were synthesized. As our results were compared to

previous studies of α-peptoids we also synthesized two new α-peptoid models containing a trifluoroacetyl group and an *N*-terminal thioamide, respectively. The investigation of these model systems show that some of the trends seen in α-peptoids translate directly to the β-peptoids. As such, it was shown that a preference for the *cis*-conformation could be induced upon introduction of an s1npe side chain, whereas the *trans*-conformation was exclusively populated when *N*-aryl type side chains are installed. We found that both a bulky substituent and α-branching is required to induce a preference for the *cis*-conformation, as a diphenyl substituted bnz side chain did not present a sufficient bulk. To probe if the backbone amides were participating in any electronic interactions we altered the stereoelectronic properties. Through an NMR investigation of these models evidence of an interaction between an amide/thioamide lone pair and an aromatic side chain moiety was found. However, we found no evidence of interactions between the carbonyl groups in our monomer model systems. Further, we were able to solve the X-ray crystal structure for two compounds, both having fully extended backbones, not allowing interactions between the termini in either *cis*- nor *trans*-conformation.

We also solved the X-ray crystal structure of a thioamide containing α-peptoid, and supported by DFT calculations and chemical shifts from NMR analysis, this structure indicated the presence of a stabilizing effect through a thioamide–aromatic interaction by a C_{sp^2}–$H\cdots S_{amide}$ "hydrogen bond".

These observations show that these stereoelectronic alterations of the backbone are valuable tools in the investigation and design of peptoid and β-peptoid structure.

3 β-Peptoid oligomers

3.1 Design of Oligomers

Since high-resolution structures of peptoids have been successfully obtained for oligomers of 4–5 residues in length, we envisioned that a hexamer might be sufficient to acquire stabilized folding. We chose two different side chains for our investigation, first the *N*spe, which has been studied for both α- and β-peptoids, and second the *N*s1npe. The latter was chosen as it has been shown to induce helicity in the crystal structure of a peptoid tetramer, and because we have shown that this side chain stabilizes the *cis*-configuration in the monomer (see chapter 2). The last point is important as a computational study of the β-peptoid backbone showed a helical structure with all amides in a *cis*-configuration to be the lowest energy conformation.[218] We reasoned, that the chances of achieving folding of this kind would be greater using residues with a predisposition for the desired local conformation.

The *N*s1npe side chain has been shown to induce helical conformations in peptoids, however, it does not induce significant control of the amide bond rotamer equilibrium of β-peptoids. Attempts to determine if this side chain induces any robust secondary structures are somewhat ambiguous.[206,207] As shown in chapter 2, introduction of a trifluoroacetyl group enhanced the preference for the *trans*-amide in the spe containing monomers, we therefore chose to include this substitution in our oligomer investigation along with the acetyl control compound. This substitution was also included for the second series of *N*s1npe oligomers, as it was shown to increase the fraction of the *cis*-amide in the monomer models (Chapter 2).

3.2 Synthesis of β-peptoid oligomers

When Hamper *et al*. first presented the β-peptoids, they described the syntheses of libraries of di- and trimers.[205] These libraries were created by SPS using a submonomer strategy, as described for the monomers in chapter 2.[205,221] The strategy involved acylation of resin-bound amines with acrylic acids followed by conjugate aza-Michael addition of the next amine. This strategy was later shown to give rise to mixtures and impure products, when extending the oligomer beyond tetramers.[207] It was further shown that this reaction was highly sensitive to the changes in solvent, as it was reported that a THF/H_2O (8:2) mixture gave better yields than the originally proposed neat dimethylsulfoxid (DMSO).[206] A solid-phase strategy using Fmoc protected building blocks, was shown to give modest yields of penta- and hexameric homo-oligomers of β-peptoids with α-chiral side chains.[207] Employing non-chiral side chains, Franzyk and co-workers later improved this strategy furnishing a 22'mer in good yield.[222]

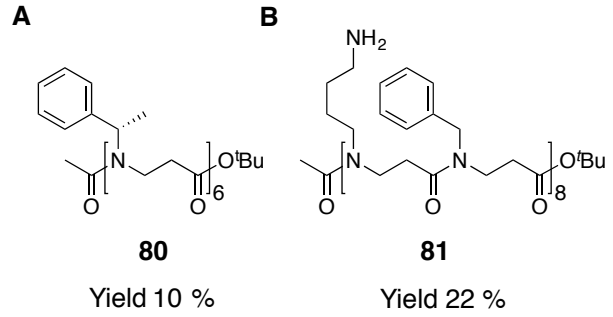

Figure 3.1. (A) Homooligomer reported by Jaroszewski and co-workers.[207] (B) Oligomer reported by Franzyk and co-workers.[222]

We experienced good yields of the aza-Michael addition using MeOH as solvent, as described by Taillefumier and co-workers.[208] However, this solvent is not optimal for SPSs, as it causes most solid-supports to contract leaving the active species inaccessible to the reactants. We chose to use a solution-phase strategy used for the synthesis of α/β-hybrid peptoids.[209] The method of choice resembled that of the monomers, starting with an aza-Michael addition of the primary amine to an acrylic compound in MeOH (Scheme 3.1). The formed secondary amine could next be acylated using acryloyl chloride in the presence of triethyl amine. By performing the acylation step in THF, the formed ammonium salts precipitated and could be removed by filtration, and the crude product undergo another Michael addition. When the desired length of the oligomer was reached it was capped with the desired capping group. This strategy calls for only one purification for each residue attached, which greatly reduces the time and effort needed to prepare β-peptoid oligomers.

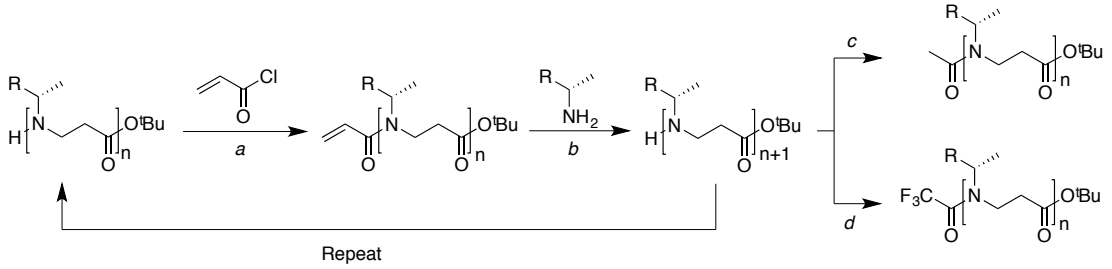

Scheme 3.1. Oligomerization and *N*-terminal functionalization of β-peptoids. a) NEt_3, THF, 0 °C. *b*) MeOH, 50. *c*) AcCl, NEt_3, 0 °C. *d*) $(CF_3CO)_2O$, NEt_3, CH_2Cl_2, 0 °C→20 °C .

In this way we prepared oligomer series **82a–86a** and **82b–86b** containing the *N*spe side chain, and **87a–91a** and **87b–91b** containing the *N*-s1npe side chain (Figure 3.2). We also chose to evaluate a non-acylated hexamer of the latter mentioned series (**91c**).

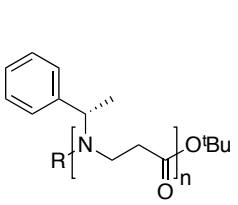

n = 2: **82a** (R = Ac), **82b** (R = COCF3)
n = 3: **83a** (R = Ac), **83b** (R = COCF3)
n = 4: **84a** (R = Ac), **84b** (R = COCF3)
n = 5: **85a** (R = Ac), **85b** (R = COCF3)
n = 6: **86a** (R = Ac), **86b** (R = COCF3)

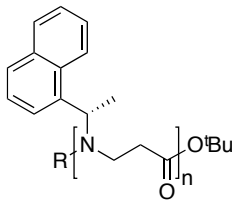

n = 2: **87a** (R = Ac), **87b** (R = COCF3)
n = 3: **88a** (R = Ac), **88b** (R = COCF3)
n = 4: **89a** (R = Ac), **89b** (R = COCF3)
n = 5: **90a** (R = Ac), **90b** (R = COCF3)
n = 6: **91a** (R = Ac), **91b** (R = COCF3)
91c (R = H)

Figure 3.2. Synthesized series of *β*-peptoid oligomers.

3.3 Structure elucidation of *β*-peptoid oligomers.

3.3.1 Preliminary NMR study of the solution structure of oligomers

First we investigated our oligomer series using NMR, to determine how elongation affects the *cis–trans* conformational preference. As expected the spectra revealed significant signal overlapping due to the identical side chains of either series. However, focusing on the shifts corresponding to the side chain methine protons the overall *cis–trans* ratios could be determined (Table 3.1).

N-(S)-1-Phenylethyl series

Compound	**82a**	**82b**	**83a**	**83b**	**84a**	**84b**	**85a**	**85b**	**86a**	**86b**
CD_3CN	0.8	0.3	0.8	0.4	0.8	0.5	0.7	0.5	0.7	0.5
C_6D_6	0.6	0.3	0.6	0.3	0.6	0.3	0.5	0.3	0.4	0.3

N-(S)-1-(1-Naphthyl)ethyl series

Compound	**87a**	**87b**	**88a**	**88b**	**89a**	**89b**	**90a**	**90b**	**91a**	**91b**
CD_3CN	5.2	5.4	5.2	6.0	5.9	7.3	–[a]	–[a]	–[a]	–[a]
C_6D_6	4.8	4.0	4.4	4.0	5.6	4.3	6.4	4.9	11.0	10.0

Table 3.1. Overall $K_{cis/trans}$ values determined by NMR. [a]A limited solubility of this compound did not allow for analysis in acetonitrile d_3.

The NMR data of the *N*spe series (**82–86**) showed no dependency on the length, with values close to those reported for their monomers. The data also suggests a rather heterogeneous mixture of configurations, consistent with the difficulties to determine if stabilized secondary structures are present, as mentioned earlier.[206,207]

The *N*-s1npe series (**87–91**) on the other hand shows increased $K_{cis/trans}$ values already at the dimer stage, as compared to the monomers. In the acetylated series, the di- and trimer (**87a–88a**) exhibits the same $K_{cis/trans}$ values, which then increases slightly as the oligomer is extended to the tetramer and pentamer. When the sixth residue is attached the $K_{cis/trans}$ value rises more steeply, giving a much more homogenous distribution of *cis*- and *trans*-conformers. It appears that this trend is not dependent on the solvent, but solely on the elongation of the oligomer.

The trifluoroacetylated series (**87b–91b**) displays the same trend, but for this series the conformational distribution appears to be solvent dependent. Going from di- to trimer the $K_{cis/trans}$ rises in acetonitrile, and remains unchanged in benzene. The same happens when going from three to four residues. Unfortunately the pentamer and hexamer were not sufficiently soluble in acetonitrile to obtain NMR-spectra. In benzene the trends continues until the hexamer, at which stage the $K_{cis/trans}$ rises steeply.
Taken together, these values may indicate a propensity of the *N*s1npe oligomers to adopt length as well as solvent dependent secondary structures.

3.3.2 Solid state structure elucidation[d]

We were able to grow crystals of all three hexamers by slow evaporation from MeOH/$CHCl_3$ or benzene solutions. Crystals of a sufficient quality were obtained for **91a** and **91c** from MeOH/$CHCl_3$ solution, and their structures were determined by X-ray crystallography at 1.05 Å and 1.00 Å resolution, respectively. The *N*-terminally non-acylated **91c** was the first structure to be solved, and revealed a helical display with exactly three residues per turn and a pitch of 9.6 Å (Figure 3.3A).

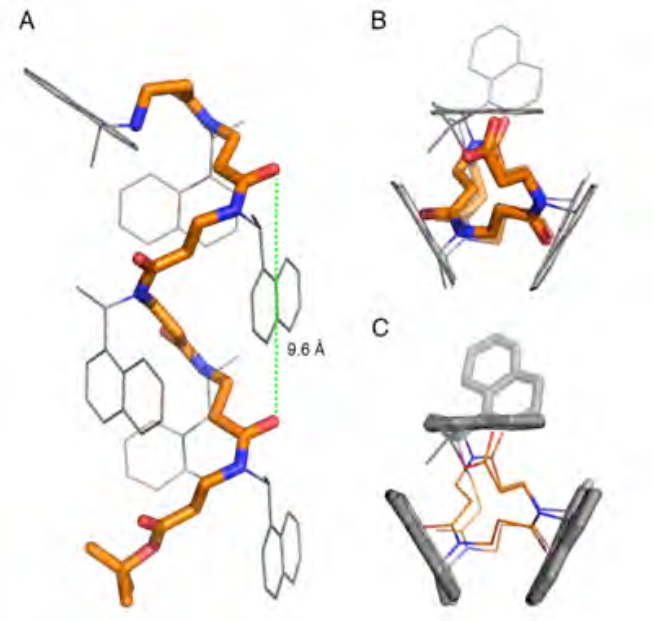

Figure 3.3. X-ray crystal structure of compound **91c**. (A) Side view. (B and C) End views from the *C*-terminal. Hydrogens are omitted for clarity.

The side chain of the *N*-terminal residue is twisted away from the core of the helix. The remaining naphthyl groups are highly organized along each of the three faces of the helix, to give an equilateral triangle when viewed down the helical axis (Figure 3.3B, C).

[d] X-ray crystal structures were solved by Associate Professor Pernille Harris

Based on our monomer study, we envisioned that acetylation of the *N*-terminal would produce another *cisoid* configuration, aligning the last naphthyl group with the rest. The X-ray crystal structure of compound **91a** confirmed this (Figure 3.4), with only one –CH_2CON(1-(1-naphthyl)-ethyl)CH– fragment in the asymmetric unit.

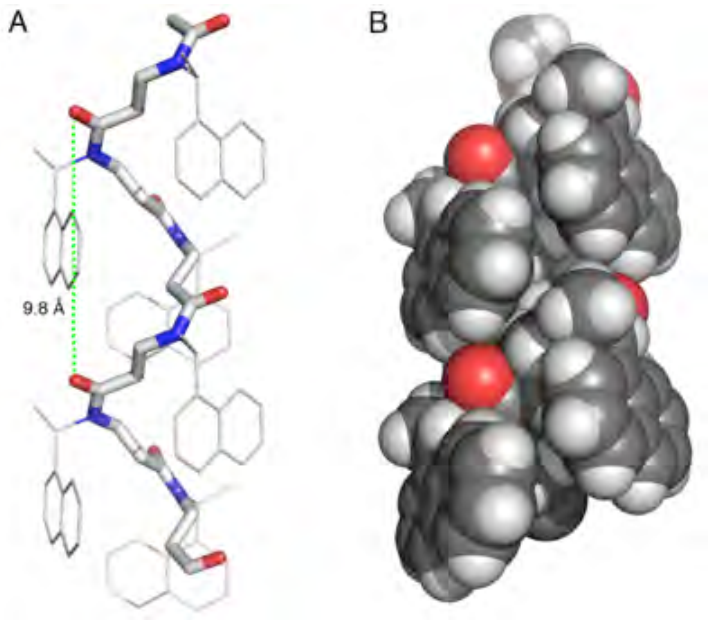

Figure 3.4. X-Ray crystal structure of compound **91a**. (A) Showing the backbone helical as sticks and side chains as lines (hydrogen atoms are omitted for clarity). (B) Space filling representation showing the packing of the naphthyl groups along the phases of the triangular prism-shaped conformation.

Thus, the crystal symmetry generates infinitely long, parallel chains, which renders the *tert*-butyl group invisible due to the 1:6 ratio of *tert*-butyl to naphthyl side chains. This results in crystal packing where the helical segments are aligned in a head to tail fashion, giving highly regular elongated triangular threads with a helical pitch of 9.8 Å (Figure 3.4A). This packing was not possible for compound **91c** due to the positioning of the *N*-terminal side chain (Figure 3.5A).

This highly ordered and tight packing of the side chains along the three phases of the helical axis (Figure 3.5B), combined with their strong *cis*-inducing properties, suggest that the *N*s1npe side chains provide a particularly strong stabilization of this novel secondary structure motif. Further, the intramolecular distances indicates interactions between the side chain naphthyl groups and backbone methylene groups. This interaction may contribute to the stabilization by protecting the helical backbone from solvation.

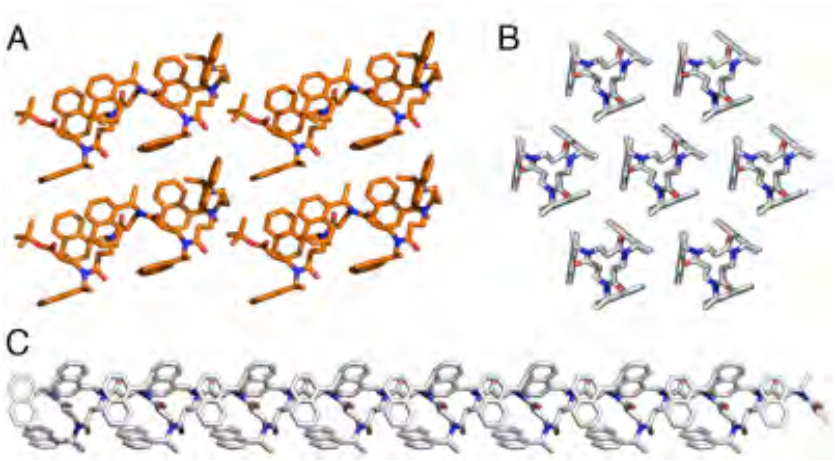

Figure 3.5. X-Ray crystal packing. A) Compound **91c**. B and C) Compound **91a**, viewed from the end and perpendicular to the helical axis, respectively. Hydrogen atoms are removed for clarity.

The torsion angles of the two helices show some similarity to one of the helical conformations suggested by Hofmann and co-workers, based on DFT-calculations.[218] These helical displays are to our knowledge the first experimental demonstration of the existence of this helical type. Most of the previously demonstrated structures of a *β*-peptidic nature have been shown to contain stabilizing hydrogen-bond networks,[63] and investigations of homologated proline-oligomers indicated *trans*-amide conformations.[112]

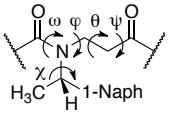

Compound **91a**[a]					
φ	θ	ψ	ω	χ_1[b]	χ_2[c]
96.3	172.5	−175.3	−13.8	53.6	−80.4
Compound **91c**[a]					
φ	θ	ψ	ω	χ_1[b]	χ_2[c]
97.4	166.0	−173.9	−13.4	56.3	−73.8
Hofmann c-1 predicted helix[d]					
φ	θ	ψ	ω	χ_1[b]	χ_2[c]
97.2	−179.2	−178.8	8.1	–	–

Table 3.2. Torsion angles of a residue within a helix. [a]Measured at residue 5 in the structures to give representative values for a residue within the helix. [b]Measured by the naphthyl substituent. [c]Measured by the methyl substituent. [d] From ref 218.

3.4 Further elucidation of solution structure

To assess if these molecules exhibited an ordered structure in solution, we evaluated the compounds by CD-spectroscopy. This method takes advantage of the fact that molecules can absorb right and left polarized light differently, to assign if they display an ordered structure. CD is a very sensitive technique, which can be used to monitor the folding and unfolding events in globular proteins. CD has also been used to elucidate the secondary structures of foldameric compounds. Based on NMR and CD

investigations of a series of β-hexa- and β-hepta-peptides, Seebach and co-workers assigned a distinct CD-pattern to the 14-helix.[103] However, further investigations showed that this pattern was not unique to the 14-helix, as it was shown that a similar sequence containing substituents in axial positions, and thereby unable to display this secondary structure, exhibited the same CD-pattern.[223] Further, CD-spectra of the cyclically constrained β-peptides, shown to fold into 14-helices, differ from the assigned pattern.[94] On this background a study combining theoretical calculations and experimental data was undertaken.[224] Since it was possible to reproduce the CD-spectra by computational methods, factors affecting the spectra could thus be evaluated *in silico*. It was concluded that the exhibited CD-pattern of these oligomeric molecules where a combination of the different conformation found in solution, why a given pattern can not be exclusively assigned to a given secondary structure. As such, no conclusions on the secondary structure of a given foldameric compound can be made on the basis of CD-spectra alone.

3.4.1 Circular dichroism of β-peptoid oligomers

As expected, the CD-spectra of the compounds containing the *N*-s1npe side chain (**84a–86a**) were similar to those previously reported with this side chain (Figure 3.6).[207] The trifluoroacetylated oligomers (**84b–86b**) showed tsimilar spectra as the acetylated, indicating that this capping group does not provide any structure stabilizing effect (Figure 3.6B).

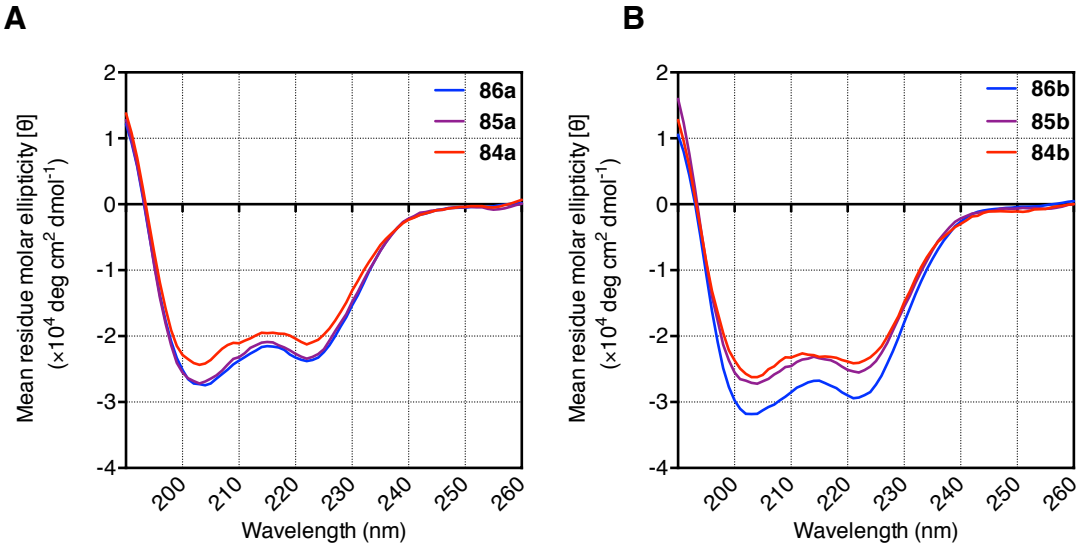

Figure 3.6. CD-spectra of oligomers **84a–86a** (**A**) and **84b–86b** (**B**). The spectra were recorded in MeCN at a concentration of 60 μM and 298 K.

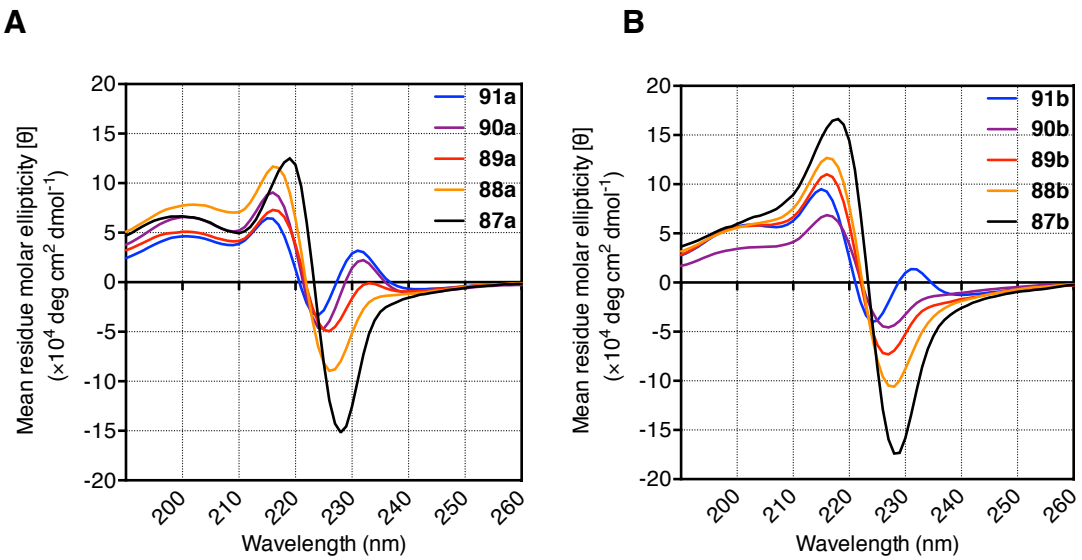

Figure 3.7. CD-spectra of oligomers **87a–91a** (**A**) and **87b–91b** (**B**). The spectra were recorded in MeCN at a concentration of 60μM and 298 K.

The oligomers carrying the *N*-s1npe side chain all revealed a minimum at 224–228 nm and a maximum at 218–220 nm (Figure 3.7A). The intensity of the signals was decreasing with the length of the oligomer, which was unexpected. However, inspection of the monomer revealed the same minimum and maximum, which disappeared upon removal of the acetyl group, which indicates that these signals are not indicative of secondary structure, but rather a signature of the a specific *cis*- or trans-amide motif. Starting at the tetramer length a positive signal appears near 232 nm, and increases in intensity as the oligomer grows. This trend is indicative of length-dependent secondary structure formation. We also obtained CD-spectra for the trifluoroacetylated oligomers (**87b–91b**), which exhibited the same overall spectral shape as the acetylated (Figure 3.7B). It is noteworthy that the signal that we assign to secondary structure formation only appears for the hexamer. In our monomer study the trifluoroacetyl group was stabilizing the *cis*-configuration, but apparently this stabilization does not translate into a stabilizing effect on the secondary structure of the oligomers. The lack of stabilization might be explained by the trifluoroacetyl group clashing with the first methylene of the backbone.

Finally we wanted to assess whether the positive signal at 232 nm was indicative of folding. Therefore we collected a series of CD-spectra at increasing temperatures in the range 20–75 °C (Figure 3.8A). We observed a gradual decrease in the signal at 232 nm upon heating, which is indicative of temperature mediated denaturation.

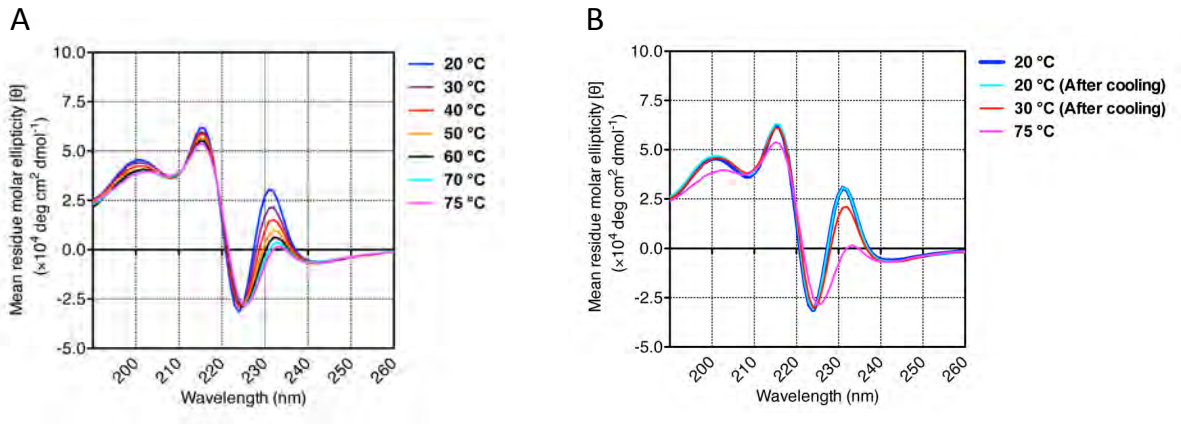

Figure 3.8. CD-spectra of **91a** at varying temperatures in acetonitrile.

At the same time the remaining spectral shape was not affected, which is in accordance with our hypothesis that it is not related to secondary structure. Further more, spectra recorded upon cooling of the sample were identical to those obtained before heating, indicating that refolding occurs (Figure 3.8B).

3.4.2 Concluding remarks

By utilizing the data obtained from our monomer study, we designed two series of oligomers, one of which should be prone to fold in a specific manner, based on a computational study[218]. In doing so we produced the first high-resolution structure for a linear *β*-peptoid oligomer, which are also the longest of any peptoid oligomer determined by X-ray crystallography to date. The novel helical display definitively validates the addition of *β*-peptoids to the ensample of accessible foldamers. The crystal structure of two hexameric compounds revealed highly regular equilateral triangular prism shaped conformations in the solid state. The hexamers were achieved by synthesis in a submonomer fashion using the highly *cis*-inducing side chain *N*s1npe. The existence of length- and temperature dependent secondary structure formation in organic solution were supported by both ^{1}H-NMR and CD-spectroscopy. For the first time control of *β*-peptoid folding has been demonstrated, enabled by backbone composition and stabilized by the tight alignment of the naphthylethyl side chains along the three phases of the helical axis. These results open the possibility of taking advantage of *β*-peptoids in designing new well-defined biomimetic materials.

4 Membrane active α-peptide/β-peptoid-hybrids

4.1 Introduction

Since its introduction of penicillin, antibiotics have been a standard part of the therapeutic arsenal for treating infectious diseases, and a number of different antibiotics are being marketed. However, resistance to conventional antibiotics is an increasing concern, which has been increasing over the last decades. This has left the selection of antibiotics for treating complicated infections limited.[225] It has also been noted that the increased amount of multi-resistant bacteria seems to correlate with an increase in the consumption of broad spectrum antibiotics.[225] To be able to continue antibiotic treatment novel antibiotic compounds are needed, which has led to a series of modifications to already existing drugs.[226] Unfortunately this strategy may accelerate the development of resistance, as the mechanism of action is highly similar to that of the parent compound.[227] The development of resistance to known classes of antibiotics has given rise to an intensified search for alternative classes of antibacterial compounds. Amongst these the antimicrobial peptides (AMP's) are a promising candidate, being naturally found as part of the antimicrobial defense of many forms of life including human.[228,229] The AMP's are especially attractive as they target the distinct structure of the bacterial membrane.[230] Unfortunately the naturally occurring AMP's suffer from a number of inherent drawbacks in regard to being distributed as an antimicrobial drug. Given their natural origin, they are recognized by the proteases limiting their bioavailability, which is accompanied by high production cost.[4] To overcome these issues synthetic modifications and mimics of the natural AMP's have shown great promise in development of effective antimicrobials with limited toxicity.

4.2 Natural antimicrobial peptides

AMP's are a group of compounds which are ubiquitous in all species of life.[231,232] Such peptides are components of the innate immune response with broad antimicrobial activities.[231] As the AMP's are naturally produced in the body and have been an effective part of the primary immune defense for millions of years,[233] they have attracted great interest for their ability to overcome antibiotic resistance.[234,235] This research has led to the discovery of a wide range of AMP's, of which some have proven to be valuable drug candidates.[4,236]

4.2.1 Structure of antimicrobial peptides

Within the class of AMP's more than 2000 compounds have been identified, all sharing the common feature of an overall charge.[237] Though anionic AMP's have shown to be part of the innate immune defenses,[238] the vast majority of AMP's have an overall cationic nature.[239]

The cationic AMP's are defined as peptides of less than 50 residues, a net charge of +2 to +9, facilitated by basic residues as lysine and arginine, and a substantial portion

(above 30%) of hydrophobic residues.[4] Though this may seem that these criteria might limit diversity of AMP's, However, the same peptide is rarely found in two different species.[230] This diversification enables the host to better cope with the microbial challenges of its ecological niche.[240] Due to the large sequence diversity amongst the AMP's they are classified based on their secondary structures.[241] α-helical and β-sheet structures are the most frequently encountered, though loops and extended structures are known.[242] Typically, however, these peptides display unordered structures in aqueous solution,[243] and frequently fold into an ordered arrangement upon contact with model membranes or membrane mimetics.[244,245]

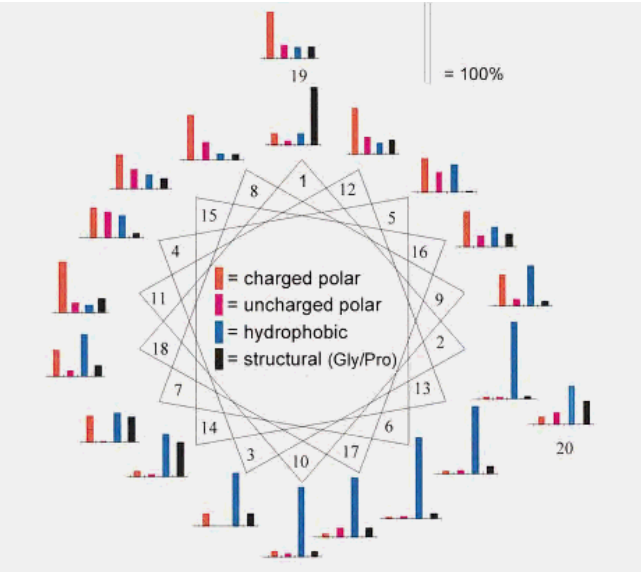

Figure 4.1. Helical wheel projection of the residue distribution in the 20 *N*-terminal residues of 150 α-helical natural AMP's.[147]

The α-helical AMP's are the most abundant class, which will fold into an amphipathic helix upon contact with membranes, displaying the hydrophobic side chains predominantly on the one phase of the helix, and the polar on the other.[245] Though these peptides show little conservatism of the amino acid sequence, there is a pronounced trend in the distribution of the type of residue (Figure 4.1).[147]

β-sheet peptides are often present as antiparallel β-sheets stabilized by two or more disulfide bonds.[242]

4.3 Cell membranes, the target of antimicrobial peptides

Despite the discovery of many novel AMP's during the past few decades, and the extensive work in the field, the mechanism of action is still under some debate.[246,247] A number of studies have pointed to mebrane activity as the reason for AMP-mediated cell-death, while others have indicated intracellular activity.[248] However, it is generally agreed that the cytoplasmic membrane is a target for most cationic AMP's, [249,250] and many studies have shown membrane permeabilization as a strong factor in the killing of cells.[251] In this regard, the cationic nature of AMP's have proved to be of

particular importance for the antimicrobial activity.[252] Also the ability to form amphipathic structures, providing a structure with separated hydrophobic- and hydrophilic regions, has been identified as an important characteristic of the AMP's.[253] These characteristics are important for the activity and in some cases also the selectivity of the AMP's due to the structure and lipid composition of the membranes on which they act.

Whether the mechanism of action is membrane activity or intracelular activity, interactions with the membrane of the cell is inevitable. The cells of bacteria, fungi and mammals are composed of different lipids. This composition gives rise to the interaction of AMP's, and their selectivity towards specific cell types. In most bacterial membranes the zwitterionic phospholipid phosphatidylethanolamine (PE) is the most abundant component.[254] In addition to PE, the bacterial membranes contain a significant portion of negatively charged phosphatidylglycerol (PG), cardiolipin (CL) and phosphatidylserine (PS), which gives the membrane an overall negative charge, at physiological pH (Figure 4.2).[250] The anionic phospholipids are stabilized by divalent cations such as Ca^{2+} or Mg^{2+}.[247] It is this charge that is responsible for the attraction and membrane activity of AMP's.[250] In contrast to bacterial cell membranes, mammalian cell membranes are composed mainly of zwitterionic phospholipids. The outer monolayer of mammalian cells primarily consist of phosphatidylcholine (PC) and sphingomyelin (SM), while the inner layer mainly consist of PE.[255] Furthemore the presence of cholesterole affects the membrane fluidity which stabilizes the lipid bilayers, reducing the affinity of AMP's to these cells.[247]

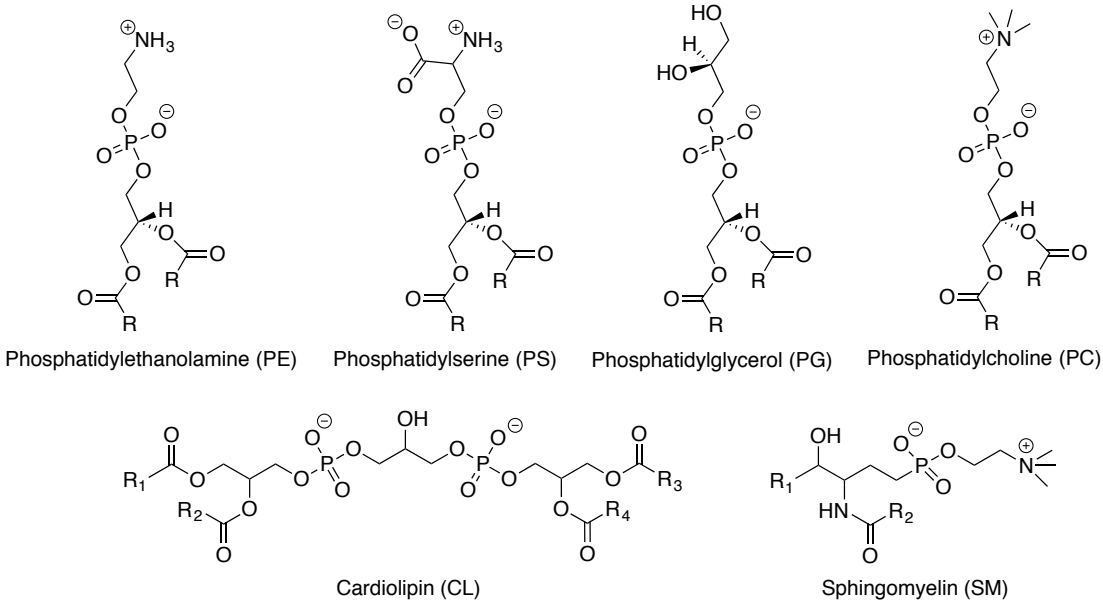

Figure 4.2. Structures of the most components in bacterial- and mammalian cell membranes.

Bacterial cells are divided into two classes, the Gram-positive and the Gram-negative, depending on the cell membrane. The lipid composition of Gram-positive cell membranes is not significantly different from that of Gram-negative. The cell wall of

Gram-positive bacteria consist of a thicker peptidoglycan layer (20–40 nm), to which acidic polysaccharides (lipoteichoic acids) are bound (Figure 4.3). Membranes of Gram-negative bacteria consist of a thin peptidoglycan layer (2–7 nm), in addition to this an outer-membrane not seen in Gram-positive cells are present. This outer membrane is covered in lipopolysaccharide (LPS) molecules. The polysaccharides present on the outer-membrane of both Gram-positive and Gram-negative cell-membranes contribute to the net negative charge making these bacteria more prone to attack from cationic AMP's.[256]

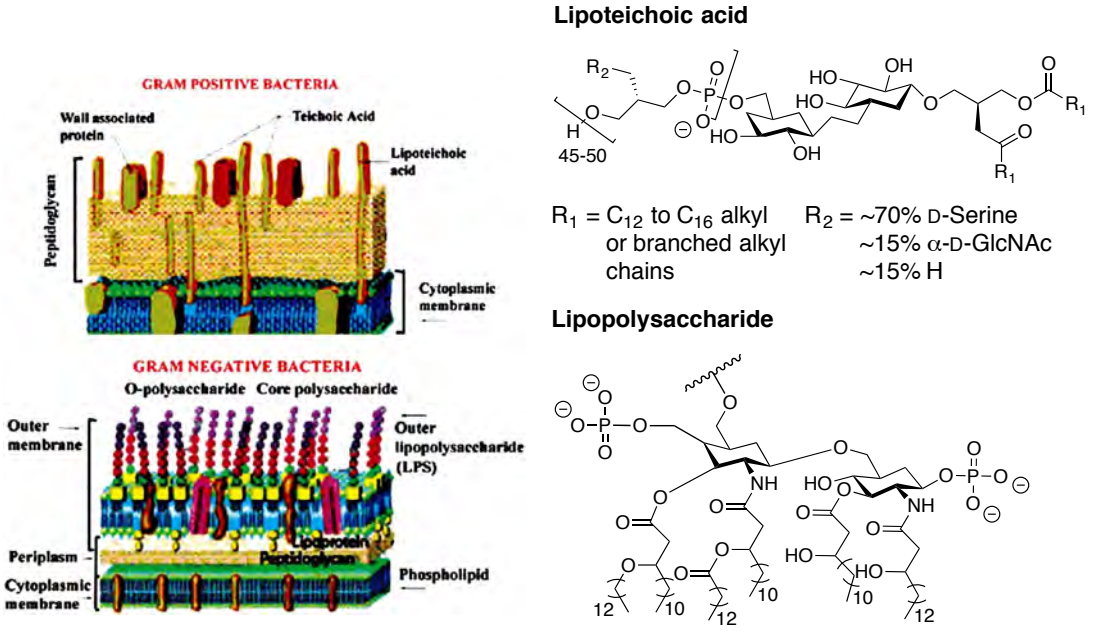

Figure 4.3. Cell membrane structure of Gram-positive and Gram-negative bacteria.

The AMP's have been shown to have a higher affinity for the polysaccharides in the outer leaflet of the membranes than metal ions such as Mg^{2+} and Ca^{2+}, which naturally counters the negative charge.[235] After the initial association with the cells an outer layer has to be breached before the peptides can interact with the cytoplasmic membrane, for the Gram-positive cells it is the peptidoglycan layer and for the Gram-negative the outer membrane.[237] The cell wall of Gram-positive bacteria is composed of peptidoglycan, embedded with polymers of teichoic acids.[257] A model that describes how the AMP's traverse this layer is yet to be made, other than the attractive ionic forces facilitate peptide accumulation in the cell wall, which eventually reaches the plasma membrane.[257] The breaching of the outer membrane of Gram-negative bacteria, on the other hand, has been more extensively studied and is hence much better understood. Upon displacement of the cationic species from the surface, the bulkiness of AMP's relative to the metal ions disrupt the normal barrier properties of the membrane.[258] This is believed to cause "cracks" in the outer membrane, which permits passage of molecules including the AMP itself, this mechanism is hence called the self-promoted uptake pathway.[234] The ability to disrupt the barrier function of the outer membrane also offer an explanation to why some studies have shown that AMP's increase the activity of conventional antibiotics.[259]

4.4 Antimicrobial peptides mechanism of action

Following the initial attachment, several different models have been proposed explaining how AMP's inserts into the cytoplasmic membrane forming trans-membrane pores (Figure 4.4). In all models the amphipathic nature of the AMP's is a key feature, as a hydrophobic region is necessary to interact with the lipid component of the membrane, while the hydrophilic part is responsible for interactions with the lipid head groups or face the lumen of the formed pores.[260] In general these models can explain the ability to form pores of α-helical AMP's, while the ability of β-sheet AMP's are much less studied, and though these compounds form amphipathic displays no experimental evidence exist to tell which model is applicable.

All models initially propose an interaction of the AMP and the negatively charged lipid head groups of the membrane surface, placing the AMP's parallel to the surface. In the first model, known as the aggregate model, the peptides reorient to span the membrane as an aggregate with micelle-like complexes of peptides and lipids.[261] In this model the peptides does not adopt a particular orientation, leading to formation of channels that vary in size and structure (Figure 4.4A). This model is used to explain how cationic AMP's can act through both membrane permeabilization an attack internal targets.[262]

In a similar model, the toroidal pore model, the formed aggregates of peptides insert themselves in an orientation perpendicular to the membrane forming more defined pores. The insertion of the peptide causes the membrane to bend, with the head-groups facing the pore, which is lined by the peptides (Figure 4.4B).[263]

The barrel-stave model calls for an even higher degree of ordering of the peptides, which in this model is oriented as the staves in a barrel, forming a cluster perpendicular to the membrane.[264] Unlike the toroidal pore model the head-groups of the membrane lipids are not part of the pore. The hydrophobic regions of each peptide in the cluster are associated with the lipid core, while the hydrophilic regions face the lumen of the pore (Figure 4.4C). This model has been used to explain voltage-dependant ion-permeable channels in planar lipid membranes, which has a similar well defined size and lifetime.[265]

A model, the carpet model, proposes that at high enough concentrations the cytoplasmic membrane can be saturated by the AMP, causing patches of the membrane to break up into micelles.[266] These local disturbances causes a decrease in membrane stability, which can lead to the formation of holes (Figure 4.4D).

Even though an exact model explaining all cases of AMP activity has not been presented, it is important to recognize that under a given set of conditions all of the above models have been validated.[260] Also, an examination of a broad range of peptides with different size and structure indicated that they interacted quite differently with membranes.[267]

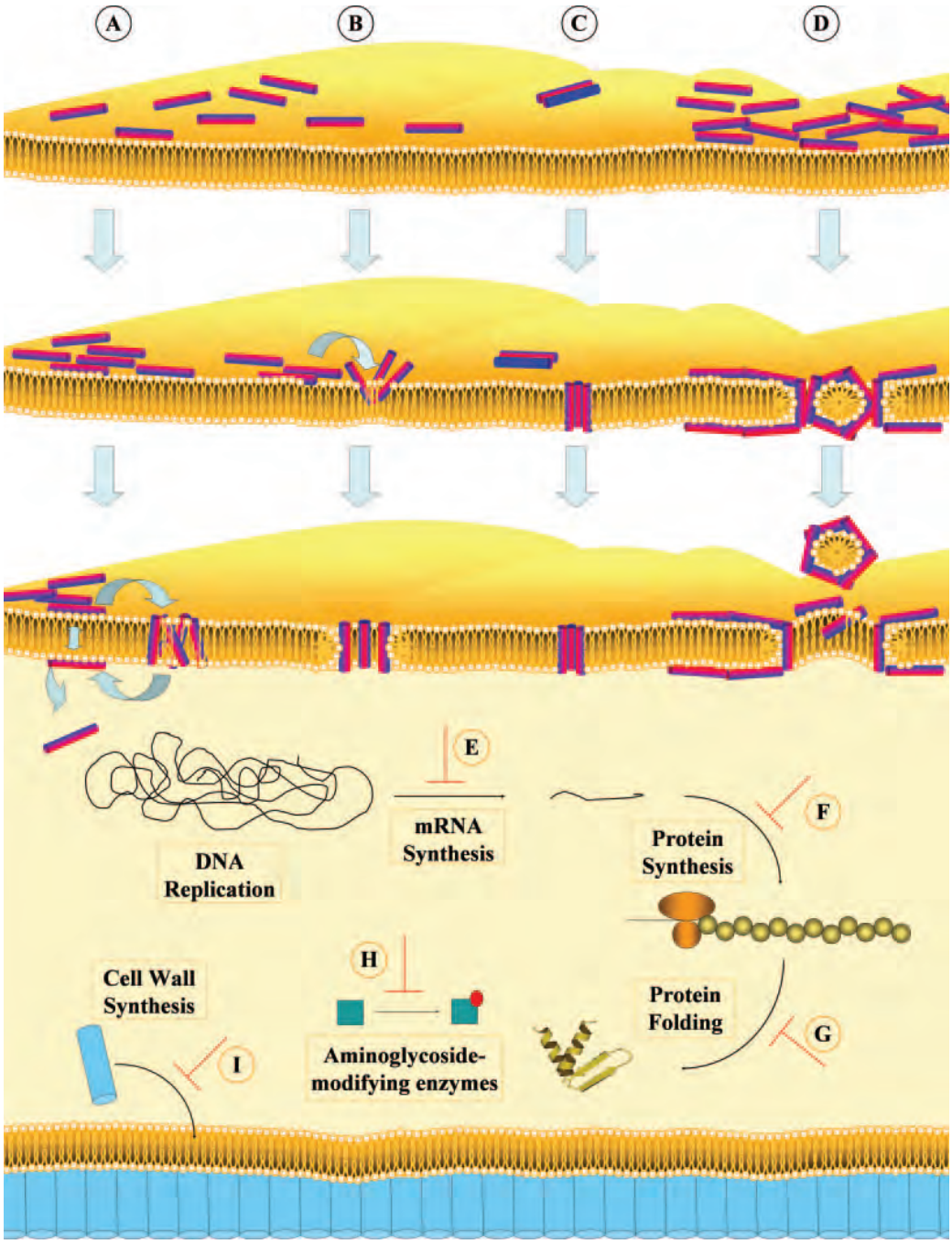

Figure 4.4. Different proposed mechanisms of action for AMP's.[260]

Not all AMP's kill bacterial cells by disrupting their membranes, and it has been established that several AMP's do not cause membrane disruption at the minimum effective concentrations.[260] A growing number of peptides have been shown to accumulate intracellularly, where they target a variety of processes leading to cell death. Amongst these are inhibition of nucleic acid synthesis, protein synthesis, enzymatic activity and cell wall synthesis.[237]

The frog derived AMP buforin II has been shown to translocate through the bacterial membranes, without causing disruption, and bind to both DNA and RNA within the cytoplasm.[268] In the same fashion α-helical peptide derivatives of the fish-derived

pleuricidin and dermaseptin from frogskin, cause inhibition of DNA- and RNA synthesis at their minimal inhibitory concentration (Figure 4.4E).[269,270] Different structural classes of AMP's have also been demonstrated to inhibit the synthesis of nucleic acids. Amongst these are the human defensins, HNP-1,[251] and the extended structure of the bovine peptide indolicidin.[270] Also some of these peptides have been shown to interfere with protein synthesis. Pleuricidin and dermaseptin can block tritiated leucine uptake in *E. Coli*, and indolicidin-treated cells exhibit reduced protein synthesis rates (Figure 4.4F).[269-271] Pyrrhocidin has been shown to inhibit enzymatic activity by binding to DnaK, a heat shock protein, which is involved in chaperone assisted protein folding, leading to accumulation of misfolded protein and cell death (Figure 4.4G). [272,273] AMP's can also target the formation of structural components, such as the cell wall. Highly cationic peptides have been shown to bind to aminoglycoside modifying enzymes, which contain an anionic binding site, causing inhibition of the enzyme (Figure 4.4H).[274] The bacterially produced peptide mersacidin interferes with the transglycocylation of lipid II, a necessary step in the synthesis of peptidoglycan (Figure 4.4I).[275]

It is likely that the action of the individual AMP's vary according to the particular target, the concentration at which the assay is performed and the physical properties of the membrane.[260] It is also likely that that the AMP's utilize more than one specific mode of action, such as destabilization of the membrane in combination with the targeting of one or more intracellular targets.[242] This high degree of complexity in mechanism of action is a very likely reason why it is extremely difficult to select a mutant that is resistant to cationic-peptides.[276,277]

4.5 Unnatural antimicrobial compounds

As described in the previous sections, the AMP's are an important part of the immune defense, but as eluted to in chapter 1, they suffer from an intrinsic instability towards proteases. This makes them unfit for treating infectious deceases in humans. For this reason an extensive amount of compounds aimed at mimicking the function of the AMP's has been proposed.

4.5.1 Unnatural Antimicrobial peptide-mimics

In 1999 DeGrado and co-workers reported the first antibacterial foldamer, which was based on a 14-helical β-peptide scaffold, consisting purely of β^3-residues.[113] From this study compounds with an efficiency matching that of the natural AMP's where found. However, these compounds turned out to cause hemolysis near the active concentration. In another study, Gellman and co-workers used a β-peptide based on a 12-helix which showed significant selectivity for bacterial cells over mammalian red blood cells, and still retained a high antibacterial activity (**92**).[278] In a later study Seebach and co-workers showed that the 14-helical scaffold can also be used to produce selective antimicrobials, e.g. compound **28** which was also used to demonstrate inhibition of lipid uptake.[114] In this study it was also demonstrated that

the exact structure of the side chains, and not just the overall amphiphilicity, is important in determining both activity and selectivity of antimicrobial β-peptides. Investigations of this class of AMP-mimics have shown them to act in a similar manner to the natural AMP's.[148,279,280]

Unnatural AMP-mimics have also been constructed from heterogeneous backbones, consisting of mixed α- and β-peptides (**92**) as it was shown that these hybrids formed stable helices.[281-283] Further studies of this hybrid system was aimed at mechanistic studies[284,285] and the relationship between the choice of side chain and the activity.[286,287] Surprisingly, it was revealed that the overall amphiphilicity is not a requirement for antimicrobial activity, as some scrambled control sequences without an overall amphiphilic motif in the folded state turned out to be potent antimicrobials.[283]

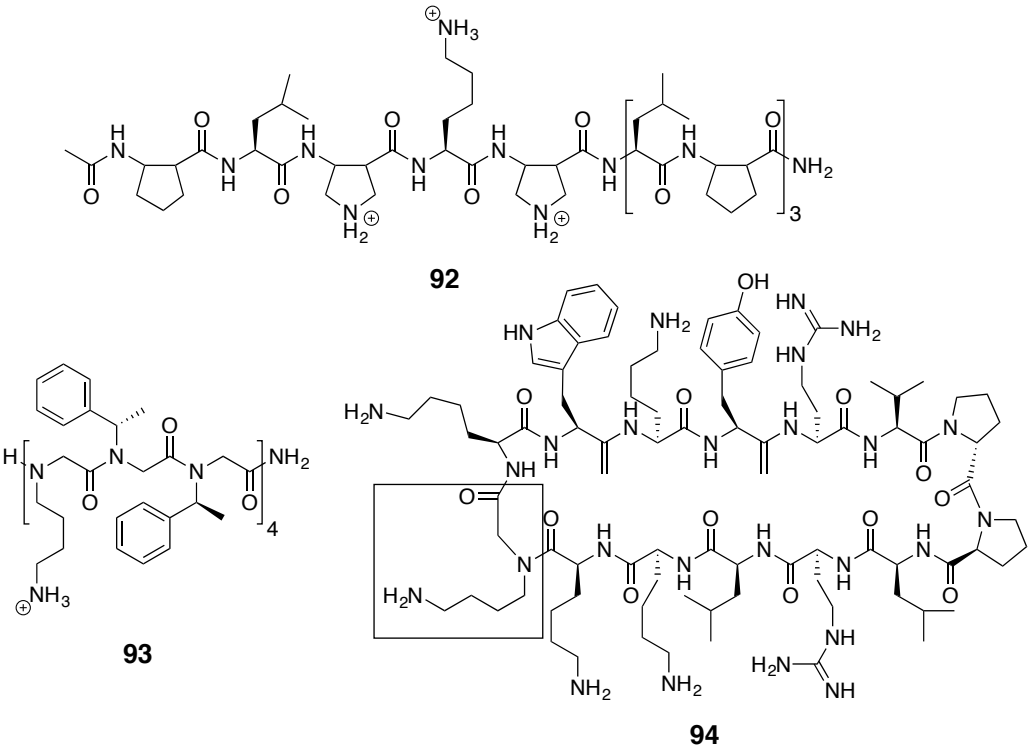

Figure 4.5. Example of unnatural AMP-mimics.

Pure- and hybrid-peptoids have also been used to furnish rather potent and selective antimicrobial compounds.[9,288] Using the polyproline-type-1-like peptoid helix, Barron and co-workers produced a series of very active mimics of the AMP magainin-2-amide.[194] This helix was designed to be amphipathic, with 1/3 hydrophilic side chains, and 2/3 of hydrophobic side chains (**93**). As for other classes of backbones it was shown that the identity of the sequence and side chain composition had a great importance on the activity and selectivity of the compounds.[162] Analogues of natural AMP's containing single or a few peptoid substitutions have also been shown to furnish potent compounds. A cyclized mimic of the hairpin-structured protegrin-1, which upon substitution of a lysine to *N*-lysine (**94**) showed a slightly increased

activity, and a much lower hemolytic activity than the natural compound.[289] The membrane-active and non-selective bee-venom derived melittin also showed increased selectivity for bacterial cells upon peptoid substitutions.[290]

4.5.2 Peptide mimics with α-peptide/β-peptoid hybrid backbones

Sequences consisting exclusively of β-peptoids have proved difficult to synthesize in lengths exceeding pentamers. However, it has been found that by synthesizing di- and trimer building blocks, longer sequences (9 to19 mers) can be formed by solid-phase coupling of these building blocks.[291] At best these compounds exhibited an antimicrobial activity which was about an order of magnitude lower than natural AMP's such as magainin.

In an approach to circumvent the difficulties of synthesis, the β-peptoids were coupled to α-amino acids, furnishing hybrid dimer building blocks. These building blocks were efficiently coupled using Fmoc SPS (see section 1.2.1), giving an alternating sequences of α-amino acids and β-peptoids (Figure 4.5).[11] Gram-scale synthesis of a series of such dimeric building blocks,[292] and an efficient solid-phase strategy giving good yields have furnished hybrid-α-peptide/β-peptoid compounds up to the hexadecamer length.[11,293]

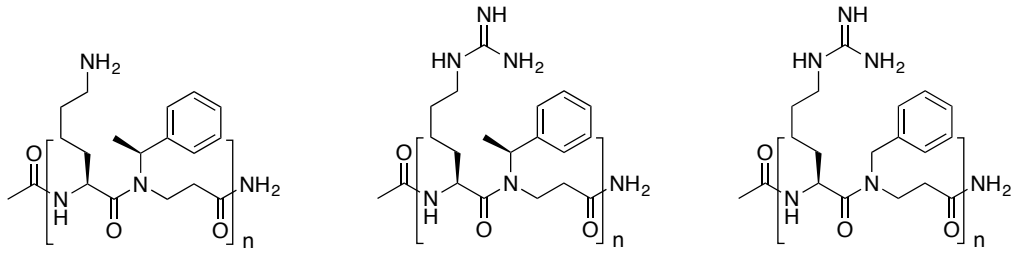

95_n [Ac-(Lys-β-*N*spe)$_n$-NH_2] **96_n** [Ac-(*h*Arg-β-*N*spe)$_n$-NH_2] **97_n** [Ac-(*h*Arg-β-*N*phe)$_n$-NH_2]

Figure 4.6. α-peptide/β-peptoid hybrids designed to extend the structural space of peptidomimetic.

The compounds in figure 4.6 were initially designed to resemble the heteromeric backbone of α/β-peptides, and due to the different side chain positioning extend the structural space.[11] Also the incorporation of α-amino acids introduce the possibility of hydrogen bonding, which should increase the stability of potential secondary structures. Like the observed non-amphipathic antimicrobial α/β-peptide sequences, reported by Gellman and co-workers,[283] these oligomers are not expected to display a global amphipathic secondary structure. CD-spectroscopy was initially performed on dodecamers of the two series with α-chiral side chains (**95_6** and **96_6**), which in various solvents showed indications of secondary structure formation, which disappeared as the chirality was lost in the third series (**97_6**).[11] It was further shown that the formation of secondary structure became stronger as the oligomers were elongated to the tetradeca- and hexadecamers. In the initial study it was also shown that all of these hybrid oligomers exhibited good antimicrobial activity towards both Gram-positive and Gram-negative bacteria whilst being non-hemolytic and proteolytically stable.[11]

These data also indicated that secondary structure was not essential for the antimicrobial activity, as the achiral series was twice as active as the chiral. In a following study these oligomers were shown to also posses antiplasmoidal activity, for which α-chiral side chains increased the potency.[13]

The oligomers from figure 4.6, including 5(6)-carboxyfluorescein (CF) labeled analogues of the hexamers (**99**–**101**) were further tested against a broader spectrum of bacteria (Table 4.1).[12]

Comp.	Sequence	MIC measurements for various pathogens (ug/mL)					HC10 (ug/mL)
		MRSA	VRE	*E. coli*	*P. aureg.*	*C. albic.*	hRBCs
Amino a-chiral							
95_5	Ac-(Lys-βNspe)$_5$-NH_2	>500	500	>500	125	>500	>500
95_6	Ac-(Lys-βNspe)$_6$-NH_2	500	250	63	63	125	>500
95_7	Ac-(Lys-βNspe)$_7$-NH_2	250	125	63	31	63	>500
95_8	Ac-(Lys-βNspe)$_8$-NH_2	125	63	31	16	63	>500
Guanidino, a-chiral							
96_5	Ac-(hArg-βNspe)$_5$-NH_2	16	32	8	125	250	>500
96_6	Ac-(hArg-βNspe)$_6$-NH_2	16	16	16	63	125	>500
96_7	Ac-(hArg-βNspe)$_7$-NH_2	9	9	16	37	148	>500
96_8	Ac-(hArg-βNspe)$_8$-NH_2	16	8	16	31	31	>500
Guanidino, non-chiral							
97_5	Ac-(hArg-βNphe)$_5$-NH_2	143	71	9	143	71	>500
97_6	Ac-(hArg-βNphe)$_6$-NH_2	67	17	4	67	33	>500
97_7	Ac-(hArg-βNphe)$_7$-NH_2	64	16	16	64	32	>500
97_8	Ac-(hArg-βNphe)$_8$-NH_2	34	9	34	34	34	>500
Guanidino, α-chiral lipophilic							
98	Ac-(hArg-βNsce)$_6$-NH_2	8	4	8	64	16	25
5(6)-Carboxyfluorescein-labeled							
99	CF-(Lys-βNspe)$_6$-NH_2	>256	128	256	>256	256	ND
100	CF-(hArg-βNspe)$_6$-NH_2	256	64	128	256	256	ND
101	CF-(hArg-βNphe)$_6$-NH_2	128	64	64	256	128	ND
Antimicrobial peptides							
Melittin	H-GIGAVLKVLTTGLPALISWIKRKRQQ-NH2	8	8	64	256	32	2
Magainin-2	GIGKFLHSAKKFGKAFVGEIMNS-NH2	500	250	125	250	500	>500
Pexiganan	GIGFLKKAKKFGKAFVKILKK-NH2	63	16	16	16	63	40

Table 4.1. Antimicrobial activity of hybrid α-peptide/β-peptoids and antimicrobial peptides. MRSA = methicillin-resistant *Staphylococcus aureus* (ATCC 33591), VRE = vancomycin-resistant *Enterococcus facium* (ATCC 700221, *E. coli* = *Eschericia coli* (ATCC 25922), *P. aureg* = *Pseudomonas aureginosa* (ATCC 27853), *C. albic* = *Candida albicans* (ATCC 200955), HC_{10} = concentration that causes 10% hemolysis. hRBCs = human red blood cells. MIC values from ref. 12.

From this investigation it is apparent that elongation of the compounds enhance their activity towards most pathogens.[12] However, this trend was diminished or even reversed for the two series containing guanidino- rather than amino functionalities, when tested against *E. coli*. It was also shown that the guanidino versions were generally more efficient against all pathogens except *P. aereginosa*, where the hexadecamer of the amino series was more active than both guanidino containing hexadecamer analogues.[12] A hexamer with cyclohexyl ethyl side chains (**98**) instead of phenyl ethyl, showed high activity, however, the activity was accompanied by a large increase in hemolytic activity as well. It is also noteworthy that most of the compounds exhibit comparable or even better MIC values than the natural AMP's melittin, magainin-2 and the synthetically derived pexiganan (from magainin). This activity is accompanied by higher HC_{10} values than seen for the natural AMP's, making the hybrid structures attractive as lead drug candidates. Unlike the

preliminary study, it was shown that the compounds containing chiral *β*-peptoids and a guanidino functionality was more potent than those with achiral *β*-peptoids and guanidino groups.[12,294] The opposite only seems to be the case when the dodecamers are tested against *E. coli*, which were the case in the preliminary study.[11] Also *C. albic*, the only fungus in the panel, showed more sensitivity towards the achiral oligomers.[12] Finally it was shown that for the oligomers containing an amino functionality, the CF-tag increased the activity against MRSA and VRE, whereas a decrease was observed for other pathogens and when having a guanidine functionalized oligomer.[12]

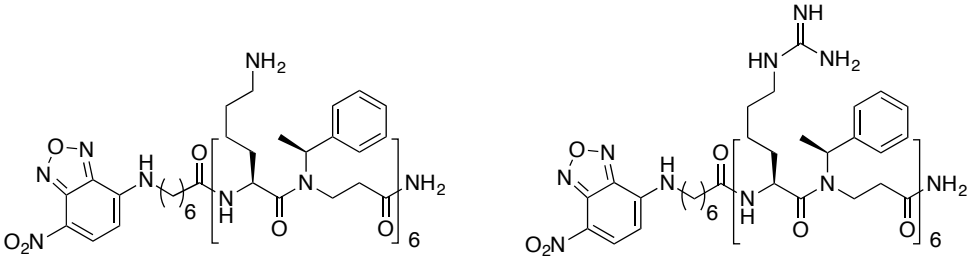

102 [NBD-(Lys-*β*-*N*spe)$_6$-NH$_2$] **103** [NBD-(*h*Arg-*β*-*N*spe)$_6$-NH$_2$]

Figure 4.7. NBD tagged hybrid *a*-peptide/*β*-peptoid compounds.

For the studies described in the following sections of this chapter, we wanted to evaluate the importance of the cationic group further. For this purpose we synthesized compounds **95$_6$** and **96$_6$**, along with a nitrobenzoxadiazole (NBD) labeled analogues (**102** and **103**). To assure that our compounds were active they were tested against five selected pathogens, for which the results described above was confirmed, however, we found that when labeling the compounds with NBD the compounds retained their activity. To validate that the fluorophore did not cause this increase itself, we decided to test it (**104**) alone, in which case we saw no activity.

Comp.	Sequence	MIC measurements for selected pathogens (ug/mL / uM)				
		Gram-negative				Gram-positive
		E. coli	*E. coli*	*K. pneumoniae*	*V. vulnificus*	*S. aureus*
95$_6$	Ac-(Lys-*β*Nspe)$_6$-NH2	128/50	128/50	256–512	64/25	64–128/25–50
102	NBD-(Lys-*β*Nspe)$_6$-NH$_2$	32/11	32/11	128/44	64/22	32/11
96$_6$	Ac-(hArg-*β*Nspe)$_6$-NH$_2$	3-Aug	16/3	16–32/3–6	3-Aug	4/1.5
103	NBD-(hArg-*β*Nspe)$_6$-NH$_2$	16/5	32/10	64/20	16/5	16/5
104	*ε*-N-NBD-6-aminohexanamide	>128/>436	>128/>436	>128/>436	>128/>436	>128/>436

Table 4.2. Antimicrobial activity of two hexameric hybrid oligomers and their NBD labeled analogues. *E. coli* = *Escherichia coli* (ATCC 25922), *K. pneumoniae* = *Klebsiella pneumonia* (ATCC 13883), *V. vulnificus* = *Vibrio vulnificus* (ATCC 27562), *S. aureus* = *Staphyllococcus aureus* (8325-4). [a] Extended Spectrum Beta-Lactamase (ESBL)-producing clinical strain isolated from a Danish patient in 2007 (AAS-EC-009).

Such labeled compounds are of great value in studying the interactions with live bacteria using confocal fluorescence microscopy. In fact, such an investigation led to

the observation that the hybrid compounds internalize into HeLa cells.[13] Further studies of this property led to the conclusion that the alternating α-peptide/β-peptoids have good cell penetrating abilities.[292] In this regard, the application of a fluorophore that does not affect the activity of the hybrid-oligomes could be of great value.

4.5.3 Backbone composition

To improve on the stability of peptidic lead compounds, replacement of single residues, fragments or entire sequences with peptidomimetic residues described in this thesis, amongst others, have been carried out. Still focusing on the ability to inhibit bacterial cell growth, a study aimed at comparing the efficiency of these mimics, and their hybrids has recently been performed.[222] To obtain knowledge concerning the importance of the composition of the backbone, a library consisting of alternating lysine and phenylalanine residues and combinations of their mimics was synthesized (Figure 4.8).

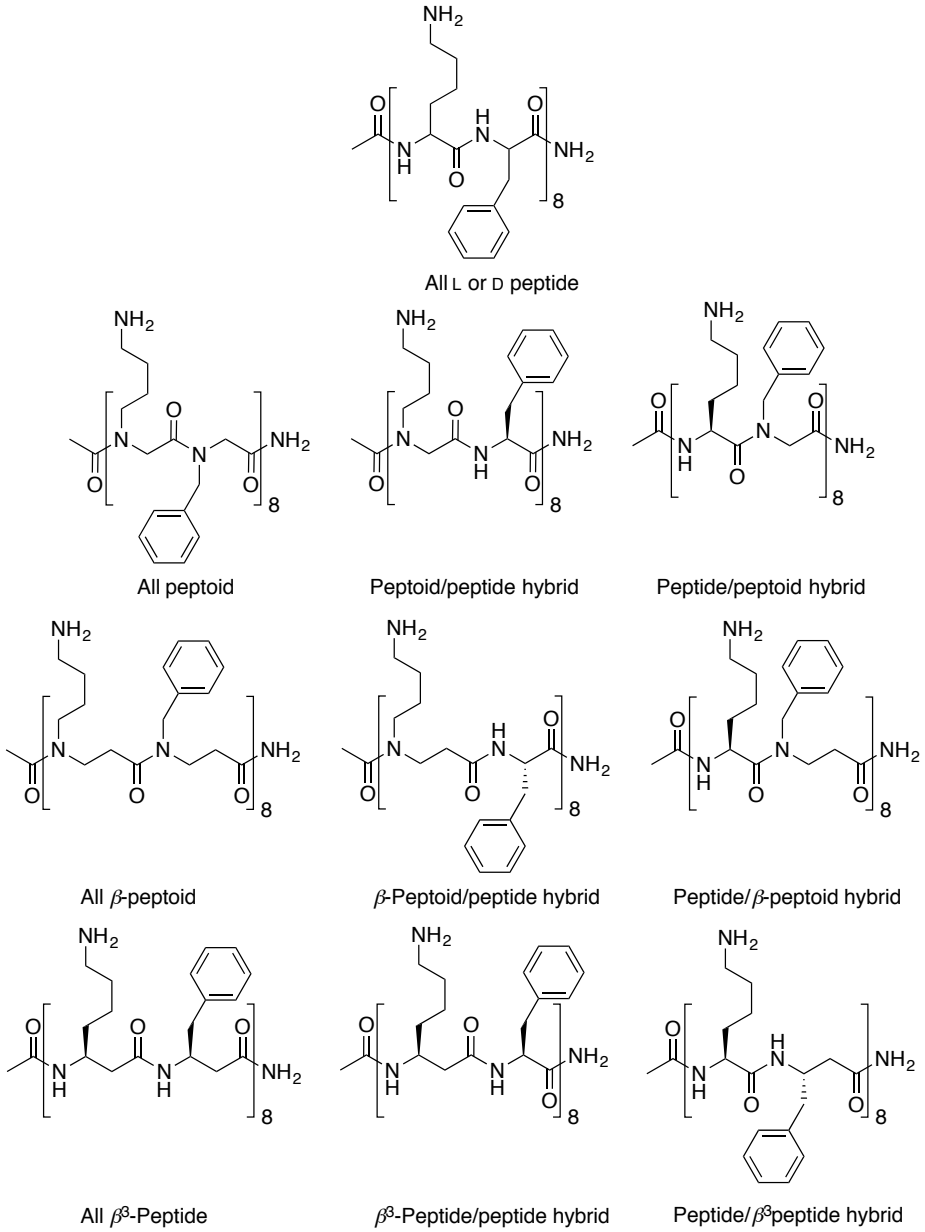

Figure 4.8. Library consisting of different combinations of various mimics and amino acids.

The activity of this library was tested against a series of multidrug resistant *E. coli* and *K. pneumoniae* strains. It was shown that all mimics had lower MIC values than the parent peptide sequence (Table 4.3).[222] The data also show that hybrid compounds seem to have improved antimicrobial activity compared to the pure mimic sequences.

Sequence	*E. coli*				*K. pneumoniae*		
	ATCC 25922	ESBL	AmpC	NDM-1	KPC-2	NDM-1	MRSA
All L-aa peptide	>256	>256	>256	128	>256	>256	16
All D-aa peptide	128	256	256	128	256	256	16
Peptoid	32	64	32	32	256	256	256
Peptoid/peptide	16	16	32	32	256	256	>256
Peptide/peptoid	4	8	8	2	128	128	256
β-peptoid	16	8	16	4	256	256	256
β-Peptoid/peptide	8	16	16	2	64	256	256
Peptide/*β*-peptoid	8	4	8	4	128	256	>256
β^3-peptide	16	32	32	32	32	32	16
β^3peptide/peptide	8	8	16	4	128	256	256
Peptide/β^3-peptide	64	32	32	64	128	128	32

Table 4.3. Antimicrobial activity of various combinations of mimics and amino acids.MIC values from ref. 222.

These results clearly indicate that by choosing the right backbone composition a gain in activity can be obtained. This also shows that factors other than the amount of hydrophobic or hydrophilic residues are important for the activity, and that these systems can be optimized in different ways, also depending on the particular system on which they are thought to act.

4.6 Synthesis of hybrid oligomers

Synthesis of the hybrid oligomers were achieved by the creation of dimeric building blocks, formed by coupling of *N*ε-Boc-protected lysine with an *N*-terminal Fmoc proteting group and the *C*-terminally *tert*-butyl protected spe *β*-peptoid monomer (**63A**) to form compound **105**. As opposed to the literature procedure, we used prolonged reaction times rather than microwave heating,[293] as we found this to give satisfying yields. Selective and simultaneous removal of the *tert*-butyl and the Boc-groups, in the presence of Fmoc, could be achieved upon treatment with 50% TFA in CH_2Cl_2 furnishing **106**. The resulting compound with free acid and amino functionalities was then selectively re-protected at the *N*ε-amine. Aiming to use an Fmoc based solid support strategy we chose to synthesize two series of oligomers incorporating either protecting groups allowing for simultaneous cleavage and deprotection, or which could be removed without cleaving the compound from the resin. For the first scenario we chose to reinstall the Boc-group (**107**), which is a classic solution for the Fmoc strategy. In order to establish an on-resin functionalization we incorporated an orthogonal 1-(4,4-dimethyl-2,6-dioxacyclohexylidene)ethyl (Dde) group (**108**).[295,296]

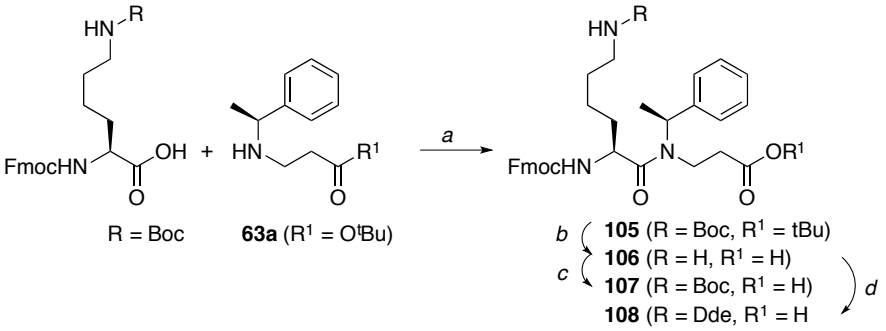

Scheme 4.1. Synthesis of hybrid dimer building blocks. . *a*) Fmoc-Lys(Boc)-OH (1.7 equiv), HBTU (1.7 equiv), *i*Pr_2NEt (4 equiv), DMF, 18 h. *b*) TFA–CH_2Cl_2 (4:6), 2 h. *c*) Boc_2O (1.5 equiv), *i*Pr_2NEt (2 equiv), DMF, 0 °C for 1 h then rt 2 h, *d*) Acetyl dimedone (1.7 equiv), *i*Pr_2NEt (2.7 equiv), DMF, 18 h.

Oligomerization of these building blocks was performed on a ChemMatrix resin using a rink linker, as a *C*-terminal amide was desired. After six rounds of coupling/deprotection of **108**, the resin bound dodecamer was achieved (**109**), the *N*-terminal was then capped with an acetyl group and the Dde groups removed to give **110**. At this point the compound could either be cleaved to give $\mathbf{95_6}$, or undergo a functionalization using **111** to give the corresponding guanidinylated compound, which upon simultaneous cleavage and deprotection gave $\mathbf{96_6}$.[297]

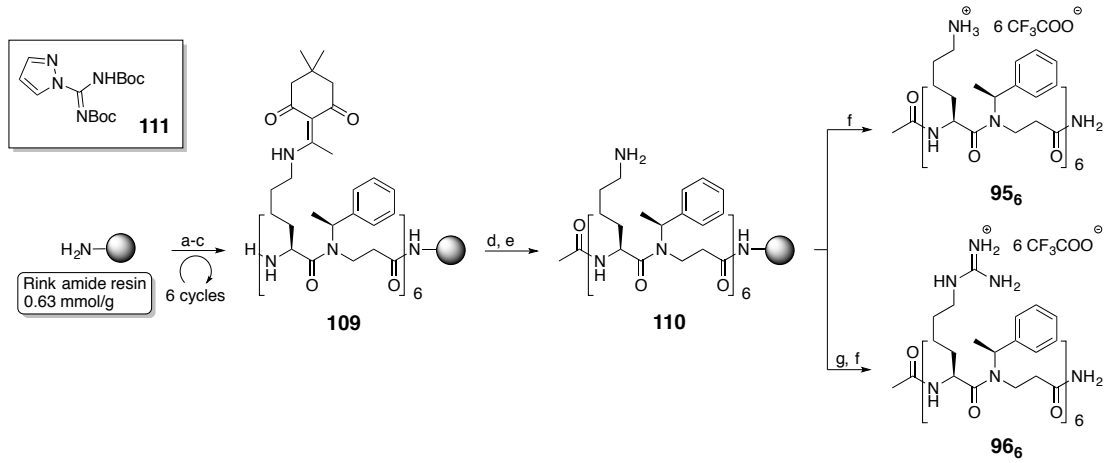

Scheme 4.2. Oligomerization of hybrid dimer building blocks. *a*) **108** (4.5 equiv), HBTU (4.5 equiv), *i*Pr_2NEt (9 equiv), DMF, 18 h. *b)* Piperidine–DMF (1:4), 2 × 10 min. *c*) DBU–piperidine–DMF (2:2:96), 20 min. *d*) Ac_2O–*i*Pr_2NEt–DMF (1:2:3), 2 h. (*e*) Hydrazine–DMF (2:98), 2 × 45 min. *f*) 50% TFA–CH_2Cl_2, 2 × 1 h. (*g*) *N,N'*-Bis(*tert*-butoxycarbonyl)-1*H*-pyrazole-1-carboxamidine (**111**, 36 equiv), *i*Pr_2NEt (72 equiv), DMF, 18 h. HBTU = *O*-(Benzotriazol-1-yl)-*N,N,N′,N′*-tetramethyluronium hexafluorophosphate.

We also tried to incorporate the NBD fluorophore building block **113** following this procedure. This, however, did not give the desired products (**102** and **102**) upon cleavage from the solid support. Due to a change in the resin color from bright yellow to a pale orange upon undergoing Dde deprotection, we believe that the chosen fluorophore is sensitive to hydrazine, used in the deprotection step. For the formation of **102** and **103** we therefore decided to oligomerize **107**, and luckily the fluorophore was stable to the cleavage/deprotection conditions required. Unfortunately this meant that the guanidino groups had to be installed in solution. As the crude product from

the cleavage of **112** (**102**) was fairly pure, the guanidino-functionalization was performed without purification of the crude **102**, eliminating an additional purification steps.

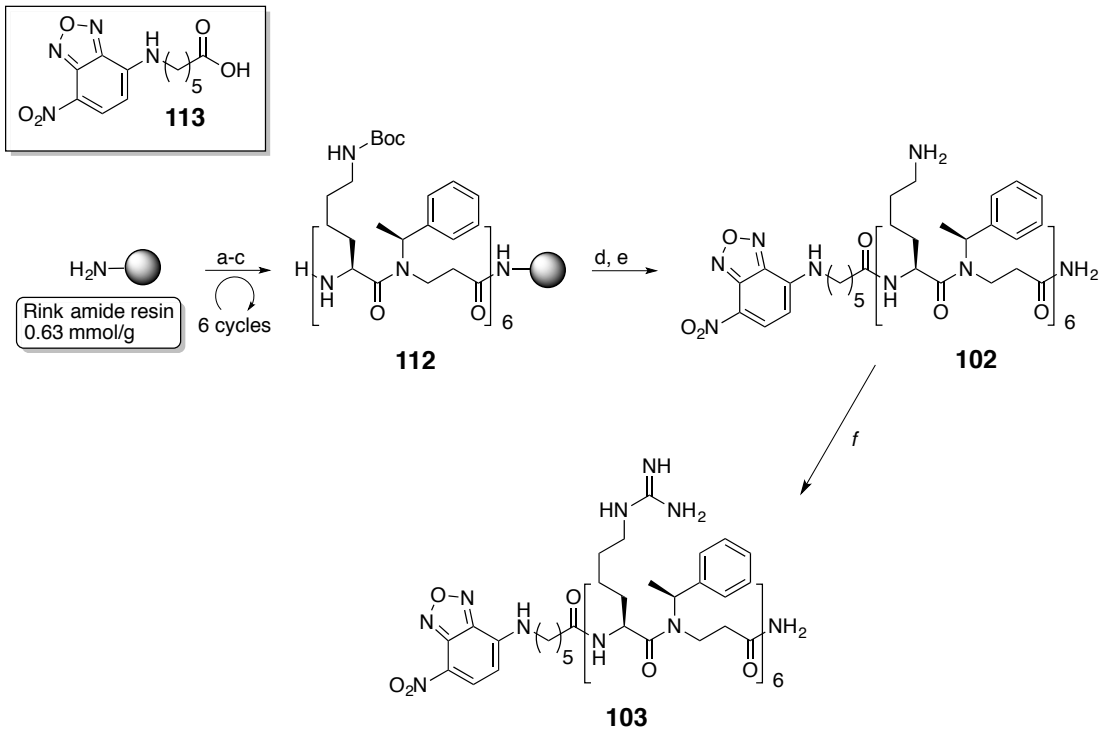

Scheme 4.3. NBD-labeling of dodecamers on solid support. **107** (4.5 equiv), HBTU (4.5 equiv), *i*Pr_2NEt (9 equiv), DMF, 18 h. (*b*) piperidine–DMF (1:4), 2 × 10 min. (*c*) DBU–piperidine–DMF (2:2:96), 20 min. (*d*) **113** (6.5 equiv), PyBOP (7.5 equiv), *i*Pr_2NEt (13 equiv), DMF, 18 h. (*e*) TFA–CH_2Cl_2 (1:1), 2 × 1 h. (*f*) *N*,*N*'-Bis(*tert*-butoxycarbonyl)-1*H*-pyrazole-1-carboxamidine (**111**, 36 equiv), *i*Pr_2NEt (72 equiv), DMF, 18 h.

Finally **113** was attached directly to the resin, and then cleaved to give an amide as the *C*-terminal functionality (**103**).

4.7 Membrane study

Whether the mechanism of action involves disruption of the membrane or perturbation of intracellular targets, an initial interaction of the antimicrobial compound and the cell surface is inevitable. A better fundamental understanding of these interactions is therefore important for further optimization of future antibiotics. The structure of cell membranes is rather complex and are currently not applicable for highly sensitive surface X-ray scattering methods.[298-300] Previous studies of the membrane-destabilizing effect of α-peptide/β-peptoid hybrids have been performed in model liposomes prepared from PC, which is predominantly found in eukaryotic cells.[292] For this reason PC-containing systems do not represent the bacterial envelope sufficiently. Furthermore, the interactions of this class of compounds with model membranes have never been investigated using sensitive X-ray methods. To create a better model for the investigation of the interactions between the hybrids and the outer surface of Gram-positive and Gram-negative bacteria, monolayers of 1,2-dipalmitoyl-

sn-glycero-3-phosphatidylglycerol (DPPG) and truncated LPS Kdo-2-lipid A, respectively, were prepared (Figure 4.9). As the hydrophobic core of the LPS envelope of most Gram-negative bacteria consist of Kdo-2 lipid A, while PG are a predominant phospholipid species in the cytoplasmic membrane of Gram-positive bacteria, we believe these to more closely resemble the actual cell surfaces.

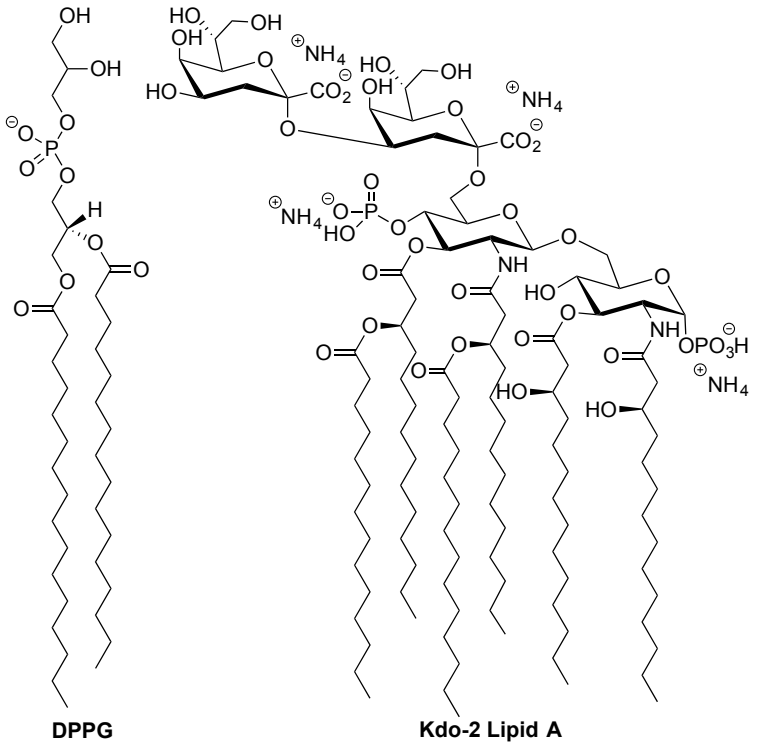

Figure 4.9. Lipids used to study the membrane interactions of the hybrid oligomers.

This approach has been used to study the lysis of bacterial membranes by human AMP LL-37,[300] protegrin-1[298,301] and gramicidin[302] by liquid surface X-ray scattering.

4.7.1 Epifluorescence microscopy[e]

First it was tested whether the hybrid oligomers would disrupt the model monolayers, which was done by exposing monolayers doped with Texas red dye to the oligomers. The first frame in figure 4.10 Show the monolayers prior to the exposure, using an epifluorescence microscope. The image shows the DPPG monolayer as branched dark domains, separated by brightly colored fluid areas. After injection of $\mathbf{95_6}$ (Figure 4.10A) and $\mathbf{96_6}$ (Figure 4.10B) it is apparent that after 4 min. the morphology of the surface is changed to contain less of the condensed lipid phase. In the next two frames the ordered phase is eliminated and the majority of the film is found in the liquid-disordered phase after 15-20 min. At the end of the experiment, ordered regions are either destroyed or too small for the microscope to see (<1 μm). This shows that both

[e] Epifluorescence microscopy was performed by Konstantin Andreev, Christopher Bianchi and Professor David Gidalevitz, at Illinois Institute of Technology, Chicago, USA.

types of cations display crystallinity-disruptive behavior, at least on the micrometer scale.

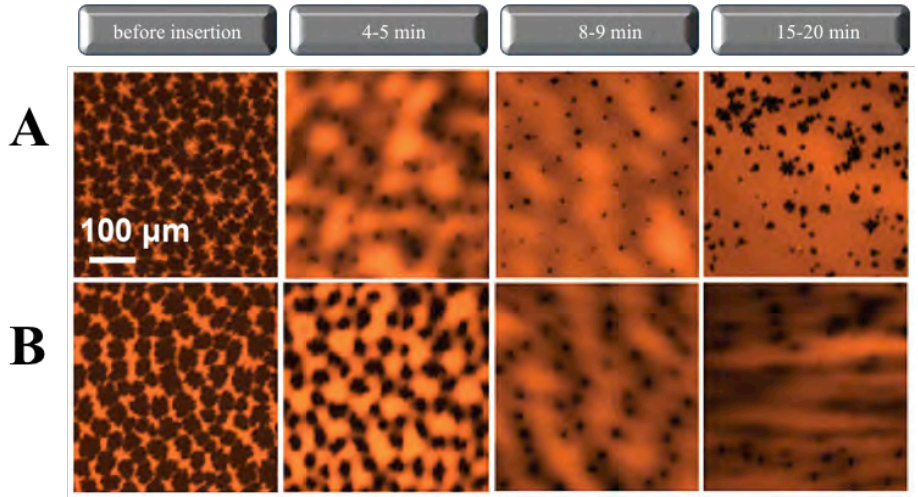

Figure 4.10. Epifluorescence images of DPPG monolayers after injection of compound 95_6 (A) and 96_6 (B) at concentrations corresponding to 20% of their MIC values against *S. aureus*.

4.7.2 Specular X-ray reflectivity[f]

X-ray reflectivity (XR) is a technique that gives information on the electron density along a plane perpendicular to the surface of a monolayer and the thickness of that layer. A slab-model, or box model, can be used to fit the data giving information about the thickness and electron densities of the individual slabs.[303]

Figure 4.11 shows the profile of the electron density along the surface normal obtained by model-independent stochastic fitting, of data extracted from reflectivity measurements. The lipid film shows no electron density at the air–water interface, then through the hydrocarbon-tail region the electron density rises sharply reaching the maximum density in the head group region at a distance of ~20-25 Å from the air–water interface. The pure DPPG monolayers were modeled as two slabs, one corresponding to the hydrocarbon region and the next to the head group region. Analysis of the obtained XR-data revealed the acyl chain slab to have a thickness of 16.5 Å and an electron density of 0.312 $e^-/Å^3$. The thickness of the head group slab was found to be 8.3 Å and have an electron density of 0.477 $e^-/Å^3$. The data for the Kdo-2 Lipid A revealed a 12.0 Å thick hydrocarbon layer with an electron density of 0.31 $e^-/Å^3$. The second slab corresponding to the layer of the carbohydrate 3-deoxy-D-mannooctulosonic acid (known as Kdo) had a thickness of 12.8 Å and an electron density of 0.485 $e^-/Å^3$. Insertion of the antimicrobials into the monolayer results in extra electrons per lipid molecule in each slab, which can be calculated using equation 1. Here, l_{slab} and ϱ_{slab} are thickness and electron density of the slab, respectively; $A_{lipid} + \Delta A_{lipid}$ is the area per lipid molecule upon insertion and $N_{initial}\, e^-_{slab}$ is the number of electrons in the slab of the original untreated monolayer.

[f] Specular X-ray reflectivity measurements and interpretation was performed by Konstantin Andreev, Christopher Bianchi and Professor David Gidalevitz, at Illinois Institute of Technology, Chicago, USA.

$$N_{extra}\, e^{-}_{slab} = l_{slab} \times \varrho_{slab} \times (A_{lipid} + \Delta A_{lipid}) - N_{initial}\, e^{-}_{slab} \quad \text{(eq. 1)}$$

Upon insertion of **95$_6$** the minimum of the reflectivity curve were shifted from a $q_z \approx 0.24$ Å^{-1} to a higher q_z value moving the peak of electron density towards the air–water interface. This indicates a decrease in thickness of the film as a result of the insertion. However, injection of compound **96$_6$** did not result in a thinning of the DPPG monolayer, but led to appearance of two distinct minima on the reflectivity profile at $q_z \approx 0.21$ Å^{-1} and 0.35 Å^{-1} giving a notable bump in the electron density curve within the range of 20–40 Å away from air-water interface. This might be due to an additional layer of distinct electron density higher than the electron density of subphase present underneath the head group region.

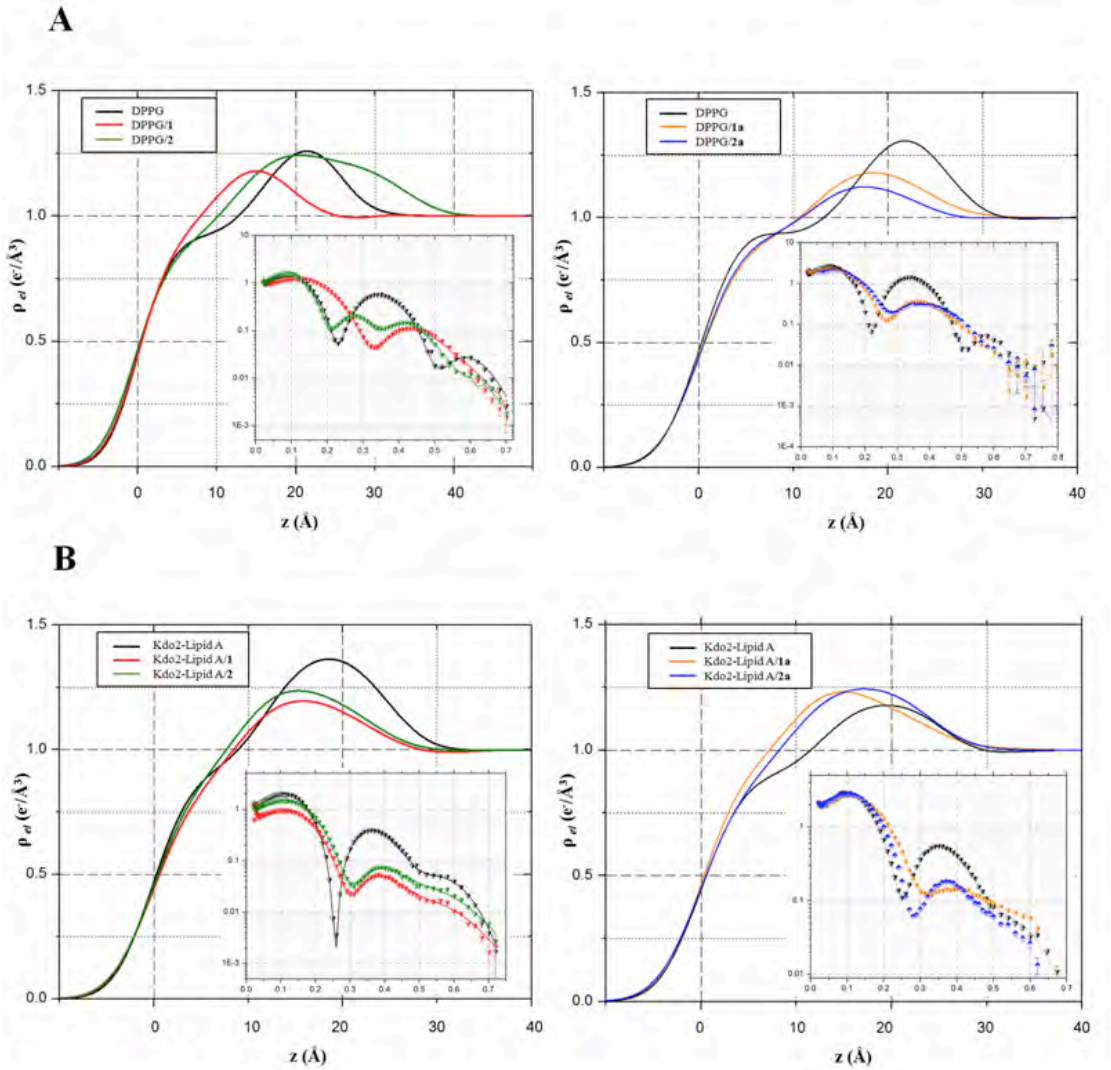

Figure 4.11. Electron density profiles and reflectivity curves for DPPG (A) and Kdo2-Lipid A (B) monolayers at 30 mN x m^{-1}.

The data were treated using a model dependent analysis which are summarized in table 4.4. As mentioned this system is best fitted using a two-slab model, however, the occurrence of the second minimum in the reflectivity upon insertion of **96$_6$** was best modeled using a third slab. The lower increase in area per lipid molecule upon

addition of **96$_6$** compared to **95$_6$** can be explained by dimerization or aggregation of **96$_6$** on the outer surface of the DPPG monolayer (Table 4.4).

Sample[a]	l_T (Å)	ρ_T (e^-/Å^3)	Extra e^-_T[b]	l_H (Å)	ρ_H (e^-/Å^3)	Extra e^-_H	l_{OL} (Å)	ρ_{OL} (e^-/Å^3)	Extra e^-_{OL}	Area per lipid molecule (Å^2)[c]
DPPG	16,5	0,312	-	8,3	0,477	-				45,5
DPPG/**95$_6$**	11,0	0,320	0	7,1	0,450	53				66
DPPG/**102**	12,0	0,314	0	11,6	0,410	112				57
DPPG/**96$_6$**	12,3	0,314	0	12,1	0,430	167	9,6	0,405	43	63
DPPG/103	12,1	0,317	89	9,7	0,408	197				90
Kdo 2 Lipid A	12,0	0,310	-	12,8	0,485	-				125
Kdo 2 Lipid A/**95$_6$**	8,9	0,293	0	14,0	0,451	234				158
Kdo 2 Lipid A/**102**	8,4	0,283	5	14,1	0,420	389				195
Kdo 2 Lipid A/**96$_6$**	8,9	0,300	0	13,7	0,445	256				168
Kdo 2 Lipid A/**103**	9,2	0,255	0	14,9	0,441	489				191

Table 4.4. Parameters of DPPG and Kdo-2-Lipid A monolayers before and after introduction of oligomers. [a] Subscripts: T, tails; H, heads; and OL, outer layer. [b] Extra electrons calculated using Eq. 1. [c] Area per lipid molecule (A_{lipid}) = $N_{lipid\ molecules}$ / A_{total}.

From the number of extra electrons it is seen that both **95$_6$** and **96$_6$** readily inserts into the polar domain of both DPPG and Kdo-2 Lipid A, resulting in a reduced electron density in the bottom slab. It is also seen that neither of the compounds are able to penetrate into the overlaying hydrophobic region. A more substantial decrease in electron density of the DPPG head group region, along with three times more additional electrons being present upon introduction of **96$_6$** points to a higher Gram-positive membrane disruptive potential of guanidino-containing oligomer compared to the amino-containing analogue. The same general trend was observed for the labeled analogues **102** and **103**. However, the guanidino containing analogue was shown to penetrate the entire depth of the monolayer including the hydrophobic tail region. Furthermore, the addition of **103** led to a greater number of added electrons in total, as well as a four-fold increase in area per lipid molecule, which is indicative of a favorable effect of the guanidine groups on the insertion.

Contrary to the observations from DPPG monolayers, the reflectivity curves for the Kdo-2 Lipid A monolayer after insertion of **95$_6$** and **96$_6$** looks nearly identical (Figure 4.11B). For the model-dependent analysis revealed very similar mechanisms of action for the two compounds against the Gram-negative membrane mimic. The similarity in mode of action between **95$_6$** and **96$_6$,** as well as between **102** and **103** was confirmed by similar changes in thickness of respective slabs within the monolayer and by similar number of contributed extra electrons. The increase in area per lipid molecule in both pairs of compounds was also similar.

4.7.3 Grazing incidence X-ray diffraction[g]

Grazing incidence X-ray diffraction (GIXD) data obtained for the DPPG monolayer before and after injection of the four compounds are shown in figure 4.12. It is seen that the pure DPPG monolayer display two distinct Bragg peaks at Q_{xy} = 1.39 Å^{-1} and Q_{xy} = 1.47 Å$^{-1,}$ which is indicative of an ordered structure being present. From the peaks the unit cell has the dimensions 5.32 x 8.54 Å, giving a total area per DPPG molecule of 45.5 Å^2. Insertion of **96$_6$** and **103** fully disrupted the crystallinity of the monolayer, seen by the total absence of the Bragg peaks. Surprisingly, insertion of **95$_6$** and **102** only caused one of the Bragg peaks to disappear, indicative of a rearrangement of the monolayer. Further, the labeled compound **102** was shown to decrease the size of the crystallized domains as well as the order of crystallinity to a greater extent than the non-labeled compound.

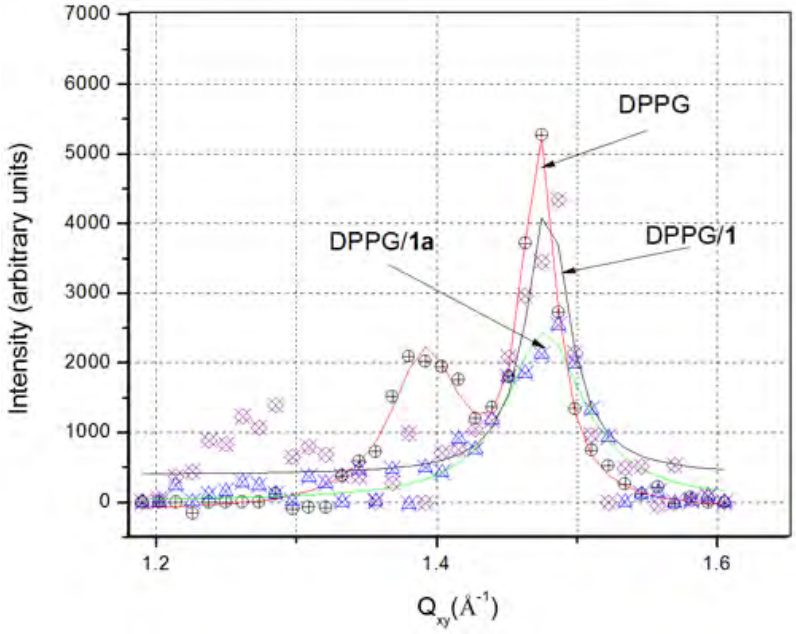

Figure 4.12. Bragg peaks plot of scattering vector as a function of intensity.

4.8 Concluding remarks

The data presented provide solid evidence of a higher membrane activity against Gram-positive bacteria of guanidine containing α-peptide/β-peptoid hybrids than their amino analogues. Guanidino containing compounds were found to possess improved membrane disruptive capabilities against DPPG monolayers, mimicking the outer leaflet of Gram-positive bacteria cell membranes. Somewhat surprisingly, this guanidine effect was not present when tested against a LPS (Kdo-2 Lipid A), mimicking the external leaflet of Gram-negative bacteria membranes. The obtained XR data are hence in good agreement with the previously published results from biological assays, especially as the length of the hybrid oligomers are increased.[12,294]

[g] Grazing incidence X-ray diffraction measurements and interpretation was performed by Konstantin Andreev, Christopher Bianchi and Professor David Gidalevitz, at Illinois Institute of Technology, Chicago, USA.

Figure 4.13 shows a cartoon representation of the proposed mode of interaction between the hybrid oligomers and the monolayers.

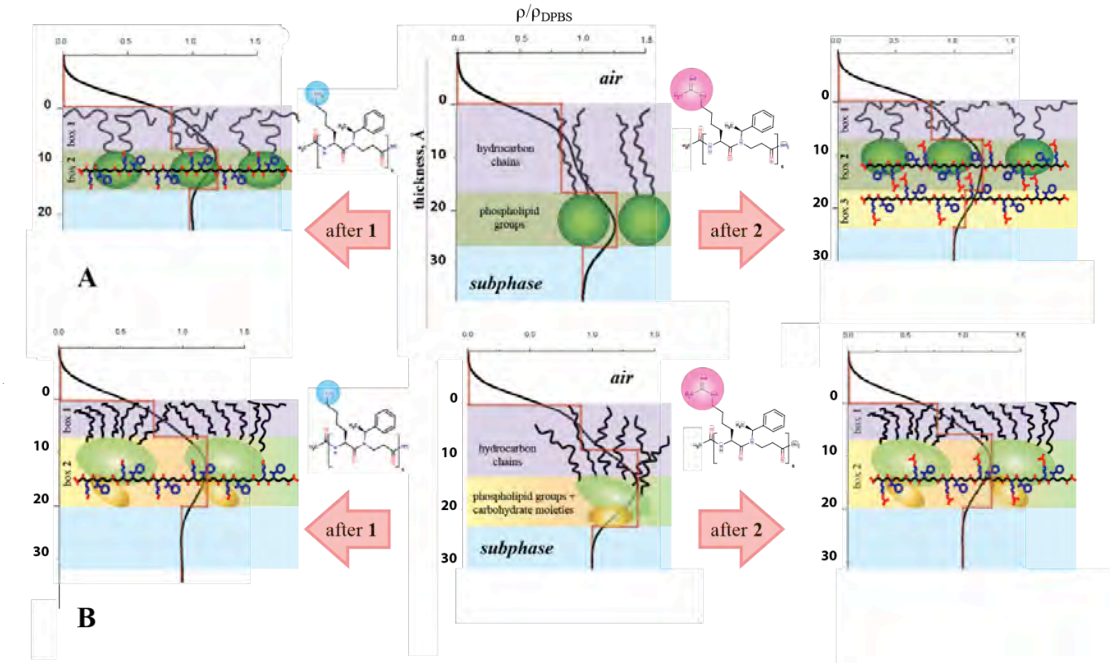

Figure 4.13. Cartoon representation of possible interaction of compound $\mathbf{95}_6$ and $\mathbf{96}_6$with DPPG (A) and Kdo2-Lipid A (B).

Since both types of cation are fully protonated at physiological pH we believe that the ability of the guanidino group to engage in more stable bidentate electrostatic interaction with the negatively charged phosphodiester moieties affects the DPPG lipids to a greater extent than Kdo-2 Lipid A due to the more rigid structure of the latter. These findings thus provide fundamental insights that should be useful in the future design of optimized synthetic peptidomimetics with selective antibiotic effects. Finally, labeling with the NBD fluorophore did not reduce the observed activity of the tested hybrids, which correlate with the observed retained antimicrobial potency against bacteria *in vitro*. In addition the NBD-labeled compounds demonstrated an even greater ability to destroy both DPPG, than their non-tagged analogues.

5 Conclusion

Mimetic compounds of natural oligomers may well serve as a valuable addition to the existing arsenal of existing drugs, as they deal with some of the inherent problems of using therapeutics based on natural compounds such as cost of production and proteolytic stability. Furthermore, even by introducing minimal perturbations to the natural design, a vast amount of modifications are made possible. Common for these modified compounds are the goal of mimicking the folding patterns of the natural proteins, to achieve protein-like functions.

Inspired by earlier work for similar foldameric compounds, we sought to obtain a better understanding of the folding propensities of β-peptoids, by synthesizing and evaluating series of monomeric model systems. Through this evaluation we saw that the identity of the side chains could be used to gain control over the rotation of the amide bond, in a similar way to that observed for α-peptoids. We also introduced alterations to the stereoelectronic properties of the backbone, which revealed a novel aromatic–thioamide interaction. It was shown that the introduction of an increased steric bulk in the backbone, rather than the side chains, could be used to impact the *cis-trans* equilibrium. These findings provide two new ways to affect the conformations of peptoidic residues, enabling a more rational design using these residues.

We next synthesized a homo-oligomer consisting of residues we found most prone to fit a helical display proposed based on DFT-calculations. A preliminary NMR-study revealed an increasing homogeneity as the oligomer was elongated. We were able to solve the X-ray crystal structure for two hexameric compounds with a free *N*-terminal amine and with an *N*-terminal acetyl group, respectively. These are the first examples of high-resolution structures of linear β-peptoid oligomers, and clearly show that these compounds form unique helical arrangements. These helices thus definitively validate the addition of β-peptoids to the already existing ensemble of foldamer designs.

The type of helix displayed by β-peptoids is unique to other peptidomimetic helices as one turn consists of exactly three residues, leaving the side chains perfectly aligned, while stretched to give a pitch of almost 10 Å. This display allows for the separation of three types of functionalities, e.g. the separation of apolar and charged side chains on two phases, and another functionality along the third. Given the excellent cell-penetrating properties of amphipathic peptoids, this setup might be highly useful for transport across membranes. However, oligomers of the same backbone carrying a different side chain did not exhibit the same homogeneity, expressing the need to investigate what substitutions are tolerated in this helical display. Given the obtained results on β-peptoid amide bond rotational behavior we have enabled the possibility of a more rational design of this and other motifs.

During the course of the Ph.D. project we also engaged in a collaboration with the laboratory of Prof. David Gidalevitz, to further elucidate the membrane interaction of cationic antimicrobial α-peptide/β-peptoid hybrid compounds. Using X-ray surface scattering techniques the interaction of two oligomers, containing different cationic moieties, and model lipid membranes mimicking Gram-positive and Gram-negative bacterial membranes, respectively, were investigated. Through these measurements we were able to obtain data on the binding interactions of the membrane mimics and our oligomeric compounds useful for future design of antimicrobial agents. Furthermore, we identified a fluorophore that allows labeling of the compound without diminishing antimicrobial activity. Such fluorophores are valuable tools for future studies of the mechanism and distribution of these compounds.

Applications of peptidomimetic compounds have been developed through the understanding of folding propensities. The investigations made throughout this project, provides fundamental knowledge on some of the important factors governing the conformational preferences of β-peptoids. Providing the first high-resolution data, we have presented the first example of a unique secondary structure available to this class of peptidomimetics. These structures validate the addition of β-peptoids to the existing peptidomimetic foldamers, expanding the structural space available to this class of compounds. The bioactivity of β-peptoids are already established, and I believe that our findings constitute an important step toward a structure based design, with novel bioactivity or enhancement of the activity towards existing targets.

6 References

(1) Lee, D.; Redfern, O.; Orengo, C. Nat. Rev. Mol. Cell Biol. 2007, 8, 995.
(2) Dill, K. A. Biochemistry 1990, 29, 7133.
(3) Schueler-Furman, O.; Wang, C.; Bradley, P.; Misura, K.; Baker, D. Science 2005, 310, 638.
(4) Hancock, R. E. W.; Sahl, H. G. Nat. Biotechnol. 2006, 24, 1551.
(5) Leader, B.; Baca, Q. J.; Golan, D. E. Nat. Rev. Drug Discovery 2008, 7, 21.
(6) Guichard, G.; Huc, I. Chem. Commun. 2011, 47, 5933.
(7) Bautista, A. D.; Craig, C. J.; Harker, E. A.; Schepartz, A. Curr. Opin. Chem. Biol. 2007, 11, 685.
(8) Hill, D. J.; Mio, M. J.; Prince, R. B.; Hughes, T. S.; Moore, J. S. Chem. Rev. 2001, 101, 3893.
(9) Horne, W. S. Expert Opin. on Drug Discovery 2011, 6, 1247.
(10) Gellman, S. H. Acc. Chem. Res. 1998, 31, 173.
(11) Olsen, C. A.; Bonke, G.; Vedel, L.; Adsersen, A.; Witt, M.; Franzyk, H.; Jaroszewski, J. W. Org. Lett. 2007, 9, 1549.
(12) Olsen, C. A.; Ziegler, H. L.; Nielsen, H. M.; Frimodt-Moller, N.; Jaroszewski, J. W.; Franzyk, H. Chembiochem 2010, 11, 1356.
(13) Vedel, L.; Bonke, G.; Foged, C.; Ziegler, H.; Franzyk, H.; Jaroszewski, J. W.; Olsen, C. A. Chembiochem 2007, 8, 1781.
(14) Venkatraman, J.; Shankaramma, S. C.; Balaram, P. Chem. Rev. 2001, 101, 3131.
(15) Wu, H. Am. J. Physiol. 1929, 90, 562.
(16) Wu, H.; Yang, E.-F. Chin. J. Physiol. 1931, 5, 301.
(17) Anson, M. L.; Mirsky, A. E. J. Gen. Physiol. 1934, 17, 393.
(18) Pauling, L.; Corey, R. B.; Branson, H. R. Proc. Natl. Acad. Sci. U. S. A. 1951, 37, 205.
(19) Pauling, L.; Corey, R. B. Proc. Natl. Acad. Sci. U. S. A. 1951, 37, 251.
(20) Barlow, D. J.; Thornton, J. M. J. Mol. Biol. 1988, 201, 601.
(21) Toniolo, C.; Benedetti, E. Trends Biochem. Sci. 1991, 16, 350.
(22) Crisma, M.; Formaggio, F.; Moretto, A.; Toniolo, C. Biopolymers 2006, 84, 3.
(23) Voet, D.; Voet, J. G. John Wiley and sons, Inc. 1995.
(24) Salemme, F. R. Prog. Biophys. Mol. Bio. 1983, 42, 95.
(25) Weatherford, D. W.; Salemme, F. R. Proc. Natl. Acad. Sci. U. S. A. 1979, 76, 19.
(26) Venkatac, C. Biopolymers 1968, 6, 1425.
(27) Toniolo, C. Crit. Rev. Biochem. 1980, 9, 1.
(28) Guzman, F.; Barberis, S.; Illanes, A. Electron. J. Biotechno. 2007, 10, 279.
(29) Merrifield, R. B. J. Am. Chem. Soc. 1963, 85, 2149.
(30) Dawson, P. E.; Muir, T. W.; Clarklewis, I.; Kent, S. B. H. Science 1994, 266, 776.
(31) Meldal, M. In Solid-Phase Peptide Synthesis; Fields, G. B., Ed.; Elsevier Academic Press Inc: San Diego, 1997; Vol. 289, p 83.
(32) Zalipsky, S.; Chang, J. L.; Albericio, F.; Barany, G. React. Polym. 1994, 22, 243.
(33) Cote, S.; MATRIX INNOVATION INC (MATR-Non-standard) COTE S (COTE-Individual), p 1687343.
(34) Garcia-Martin, F.; Quintanar-Audelo, M.; Garcia-Ramos, Y.; Cruz, L. J.; Gravel, C.; Furic, R.; Cote, S.; Tulla-Puche, J.; Albericio, F. J. Comb. Chem. 2006, 8, 213.

(35) Barlos, K.; Gatos, D.; Kallitsis, J.; Papaphotiu, G.; Sotiriu, P.; Yao, W. Q.; Schafer, W. Tet. Lett. 1989, 30, 3943.
(36) Barlos, K.; Chatzi, O.; Gatos, D.; Stavropoulos, G. Int. J. Pept. Protein Res. 1991, 37, 513.
(37) Rink, H. Tet. Lett. 1987, 28, 3787.
(38) Atherton, E.; Gait, M. J.; Sheppard, R. C.; Williams, B. J. Bioorg. Chem. 1979, 8, 351.
(39) Holmes, C. P.; Jones, D. G. J. Org. Chem. 1995, 60, 2318.
(40) Jensen, K. J.; Alsina, J.; Songster, M. F.; Vagner, J.; Albericio, F.; Barany, G. J. Am. Chem. Soc. 1998, 120, 5441.
(41) Jursic, B. S.; Zdravkovski, Z. Synth. Commun. 1993, 23, 2761.
(42) Valeur, E.; Bradley, M. Chem. Soc. Rev. 2009, 38, 606.
(43) Sheehan, J. C.; Hess, G. P. J. Am. Chem. Soc. 1955, 77, 1067.
(44) Anderson, G. W.; Callahan, F. M. J. Am. Chem. Soc. 1958, 80, 2902.
(45) Konig, W.; Geiger, R. Chem. Ber. 1970, 103, 788.
(46) Albericio, F.; Bofill, J. M.; El-Faham, A.; Kates, S. A. J. Org. Chem. 1998, 63, 9678.
(47) Carpino, L. A.; Han, G. Y. J. Am. Chem. Soc.1970, 92, 5748.
(48) Atherton, E.; Fox, H.; Harkiss, D.; Logan, C. J.; Sheppard, R. C.; Williams, B. J. J. Chem. Soc. Chem. Commun. 1978, 537.
(49) Anderson, G. W.; McGregor, A. C. J. Am. Chem. Soc.1957, 79, 6180.
(50) Isidro-Llobet, A.; Alvarez, M.; Albericio, F. Chem. Rev. 2009, 109, 2455.
(51) Hecht, S.; Huc, I. Foldamers, Structure, Properties, and Applications; WILEY-VCH, 2007.
(52) Deshayes, K.; Broene, R. D.; Chao, I.; Knobler, C. B.; Diederich, F. J. Org. Chem.1991, 56, 6787.
(53) Gange, D.; Magnus, P.; Bass, L.; Arnold, E. V.; Clardy, J. J. Am. Chem. Soc.1980, 102, 2134.
(54) Kiupel, B.; Niederalt, C.; Nieger, M.; Grimme, S.; Vogtle, F. Ang. Chem. Int. Ed. 1998, 37, 3031.
(55) Gong, B.; Zeng, H. Q.; Zhu, J.; Yuan, L. H.; Han, Y. H.; Cheng, S. Z.; Furukawa, M.; Parra, R. D.; Kovalevsky, A. Y.; Mills, J. L.; Skrzypczak-Jankun, E.; Martinovic, S.; Smith, R. D.; Zheng, C.; Szyperski, T.; Zeng, X. C. Proc. Natl. Acad. Sci. U. S. A 2002, 99, 11583.
(56) Berl, V.; Huc, I.; Khoury, R. G.; Lehn, J. M. Chem. Eur. J. 2001, 7, 2798.
(57) Wu, Z. Q.; Jiang, X. K.; Zhu, S. Z.; Li, Z. T. Org. Lett. 2004, 6, 229.
(58) Zhu, J.; Wang, X. Z.; Chen, Y. Q.; Jiang, X. K.; Chen, X. Z.; Li, Z. T. J. Org. Chem. 2004, 69, 6221.
(59) Itai, A.; Toriumi, Y.; Saito, S.; Kagechika, H.; Shudo, K. J. Am. Chem. Soc. 1992, 114, 10649.
(60) Tanatani, A.; Kagechika, H.; Azumaya, I.; Fukutomi, R.; Ito, Y.; Yamaguchi, K.; Shudo, K. Tet. Lett. 1997, 38, 4425.
(61) Tanatani, A.; Yamaguchi, K.; Azumaya, I.; Fukutomi, R.; Shudo, K.; Kagechika, H. J. Am. Chem. Soc.1998, 120, 6433.
(62) Hintermann, T.; Gademann, K.; Jaun, B.; Seebach, D. Helv. Chim. Acta 1998, 81, 983.
(63) Seebach, D.; Beck, A. K.; Bierbaum, D. J. Chem. Biodivers. 2004, 1, 1111.
(64) Gante, J. Synthesis 1989, 405.
(65) Han, H.; Janda, K. D. J. Am. Chem. Soc.1996, 118, 2539.

(66) Lee, H. J.; Ahn, I. A.; Ro, S.; Choi, K. H.; Choi, Y. S.; Lee, K. B. J. Pept. Res. 2000, 56, 35.
(67) Andre, F.; Boussard, G.; Bayeul, D.; Didierjean, C.; Aubry, A.; Marraud, M. J. Pept. Res. 1997, 49, 556.
(68) Lelais, G.; Seebach, D. Helv. Chim. Acta 2003, 86, 4152.
(69) Salaun, A.; Favre, A.; Le Grel, B.; Potel, M.; Le Grel, P. J. Org. Chem.2006, 71, 150.
(70) Salaun, A.; Potel, M.; Roisnel, T.; Gall, P.; Le Grel, P. J. Org. Chem.2005, 70, 6499.
(71) Fischer, L.; Claudon, P.; Pendem, N.; Miclet, E.; Didierjean, C.; Ennifar, E.; Guichard, G. Ang. Chem. Int. Ed. 2010, 49, 1067.
(72) Yang, D.; Ng, F. F.; Li, Z. J.; Wu, Y. D.; Chan, K. W. K.; Wang, D. P. J. Am. Chem. Soc.1996, 118, 9794.
(73) Yang, D.; Qu, J.; Li, B.; Ng, F. F.; Wang, X. C.; Cheung, K. K.; Wang, D. P.; Wu, Y. D. J. Am. Chem. Soc.1999, 121, 589.
(74) Yang, D.; Li, B.; Ng, F. F.; Yan, Y. L.; Qu, J.; Wu, Y. D. J. Org. Chem.2001, 66, 7303.
(75) Li, X.; Yang, D. Chem. Commun. 2006, 3367.
(76) Yang, D.; Zhang, D. W.; Hao, Y.; Wu, Y. D.; Luo, S. W.; Zhu, N. Y. Ang. Chem. Int. Ed. 2004, 43, 6719.
(77) Weinstock, H. H.; Mitchell, H. K.; Pratt, E. F.; Williams, R. J. J. Am. Chem. Soc.1939, 61, 1421.
(78) Perezgrau, L.; Munozguerra, S.; Subirana, J. A. Micron Microsc. Acta 1984, 15, 147.
(79) Fernandezsantin, J. M.; Munozguerra, S.; Rodriguezgalan, A.; Aymami, J.; Lloveras, J.; Subirana, J. A.; Giralt, E.; Ptak, M. Macromolecules 1987, 20, 62.
(80) Bella, J.; Aleman, C.; Fernandezsantin, J. M.; Alegre, C.; Subirana, J. A. Macromolecules 1992, 25, 5225.
(81) Lopezcarrasquero, F.; Aleman, C.; Munozguerra, S. Biopolymers 1995, 36, 263.
(82) Banerjee, A.; Balaram, P. Current Science 1997, 73, 1067.
(83) Cheng, R. P.; Gellman, S. H.; DeGrado, W. F. Chem. Rev. 2001, 101, 3219.
(84) Seebach, D.; Abele, S.; Gademann, K.; Guichard, G.; Hintermann, T.; Jaun, B.; Matthews, J. L.; Schreiber, J. V. Helv. Chim. Acta 1998, 81, 932.
(85) Appella, D. H.; Christianson, L. A.; Karle, I. L.; Powell, D. R.; Gellman, S. H. J. Am. Chem. Soc.1996, 118, 13071.
(86) Appella, D. H.; Christianson, L. A.; Klein, D. A.; Powell, D. R.; Huang, X. L.; Barchi, J. J.; Gellman, S. H. Nature 1997, 387, 381.
(87) Seebach, D.; Gademann, K.; Schreiber, J. V.; Matthews, J. L.; Hintermann, T.; Jaun, B.; Oberer, L.; Hommel, U.; Widmer, H. Helv. Chim. Acta 1997, 80, 2033.
(88) Chung, Y. J.; Christianson, L. A.; Stanger, H. E.; Powell, D. R.; Gellman, S. H. J. Am. Chem. Soc.1998, 120, 10555.
(89) Krauthauser, S.; Christianson, L. A.; Powell, D. R.; Gellman, S. H. J. Am. Chem. Soc.1997, 119, 11719.
(90) Seebach, D.; Overhand, M.; Kuhnle, F. N. M.; Martinoni, B.; Oberer, L.; Hommel, U.; Widmer, H. Helv. Chim. Acta 1996, 79, 913.
(91) Seebach, D.; Hook, D. F.; Glattli, A. Biopolymers 2006, 84, 23.

(92) Hart, S. A.; Bahadoor, A. B. F.; Matthews, E. E.; Qiu, X. Y. J.; Schepartz, A. J. Am. Chem. Soc.2003, 125, 4022.
(93) Raguse, T. L.; Lai, J. R.; Gellman, S. H. J. Am. Chem. Soc.2003, 125, 5592.
(94) Appella, D. H.; Christianson, L. A.; Karle, I. L.; Powell, D. R.; Gellman, S. H. J. Am. Chem. Soc.1999, 121, 6206.
(95) Appella, D. H.; Christianson, L. A.; Klein, D. A.; Richards, M. R.; Powell, D. R.; Gellman, S. H. J. Am. Chem. Soc.1999, 121, 7574.
(96) Hetenyi, A.; Mandity, I. M.; Martinek, T. A.; Toth, G. K.; Fulop, F. J. Am. Chem. Soc.2005, 127, 547.
(97) Claridge, T. D. W.; Goodman, J. M.; Moreno, A.; Angus, D.; Barker, S. F.; Taillefumier, C.; Watterson, M. P.; Fleet, G. W. J. Tet. Lett. 2001, 42, 4251.
(98) Doerksen, R. J.; Chen, B.; Yuan, J.; Winkler, J. D.; Klein, M. L. Chem. Commun. 2003, 2534.
(99) Mathad, R. I.; Gessier, F.; Seebach, D.; Jaun, B. Helv. Chim. Acta 2005, 88, 266.
(100) Barchi, J. J.; Huang, X. L.; Appella, D. H.; Christianson, L. A.; Durell, S. R.; Gellman, S. H. J. Am. Chem. Soc.2000, 122, 2711.
(101) Appella, D. H.; Barchi, J. J.; Durell, S. R.; Gellman, S. H. J. Am. Chem. Soc.1999, 121, 2309.
(102) Seebach, D.; Ciceri, P. E.; Overhand, M.; Jaun, B.; Rigo, D.; Oberer, L.; Hommel, U.; Amstutz, R.; Widmer, H. Helv. Chim. Acta 1996, 79, 2043.
(103) Seebach, D.; Schreiber, J. V.; Abele, S.; Daura, X.; van Gunsteren, W. F. Helv. Chim. Acta 2000, 83, 34.
(104) Appella, D. H.; LePlae, P. R.; Raguse, T. L.; Gellman, S. H. J. Org. Chem.2000, 65, 4766.
(105) Arvidsson, P. I.; Rueping, M.; Seebach, D. Chem. Commun. 2001, 649.
(106) Cheng, R. P.; DeGrado, W. F. J. Am. Chem. Soc.2001, 123, 5162.
(107) Abele, S.; Guichard, G.; Seebach, D. Helv. Chim. Acta 1998, 81, 2141.
(108) Wang, X. F.; Espinosa, J. F.; Gellman, S. H. J. Am. Chem. Soc.2000, 122, 4821.
(109) Lee, H. S.; Syud, F. A.; Wang, X. F.; Gellman, S. H. J. Am. Chem. Soc.2001, 123, 7721.
(110) Seebach, D.; Abele, S.; Gademann, K.; Jaun, B. Ang. Chem. Int. Ed. 1999, 38, 1595.
(111) Huck, B. R.; Langenhan, J. M.; Gellman, S. H. Org. Lett. 1999, 1, 1717.
(112) Abele, S.; Vogtli, K.; Seebach, D. Helv. Chim. Acta 1999, 82, 1539.
(113) Hamuro, Y.; Schneider, J. P.; DeGrado, W. F. J. Am. Chem. Soc.1999, 121, 12200.
(114) Arvidsson, P. I.; Frackenpohl, J.; Ryder, N. S.; Liechty, B.; Petersen, F.; Zimmermann, H.; Camenisch, G. P.; Woessner, R.; Seebach, D. Chembiochem 2001, 2, 771.
(115) Wender, P. A.; Mitchell, D. J.; Pattabiraman, K.; Pelkey, E. T.; Steinman, L.; Rothbard, J. B. Proc. Natl. Acad. Sci. U. S. A 2000, 97, 13003.
(116) Umezawa, N.; Gelman, M. A.; Haigis, M. C.; Raines, R. T.; Gellman, S. H. J. Am. Chem. Soc.2002, 124, 368.
(117) Rueping, M.; Mahajan, Y.; Sauer, M.; Seebach, D. Chembiochem 2002, 3, 257.
(118) Werder, M.; Hauser, H.; Abele, S.; Seebach, D. Helv. Chim. Acta 1999, 82, 1774.

(119) Lind, R.; Greenhow, D.; Perry, S.; Kimmerlin, T.; Seebach, D. Chem. Biodivers. 2004, 1, 1391.
(120) Wiegand, H.; Wirz, B.; Schweitzer, A.; Gross, G.; Perez, M. I. R.; Andres, H.; Kimmerlin, T.; Rueping, M.; Seebach, D. Chem. Biodivers. 2004, 1, 1812.
(121) Wiegand, H.; Wirz, B.; Schweitzer, A.; Camenisch, G. P.; Perez, M. I. R.; Gross, G.; Woessner, R.; Voges, R.; Arvidsson, P. I.; Frackenpohl, J.; Seebach, D. Biopharm. Drug Dispos. 2002, 23, 251.
(122) Gallo, S. A.; Finnegan, C. M.; Viard, M.; Raviv, Y.; Dimitrov, A.; Rawat, S. S.; Puri, A.; Durell, S.; Blumenthal, R. BBA. Biomembranes 2003, 1614, 36.
(123) Stephens, O. M.; Kim, S.; Welch, B. D.; Hodsdon, M. E.; Kay, M. S.; Schepartz, A. J. Am. Chem. Soc.2005, 127, 13126.
(124) Weissenhorn, W.; Dessen, A.; Harrison, S. C.; Skehel, J. J.; Wiley, D. C. Nature 1997, 387, 426.
(125) Bautista, A. D.; Stephens, O. M.; Wang, L. G.; Domaoal, R. A.; Anderson, K. S.; Schepartz, A. Bioorg. Med. Chem. Lett. 2009, 19, 3736.
(126) Johnson, L. M.; Horne, W. S.; Gellman, S. H. J. Am. Chem. Soc.2011, 133, 10038.
(127) Horne, W. S.; Johnson, L. M.; Ketas, T. J.; Klasse, P. J.; Lu, M.; Moore, J. P.; Gellman, S. H. Proc. Natl. Acad. Sci. U. S. A 2009, 106, 14751.
(128) Vousden, K. H.; Lane, D. P. Nat. Rev. Mol. Cell Biol. 2007, 8, 275.
(129) Murray, J. K.; Gellman, S. H. Biopolymers 2007, 88, 657.
(130) Kussie, P. H.; Gorina, S.; Marechal, V.; Elenbaas, B.; Moreau, J.; Levine, A. J.; Pavletich, N. P. Science 1996, 274, 948.
(131) Kritzer, J. A.; Lear, J. D.; Hodsdon, M. E.; Schepartz, A. J. Am. Chem. Soc.2004, 126, 9468.
(132) Harker, E. A.; Daniels, D. S.; Guarracino, D. A.; Schepartz, A. Bioorg. Med. Chem. 2009, 17, 2038.
(133) Michel, J.; Harker, E. A.; Tirado-Rives, J.; Jorgensen, W. L.; Schepartz, A. J. Am. Chem. Soc.2009, 131, 6356.
(134) Harker, E. A.; Schepartz, A. Chembiochem 2009, 10, 990.
(135) Bautista, A. D.; Appelbaum, J. S.; Craig, C. J.; Michel, J.; Schepartz, A. J. Am. Chem. Soc.2010, 132, 2904.
(136) Adams, J. M.; Cory, S. Oncogene 2007, 26, 1324.
(137) Sattler, M.; Liang, H.; Nettesheim, D.; Meadows, R. P.; Harlan, J. E.; Eberstadt, M.; Yoon, H. S.; Shuker, S. B.; Chang, B. S.; Minn, A. J.; Thompson, C. B.; Fesik, S. W. Science 1997, 275, 983.
(138) Sadowsky, J. D.; Schmitt, M. A.; Lee, H. S.; Umezawa, N.; Wang, S. M.; Tomita, Y.; Gellman, S. H. J. Am. Chem. Soc.2005, 127, 11966.
(139) Sadowsky, J. D.; Fairlie, W. D.; Hadley, E. B.; Lee, H. S.; Umezawa, N.; Nikolovska-Coleska, Z.; Wang, S. M.; Huang, D. C. S.; Tomita, Y.; Gellman, S. H. J. Am. Chem. Soc.2007, 129, 139.
(140) Lee, E. F.; Sadowsky, J. D.; Smith, B. J.; Czabotar, P. E.; Peterson-Kaufman, K. J.; Colman, P. M.; Gellman, S. H.; Fairlie, W. D. Ang. Chem. Int. Ed. 2009, 48, 4318.
(141) Murray, J. K.; Sadowsky, J. D.; Scalf, M.; Smith, L. M.; Tomita, Y.; Gellman, S. H. J. Comb. Chem. 2008, 10, 204.
(142) Sadowsky, J. D.; Murray, J. K.; Tomita, Y.; Gellman, S. H. Chembiochem 2007, 8, 903.
(143) Horne, W. S.; Boersma, M. D.; Windsor, M. A.; Gellman, S. H. Ang. Chem. Int. Ed. 2008, 47, 2853.

(144) Lee, E. F.; Smith, B. J.; Horne, W. S.; Mayer, K. N.; Evangelista, M.; Colman, P. M.; Gellman, S. H.; Fairlie, W. D. Chembiochem 2011, 12, 2025.
(145) Gura, T. Science 2001, 291, 2068.
(146) Oren, Z.; Shai, Y. Biopolymers 1998, 47, 451.
(147) Tossi, A.; Sandri, L.; Giangaspero, A. Biopolymers 2000, 55, 4.
(148) Porter, E. A.; Weisblum, B.; Gellman, S. H. J. Am. Chem. Soc.2002, 124, 7324.
(149) Heitz, F.; Morris, M. C.; Divita, G. British J. Pharmacol. 2009, 157, 195.
(150) Foged, C.; Nielsen, H. M. Expert Opin. Drug Deliv. 2008, 5, 105.
(151) Potocky, T. B.; Menon, A. K.; Gellman, S. H. J. Biol. Chem. 2003, 278, 50188.
(152) Seebach, D.; Namoto, K.; Mahajan, Y. R.; Bindschadler, P.; Sustmann, R.; Kirsch, M.; Ryder, N. S.; Weiss, M.; Sauer, M.; Roth, C.; Werner, S.; Beer, H. D.; Munding, C.; Walde, P.; Voser, M. Chem. Biodivers. 2004, 1, 65.
(153) Potocky, T. B.; Menon, A. K.; Gellman, S. H. J. Am. Chem. Soc.2005, 127, 3686.
(154) Potocky, T. B.; Silvius, J.; Menon, A. K.; Gellman, S. H. Chembiochem 2007, 8, 917.
(155) Simon, R. J.; Kania, R. S.; Zuckermann, R. N.; Huebner, V. D.; Jewell, D. A.; Banville, S.; Ng, S.; Wang, L.; Rosenberg, S.; Marlowe, C. K.; Spellmeyer, D. C.; Tan, R. Y.; Frankel, A. D.; Santi, D. V.; Cohen, F. E.; Bartlett, P. A. Proc. Natl. Acad. Sci. U. S. A 1992, 89, 9367.
(156) Zuckermann, R. N.; Kerr, J. M.; Kent, S. B. H.; Moos, W. H. J. Am. Chem. Soc. 1992, 114, 10646.
(157) Culf, A. S.; Ouellette, R. J. Molecules 2010, 15, 5282.
(158) Zuckermann, R. N.; Martin, E. J.; Spellmeyer, D. C.; Stauber, G. B.; Shoemaker, K. R.; Kerr, J. M.; Figliozzi, G. M.; Goff, D. A.; Siani, M. A.; Simon, R. J.; Banville, S. C.; Brown, E. G.; Wang, L.; Richter, L. S.; Moos, W. H. J. Med. Chem. 1994, 37, 2678.
(159) Liu, B.; Alluri, P. G.; Yu, P.; Kodadek, T. J. Am. Chem. Soc.2005, 127, 8254.
(160) Miller, S. M.; Simon, R. J.; Ng, S.; Zuckermann, R. N.; Kerr, J. M.; Moos, W. H. Bioorg. Med. Chem. Lett. 1994, 4, 2657.
(161) Kwon, Y. U.; Kodadek, T. J. Am. Chem. Soc.2007, 129, 1508.
(162) Chongsiriwatana, N. P.; Patch, J. A.; Czyzewski, A. M.; Dohm, M. T.; Ivankin, A.; Gidalevitz, D.; Zuckermann, R. N.; Barron, A. E. Proc. Natl. Acad. Sci. U. S. A 2008, 105, 2794.
(163) Fowler, S. A.; Stacy, D. M.; Blackwell, H. E. Org. Lett. 2008, 10, 2329.
(164) Schroder, T.; Schmitz, K.; Niemeier, N.; Balaban, T. S.; Krug, H. F.; Schepers, U.; Brase, S. Bioconjugate Chem. 2007, 18, 342.
(165) Levine, P. M.; Imberg, K.; Garabedian, M. J.; Kirshenbaum, K. J. Am. Chem. Soc.2012, 134, 6912.
(166) Fischer, G. Chem. Soc. Rev. 2000, 29, 119.
(167) Armand, P.; Kirshenbaum, K.; Goldsmith, R. A.; Farr-Jones, S.; Barron, A. E.; Truong, K. T. V.; Dill, K. A.; Mierke, D. F.; Cohen, F. E.; Zuckermann, R. N.; Bradley, E. K. Proc. Natl. Acad. Sci. U. S. A 1998, 95, 4309.
(168) Wu, C. W.; Kirshenbaum, K.; Sanborn, T. J.; Patch, J. A.; Huang, K.; Dill, K. A.; Zuckermann, R. N.; Barron, A. E. J. Am. Chem. Soc. 2003, 125, 13525.
(169) Wu, C. W.; Sanborn, T. J.; Zuckermann, R. N.; Barron, A. E. J. Am. Chem. Soc. 2001, 123, 2958.

(170) Wu, C. W.; Sanborn, T. J.; Huang, K.; Zuckermann, R. N.; Barron, A. E. J. Am. Chem. Soc. 2001, 123, 6778.
(171) Huang, K.; Wu, C. W.; Sanborn, T. J.; Patch, J. A.; Kirshenbaum, K.; Zuckermann, R. N.; Barron, A. E.; Radhakrishnan, I. J. Am. Chem. Soc. 2006, 128, 1733.
(172) Shin, S. B. Y.; Yoo, B.; Todaro, L. J.; Kirshenbaum, K. J. Am. Chem. Soc. 2007, 129, 3218.
(173) Vaz, B.; Brunsveld, L. Org. Biomol. Chem. 2008, 6, 2988.
(174) Holub, J. M.; Jang, H. J.; Kirshenbaum, K. Org. Lett. 2007, 9, 3275.
(175) Shah, N. H.; Butterfoss, G. L.; Nguyen, K.; Yoo, B.; Bonneau, R.; Rabenstein, D. L.; Kirshenbaum, K. J. Am. Chem. Soc. 2008, 130, 16622.
(176) Gorske, B. C.; Stringer, J. R.; Bastian, B. L.; Fowler, S. A.; Blackwell, H. E. J. Am. Chem. Soc. 2009, 131, 16555.
(177) Gorske, B. C.; Bastian, B. L.; Geske, G. D.; Blackwell, H. E. J. Am. Chem. Soc. 2007, 129, 8928.
(178) Roy, O.; Caumes, C.; Esvan, Y.; Didierjean, C.; Faure, S.; Taillefumier, C. Org. Lett. 2013, 15, 2246.
(179) Caumes, C.; Roy, O.; Faure, S.; Taillefumier, C. J. Am. Chem. Soc. 2012, 134, 9553.
(180) Toth, G.; Kover, K. E.; Murphy, R. F.; Lovas, S. J. Phys. Chem. B 2004, 108, 9287.
(181) Gamez, P.; Mooibroek, T. J.; Teat, S. J.; Reedijk, J. Acc. Chem. Res. 2007, 40, 435.
(182) Egli, M.; Sarkhel, S. Acc. Chem. Res. 2007, 40, 197.
(183) Pedersen, B. F.; Pedersen, B. Tet. Lett. 1965, 2995.
(184) Hinderaker, M. P.; Raines, R. T. Protein Sci. 2003, 12, 1188.
(185) DeRider, M. L.; Wilkens, S. J.; Waddell, M. J.; Bretscher, L. E.; Weinhold, F.; Raines, R. T.; Markley, J. L. J. Am. Chem. Soc. 2002, 124, 2497.
(186) Burgi, H. B.; Dunitz, J. D.; Shefter, E. J. Am. Chem. Soc. 1973, 95, 5065.
(187) Choudhary, A.; Gandla, D.; Krow, G. R.; Raines, R. T. J. Am. Chem. Soc. 2009, 131, 7244.
(188) Bowden, Z. S.; Kufe, T. A.; Nelson, R. C.; Gorske, B. C. Abstr. Pap. Am. Chem. Soc. 2013, 245.
(189) Butterfoss, G. L.; Renfrew, P. D.; Kuhlman, B.; Kirshenbaum, K.; Bonneau, R. J. Am. Chem. Soc. 2009, 131, 16798.
(190) Butterfoss, G. L.; Yoo, B.; Jaworski, J. N.; Chorny, I.; Dill, K. A.; Zuckermann, R. N.; Bonneau, R.; Kirshenbaum, K.; Voelz, V. A. Proc. Natl. Acad. Sci. U. S. A 2012, 109, 14320.
(191) Stringer, J. R.; Crapster, J. A.; Guzei, I. A.; Blackwell, H. E. J. Am. Chem. Soc. 2011, 133, 15559.
(192) Crapster, J. A.; Guzei, I. A.; Blackwell, H. E. Ang. Chem. Int. Ed. 2013, 52, 5079.
(193) Goodson, B.; Ehrhardt, A.; Ng, S.; Nuss, J.; Johnson, K.; Giedlin, M.; Yamamoto, R.; Moos, W. H.; Krebber, A.; Ladner, M.; Giacona, M. B.; Vitt, C.; Winter, J. Antimicrob. Chemother 1999, 43, 1429.
(194) Patch, J. A.; Barron, A. E. J. Am. Chem. Soc.2003, 125, 12092.
(195) Tan, N. C.; Yu, P.; Kwon, Y. U.; Kodadek, T. Bioorg. Med. Chem. 2008, 16, 5853.
(196) Schroder, T.; Niemeier, N.; Afonin, S.; Ulrich, A. S.; Krug, H. F.; Brase, S. J. Med. Chem. 2008, 51, 376.

(197) Sternberg, U.; Birtalan, E.; Jakovkin, I.; Luy, B.; Schepers, U.; Brase, S.; Muhle-Goll, C. Org. Biomol. Chem. 2013, 11, 640.
(198) Unciti-Broceta, A.; Diezmann, F.; Ou-Yang, C. Y.; Fara, M. A.; Bradley, M. Bioorg. Med. Chem. 2009, 17, 959.
(199) Dhaliwal, K.; Escher, G.; Unciti-Broceta, A.; McDonald, N.; Simpson, A. J.; Haslett, C.; Bradley, M. Medchemcomm 2011, 2, 1050.
(200) Palleboina, D.; Waring, A. J.; Notter, R. H.; Booth, V.; Morrow, M. Eur. Biophys. J. Biophy. 2012, 41, 755.
(201) Seurynck-Servoss, S. L.; Dohm, M. T.; Barron, A. E. Biochemistry 2006, 45, 11809.
(202) Hara, T.; Durell, S. R.; Myers, M. C.; Appella, D. H. J. Am. Chem. Soc. 2006, 128, 1995.
(203) Elgersma, R. C.; Mulder, G. E.; Kruijtzer, J. A. W.; Posthuma, G.; Rijkers, D. T. S.; Liskamp, R. M. J. Bioorg. Med. Chem. Lett. 2007, 17, 1837.
(204) Fowler, S. A.; Blackwell, H. E. Org. Biomol. Chem. 2009, 7, 1508.
(205) Hamper, B. C.; Kolodziej, S. A.; Scates, A. M.; Smith, R. G.; Cortez, E. J. Org. Chem.1998, 63, 708.
(206) Norgren, A. S.; Zhang, S. D.; Arvidsson, P. I. Org. Lett. 2006, 8, 4533.
(207) Olsen, C. A.; Lambert, M.; Witt, M.; Franzyk, H.; Jaroszewski, J. W. Amino Acids 2008, 34, 465.
(208) Roy, O.; Faure, S.; Thery, V.; Didierjean, C.; Taillefumier, C. Org. Lett. 2008, 10, 921.
(209) Hjelmgaard, T.; Faure, S.; Caumes, C.; De Santis, E.; Edwards, A. A.; Taillefumier, C. Org. Lett. 2009, 11, 4100.
(210) De Santis, E.; Hjelmgaard, T.; Faure, S.; Roy, O.; Didierjean, C.; Alexander, B. D.; Siligardi, G.; Hussain, R.; Javorfi, T.; Edwards, A. A.; Taillefumier, C. Amino Acids 2011, 41, 663.
(211) Caumes, C.; Fernandes, C.; Roy, O.; Hjelmgaard, T.; Wenger, E.; Didierjean, C.; Taillefumier, C.; Faure, S. Org. Lett. 2013, 15, 3626.
(212) De Santis, E.; Hjelmgaard, T.; Caumes, C.; Faure, S.; Alexander, B. D.; Holder, S. J.; Siligardi, G.; Taillefumier, C.; Edwards, A. A. Org. Biomol. Chem. 2012, 10, 1108.
(213) Allred, A. L. J. Inorg. Nucl. Chem. 1961, 17, 215.
(214) Pedersen, B. S.; Scheibye, S.; Nilsson, N. H.; Lawesson, S. O. Bull. Soc. Chim. Belg. 1978, 87, 223.
(215) Scheibye, S.; Pedersen, B. S.; Lawesson, S. O. Bull. Soc. Chim. Belg. 1978, 87, 229.
(216) Jesberger, M.; Davis, T. P.; Barner, L. Synthesis 2003, 1929.
(217) Hodges, J. A.; Raines, R. T. Org. Lett. 2006, 8, 4695.
(218) Baldauf, C.; Gunther, R.; Hofmann, H. J. Phys. Biol. 2006, 3, S1.
(219) Choudhary, A.; Fry, C. G.; Raines, R. T. Arkivoc 2010, 251.
(220) Bartlett, G. J.; Choudhary, A.; Raines, R. T.; Woolfson, D. N. Nat. Chem. Biol. 2010, 6, 615.
(221) Hamper, B. C.; Kesselring, A. S. In Solid-Phase Organic Syntheses; John Wiley & Sons, Inc.: 2001, p 55.
(222) Jahnsen, R. D.; Frimodt-Moller, N.; Franzyk, H. J. Med. Chem. 2012, 55, 7253.
(223) Seebach, D.; Sifferlen, T.; Mathieu, P. A.; Hane, A. M.; Krell, C. M.; Bierbaum, D. J.; Abele, S. Helv. Chim. Acta 2000, 83, 2849.

(224) Glattli, A.; Daura, X.; Seebach, D.; van Gunsteren, W. F. J. Am. Chem. Soc.2002, 124, 12972.
(225) Jensen, U. S.; Skjot-Rasmussen, L.; Olsen, S. S.; Frimodt-Moller, N.; Hammerum, A. M.; Grp, D. S. J. Antimicrob. Chemother. 2009, 63, 812.
(226) Fischbach, M. A.; Walsh, C. T. Science 2009, 325, 1089.
(227) Livermore, D. M.; British Soc, A. J. Antimicrob. Chemother. 2011, 66, 1941.
(228) Yeung, A. T. Y.; Gellatly, S. L.; Hancock, R. E. W. Cell Mol. Life Sci. 2011, 68, 2161.
(229) Maroti, G.; Kereszt, A.; Kondorosi, E.; Mergaert, P. Res. Microbiol. 2011, 162, 363.
(230) Zasloff, M. Nature 2002, 415, 389.
(231) Hancock, R. E. W.; Diamond, G. Trends Microbiol. 2000, 8, 402.
(232) Hancock, R. E.; Falla, T.; Brown, M. Adv. microb. physiol. 1995, 37, 135.
(233) Perron, G. G.; Zasloff, M.; Bell, G. Proc. R. Soc. London B, 2006, 273, 251.
(234) Hancock, R. E. W. Lancet 1997, 349, 418.
(235) Hancock, R. E. W.; Chapple, D. S. Antimicrob. Agents Chemother. 1999, 43, 1317.
(236) Boman, H. G. J. Int. Med. 2003, 254, 197.
(237) Brogden, K. A. Nat. Rev. Microbiol. 2005, 3, 238.
(238) Harris, F.; Dennison, S. R.; Phoenix, D. A. Curr. Protein Pept. Sci. 2009, 10, 585.
(239) Vizioli, J.; Salzet, M. Trends Pharmacol. Sci. 2002, 23, 494.
(240) Patil, A.; Hughes, A. L.; Zhang, G. L. Physiol. Genomics 2004, 20, 1.
(241) Hancock, R. E. W.; Lehrer, R. Trends Biotechnol 1998, 16, 82.
(242) Powers, J. P. S.; Hancock, R. E. W. Peptides 2003, 24, 1681.
(243) Javadpour, M. M.; Eilers, M.; Groesbeek, M.; Smith, S. O. Biophys. J. 1999, 77, 1609.
(244) Friedrich, C.; Scott, M. G.; Karunaratne, N.; Yan, H.; Hancock, R. E. W. Antimicrob. Agents Chemother. 1999, 43, 1542.
(245) McPhee, J. B.; Scott, M. G.; Hancock, R. E. W. Comb. Chem. High Throughput Screening 2005, 8, 257.
(246) Zhang, L. J.; Rozek, A.; Hancock, R. E. W. J. Biol. Chem. 2001, 276, 35714.
(247) Pasupuleti, M.; Schmidtchen, A.; Malmsten, M. Crit. Rev. Biotechnol. 2012, 32, 143.
(248) Shai, Y. Biopolymers 2002, 66, 236.
(249) Boman, H. G. Annu. Rev. Immunol. 1995, 13, 61.
(250) Teixeira, V.; Feio, M. J.; Bastos, M. Prog. Lipid Res. 2012, 51, 149.
(251) Lehrer, R. I.; Barton, A.; Daher, K. A.; Harwig, S. S. L.; Ganz, T.; Selsted, M. E. J. Clin. Invest. 1989, 84, 553.
(252) Wu, M. H.; Hancock, R. E. W. Antimicrob. Agents Chemother. 1999, 43, 1274.
(253) Scheller, A.; Oehlke, J.; Wiesner, B.; Dathe, M.; Krause, E.; Beyermann, M.; Melzig, M.; Bienert, M. J. Pept. Sci. 1999, 5, 185.
(254) Epand, R. M.; Epand, R. F. J. Pept. Sci. 2011, 17, 298.
(255) Verkleij, A. J.; Zwaal, R. F. A.; Roelofse.B; Comfuriu.P; Kastelij.D; Vandeene.Ll Biochim. Biophys. Acta 1973, 323, 178.
(256) Silhavy, T. J.; Kahne, D.; Walker, S. Cold Spring Harbor Perspectives in Biology 2010, 2.
(257) Peschel, A.; Collins, L. V. Peptides 2001, 22, 1651.
(258) Hancock, R. E. W. Trends Microbiol. 1997, 5, 37.

(259) Cassone, M.; Otvos, L. Expert Rev Anti Infect. Ther. 2010, 8, 703.
(260) Jenssen, H.; Hamill, P.; Hancock, R. E. W. Clin. Microbiol. Rev. 2006, 19, 491.
(261) Wu, M. H.; Maier, E.; Benz, R.; Hancock, R. E. W. Biochemistry 1999, 38, 7235.
(262) Hale, J. D.; Hancock, R. E. Expert Rev. Anti Infect. Ther. 2007, 5, 951.
(263) Ludtke, S. J.; He, K.; Heller, W. T.; Harroun, T. A.; Yang, L.; Huang, H. W. Biochemistry 1996, 35, 13723.
(264) Ehrenstein, G.; Lecar, H. Q. Rev. Biophys. 1977, 10, 1.
(265) Kordel, M.; Benz, R.; Sahl, H. G. J. Bacteriol. 1988, 170, 84.
(266) Shai, Y. Trends Biochem. Sci. 1995, 20, 460.
(267) Zhang, L. J.; Scott, M. G.; Yan, H.; Mayer, L. D.; Hancock, R. E. W. Biochemistry 2000, 39, 14504.
(268) Park, C. B.; Kim, H. S.; Kim, S. C. Biochem. Biophys. Res. Commun. 1998, 244, 253.
(269) Patrzykat, A.; Friedrich, C. L.; Zhang, L. J.; Mendoza, V.; Hancock, R. E. W. Antimicrob. Agents Chemother. 2002, 46, 605.
(270) Subbalakshmi, C.; Sitaram, N. Fems Microbiol. Lett. 1998, 160, 91.
(271) Friedrich, C. L.; Rozek, A.; Patrzykat, A.; Hancock, R. E. W. J. Biol. Chem. 2001, 276, 24015.
(272) Kragol, G.; Lovas, S.; Varadi, G.; Condie, B. A.; Hoffmann, R.; Otvos, L. Biochemistry 2001, 40, 3016.
(273) Otvos, L.; O, I.; Rogers, M. E.; Consolvo, P. J.; Condie, B. A.; Lovas, S.; Bulet, P.; Blaszczyk-Thurin, M. Biochemistry 2000, 39, 14150.
(274) Boehr, D. D.; Draker, K. A.; Koteva, K.; Bains, M.; Hancock, R. E.; Wright, G. D. Chem. Biol. 2003, 10, 189.
(275) Brotz, H.; Bierbaum, G.; Reynolds, P. E.; Sahl, H. G. Eur. J. Biochem. 1997, 246, 193.
(276) Steinberg, D. A.; Hurst, M. A.; Fujii, C. A.; Kung, A. H. C.; Ho, J. F.; Cheng, F. C.; Loury, D. J.; Fiddes, J. C. Antimicrob. Agents Chemother. 1997, 41, 1738.
(277) Zhang, L. J.; Parente, J.; Harris, S. A.; Woods, D. E.; Hancock, R. E. W.; Falla, T. J. Antimicrob. Chemother 2005, 49, 2921.
(278) Porter, E. A.; Wang, X. F.; Lee, H. S.; Weisblum, B.; Gellman, S. H. Nature 2000, 404, 565.
(279) Liu, D. H.; DeGrado, W. F. J. Am. Chem. Soc.2001, 123, 7553.
(280) Arvidsson, P. I.; Ryder, N. S.; Weiss, H. M.; Gross, G.; Kretz, O.; Woessner, R.; Seebach, D. Chembiochem 2003, 4, 1345.
(281) De Pol, S.; Zorn, C.; Klein, C. D.; Zerbe, O.; Reiser, O. Ang. Chem. Int. Ed. 2004, 43, 511.
(282) Hayen, A.; Schmitt, M. A.; Ngassa, F. N.; Thomasson, K. A.; Gellman, S. H. Ang. Chem. Int. Ed. 2004, 43, 505.
(283) Schmitt, M. A.; Weisblum, B.; Gellman, S. H. J. Am. Chem. Soc.2004, 126, 6848.
(284) Epand, R. F.; Schmitt, M. A.; Gellman, S. H.; Epand, R. M. BBA. Biomembranes 2006, 1758, 1343.
(285) Epand, R. F.; Schmitt, M. A.; Gellman, S. H.; Sen, A.; Auger, M.; Hughes, D. W.; Epand, R. M. Mol. Membr. Biol. 2005, 22, 457.
(286) Arvidsson, P. I.; Ryder, N. S.; Weiss, H. M.; Hook, D. F.; Escalante, J.; Seebach, D. Chem. Biodivers. 2005, 2, 401.

(287) Schmitt, M. A.; Weisblum, B.; Gellman, S. H. J. Am. Chem. Soc. 2007, 129, 417.
(288) Olsen, C. A. Chembiochem 2010, 11, 152.
(289) Shankaramma, S. C.; Moehle, K.; James, S.; Vrijbloed, J. W.; Obrecht, D.; Robinson, J. A. Chem. Commun. 2003, 1842.
(290) Zhu, W. L.; Song, Y. M.; Park, Y.; Park, K. H.; Yang, S. T.; Kim, J. I.; Park, I. S.; Hahm, K. S.; Shin, S. Y. BBA. Biomembranes 2007, 1768, 1506.
(291) Shuey, S. W.; Delaney, W. J.; Shah, M. C.; Scialdone, M. A. Bioorg. Med. Chem. Lett. 2006, 16, 1245.
(292) Foged, C.; Franzyk, H.; Bahrami, S.; Frokjaer, S.; Jaroszewski, J. W.; Nielsen, H. M.; Olsen, C. A. BBA. Biomembranes 2008, 1778, 2487.
(293) Bonke, G.; Vedel, L.; Witt, M.; Jaroszewski, J. W.; Olsen, C. A.; Franzyk, H. Synthesis 2008, 2381.
(294) Hein-Kristensen, L.; Knapp, K. M.; Franzyk, H.; Gram, L. BMC Microbiol. 2011, 11.
(295) Chan, W. C.; Bycroft, B. W.; Evans, D. J.; White, P. D. J. Chem. Soc. Chem. Commun. 1995, 2209.
(296) Diaz-Mochon, J. J.; Bialy, L.; Bradley, M. Org. Lett. 2004, 6, 1127.
(297) Bernatowicz, M. S.; Wu, Y. L.; Matsueda, G. R. Tet. Lett. 1993, 34, 3389.
(298) Gidalevitz, D.; Ishitsuka, Y. J.; Muresan, A. S.; Konovalov, O.; Waring, A. J.; Lehrer, R. I.; Lee, K. Y. C. Proc. Natl. Acad. Sci. U. S. A 2003, 100, 6302.
(299) Ivankin, A.; Livne, L.; Mor, A.; Caputo, G. A.; DeGrado, W. F.; Meron, M.; Lin, B.; Gidalevitz, D. Ang. Chem. Int. Ed. 2010, 49, 8462.
(300) Neville, F.; Cahuzac, M.; Konovalov, O.; Ishitsuka, Y.; Lee, K. Y. C.; Kuzmenko, I.; Kale, G. M.; Gidalevitz, D. Biophys. J. 2006, 90, 1275.
(301) Neville, F.; Ishitsuka, Y.; Hodges, C. S.; Konovalov, O.; Waring, A. J.; Lehrer, R.; Lee, K. Y. C.; Gidalevitz, D. Soft Matter 2008, 4, 1665.
(302) Whitehouse, C.; Gidalevitz, D.; Cahuzac, M.; Koeppe, R. E.; Nelson, A. Langmuir 2004, 20, 9291.
(303) Schalke, M.; Losche, M. Adv. Colloid Interface Sci. 2000, 88, 243.

7 Appendix

"Cis−Trans Amide Bond Rotamers in β-Peptoids and Peptoids: Evaluation of Stereoelectronic Effects in Backbone and Side Chains"
Jonas S. Laursen, Jens Engel-Andreasen, Peter Fristrup, Pernille Harris, and Christian A. Olsen. *J. Am. Chem. Soc.* **2013**, *135*, 2835

"*Trianguler Prism-Shaped Helices—Synthesis and StructuralDetermination of β-Peptoid Oligomers"*
Jonas S. Laursen, Pernille Harris, and Christian A. Olsen. *In preparation*

"*Guanidino Groups Greatly Enhance the Action of Antimicrobial Peptidomimetics Against Lipid Monolayers Mimicking Gram-positive Bacteria Membranes"*
Konstantin Andreev, Christopher Bianchi, Jonas S. Laursen, Line Hein-Kristensen, Lone Gram, Ivan Kuzmenko, Christian A. Olsen, David Gidalevitz. *In preparation.*

JACS
JOURNAL OF THE AMERICAN CHEMICAL SOCIETY

Article

pubs.acs.org/JACS

Cis–Trans Amide Bond Rotamers in β-Peptoids and Peptoids: Evaluation of Stereoelectronic Effects in Backbone and Side Chains

Jonas S. Laursen, Jens Engel-Andreasen, Peter Fristrup, Pernille Harris, and Christian A. Olsen*

Department of Chemistry, Technical University of Denmark, Kemitorvet 207, DK-2800, Kongens Lyngby, Denmark

Supporting Information

ABSTRACT: Non-natural peptide analogs have significant potential for the development of new materials and pharmacologically active ligands. One such architecture, the β-peptoids (N-alkyl-β-alanines), has found use in a variety of biologically active compounds but has been sparsely studied with respect to folding propensity. Thus, we here report an investigation of the effect of structural variations on the *cis–trans* amide bond rotamer equilibria in a selection of monomer model systems. In addition to various side chain effects, which correlated well with previous studies of α-peptoids, we present the synthesis and investigation of *cis–trans* isomerism in the first examples of peptoids and β-peptoids containing thioamide bonds as well as trifluoroacetylated peptoids and β-peptoids. These systems revealed an increase in the preference for *cis*-amides as compared to their parent compounds and thus provide novel strategies for affecting the folding of peptoid constructs. By using NMR spectroscopy, X-ray crystallographic analysis, and density functional theory calculations, we present evidence for the presence of thioamide–aromatic interactions through C_{sp^2}–H···S_{amide} hydrogen bonding, which stabilize certain peptoid conformations.

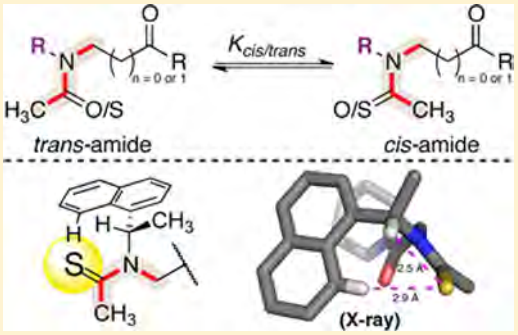

INTRODUCTION

The 20 canonical α-amino acids constitute the fundamental set of building blocks necessary for human ribosomal synthesis of the major class of biopolymers comprised of proteins and peptides. In traditional medicinal chemistry, this class of compounds has not been considered suitable for drug development, due to susceptibility to proteolytic degradation in cellular environments and often poor cell permeability properties. Nevertheless, recent tendencies in the pharmaceutical industry have revealed an increased interest in the development of so-called biologics. This may, at least in part, be due to the successful approval and marketing of several monoclonal antibodies as therapeutics during the past decade. In order to circumvent the inherent stability problems, however, extensive research in the field of peptidomimetic designs has been undertaken. In addition to the nature of the functional groups themselves, bioactive α-peptides realize their high potency and selectivity due to stabilized secondary structure formation, which displays these functionalities accurately in three-dimensional space. Non-natural compounds that are capable of adopting stabilized three-dimensional structures mimicking or complementing those found in nature are therefore of great interest, and as a class of compounds, these various chemotypes have been coined "foldamers".[1] A wide variety of foldamers have been developed and extensively studied,[2] with some of the prominent peptidomimetic examples being β-peptides[3] and peptoids (N-alkylglycines)[4] (Figure 1A).

The tertiary amide backbone architecture in peptoids renders them unable to stabilize putative folded structures by forming intramolecular hydrogen-bond networks. Furthermore, the presence of tertiary backbone amide bonds gives rise to increased flexibility due to a low-energy barrier between *cis* and *trans* configurations. Thus, a high degree of *cis*-amide bonds may occur in peptoids, which is almost exclusively observed at proline in natural peptides and proteins (Figure 1B)[5] and have been enhanced by introduction of synthetic proline derivatives.[6] The effect of various N-alkyl side chain functionalities on this *cis–trans* equilibrium in peptoids has been studied by NMR spectroscopy.[7−10] Despite the inherent flexibility of peptoids, secondary structures of oligomeric and cyclic peptoids have been studied in some detail in solution by NMR spectroscopy[11−13] and in the solid state by X-ray crystallography, and some requirements for the formation of secondary peptoid structure have been identified.[13−16] For instance, the handedness of a helical conformation depends on the enantiomeric nature of α-chiral N-alkyl side chains, and the helix formation is favored by the presence of bulky and aromatic substituents.[11,16−18] Electronic n → π* interactions[19] have also been proposed to take part in the stabilization of secondary structures of peptoids.[8,9] These interactions involve donation of a lone pair from a carbonyl oxygen atom into an empty π* orbital of carbon atom of another carbonyl or an aromatic ring (Figure 1C)[20] and are optimal when mimicking the Bürgi–Dunitz trajectory for nucleophilic attack.[21] The β-peptides (Figure 1A), on the other hand, retain the capability to form intramolecular hydrogen-bond networks to stabilize secondary

Received: December 22, 2012
Published: January 23, 2013

   dx.doi.org/10.1021/ja312532x | J. Am. Chem. Soc. 2013, 135, 2835−2844

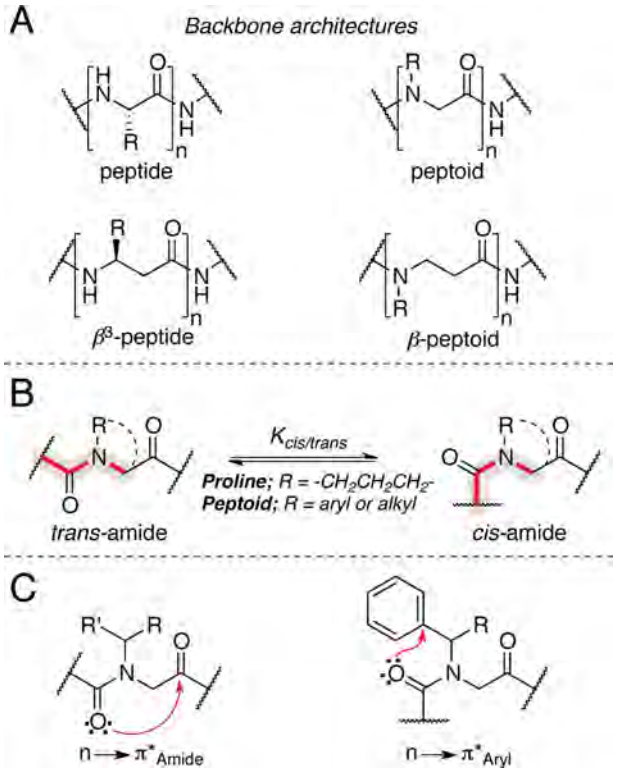

Figure 1. (A) Generic structures of the backbone architectures of peptides (i.e., α-peptides), peptoids (i.e., α-peptoids), β^3-peptides (β^2- and disubstituted β-peptides are not shown), and β-peptoids. (B) Depiction of the equilibrium of *trans*- and *cis*-amide conformations in proline and peptoid residues. (C) Examples of n → π^* interactions previously reported to exist in peptoids.[8]

structures, while the geometry of known helices is unlikely to be stabilized by n → π^* interactions.[2,3]

By combining the features of β-peptides and peptoids, the ensembles of available foldameric scaffolds may be expanded with β-peptoids, and several examples of biologically active compounds containing this motif have been reported.[22] The structural properties of compounds with a β-peptoid backbone architecture, however, have been studied to a far lesser extent than its parent compounds since the first examples were reported by Hamper et al. in 1998.[23] The first three-dimensional structure of a β-peptoid, which was achieved for a cyclic tetramer, was thus reported by Taillefumier and co-workers in 2008.[24] Computational studies of linear oligomeric β-peptoids have predicted several possible helical conformations,[25] containing both the *cis*- and *trans*-amides, but studies based on circular dichroism (CD) spectroscopy have been inconclusive.[26] To obtain experimental data regarding the folding propensity of these molecules, we decided to prepare a series of β-peptoid monomers and evaluate the structural influence on *cis*–*trans* amide bond isomerization by NMR spectroscopy under various conditions. Our collection of model compounds was designed to investigate how stereoelectronic effects and substituent bulk affect the conformational preferences of β-peptoid monomers.

RESULTS AND DISCUSSION

Design and Synthesis. All our model compounds were based on acylated β-peptoid monomers. This minimal design was chosen to mimic the local interactions of a residue within an oligomer structure. In this way the effect of side chains may be investigated with respect to steric and stereoelectronic interactions. Furthermore, it was the scope of this work to assess whether changes in the electronic properties of the backbone would alter the conformational preferences of the residues.

The first array of monomers was designed to include a structurally diverse set of N-alkyl side chains accommodating variations in steric bulk, α-branching, aromatic vs saturated substituents and finally including an N-aryl substituent (phenyl). The chosen set of eight different side chains (**a**–**h**) was installed in two different monomer series: (1) **3a**–**h** containing a C-terminal ester functionality and (2) **4a**–**h** containing a C-terminal tertiary amide functionality thought to better mimic the local environment of a single residue within an oligomeric structure (Scheme 1A). The *tert*-butylester series was prepared since these can be readily deprotected, which allows for further coupling reactions as well as installation of additional C-teminal functionalities. To probe the effects of the various side chains on the rotameric preference of the β-peptoid amide bond (the *cis*–*trans* equilibrium), acetyl groups were installed to give N-terminal tertiary amides, as also investigated in α-peptoid model systems.[8−10] Analogous to those studies, the *trans*–*cis* isomerism in our compounds could then be determined by integration of the ^{1}H NMR peaks assigned to each rotamer.

Syntheses of the β-peptoid monomers were achieved by aza Michael addition of a primary amine to acrylester (**1**) or acrylamide (**2**) in MeOH,[24] which has turned out to be an ideal solvent for this tranformation as opposed to the originally reported reactions in DMSO (Scheme 1A).[23] This was followed by acetylation to give the two series of monomer model compounds (**5a**–**h** and **6a**–**h**) for evaluation by NMR spectroscopy.

In addition to the various N-alkyl side chains and differences in C-terminal functionality, we were also interested in probing the possibility of local n → π^* interactions by altering the electronic properties of amide carbonyls. The N-terminal amides were therefore modified by introduction of trifluoroacetyl groups in place of the acetyl groups in selected compounds (Scheme 1B). These were readily prepared from **3a**,**e**,**f** and **4a**,**e**,**f** by treatment with trifluoroacetic anhydride (Scheme 1B).

Finally, we substituted carbonyl oxygen atoms with sulfur in a selection of compounds to achieve introduction of minimal peptide bond surrogates with altered electronic properties.[27] Both amides in compounds **6a**,**e**,**f** were individually mutated to thioamides to give **10a**,**e**,**f** and **12a**,**e**,**f**, respectively (Scheme 1C,D). For their preparation, we utilized Lawesson's reagent,[28] which selectively converts amides to thioamides in the presence of esters. Preparation of the C-terminal thioamides **10a**,**e**,**f**, were achieved by treating precursors **4a**,**e**,**f** with Lawesson's reagent to give **9a**,**e**,**f**, which were then acetylated to give the target compounds (Scheme 1C). The N-terminal thioamides **12a**,**e**, **f**, on the other hand, were synthesized by treating **5a**,**e**,**f** with Lawesson's reagent to give **11a**,**e**,**f**, followed by *tert*-butylester cleavage and coupling to morpholine to yield the target compounds (Scheme 1D). These changes were thus quite efficiently introduced from common precursors to alter the donor and acceptor capabilities of the two carbonyl groups.

NMR Spectroscopy of Acetylated Monomers. In order to take possible solvent effects into consideration in our evaluation of the monomers, we recorded NMR spectra in six

dx.doi.org/10.1021/ja312532x | J. Am. Chem. Soc. 2013, 135, 2835−2844

Scheme 1. Synthesis of β-Peptoid Model Compounds[a]

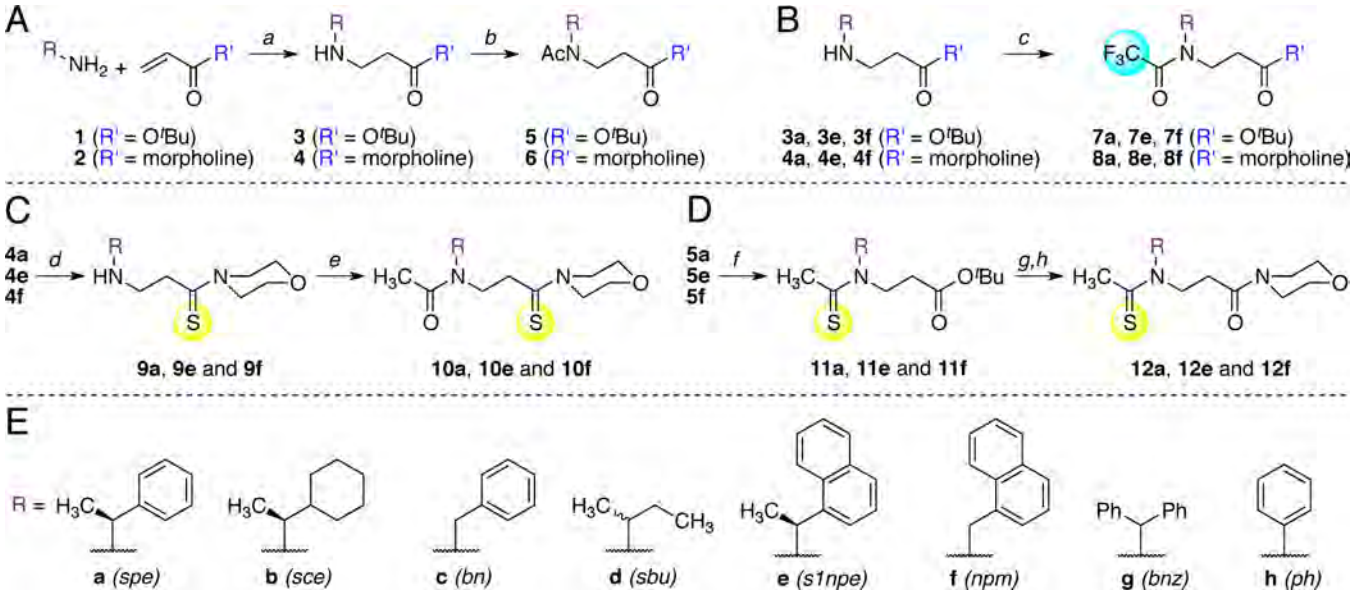

[a](A) Acetylated monomers **5a–h** and **6a–h**. Reagents and conditions: (a) MeOH, 50 °C, 16 h; (b) (i) for esters Ac_2O (2 equiv), pyridine (2 equiv), DMF, 0 °C → rt, 4 h or (ii) for amides AcCl (2 equiv), pyridine (2 equiv), DMF, CH_2Cl_2, 0 °C, 1 h. (B) Synthesis of trifluoroacetylated monomers **7a,e,f** and **8a,e,f**. Reagents and conditions: (c) Trifluoroacetic anhydride (2 equiv), pyridine (2 equiv), CH_2Cl_2, 0 °C, 4 h. (C and D) Synthesis of thioamide-containing β-peptoid monomeric model compounds. Reagents and conditions: (d) Lawesson's reagent (1.5 equiv), toluene, 110 °C, 3 h; (e) AcCl (2 equiv), *i*-Pr_2NEt (2 equiv), CH_2Cl_2, 0 °C, 3 h; (f) Lawesson's reagent (0.6 equiv), toluene, 110 °C, 1 h; (g) 1 M $LiOH_{aq}$–DMF 1:1, rt, 16 h; (h) morpholine (2 equiv), HBTU (2 equiv), *i*-Pr_2NEt (2 equiv) CH_2Cl_2, rt, 16 h. (E) Abbreviations for N-alkyl side chains used are as follows: spe = (*S*)-1-phenylethyl, sce = (*S*)-1-cyclohexylethyl, bn = benzyl, sbu = *sec*-butyl, s1npe = (*S*)-1-(1-naphthyl)ethyl, npm = 1-naphthylmethyl, bnz = benzhydryl, ph = phenyl.

Table 1. Rotamer Equilibrium Constants ($K_{cis/trans}$) for Acetylated β-Peptoid Monomers in Various Solvents[a] **and Their Corresponding Differences in Free Energy (ΔG values given in kJ × mol^{-1})**[b]

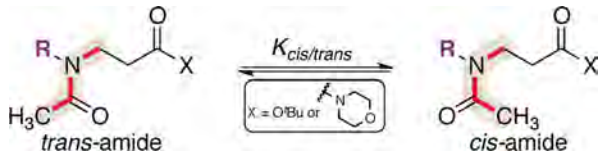

		D_2O		DMSO-d_6		CD_3OD		CD_3CN		$CDCl_3$		C_6D_6	
compd	side chain	$K_{cis/trans}$	ΔG	$K_{cis/trans}$	ΔG	$K_{cis/trans}$	ΔG	$K_{cis/trans}$	ΔG	$K_{cis/trans}$	ΔG	$K_{cis/trans}$	ΔG
C-terminal esters													
5a	spe	0.8	0.5	0.8	0.5	0.7	0.9	0.8	0.5	0.9	0.3	0.8	0.5
5b	sce	0.5	1.7	0.6	1.2	0.4	2.2	0.5	1.7	0.4	2.2	0.5	1.7
5c	bn	1.0	0	0.9	0.3	0.9	0.3	0.9	0.3	0.7	0.9	0.7	0.9
5d	sbu	0.5	1.7	0.5	1.7	0.4	2.2	0.4	2.2	0.5	1.7	0.4	2.2
5e	s1npe	n.s.[c]	–	3.6	−3.1	5.6	−4.2	3.6	−3.1	5.3	−4.1	6.3	−4.5
5f	npm	n.s.[c]	–	0.7	0.9	0.9	0.3	0.7	0.9	0.9	0.3	0.9	0.3
5g	bnz	n.s.[c]	–	0.9	0.3	0.6	1.2	0.9	0.3	0.7	0.9	0.5	1.7
5h	ph	0.2	3.9	all *trans*	–	all *trans*	–	all *trans*	–	all *trans*	–	all *trans*	–
C-terminal amides													
6a	spe	0.7	0.9	0.8	0.5	0.5	1.7	0.8	0.5	0.4	2.2	0.4	2.2
6b	sce	0.3	2.9	0.5	1.7	0.3	2.9	0.4	2.2	0.4	2.2	0.3	2.9
6c	bn	1.0	0	0.9	0.3	0.7	0.9	0.9	0.3	0.3	2.9	0.3	2.9
6d	sbu	0.2	3.9	0.5	1.7	0.2	3.9	0.4	2.2	0.1	5.6	0.1	5.6
6e	s1npe	2.9	−2.6	3.0	−2.7	3.0	−2.7	3.1	−2.8	2.9	−2.6	3.5	−3.1
6f	npm	0.9	0.3	0.6	1.2	0.9	0.3	0.8	0.5	0.4	2.2	0.5	1.7
6g	bnz	0.8	0.5	0.9	0.3	0.5	1.7	0.9	0.3	0.4	2.2	0.5	1.7
6h	ph	n.s.[c]	–	all *trans*	–	all *trans*	–	all *trans*	–	all *trans*	–	all *trans*	–

[a]Determined by integration of ^{1}H NMR spectra of 12 mM compound solutions at ambient temperature. [b]$\Delta G = -RT \times \ln(K_{cis/trans})$. [c]Not soluble.

different deuterated solvents of varying polarities (Table 1). First, we looked at compound **5a** containing the (*S*)-1-phenylethyl side chain, which is one of the most well-studied functionalities with respect to folding propensity of α-

dx.doi.org/10.1021/ja312532x | *J. Am. Chem. Soc.* 2013, 135, 2835–2844

Table 2. Rotamer Equilibrium Constants ($K_{cis/trans}$) for Trifluoroacetylated β-Peptoid Monomers in Various Solvents[a] and Their Corresponding Differences in Free Energy (ΔG values given in kJ × mol^{-1})[b]

		D_2O		DMSO-d_6		CD_3OD		CD_3CN		$CDCl_3$		C_6D_6	
compd	side chain	$K_{cis/trans}$	ΔG	$K_{cis/trans}$	ΔG	$K_{cis/trans}$	ΔG	$K_{cis/trans}$	ΔG	$K_{cis/trans}$	ΔG	$K_{cis/trans}$	ΔG
C-terminal esters													
7a	spe	n.s.[c]	–	0.4	2.2	0.3	2.9	0.4	2.2	0.3	2.9	0.3	2.9
7e	s1npe	n.s.[c]	–	6.8	−4.7	6.3	−4.3	6.6	−4.6	6.3	−4.3	6.3	−4.3
7f	npm	n.s.[c]	–	0.8	0.5	0.8	0.5	0.8	0.5	0.9	0.3	1.0	0
C-terminal amides													
8a	spe	0.4	2.2	0.4	2.2	0.3	2.9	0.4	2.2	0.2	3.9	0.2	3.9
8e	s1npe	n.s.[c]	–	5.6	−4.2	5.0	−3.9	5.5	−4.1	4.8	−3.8	4.5	−3.7
8f	npm	n.s.[c]	–	0.8	0.5	1.0	0	0.8	0.5	0.7	0.9	0.6	1.2

[a]Determined by integration of ^{1}H NMR spectra of 12 mM compound solutions at ambient temperature. [b]$\Delta G = -RT \times \ln(K_{cis/trans})$. [c]Not soluble.

peptoids[17] and has been studied briefly by CD spectroscopy in β-peptoids.[26] This model β-peptoid exhibited a slight preference for the *trans*-amide configuration without any notable solvent effect, and expectedly, we further showed that the chiral identity had no influence on the conformational distribution, by synthesizing the corresponding racemate and the (*R*)-enantiomer (see Figure S1Supporting Information). As no significant effects of the concentration on the $K_{cis/trans}$ had previously been reported for peptoids,[9] we gratifyingly found that to be true for β-peptoid solutions in $CDCl_3$ between 6−200 mM as well (Figure S2). Finally, we performed rotating frame Overhauser effect spectroscopy (ROESY) experiments on selected compounds (e.g., see Figure S3) in order to show that the methyne group exhibiting the most downfield chemical shift arises from the *cis*-amide conformation, which is in agreement with previously published peptoid studies.[8−10]

Next, we compared the $K_{cis/trans}$ data for **5a** with those obtained for **5b**, which is a nonaromatic, fully saturated version of **5a**. The loss of aromaticity with only a slight increase in steric bulk gave rise to an increase in the preference for the *trans* conformation. This, in turn, indicates that the aromatic moiety may cause a slight shift toward the *cis*-amide, which is consistent with previous findings reported by Blackwell and coworkers for peptoids.[9] Likewise, this was also the case when we decreased the steric congestion of the side chain by introducing a benzyl group (**5c**), as the recorded $K_{cis/trans}$ values were comparable to those of **5a** in all the tested solvents. We then evaluated a combination of decrease in steric bulk further and removal of aromaticity using the *sec*-butyl side chain (**5d**). Similar equilibrium constants were observed for **5b** and **5d**, which was in accordance with α-peptoid findings,[9] as was the significant preference for *cis*-amide configuration induced by the (*S*)-1-(1-naphthyl)ethyl side chain (**5e**).[15]

Interestingly, introduction of a 1-naphtylmethyl side chain (**5f**) resulted in approximately a 1:1 mixture of rotamers as observed for **5a** and **5b**, showing that the naphthyl group itself is not sufficient to induce a predominant amount of the *cis*-amide. Thus, it would seem that the lack of α-branching enables the naphthyl group to avoid structure inducing steric interactions. Furthermore, we altered the bulk of the side chain by introducing the disubstituted benzhydryl group (**5g**), which, perhaps somewhat suprisingly, also gave rise to similar $K_{cis/trans}$ values as found for compound **5a**. This shows that α-branching only in combination with a very bulky group will promote induction of the *cis*-conformation, which apparently is uniquely well represented in the (*S*)-1-(1-naphthyl)-ethyl side chain. However, alternative constructs, taking advantage of a putative n → π^*_{aryl} interaction (Figure 1C) by introducing electron-deficient aromatic substituents instead of increasing the steric bulk, have been reported for peptoids as well.[9,29]

Finally, peptoid studies have also shown that direct attachment of a phenyl group to the nitrogen atom (i.e., prepared from aniline subunits) leads to a very strong preference for *trans*-amides.[13] A single β-peptoid model system of this type (**5h**) was evaluated and exhibited the expected selectivity, by virtually giving rise to single sets of signals in all tested solvents when analyzed by ^{1}H NMR. As mentioned, we also evaluated the entire series of side chains **a**−**h** in model systems having C-terminal amides (**6a**−**6h**) instead of esters, to mimic the environment of a β-peptoid residue within an oligomer more appropriately. The data are shown in the lower panel of Table 1, and inspection of the results reveals the same trends as discussed for the C-terminal *tert*-butylesters.

Taken together, our side chain investigations indicate that there may be a slight intrinsic preference for the *trans*-amide rotamer in β-peptoid model systems (**5d** and **6d**), which is in agreement with results from peptoids containing methyl or ethyl side chains.[9] The equilibrium then shifts toward the *cis*-amide rotamer to approximately 1:1 mixtures when adding aromatic functionalities as substituents in the α-position of the side chains. Based on the results of **5a** vs **5b** as well as **6a** vs **6b** (in the polar solvents), it seems plausible that an n → π^*_{aryl} interaction could play a role. Though, this interaction, in the case of a phenyl or naphthyl group, is too weak to induce the *cis*-amide as the preferred conformation. However, it is not possible to unambiguously attribute this effect of the aromaticity on $K_{cis/trans}$ to an n → π^*_{aryl} interaction based on our side chain experiments alone. Furthermore, the only examples of a strong preference for the *cis*-amide required quite specific steric properties of the side chain (**5e** and **6e**). In an attempt to gain further insight regarding possible stereoelectronic effects on $K_{cis/trans}$ in β-peptoids, we turned our attention to model systems containing carbonyls with altered electronic properties.

NMR Spectroscopy of Trifluoroacetylated Analogs. As we found that the β-peptoid model systems display the same behavior as peptoids upon side chain substitutions, we turned our attention to backbone modifications. Examples of such investigations have been reported for proline but have not, to the best of our knowledge, been utilized for interrogation of peptoid structure and conformational preference.

Noncovalent n → π^*_{amide} (Figure 1C) interactions contribute to stabilization of protein secondary structures[30] and have been studied extensively in relation to collagen polyproline type-II helical conformations.[31] The presence of this type of interaction has also been suggested in certain peptoid model systems.[8]

Table 3. Rotamer Equilibrium Constants ($K_{cis/trans}$) for Thioamide-Containing β-Peptoid Monomers in Various Solvents[a] and Their Corresponding Differences in Free Energy (ΔG values given in kJ × mol^{-1})[b]

		D_2O		DMSO-d_6		CD_3OD		CD_3CN		$CDCl_3$		C_6D_6	
compd	side chain	$K_{cis/trans}$	ΔG	$K_{cis/trans}$	ΔG	$K_{cis/trans}$	ΔG	$K_{cis/trans}$	ΔG	$K_{cis/trans}$	ΔG	$K_{cis/trans}$	ΔG
10a	spe	0.4	2.2	0.5	1.7	0.5	1.7	0.5	1.7	0.2	3.9	0.2	3.9
10e	s1npe	n.s.[c]	–	2.0	−1.7	3.4	−3.0	2.8	−2.5	2.2	−1.9	2.6	−2.3
10f	npm	n.s.[c]	–	0.9	0.3	0.8	0.5	0.9	0.3	0.3	2.9	0.3	2.9
12a	spe	0.7	0.9	0.9	0.3	0.4	2.2	0.7	0.9	0.5	1.7	0.5	1.7
12e	s1npe	n.s.[c]	–	5.4	−4.1	4.7	−3.8	4.5	−3.7	3.3	−2.9	5.2	−4.0
12f	npm	n.s.[c]	–	1.0	0	0.6	1.2	0.9	0.3	0.3	2.9	0.3	2.9

[a]Determined by integration of ^{1}H NMR spectra of 12 mM compound solutions at ambient temperature. [b]$\Delta G = -RT \times \ln(K_{cis/trans})$. [c]Not soluble.

Although such interactions would not be expected to have a stabilizing effect on β-peptoid secondary structure due to unfavorable geometry,[25] we were interested in testing whether the $K_{cis/trans}$ values in our model systems were sensitive to this type of interaction.

First we reasoned that substitution of the N-terminal acetyl group for a trifluoroacetyl group would significantly alter the electronic properties of the carbonyl through the strong inductive electron-withdrawing effect of fluorine. This should thus decrease the electronegativity of the N-terminal carbonyl, which would render this position weaker as donor of a lone pair from oxygen, whereas the carbonyl carbon atom would become a better acceptor. Since the alkyl side chains exhibited disfavoring of the *cis*-conformer, we chose to investigate trifluoroacetylated analogs containing aromatic side chains exclusively. We thus evaluated model compounds containing (*S*)-1-phenylethyl (**7a**), (*S*)-1-(1-napthyl)-ethyl (**7e**), and naphtylmethyl (**7f**) side chains (Table 2).

Surprisingly, at first glance, opposite effects were observed for **7a** vs **5a** and **7e** vs **5e** with a decrease and an increase in $K_{cis/trans}$, respectively, while compounds **7f** and **5f** behaved alike each other. Retrospectively, however, we hypothesize that a decrease of the *cis*-amide fraction in the (*S*)-1-phenylethyl system may in fact be explained by a weakened n → π^*_{aryl} interaction, whereas the opposite trend in the (*S*)-1-(1-napthyl)ethyl system is most likely of entirely steric nature. The trifluoromethyl group is more sterically demanding than the methyl, which may indeed be of particular significance in the already congested amide bond of **7e**. In support of this hypothesis, we recently became aware of a study by Raines and co-workers, in which it was shown that the rotamer equilibrium of a trifluoroacetylated proline derivative was governed by sterics, while the corresponding mono- and difluorinated analogs were affected by the electron-withdrawing inductive effect of fluorine.[29] It was also suggested by Raines and co-workers that fluorine may act as donor of an electron pair to an antibonding π^* orbital of the adjacent carbonyl, which would then results in the opposite of the anticipated inductive effect. Such interactions are indeed precedented in the literature, for example, by using molecular torsion balance double mutant systems.[32]

We also tested the morpholine analogs (**8a,e,f**), and again these exhibited trends that were similar to the *tert*-butylesters. Thus, it seems unlikely that the C-terminal carbonyl should be involved in the stabilization of monomer conformations. Although we are not able to propose unequivocal guidelines for the effects of introducing fluorine atoms in peptoid or peptide backbones, we believe that this could prove to be a useful addition to the arsenal of strategies for future design of peptide mimics.

NMR Spectroscopy of Thioamide Analogs. Inspired by another study of prolines by Raines and co-workers,[27] we next altered the carbonyl-donor capabilities by individually substituting the oxygen atoms with sulfur to increase the "nucleophilicity". If any carbonyl−carbonyl interactions (in the N → C or C → N directionality) were to be playing a significant role on the β-peptoid conforms, these sulfur substitutions should give rise to differences in the $K_{cis/trans}$ values as compared to the corresponding oxygen-containing compounds. Evaluating first the thioacetylated compounds (**12a,e,f**), we found that they behaved similar to the acetylated compounds. The only difference was observed in the (*S*)-1-(1-napthyl)ethyl system (**12e**), which showed increased fractions of the *cis*-amide. This would indicate that the sulfur is interacting with the aromatic ring rather than the C-terminal carbonyl. On the other hand, substitution of the C-terminal oxygen atom with sulfur (**10a,e,f**) resulted in $K_{cis/trans}$ values very similar to those recorded for their acetylated parent monomers (**6a,e,f**) in all cases (Table 3). This indicates that an n → π^*_{amide} interaction in the C → N directionality, which in theory should stabilize the *cis* configuration, is highly unlikely. These are the first examples of thioamides in peptoids, and our results show that this minimal amide bond surrogate may be valuable for interrogation of higher oligomers and possibly also in N-alkylglycine-based peptoids.

Peptoids. To address the effects of fluorination or thioamide introduction in peptoids as well, we finally prepared compounds **13**−**15** (Chart 1). These syntheses were achieved by applying published methods for solution-phase peptoid

Chart 1. Structures and $K_{cis/trans}$ Values for the Investigated N-Alkylglycine Peptoids

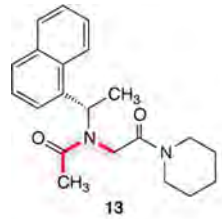

13

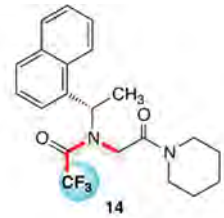

14

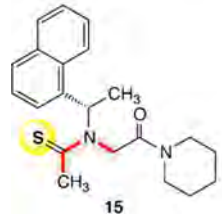

15

	$K_{cis/trans}$		
Compd.	**13**	**14**	**15**
DMSO-d_6	4.6	8.1	8.3
CD_3CN	6.7	9.2	9.1
$CDCl_3$	3.1	6.1	2.6

dx.doi.org/10.1021/ja312532x | J. Am. Chem. Soc. 2013, 135, 2835−2844

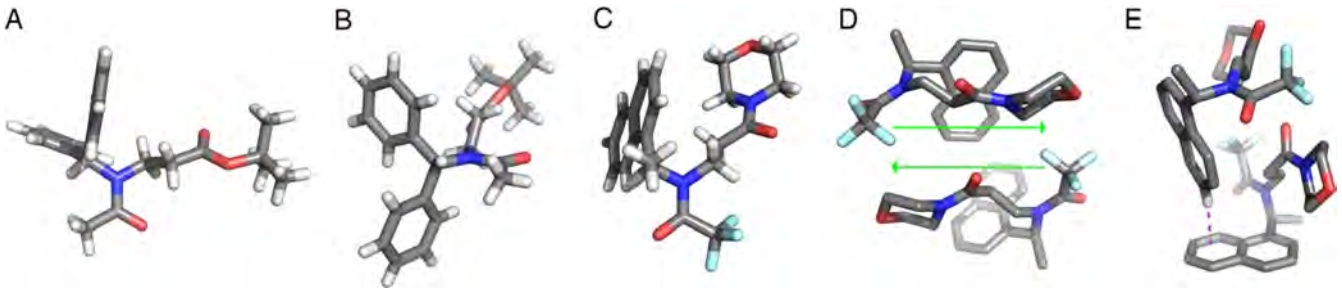

Figure 2. Solid-state structures of compound **5g** (A and B) and compound **8e** (C–E) determined by X-ray crystallography. Atom coloring: gray, carbon; white, hydrogen; red, oxygen; blue, nitrogen; and turquoise, fluorine. Green arrows indicate N → C directionality (D), and the dashed magenta colored line indicates an edge to face aromatic interaction (E). The hydrogen atoms have been removed for clarity in D and E.

synthesis[33] in combination with the protocols described for *β*-peptoid functionalization *vide supra* (Scheme S1).

Compound **13**, which has been investigated previously, exhibited the same $K_{cis/trans}$ values as reported in CD_3CN and $CDCl_3$ [9] and an intermediate value in DMSO-d_6, suggesting the presence of a solvent effect in this system. Comparing these values to the ones obtained for *β*-peptoid **8e** revealed a similarly lowered $K_{cis/trans}$ value in CD_3CN as compared to the other tested solvents (Table 1). For compound **14**, an even higher preference for the *cis*-amide conformation was observed, and this was affected to a much lesser extent by a change in the solvent polarity. In analogy to the arguments presented for the trifluoroacetylated *β*-peptoids, we hypothesize that this equilibrium is primarily dictated by sterics, but also note that the additional stabilization of the *cis*-amide conformation in the peptoid (e.g., $^{DMSO}K_{cis/trans}$ for **14** vs **8e** = 7.1 and 5.6, respectively) may involve the aforementioned possibility of an interaction between fluorine and the C-terminal carbonyl. However, compelling evidence for the latter point would require further experimentation.

Finally, the thioamide analog **15**, like *β*-peptoid **12e**, exhibited higher $K_{cis/trans}$ values than its oxoamide analog (**13**) in polar solvents, and a significant decrease in the *cis*-amide fraction in $CDCl_3$ (Chart 1). This again indicates that there is an interaction between the sulfur and the aromatic residue, which results in favoring of the *cis*-amide conformation.

X-ray Crystallography. We were able to obtain diffraction quality crystals for two *β*-peptoids, **5g** and **8e**, by slow evaporation of chloroform solutions as well as the peptoid **15** by slow evaporation from an AcOEt solution. Thus, the solid-state crystal structures of these model compounds were solved by X-ray structure determination. The structure of **5g** revealed an extended backbone conformation (Figure 2A) with *trans*-amide configuration, which is consistent with the obtained $K_{cis/trans}$ = 0.7 in $CDCl_3$. Notably, the two phenyl groups adopt a periplanar relationship and are both pointed away from the acetyl CH_3 group (Figure 2B), which may also explain the relatively high *trans*-amide ratio observed in solution despite its significant steric bulk.

Compound **8e** adopted the *cis*-amide conformation in the solid state (Figure 2C), as would also be expected judging from its $K_{cis/trans}$ values. We had suspected that the attenuated electron lone-pair donor capabilities of the N-terminal carbonyl in the trifluoroacetylated compounds compared to acetylated analogs would result in a decreased n → π^*_{aryl} effect. The crystal structure of **8e** shows no such interaction, and there are no signs of fluorine–carbonyl interactions either. However, due to the very dense crystal packing with antiparallel *β*-peptoid backbones (Figure 2D) and edge to face aromatic *π*–*π* interactions (Figure 2E), the presence of n → π^*_{aryl} interactions in solution cannot be definitively excluded.

The X-ray crystal structure of the N-terminal thioamide peptoid analog **15** also revealed the presence of a *cis*-amide configuration, as would be expected from the NMR data (Figure 3). The distance between the C-terminal carbonyl and

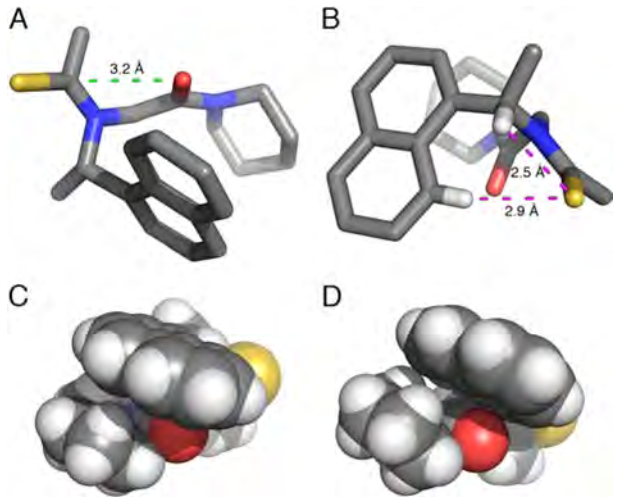

Figure 3. Solid-state structure of compound **15** determined by X-ray crystallography. Stick representations showing the C═O_{i+1}···C_i═S distance in green (A) and the distances between sulfur and its two closest hydrogen atoms in magenta (B). Space-filling representations showing hydrophobic packing of the naphthyl and the piperidine groups (C) and (D). The hydrogen atoms have been removed for clarity in A and B (except for the two hydrogens in close proximity to sulfur).

the carbon of the thioamide is consistent with the presence of an n → π^*_{amide} interaction (Figure 3A),[19,30] which may explain the higher $K_{cis/trans}$ values recorded for the glycine-based peptoids compared to the *β*-alanine-based peptoids. As was also the case for compound **8e**, the solid-state structure did not provide any evidence of an n → π^*_{aryl} interaction. Interestingly, however, the distance between one of the naphthyl hydrogen atoms and the sulfur shown in Figure 3B (2.9 Å) is consistent with an overlap of their orbitals to give rise to an aromatic C–H···S_{amide} interaction. This could offer an alternative explanation of the stabilizing effect on the *cis*-amide conformation obtained by introduction of the N-terminal thioamide functionality. In order to shed more light on the identity of the putative noncovalent carbonyl–aryl interaction in this system, we performed density functional theory (DFT) calculations on selected compounds (*vide infra*). We also

dx.doi.org/10.1021/ja312532x | J. Am. Chem. Soc. 2013, 135, 2835–2844

note that the proximity of the side chain methyne hydrogen, and the carbonyl in this crystal structure (2.5 Å) as well as in the structure of **8e** described above are consistent with the downfield shift observed in ^{1}H NMR for this proton in the *cis*-amide conformations.

Evidence for Aromatic C−H···S$_{amide}$ Interactions. To gain further insight into the molecular features responsible for a C−H···S$_{amide}$ interaction and its effect on the observed preference for the *cis*-amide configuration in the presence of the (*S*)-1-(1-napthyl)ethyl side chain, a computational study was carried out. Initially, the peptoids (**6e**, **8e**, **12e**, **13**−**15**) were built in either the *cis* or the *trans* configuration and subjected to a conformational search running 1000 steps using the OPLS-2005 force-field[34] and a GB/SA solvation model[35] for water as incorporated in Macromodel version 9.6.[36] The *cis*- or *trans*-amide conformations were retained by applying a constraint of 100 kJ × mol^{-1} × radian^{-2} to those particular dihedral angles. Furthermore, to prevent irrelevant rotamers of the morpholine headgroup to appear in the conformational search, additional dihedral constraints were applied to the N-terminal part of the molecules. The conformational search was carried out using a combination of Monte Carlo multiple minimum (MCMM) algorithm[37,38] and the "Low-Mode" search algorithm,[39] with an energy window of 21 kJ × mol^{-1}. After this initial conformational search all of the generated conformations were submitted to a further optimization with DFT using the B3LYP functional.[40] We used the 6-31G* basis set[41] along with the polarized continuum solvent model (PCM-SCRF)[42] with parameters suitable for water.

The lowest energy conformations of both **6e** and **12e** contained the *cis*-amide configuration in agreement with our $K_{cis/trans}$ data from NMR as well as the X-ray diffraction data (Figure 4). Notably, when visualizing the ensemble of conformations with energies within 21 kJ × mol^{-1} (Figure 4B,D), the more homogeneous positioning of the N-alkyl side chain in the thioamide analog indicates that there may be a stabilizing interaction between the sulfur and the naphthyl group. This is again consistent with the trends of $K_{cis/trans}$ observed by NMR, and the preferred geometry is the same as we found in the solid-state for compound **15** revealing close proximity of the proton in position eight of the naphthyl functionality with the carbonyl (Figure 4A,C).

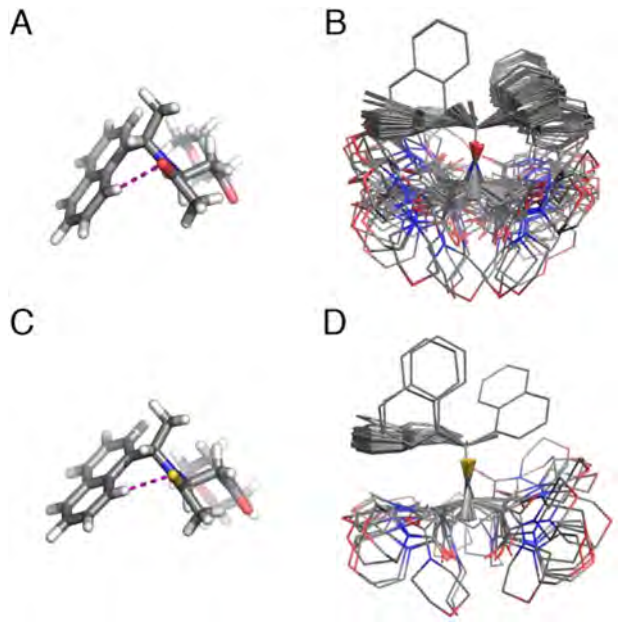

Figure 4. Calculated structures of compounds **6e** (A and B) and **12e** (C and D). All structures within 21 kJ × mol^{-1} of the global minimum were superimposed.

To further investigate the electronic properties responsible for the observed *cis*-amide preference in the thioamide series, we carried out natural bond order (NBO) analyses.[43] By inclusion of the trifluoroacetylated compounds **8e** and **14** we would be able to pinpoint the effect of this substitution in both peptoid and *β*-peptoid backbones. For this purpose, superimposable, low-energy conformations of both *cis*- and *trans*-isomers of **6e**, **8e**, **12e**, **13**−**15** were selected. When comparing the two *cis*-conformations of **6e** and **12e**, it is notable that while the longer C═S compared to C═O (1.7 vs 1.2 Å) caused the distance to the hydrogen of the naphtyl group to increase from 2.9 to 3.2 Å, the NBO analysis clearly showed that the interaction is stronger in the thioamide case.

First of all, the natural charge on the aromatic hydrogen in the thioamide (**12e**) is lower than in the amide compound (0.2436 au for **12e** vs 0.2455 au for **6e**), although both hydrogens are more electron deficient than their neighboring hydrogen, which does not have such intramolecular interactions (0.2503 au for **12e** and 0.2487 au for **6e**). In addition, second-order perturbation analyses of **12e** and **6e** revealed calculated stabilizing energies of this interaction to be 0.86 kcal × mol^{-1} and below the 0.5 kcal × mol^{-1} threshold, respectively.

In the trifluoroacetylated compound **8e**, the amide oxygen is less negatively charged as expected (−0.657 au in **8e** vs −0.716 au in **6e**). As a consequence, the electrostatic interaction with the naphthyl hydrogen is expected to be even smaller than for **6e**, however, in this case it is also below the threshold of 0.5 kcal × mol^{-1}. This suggests that the increased *cis*−*trans* ratio upon change of methyl to trifluoromethyl likely is caused by the increased steric congestion of the larger fluorine atoms rather than arising from an increased electrophilicity of the amide carbonyl carbon. Finally, the three *trans* configured structures featured a fully extended backbone with neither n → π^*_{amide} nor electrostatic C−H···S$_{amide}$ interactions.

Next, we turned our attention to the peptoid series (**13**−**15**) where the closer proximity of the other carbonyl group may allow for the possibility of n → π^*_{amide} interactions in addition to the electrostatic C−H···S$_{amide}$ interaction. For all of these compounds, the C−H···S$_{amide}$ interaction shows up in the second-order perturbation analysis part of the NBO analysis, and it is only slightly stronger for the thioamide **15** (0.63 kcal × mol^{-1}) compared to the amide **13** (0.58 kcal × mol^{-1}). For the trifluoroacetylated peptoid **14**, the value is even higher at 0.65 kcal × mol^{-1}, but the small energies considered, these differences may well be within the inaccuracy of the method. These effects on peptoid structure are currently under further investigation in our laboratories.

A comparison of the chemical shifts assigned to the naphthyl H-8 hydrogen in the *cis*-amide conformations of compounds with altered electronic properties of the carbonyl support the presence of the proposed interaction in solution as well (Figure 5). Thus, attenuation of the electron density of the oxygen by introduction of fluorine atoms should render the hydrogen less shielded and cause an upfield shift of the signal, which was indeed what the spectra showed (**6e** vs **8e**). Substitution of oxygen with sulfur (**6e** vs **12e**) should in principle affect this putative interaction in the same manner. However, the opposite

dx.doi.org/10.1021/ja312532x | J. Am. Chem. Soc. 2013, 135, 2835−2844

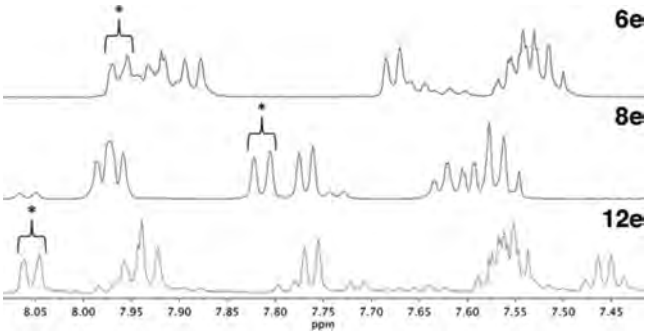

Figure 5. Aromatic region of the ^{1}H NMR spectra of **6e**, **8e**, and **12e** recorded in CD_3CN. The asterisk denotes the signal of the position eight proton of the naphthyl group (see, Figure S5 for signal assignments by COSY and HMBC NMR). The same trend was observed when comparing compounds **13**–**15** (data not shown).

effect was observed with a downfield shift of the signal (Figure 5), which gratifyingly is consistent with the calculated ensembles and the $K_{cis/trans}$ values that indicate a stronger interaction for sulfur. Although hydrogen bonds to oxoamides should be stronger than thioamides, we speculate that the geometric restraint required for formation of the eight-membered ring in our system does not allow for an optimal hydrogen-bond distance, and therefore the larger radius of the sulfur enables a higher degree of orbital overlap than the oxygen. This is supported by the NBO analysis on the β-peptoids **6e** and **12e** (see above). Additionally, the difference in polarizability of thioamides as compared to oxoamides may play a role[44] and could also provide arguments to help explain the solvent effects observed on $K_{cis/trans}$ for some thioamide compounds (*vide supra*).[44a]

CONCLUSIONS

To get a better understanding of the amide bond isomerization in peptoids, we have synthesized and evaluated several series of monomer β-peptoid model systems with varying electronic and steric properties as well as two novel N-alkylglycine (peptoid) model compounds containing a trifluoroacetyl group or an N-terminal thioamide, respectively. Our studies show that some of the trends found in peptoids are directly applicable to β-peptoids. As such, the (*S*)-1-(1-napthyl)ethyl side chain strongly induces the *cis*-amide conformation, while N-aryl gives rise to *trans*. We thus found that a bulky substituent like naphthyl in combination with α-branching is required for a *cis*-amide preference, as a diphenyl-substituted benzhydryl side chain was not sufficiently sterically demanding. In addition to the investigation of various side chain effects, we prepared model systems containing trifluoroacetyl groups as well as thioamides to probe the electronic effects of the carbonyl donor–acceptor capabilities. The NMR-based studies of these compounds provided evidence for an interaction of the N-terminal carbonyl/thiocarbonyl lone pair with the aromatic side chain, but we saw no evidence for conformational stabilization through noncovalent carbonyl–carbonyl interactions. The X-ray crystal structures of two β-peptoid model compounds were solved, which revealed one *trans*- and one *cis*-amide, respectively. Those rotamer conformations were both in agreement with the NMR experiments.

Furthermore, the X-ray crystal structure of a thioamide-containing peptoid model compound was solved, and supported by DFT calculations and NMR chemical shift analysis, this structure indicated the presence of a stabilizing effect through thioamide–aromatic interactions by C_{sp^2}–H···S_{amide} "hydrogen bonds". Whereas aromatic–sulfur interactions have been described for proteins as well as in other systems,[45] the present work, to the best of our knowledge, provides evidence for the first examples of intramolecular conformation-stabilizing effects by introduction of thioamides, which is in contrast to the destabilizing effect of thioamide introduction in α-helical peptides.[46]

Importantly, this work shows that minimal peptide bond surrogates like thioamides as well as fluorinated backbone analogs are useful for investigation of peptoid and β-peptoid structure. These modifications should therefore be considered valuable for other types of peptidomimetics as well. Thioamides, in particular, have recently found use in peptide ligands and have been site-specifically introduced into proteins to probe folding.[47] We envision that the straight forward methodology presented herein may encourage further studies of thioamide-containing peptoid and β-peptoid oligomeric systems.

ASSOCIATED CONTENT

Supporting Information

Supplementary figures , experimental methods, charaterization data, ^{1}H NMR and ^{13}C NMR spectra for all synthesized compounds, selected 2D NMR spectra, and crystallographic data (CIF). Coordinates (*X*, *Y*, *Z*) and solution phase SCF energies for global minimum found in each conformational search along with most favorable structure calculated using DFT/B3LYP, and tables of data from the NBO analyses. This material is available free of charge via the Internet at http://pubs.acs.org.

AUTHOR INFORMATION

Corresponding Author

cao@kemi.dtu.dk

Notes

The authors declare no competing financial interest.

ACKNOWLEDGMENTS

We thank Ms. Anne Hector and Dr. Charlotte H. Gotfredsen for assistance with NMR spectroscopy and Ms. Tina Gustafsson for technical assistance with UPLC-MS and HRMS. This work was supported by funds from DTU Chemistry and the Danish Independent Research Council, Natural Sciences (Steno grant no. 10-080907, C.A.O.). C.A.O. is a Lundbeck Foundation Fellow.

REFERENCES

(1) Gellman, S. H. *Acc. Chem. Res.* **1998**, *31*, 173–180.
(2) (a) Bautista, A. D.; Craig, C. J.; Harker, E. A.; Schepartz, A. *Curr. Opin. Chem. Biol.* **2007**, *11*, 685–92. (b) Goodman, C. M.; Choi, S.; Shandler, S.; DeGrado, W. F. *Nat. Chem. Biol.* **2007**, *3*, 252–62. (c) Olsen, C. A. *ChemBioChem* **2010**, *11*, 152–60. (d) Horne, W. S. *Expert Opin. Drug Discovery* **2011**, *6*, 1247–62.
(3) (a) Seebach, D.; Beck, A. K.; Bierbaum, D. J. *Chem. Biodivers.* **2004**, *1*, 1111–239. (b) Seebach, D.; Gardiner, J. *Acc. Chem. Res.* **2008**, *41*, 1366–75. (c) Wu, Y.-D.; Gellman, S. *Acc. Chem. Res.* **2008**, *41*, 1231–1232.
(4) (a) Yoo, B.; Kirshenbaum, K. *Curr. Opin. Chem. Biol.* **2008**, *12*, 714–21. (b) Yoo, B.; Shin, S. B.; Huang, M. L.; Kirshenbaum, K. *Chem.—Eur. J.* **2010**, *16*, 5528–37. (c) Brown, N. J.; Johansson, J.; Barron, A. E. *Acc. Chem. Res.* **2008**, *41*, 1409–17. (d) Zuckermann Ronald, N.; Kodadek, T. *Curr. Opin. Mol. Ther.* **2009**, *11*, 299–307.

(5) (a) Stewart, D. E.; Sarkar, A.; Wampler, J. E. *J. Mol. Biol.* **1990**, *214*, 253−260. (b) Pal, D.; Chakrabarti, P. *J. Mol. Biol.* **1999**, *294*, 271−288.
(6) (a) Halab, L.; Becker, J. A. J.; Darula, Z.; Tourwe, D.; Kieffer, B. L.; Simonin, F.; Lubell, W. D. *J. Med. Chem.* **2002**, *45*, 5353−5357. (b) Halab, L.; Lubell, W. D. *J. Am. Chem. Soc.* **2002**, *124*, 2474−2484.
(7) Sui, Q.; Borchardt, D.; Rabenstein, D. L. *J. Am. Chem. Soc.* **2007**, *129*, 12042−8.
(8) Gorske, B. C.; Bastian, B. L.; Geske, G. D.; Blackwell, H. E. *J. Am. Chem. Soc.* **2007**, *129*, 8928−9.
(9) Gorske, B. C.; Stringer, J. R.; Bastian, B. L.; Fowler, S. A.; Blackwell, H. E. *J. Am. Chem. Soc.* **2009**, *131*, 16555−67.
(10) Caumes, C.; Roy, O.; Faure, S.; Taillefumier, C. *J. Am. Chem. Soc.* **2012**, *134*, 9553−6.
(11) Armand, P.; Kirshenbaum, K.; Goldsmith, R. A.; Farr-Jones, S.; Barron, A. E.; Truong, K. T. V.; Dill, K. A.; Mierke, D. F.; Cohen, F. E.; Zuckermann, R. N.; Bradley, E. K. *Proc. Natl. Acad. Sci. U.S.A.* **1998**, *95*, 4309−4314.
(12) (a) Huang, K.; Wu, C. W.; Sanborn, T. J.; Patch, J. A.; Kirshenbaum, K.; Zuckermann, R. N.; Barron, A. E.; Radhakrishnan, I. *J. Am. Chem. Soc.* **2006**, *128*, 1733−8. (b) Butterfoss, G. L.; Renfrew, P. D.; Kuhlman, B.; Kirshenbaum, K.; Bonneau, R. *J. Am. Chem. Soc.* **2009**, *131*, 16798−807.
(13) Shah, N. H.; Butterfoss, G. L.; Nguyen, K.; Yoo, B.; Bonneau, R.; Rabenstein, D. L.; Kirshenbaum, K. *J. Am. Chem. Soc.* **2008**, *130*, 16622−16632.
(14) (a) Shin, S. B.; Yoo, B.; Todaro, L. J.; Kirshenbaum, K. *J. Am. Chem. Soc.* **2007**, *129*, 3218−25. (b) Butterfoss, G. L.; Yoo, B.; Jaworski, J. N.; Chorny, I.; Dill, K. A.; Zuckermann, R. N.; Bonneau, R.; Kirshenbaum, K.; Voelz, V. A. *Proc. Natl. Acad. Sci. U.S.A.* **2012**, *109*, 14320−5.
(15) Stringer, J. R.; Crapster, J. A.; Guzei, I. A.; Blackwell, H. E. *J. Am. Chem. Soc.* **2011**, *133*, 15559−67.
(16) Wu, C. W.; Kirshenbaum, K.; Sanborn, T. J.; Patch, J. A.; Huang, K.; Dill, K. A.; Zuckermann, R. N.; Barron, A. E. *J. Am. Chem. Soc.* **2003**, *125*, 13525−30.
(17) (a) Wu, C. W.; Sanborn, T. J.; Huang, K.; Zuckermann, R. N.; Barron, A. E. *J. Am. Chem. Soc.* **2001**, *123*, 6778−84. (b) Wu, C. W.; Sanborn, T. J.; Zuckermann, R. N.; Barron, A. E. *J. Am. Chem. Soc.* **2001**, *123*, 2958−63. (c) Kirshenbaum, K.; Barron, A. E.; Goldsmith, R. A.; Armand, P.; Bradley, E. K.; Truong, K. T. V.; Dill, K. A.; Cohen, F. E.; Zuckermann, R. N. *Proc. Natl. Acad. Sci. U.S.A.* **1998**, *95*, 4303−4308. (d) Sanborn, T. J.; Wu, C. W.; Zuckermann, R. N.; Barron, A. E. *Biopolymers* **2002**, *63*, 12−20.
(18) Paul, B.; Butterfoss, G. L.; Boswell, M. G.; Huang, M. L.; Bonneau, R.; Wolf, C.; Kirshenbaum, K. *Org. Lett.* **2012**, *14*, 926−9.
(19) Hinderaker, M. P.; Raines, R. T. *Protein Sci.* **2003**, *12*, 1188−94.
(20) Fischer, F. R.; Wood, P. A.; Allen, F. H.; Diederich, F. *Proc. Natl. Acad Sci. U.S.A.* **2008**, *105*, 17290−4.
(21) Burgi, H. B.; Dunitz, J. D.; Shefter, E. *J. Am. Chem. Soc.* **1973**, *95*, 5065−5067.
(22) (a) Shuey, S. W.; Delaney, W. J.; Shah, M. C.; Scialdone, M. A. *Bioorg. Med. Chem. Lett.* **2006**, *16*, 1245−8. (b) Olsen, C. A.; Bonke, G.; Vedel, L.; Adsersen, A.; Witt, M.; Franzyk, H.; Jaroszewski, J. W. *Org. Lett.* **2007**, *9*, 1549−52. (c) Vedel, L.; Bonke, G.; Foged, C.; Ziegler, H.; Franzyk, H.; Jaroszewski, J. W.; Olsen, C. A. *ChemBioChem* **2007**, *8*, 1781−4. (d) Foged, C.; Franzyk, H.; Bahrami, S.; Frokjaer, S.; Jaroszewski, J. W.; Nielsen, H. M.; Olsen, C. A. *Biochim. Biophys. Acta, Biomembr.* **2008**, *1778*, 2487−2495. (e) Olsen, C. A.; Ziegler, H. L.; Nielsen, H. M.; Frimodt-Moller, N.; Jaroszewski, J. W.; Franzyk, H. *ChemBioChem* **2010**, *11*, 1356−60. (f) Jahnsen, R. D.; Frimodt-Moller, N.; Franzyk, H. *J. Med. Chem.* **2012**, *55*, 7253−61. (g) Olsen, C. A.; Montero, A.; Leman, L. J.; Ghadiri, M. R. *ACS Med. Chem. Lett* **2012**, *3*, 749−753.
(23) Hamper, B. C.; Kolodziej, S. A.; Scates, A. M.; Smith, R. G.; Cortez, E. *J. Org. Chem.* **1998**, *63*, 708−718.
(24) Roy, O.; Faure, S.; Thery, V.; Didierjean, C.; Taillefumier, C. *Org. Lett.* **2008**, *10*, 921−4.
(25) Baldauf, C.; Guenther, R.; Hofmann, H.-J. *Phys. Biol.* **2006**, *3*, S1−S9.
(26) (a) Norgren, A. S.; Zhang, S.; Arvidsson, P. I. *Org. Lett.* **2006**, *8*, 4533−6. (b) Olsen, C. A.; Lambert, M.; Witt, M.; Franzyk, H.; Jaroszewski, J. W. *Amino Acids* **2008**, *34*, 465−471.
(27) Choudhary, A.; Gandla, D.; Krow, G. R.; Raines, R. T. *J. Am. Chem. Soc.* **2009**, *131*, 7244−6.
(28) (a) Pedersen, B. S.; Scheibye, S.; Nilsson, N. H.; Lawesson, S. O. *Bull. Soc. Chim. Belg.* **1978**, *87*, 223−228. (b) Scheibye, S.; Pedersen, B. S.; Lawesson, S. O. *Bull. Soc. Chim. Belg.* **1978**, *87*, 229−238.
(29) Choudhary, A.; Fry, C. G.; Raines, R. T. *ARKIVOC* **2010**, *2010*, 251−262.
(30) Bartlett, G. J.; Choudhary, A.; Raines, R. T.; Woolfson, D. N. *Nat. Chem. Biol.* **2010**, *6*, 615−20.
(31) (a) DeRider, M. L.; Wilkens, S. J.; Waddell, M. J.; Bretscher, L. E.; Weinhold, F.; Raines, R. T.; Markley, J. L. *J. Am. Chem. Soc.* **2002**, *124*, 2497−505. (b) Hodges, J. A.; Raines, R. T. *J. Am. Chem. Soc.* **2003**, *125*, 9262−3. (c) Jenkins, C. L.; Bretscher, L. E.; Guzei, I. A.; Raines, R. T. *J. Am. Chem. Soc.* **2003**, *125*, 6422−7. (d) Hodges, J. A.; Raines, R. T. *Org. Lett.* **2006**, *8*, 4695−7. (e) Kuemin, M.; Nagel, Y. A.; Schweizer, S.; Monnard, F. W.; Ochsenfeld, C.; Wennemers, H. *Angew. Chem., Int. Ed.* **2010**, *49*, 6324−7.
(32) Fischer, F. R.; Schweizer, W. B.; Diederich, F. *Angew. Chem., Int. Ed. Engl.* **2007**, *46*, 8270−3.
(33) Hjelmgaard, T.; Faure, S.; Caumes, C.; De Santis, E.; Edwards, A. A.; Taillefumier, C. *Org. Lett.* **2009**, *11*, 4100−3.
(34) Still, W. C.; Tempczyk, A.; Hawley, R. C.; Hendrickson, T. *J. Am. Chem. Soc.* **1990**, *112*, 6127−6129.
(35) Kaminski, G. A.; Friesner, R. A.; Tirado-Rives, J.; Jorgensen, W. J. *J. Phys. Chem. B* **2001**, *105*, 6474−6487.
(36) *MacroModel*, v. 9.9; Schrödinger Inc.: Cambridge, MA, 2012; http://www.schrodinger.com. Mohamadi, F.; Richards, N. G. J.; Guida, W. C.; Liskamp, R.; Lipton, M.; Caulfield, C.; Chang, G.; Hendrickson, T.; Still, W. C. *J. Comput. Chem.* 1990, *11*, 440−467.
(37) Chang, G.; Guida, W. C.; Still, W. C. *J. Am. Chem. Soc.* **1989**, *111*, 4379−4386.
(38) Saunders, M.; Houk, K. N.; Wu, Y.-D.; Still, C. W.; Lipton, M.; Chang, G.; Guida, W. C. *J. Am. Chem. Soc.* **1990**, *112*, 1419−1427.
(39) Kolossváry, I.; Guida, W. C. *J. Am. Chem. Soc.* **1996**, *188*, 5011−5019.
(40) (a) Becke, A. D. *J. Chem. Phys.* **1993**, *98*, 5648−5652. (b) Becke, A. D. *J. Chem. Phys.* **1993**, *98*, 1372−1377. (c) Lee, C.; Yang, W.; Parr, R. G. *Phys. Rev. B* **1988**, *37*, 785−789.
(41) Ditchfield, R.; Hehre, W. J.; Pople, J. A. *J. Chem. Phys.* **1971**, *54*, 724.
(42) (a) Marten, B.; Kim, K.; Cortis, C.; Friesner, R. A.; Murphy, R. B.; Ringnalda, M. N.; Sitkoff, D.; Honig, B. *J. Phys. Chem.* **1996**, *100*, 11775−11788. (b) Tannor, D. J.; Marten, B.; Murphy, R.; Friesner, R. A.; Sitkoff, D.; Nicholls, A.; Ringnalda, M.; Goddard, W. A.,, III; Honig, B. *J. Am. Chem. Soc.* **1994**, *116*, 11875−11882.
(43) Glendening, J. K. Badenhoop, A. E. Reed, J. E. Carpenter, J. A. Bohmann, C. M. Morales, and Weinhold, F. *NBO*, 5.0. ed.; Theoretical Chemistry Institute, University of Wisconsin: Madison, WI, 2001; http://www.chem.wisc.edu/∼nbo5.
(44) (a) Wiberg, K. B.; Rush, D. J. *J. Am. Chem. Soc.* **2001**, *123*, 2038−2046. (b) Huang, Y.; Jahres, G.; Fischer, G.; Lücke, C. *Chem.—Eur. J.* **2012**, *18*, 9841−9848.
(45) (a) Salonen, L. M.; Ellermann, M.; Diederich, F. *Angew. Chem., Int. Ed.* **2011**, *50*, 4808−4842. (b) Meyer, E. A.; Castellano, R. K.; Diederich, F. *Angew. Chem., Int. Ed.* **2003**, *42*, 1210−1250. (c) Tatko, C. D.; Waters, M. L. *Protein Sci.* **2004**, *13*, 2515−2522. (d) Waters, M. L. *Biopolymers* **2004**, *76*, 435−445. (e) Pranata, J. *Bioorg. Chem.* **1997**, *25*, 213−219.
(46) (a) Tran, T. T.; Zeng, J.; Treutlin, H.; Burgess, A. W. *J. Am. Chem. Soc.* **2002**, *124*, 5222−5230. (b) Reiner, A.; Wildermann, D.; Fischer, G.; Kiefhaber, T. *J. Am. Chem. Soc.* **2008**, *130*, 8079−8084.
(47) (a) Bach, A.; Eildal, J. N.; Stuhr-Hansen, N.; Deeskamp, R.; Gottschalk, M.; Pedersen, S. W.; Kristensen, A. S.; Strømgaard, K. *J. Med. Chem.* **2011**, *54*, 1333−46. (b) Goldberg, J. M.; Batjargal, S.;

Petersson, E. J. *J. Am. Chem. Soc.* **2010**, *132*, 14718−20. (c) Goldberg, J. M.; Speight, L. C.; Fegley, M. W.; Petersson, E. J. *J. Am. Chem. Soc.* **2012**, *134*, 6088−91. (d) Batjargal, S.; Wang, Y. J.; Goldberg, J. M.; Wissner, R. F.; Petersson, E. J. *J. Am. Chem. Soc.* **2012**, *134*, 9172−82.

SUPPORTING INFORMATION

Cis–Trans Amide Bond Rotamers in β-Peptoids and Peptoids: Evaluation of Stereoelectronic Effects in Backbone and Side Chains

*Jonas S. Laursen, Jens Engel-Andreasen, Peter Fristrup, Pernille Harris, and Christian A. Olsen**

Department of Chemistry, Technical University of Denmark, Kemitorvet 207, DK-2800, Kongens Lyngby, Denmark

*cao@kemi.dtu.dk

Table of Contents

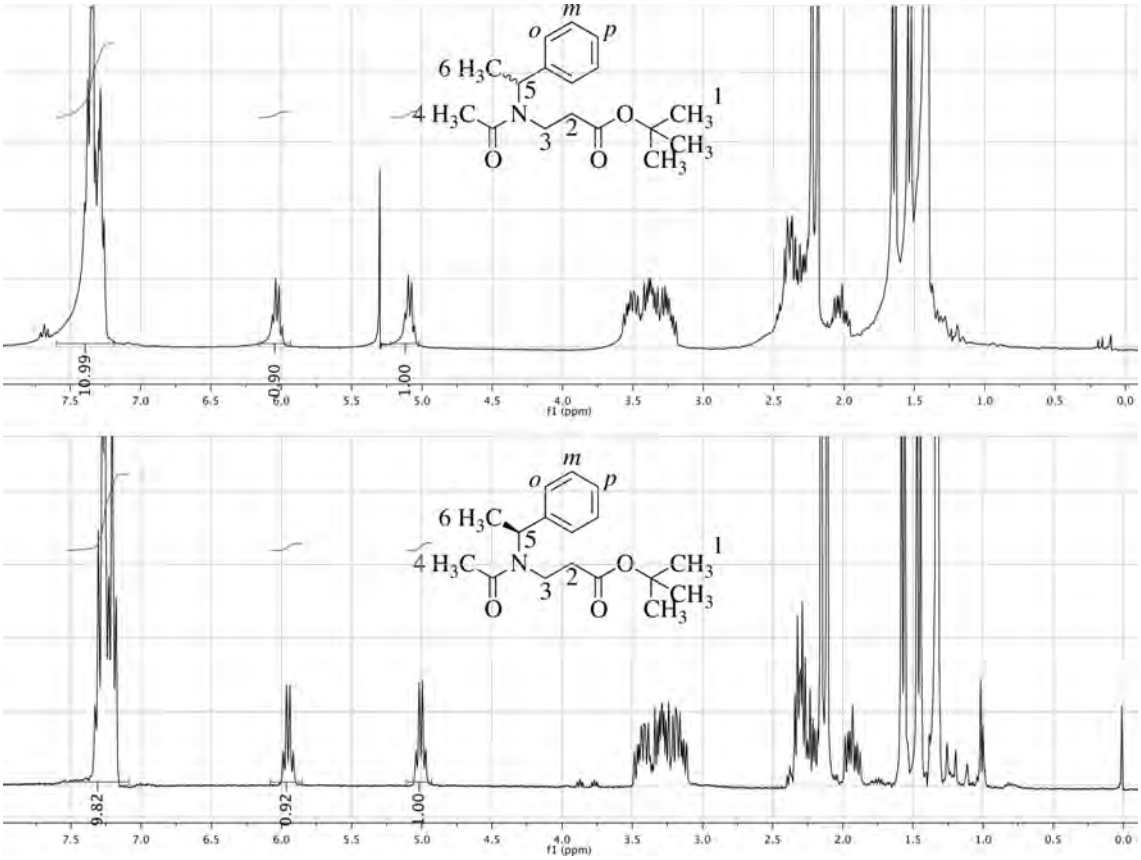

Figure S1. Comparison of the *trans–cis* rotamer ratios of enantiomerically pure and racemic versions of compound **5a**, which expectedly show no difference in equilibria.

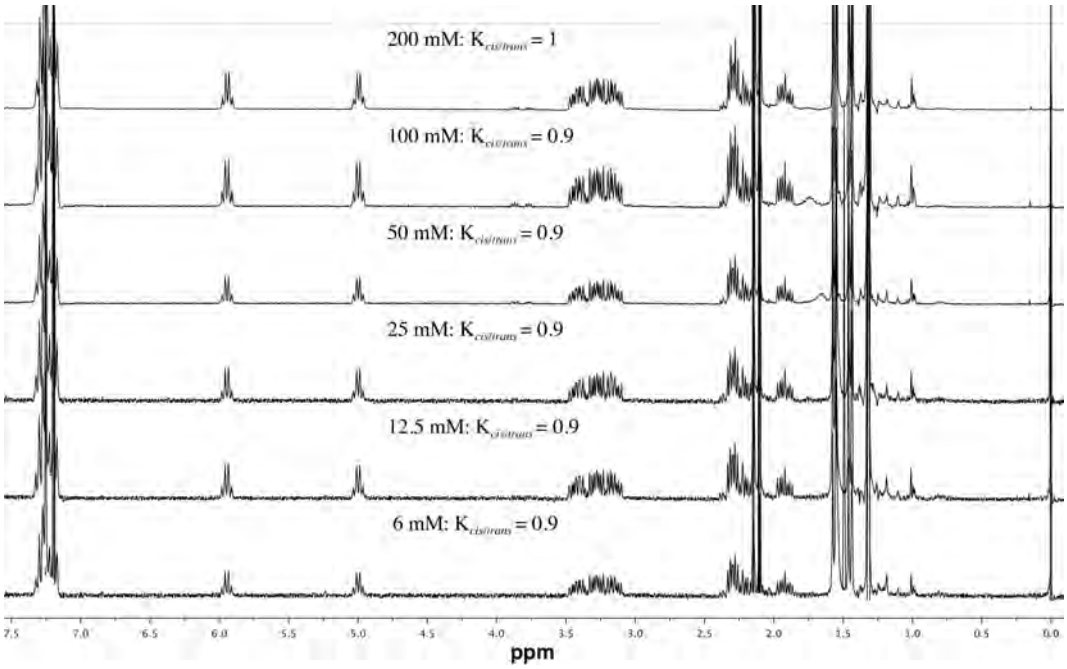

Figure S2. Concentration dependence on $K_{cis/trans}$ for compound **3a**. Spectra were recorded in $CDCl_3$ at 298 K.

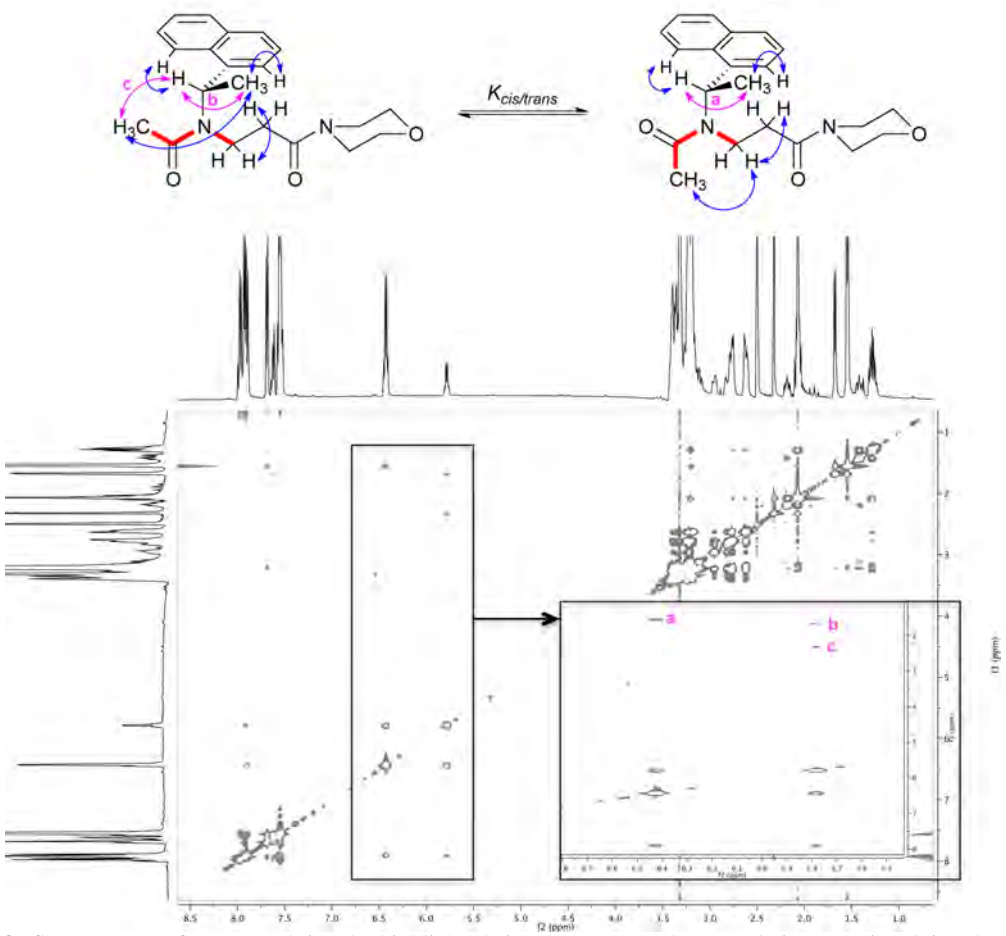

Figure S3. ROESY spectrum of compound **6e**. The highlighted signals correspond to correlations **a**–**c** involving the methyne proton as shown in the scheme above. In the *trans*-amide conformation, the methine proton (quartet) has correlations to the side chain CH_3 protons (**b**) as well as the *N*-acetyl CH_3 protons (**c**). The further down-field shiftet quartet only has an ROE correlation to the side chain CH_3 protons (**a**). Thus, the *N*-acetyl CH_3 group from the conformation with up-field shiftet signal is in closer proximity to the methine proton, which confirms the assignment of this spin system as originating from the *trans*-amide conformation.

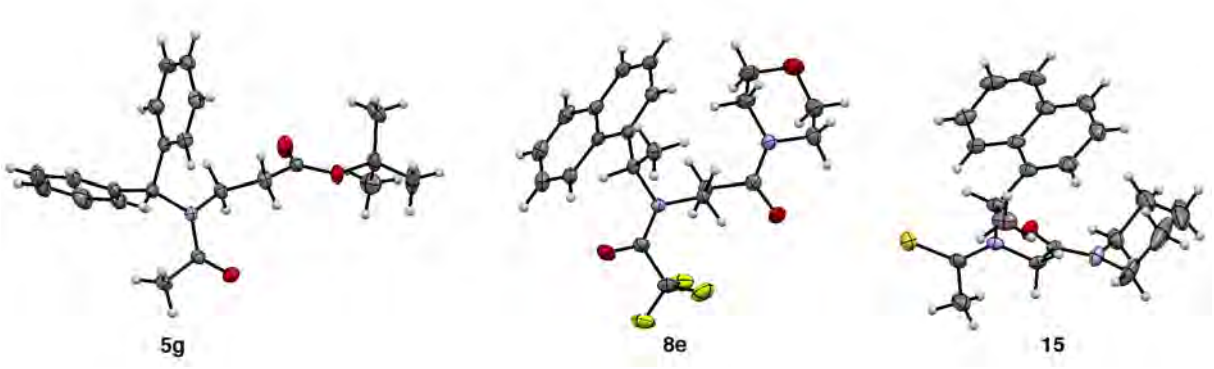

Figure S4. ORTEP representation of the solid state structures of compound **5g**, **8e**, and **15**. For crystallographic details, see the CIF files. *Atom colors:* Grey, carbon; white, hydrogen; red, oxygen; blue, nitrogen; green, fluorine; yellow, sulfur.

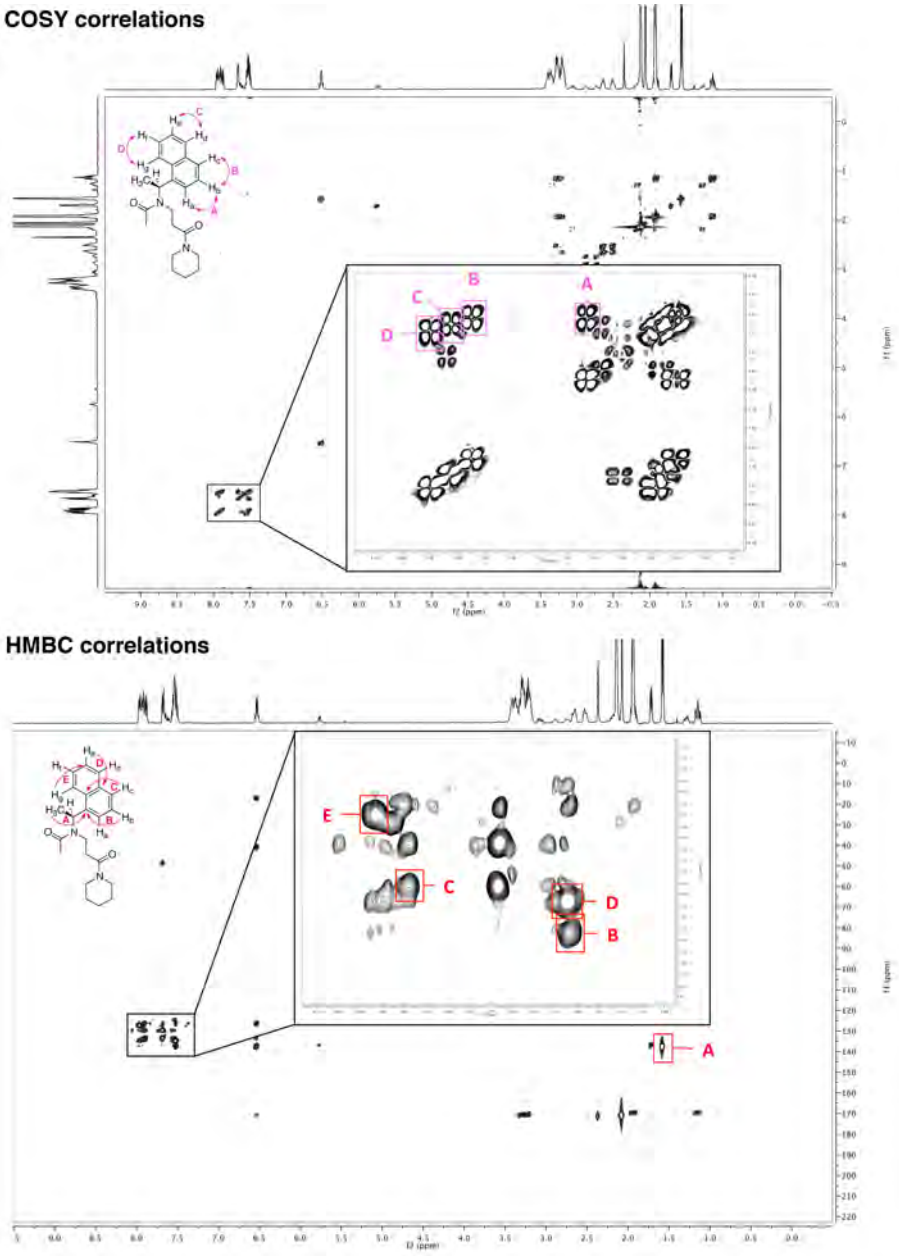

Figure S5. Assignment of the aromatic signals of compound **6e**. For full 2D spectra of this *β*-peptoid as well as **8e** and **12e**, see pages S55–S63.

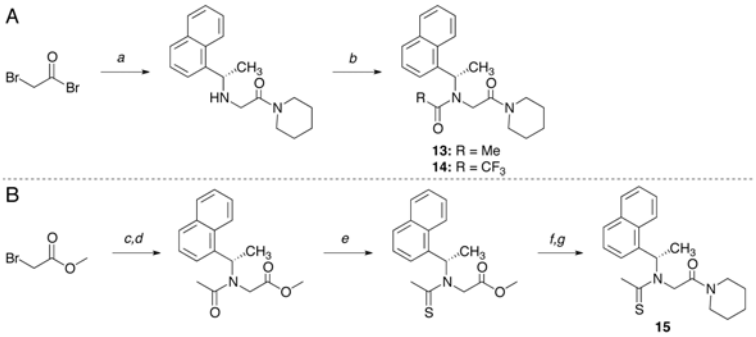

Scheme S1. Synthesis of peptoid compounds **13**–**15**. *Reagents and conditions:* (**A**) *(a) i)* piperidine (0.9 equiv), *i*-Pr_2NEt (1 equiv), THF, 0 °C, 1 h. *ii)* (*S*)-1-(1-naphthyl)ethylamine (2 equiv), NEt_3 (2 equiv), THF, 0 °C → rt, 16 h, 58%; *(b)* $(RCO)_2O$ (3 equiv), pyridine, DMF, 0 °C → rt, 16 h, [**13** (63%) and **14** (46%)]. (**B**) *(c)* (*S*)-1-(1-naphthyl)ethylamine (2 equiv), NEt_3 (2 equiv), THF, 0 °C → rt, 16 h; *(d)* Ac_2O (3 equiv), pyridine, DMF, 0 °C → rt, 16 h, 70% two steps; *(e)* Lawesson's reagent (0.6 equiv), toluene, reflux, 1h, 71%; *(f)* LiOH (2 equiv), DMF/H_2O, rt, 2h; *(g)* piperidine (2 equiv), HBTU (2 equiv), *i*-Pr_2NEt (2 equiv), CH_2Cl_2, rt, 16 h, 44% two steps.

Materials and Methods

General. All chemicals and solvents were analytical grade and used without further purification. Vacuum liquid chromatography (VLC) was performed on silica gel 60 (particle size 0.015–0.040 mm). UPLC–MS analyses were performed on a Waters Acquity ultra high-performance liquid chromatography system. A gradient with eluent I (0.1% HCOOH in water) and eluent II (0.1% HCOOH in acetonitrile) rising linearly from 0% to 95% of II during t = 0.00–2.50 min was applied at a flow rate of 1 mL/min (gradient A) or during t = 0.00–5.20 min (gradient B). Compounds, for which purity could not be assessed by UPLC-MS, were analyzed using HPLC performed on a [250 mm × 20 mm, C18 Phenomenex Luna column (5 µm, 100 Å)] using an Agilent 1260 LC system equipped with a diode array UV detector and an evaporative light scattering detector (ELSD). A gradient C with eluent III (95:5:0.1, water–MeCN–TFA) and eluent IV (0.1% TFA in acetonitrile) rising linearly from 0% to 95% of IV during t = 5–45 min was applied at a flow rate of 20 mL/min. 1D NMR spectra were recorded on a Varian Mercury 300 instrument. ^{1}H NMR, ^{13}C NMR, were recorded at 300 and 75 MHz, respectively. 2D NMR spectra were recorded on a varian INOVA 500 MHz instrument at 500 MHz for ^{1}H and 125 MHz for ^{13}C. All spectra were recorded at 298 K. Correlation spectroscopy (COSY) spectra was recorded with a relaxation delay of 1.5 sec before each scan, a spectral width of 6k × 6k, collecting 8 FIDs and 1k × 512 data points. Heteronuclear single quantum coherence (HSQC) spectra were recorded with a relaxation delay of 1.5 sec before each scan, a spectral width of 6k × 25k, collecting 16 FIDs and 1k × 128 datapoints. Heteronuclear 2-bond correlation (H2BC) spectra were recorded with a relaxation delay of 1.5 sec before each scan, a spectral width of 4k × 35k, collecting 16 FIDs at 295 K and 1k × 256 datapoints. Heteronuclear multiple-bond correlation (HMBC) spectra were recorded with a relaxation delay of 1.5 sec before each scan, a spectral width of 6k × 35 k, collecting 32 FIDs and 1k × 256 datapoints. Rotating frame Overhauser effect (ROESY) spectra were recorded with a relaxation delay of 2 sec before each scan, a spectral width of 4k × 4k, collecting 8 FIDs at 295 K, 1k × 256 datapoints, and a mixing time of 100 ms. Chemical shifts are reported in ppm relative to deuterated solvent peaks as internal standards (δH, DMSO-d_6 2.50 ppm; δC, DMSO-d_6 39.52 ppm, δH, $CDCl_3$ 7.26 ppm; δC, $CDCl_3$ 77.16 ppm. Coupling constants (*J*) are given in hertz (Hz). Multiplicities of ^{1}H NMR signals are reported as follows: s, singlet; d, doublet; t, triplet; q, quartet; m, multiplet. Signals marked with an asterisk (*) correspond to peaks assigned to the minor rotamer conformation.

General procedure for aza-Michael addition to give *tert*-butylester containing monomers.

tert-Butyl acrylate (1 equiv) was dissolved in MeOH and heated to 50 °C on an oil bath. The desired primary amine (1.2 equiv) was added and the reaction was stirred overnight. The solvent was removed *in vacuo* and the crude product was purified by vacuum liquid chromatography (VLC) (<1 gram 3 × 6 cm column CH_2Cl_2–MeOH 0.2 % gradient from 0→5%; from 1–5 grams 6 × 6 cm column CH_2Cl_2–MeOH 0.2 % gradient from 0→5%).

(*S*)-*tert*-Butyl 3-((1-phenylethyl)amino)propanoate (3a). Yield 17.3 g (85%) as a clear oil. ^{1}H NMR (300 MHz, $CDCl_3$) δ = 1.34 (d, 3H, *J* = 6.8 Hz, H-6), 1.44 (s, 9H, H-1), 1.70 (s, 1H, H-4), 2.38 (t, 2H, *J* = 6.3 Hz), 2.60–2.75 (m, 2H, H-3), 3.77 (q, 1H, *J* = 6.6 Hz, H-2), 7.20–7.27(m, 1H, H-*p*), 7.20–7.35 (m, 4H, H-*o*, H-*m*). ^{13}C NMR (75 MHz, $CDCl_3$) δ = 24.7, 28.3, 36.1, 43.4, 58.4, 80.7, 126.8, 127.1, 128.6, 145.8, 172.52. UPLC-MS gradient a, t_R = 0.96 min (>95%), MS (*m/z*) 250.3 ([M + H]$^+$ $C_{15}H_{24}NO_2^+$ calcd 250.4). $[\alpha]_{589.2}$: –29° (*c* = 2.2 , 293 K, $CHCl_3$).

(*S*)-*tert*-Butyl 3-((1-cyclohexylethyl)amino)propanoate (3b). Yield: 5.68 g (85%) as a clear oil. ^{1}H NMR (300 MHz, $CDCl_3$) δ = 0.95 (d, 3H, *J* = 6.5 Hz, H-6), 0,93–1.30 (broad m, 7H, c-Hex, H-4), 1.42 (s, 9H, H-1), 1.63–1.74 (broad m, 5H, c-Hex), 2.35–2.42 (m, 3H, H-2, H-5), 2.69–2.88 (m, 2H, H-3). ^{13}C NMR (75 MHz, $CDCl_3$) δ = 17.0, 26.7, 26.9, 27.0, 28.2, 28.3, 30.10 36.4, 43.0, 43.1, 57.7, 80.6, 172.6. UPLC-MS gradient A, t_R = 1.07 min, *m/z* 256.4 ([M + H]$^+$, $C_{15}H_{30}NO_2^+$ calcd 256.4), gradient C: >95%. $[\alpha]_{589.2}$: +8° (*c* = 1.6 , 293 K, $CHCl_3$).

***tert*-Butyl 3-(benzylamino)propanoate (3c)**. Yield: 5.24 g (40%) as a clear oil. ^{1}H NMR (300 MHz, $CDCl_3$) δ =1.44 (s, 9H, H-1), 1.73 (s, 1H, H-4), 2.45 (t, 2H, *J* = 6.6 Hz, H-2), 2.85 (t, 2H, *J* = 6.6 Hz, H-3), 3.79 (s, 2H, H-5), 7.20–7.30 (m, 1H, H-*p*), 7.31–7.32 (m, 4H, H-*o*, H-*m*). ^{13}C NMR (75 MHz, $CDCl_3$) δ = 28.4, 36.1, 45.0, 54.1, 80.7, 127.1, 128.3, 128.6, 140.5, 172.4. UPLC-MS gradient A, t_R = 0.92 min (>95%), *m/z* 236.3 ([M + H]$^+$, $C_{14}H_{22}NO_2^+$ calcd 236.3).

***tert*-Butyl 3-(*sec*-butylamino)propanoate (3d)**. Yield: 3.82 g (56%) as a clear oil. ^{1}H NMR (300 MHz, $CDCl_3$) δ = 0.79 (t, 3H, *J* = 7.4 Hz, H-8), 0.93 (d, 3H, *J* = 6.3 Hz, H-5), 1.15–1.29 (m, 1H, H-4), 1.36 (s, 9H, H-1), 2.32 (t, 2H, J = 5.9 Hz, H-2), 2.41–2.51 (m, 1H, H-6), 2.65–2.80 (m, 2H, H-3). ^{13}C NMR (75 MHz, $CDCl_3$) δ = 10.4, 19.9, 28.2, 29.7, 36.2, 42.7, 54.4, 80.5, 172.4, UPLC-MS gradient A, t_R = 1.28 min, *m/z* 202.3 ([M + H]$^+$, $C_{11}H_{24}NO_2^+$ calcd 202.3). HPLC gradient C: ELSD >95%.

(*S*)-*tert*-Butyl 3-((1-(naphthalen-1-yl)ethyl)amino)propanoate (3e). Yield 1.38 g (78%) as a yellow oil. ^{1}H NMR (300 MHz, $CDCl_3$) δ = 1.45 (s, 9H, H-1), 1.49 (d, 3H, *J* = 6.6 Hz, H-6), 1.82 (s, 1H, H-4), 2.43 (t, 2H, *J* = 6.4 Hz, H-2), 2.76–2.81 (m, 2H, H-3), 4.65 (q, 1H, *J* = 6.6, H-5),

7.44– 8.21 (5 × m, 7H, H-*a*, H-*b,* H-*c*, H-*d*, H-*e*, H-*f,* H-*g*). ^{13}C NMR (75 MHz, $CDCl_3$) δ = 24.0, 28.4, 36.4, 43.6, 53.8, 80.8, 122.9, 123.2, 125.5, 127.3, 129.2, 131.5, 134.2, 141.3, 172.5. UPLC-MS gradient A, t_R = 1.20 min (>95%), *m/z* 300.3 ([M + H]$^+$, $C_{19}H_{26}NO_2^+$ calcd 300.4). $[\alpha]_{589.2}$: –36° (*c* = 2.2 , 293 K, $CHCl_3$).

***tert*-Butyl 3-((naphthalen-1-ylmethyl)amino)propanoate (3f)**. Yield: 1.35 g (74%) as a clear oil. ^{1}H NMR (300 MHz, $CDCl_3$) δ = 1.4 (s, 9H, H-1), 1.72 (s, 1H, H-4), 2.51 (t, 2H, *J* = 6.5 Hz, H-2), 3.00 (t, 2H, *J* = 6.5 Hz), 4.25 (s, 2H, H-5), 7.41–8.16 (4 × m, 7H, H-a, H-b, H-c, H-d, H-e, H-f, H-g). ^{13}C NMR (75 MHz, $CDCl_3$) δ = 28.4, 36.3, 45.7, 51.8, 80.7, 124.00, 125.6, 125.8, 126.2, 126.3, 128.0, 128.9, 132.1, 134.1, 136.1, 172.4. UPLC-MS gradient A, *m/z* ([M + H]$^+$, $C_{18}H_{23}NO_2^+$ calcd 285.4).

***tert*-Butyl 3-(benzhydrylamino)propanoate (3g)**. Yield: 5.44 g (64%) as a white solid. ^{1}H NMR (300 MHz, $CDCl_3$) δ = 1.44 (s, 9H, H-1), 1.94 (s, 1H, H-4), 2.45 (t, 2H, *J* = 6.4 Hz, H-2), 2.80 (t, 2H, *J* = 6.4 Hz, H-3), 4.83 (s, 1H, H-5), 7.17–7.41 (3 × m, 10H, H-*o*, H-*m*, H-*p*). ^{13}C NMR (75 MHz, $CDCl_3$) δ = 28.4, 36.3, 43.9, 67.5, 80.7, 127.2, 127.5, 128.7, 144.2, 172.4. UPLC-MS gradient A, t_R = 1.32 min (>95%), *m/z* 312.4 ([M + H]$^+$, $C_{20}H_{26}NO_2^+$ calcd 312.4).

***tert*-Butyl 3-(phenylamino)propanoate (3h)**. Yield: 2.51 g (21%) as an orange oil. ^{1}H NMR (300 MHz, $CDCl_3$) δ = 1.48 (s, 9H, H-1), 2.54 (t, 2H, *J* = 6.4 Hz, H-2), 3.41 (m, 2H, H-3), 4.06 (s, 1H, H4), 6.63–7.23 (3 × m, 5H, H-*o*, H-*m*, H-*p*). ^{13}C NMR (75 MHz, $CDCl_3$) δ = 28.4, 35.3, 39.9, 81.1, 113.3, 117.8, 129.5, 148.1, 172.0. UPLC-MS gradient A, t_R = 1.94 min (>95%), *m/z* 222.3 ([M + H]$^+$, $C_{13}H_{20}NO_2^+$ calcd 222.3).

***tert*-Butyl 3-((1-phenylethyl)amino)propanoate (*rac*-3a)**. Yield: 0.71 g (80%) as a clear oil. ^{1}H NMR (300 MHz, $CDCl_3$) δ = 1.34 (d, 3H, *J* = 6.7 Hz, H-6), 1.44 (s, 9H, H-1), 1.69 (s, 1H, H-4), 2.38(t, 2H, *J* = 6.3 Hz, H-2), 2.66 (m, 2H, H-3), 3.76(q, 1H, *J* = 6.6 H-5), 7.20–7.31 (3 × m, 1H, H-p), 7.31 (d, 4H, *J* = 4.38, H-*o*, H-*m*).

(*R*)-*tert*-Butyl 3-((1-phenylethyl)amino)propanoate [(*R*)-3a]. 7.58 g (82%) as a clear oil. ^{1}H NMR (300 MHz, $CDCl_3$) δ = 1.33 (d, 3H, *J* = 6.6 Hz, H-6), 1.43 (s, 9H, H-1), 1.72 (s, 1H, H-4), 2.37 (t, 2H, *J* = 6.4 Hz, H-2), 2.68 (m, 2H, H-3), 3.8 (q, 1H, *J* = 6.6 Hz, H-5), 7.18–7.25 (m, 1H, H-*p*), 7.30–7.31 (d, 4H, H-*o*, H-*m*). ^{13}C NMR (75 MHz, $CDCl_3$) δ = 24.7, 28.3, 36.2, 43.4, 58.4, 80.6, 126.8, 127.1, 128.6, 154.8, 172.5. UPLC-MS gradient A, t_R = 1.00 min (>95%), *m/z* 250.3 ([M + H]$^+$, $C_{15}H_{24}NO_2^+$ calcd 250.4). $[\alpha]_{589.2}$: +29° (*c* = 1.3 , 293 K, $CHCl_3$).

General procedure for aza-Michael addition to give morpholine containing monomers.

N-Acryloyl morpholine (1 equiv) was dissolved in MeOH and heated to 50 °C. The primary amine (1.2 equiv) was added and the reaction was stirred overnight. The solvent was removed *in vacuo*. The crude product was purified by VLC (3 × 6 cm column, CH_2Cl_2–MeOH, 0.2% gradient from 0–>5%).

(*S*)-1-morpholino-3-((1-phenylethyl)amino)propan-1-one (4a). Yield 613 mg (56%) as a clear oil, UPLC-MS gradient B, t_R = 0.67 min (>95%), *m/z* 263.2 ([M + H]$^+$, $C_{15}H_{23}N_2O_2^+$ calcd 263.4).

(*S*)-1-morpholino-3-((1-(naphthalen-1-yl)ethyl)amino)-propan-1-one (4e). Yield: 821 mg (77%) as a yellow oil, UPLC-MS gradient B, t_R = 0.88min (85%), *m/z* 313.3 ([M + H]$^+$, $C_{19}H_{25}N_2O_2^+$ calcd 313.4).

1-morpholino-3-((naphthalen-1-ylmethyl)amino)propan-1-one (4f). Yield: 561 mg (59%) as a clear oil, UPLC-MS gradient B, t_R = 0.84min (94%), *m/z* 299.4 ([M + H]$^+$, $C_{18}H_{23}N_2O_2^+$ calcd 299.4).

General procedure for acetylation of monomers.

The monomer and pyridine (2 equiv) were dissolved in DMF (1 mL/mmol) and cooled to 0 °C. Acetic anhydride (2 equiv) was added dropwise and the temperature was allowed to rise to room temperature (r.t.). After stirring for 4h, the reaction mixture was taken up in saturated aqueous ammonium chloride (50 mL) and extracted with ethyl acetate (3 × 50 mL). The combined organic phases were dried (Na_2SO_4), filtered, and evaporated to dryness. The crude product was purified by VLC (3 × 6 cm column, hexane–EtOAc 5% gradient).

(*S*)-*tert*-Butyl 3-(*N*-(1-phenylethyl)acetamido)propanoate (5a). Yield: 548 mg (94%) as a clear oil. ^{1}H NMR (300 MHz, $CDCl_3$) δ = 1.31 (s, 9H, H-1), 1.45*/1.56 (2 × d, 3H, *J* = 7.1 Hz, H-6), 1.98*/2.32 (2 × m, 2H, H-2), 2.16/2.21* (2 × s, 3H, H-4), 3.10–3.47 (3H, H-3), 5.00/5.95 (2 × q, 1H, *J* = 7.1 Hz), 7.17–7.31 (m, 5H, H-*o*, H-*m*, H-*p*). ^{13}C NMR (75 MHz, $CDCl_3$) δ= 16.8, 18.2, 18.43, 22.17, 22.5, 28.2, 28.3 (3C), 34.7, 36.7, 39.0, 40.2, 51.1, 56.6, 126.8 (2C), 127.7, 127.8 (2C), 127.9, 128.7 (2C), 129.0 (2C), 140.4 140.8, 170.4, 170.7, 170.8, 171.4. UPLC-MS gradient A, t_R = 1.92 min

(>95%), *m/z* 292.3 ([M + H]$^+$, $C_{17}H_{25}NO_3^+$ calcd 292.4). $[\alpha]_{589.2}$: –59° (*c* = 2.7 , 293 K, $CHCl_3$).

(*S*)-*tert*-Butyl 3-(*N*-(1-cyclohexylethyl)acetamido)propanoate (5b). Yield: 120 mg (52%) as a clear oil. ^{1}H NMR (300 MHz, $CDCl_3$) δ = 0.73–0.93 (m, 2H, *c*-Hex), 1.11–1.24 (m, 3H, *c*-Hex), 1.16*/1.18 (2 × d, 3H, *J* = 7.0*/6.8 Hz, H-6), 1.35–1.53 (m, 1H, *c*-Hex), 1.43/1.46* (2 × s, 9H, H-1), 1.64–1.78 (m, 5H, *c*-Hex), 2.06/2.11* (2 × s, 3H, H-4), 2.35–2.77 (2 × m, 2H, H-2), 3.15–3.60 (3 × m, 3H, H-3, H-5). ^{13}C NMR (75 MHz, $CDCl_3$) δ = 16.9*, 17.5, 22.1*, 22.4, 25.9, 26.0*, 26.1, 26.2, 28.1* (3C), 28.1 (3C) 30.0*, 30.4*, 30.5, 30.5, 34.4, 36.6*, 37.5, 40.7*, 41.4, 59.6, 80.5, 81.3*, 170.4*, 170.6, 170.7, 171.5 . UPLC-MS gradient B, t_R = 2.22 min, *m/z* 298.3 ([M + H]$^+$, $C_{17}H_{32}NO_3^+$ calcd 298.4). HPLC gradient C: ELSD >95%. $[\alpha]_{589.2}$: +3° (*c* = 1.2, 293 K, $CHCl_3$).

***tert*-Butyl 3-(*N*-benzylacetamido)propanoate (5c)**. Yield: 355 mg (80%) as a white solid. ^{1}H NMR (300 MHz, $CDCl_3$) δ = 1.42/1.43* (2 × s, 9H, H-1), 2.11/2.23* (2 × s, 3H, H-4), 2.44*/2.54 (2 × t, 2H, *J* = 7.1 Hz, H-2), 3.52*/3.59 (2 × t, 2H, *J* = 7.0 Hz, H-3), 4.59/4.60* (2 × s, 2H, H-5), 7.15–7.39 (m, 5H, H-*o*, H-*m*, H-*p*). ^{13}C NMR (75 MHz, $CDCl_3$) δ = 22.9, 28.1, 34.1, 45.1, 80.8, 128.2, 128.3, 129.9, 142.8, 170.4, 170.8. UPLC-MS gradient A, t_R = 1.75 min (>95%), *m/z* 278.3([M + H]$^+$, $C_{16}H_{24}NO_3^+$ calcd 278.4).

***tert*-Butyl 3-(*N*-(*sec*-butyl)acetamido)propanoate (5d)**. Yield: 208 mg (85%) as a clear oil, ^{1}H NMR (300 MHz, $CDCl_3$) δ = 0.68–0.76 (m, 3H, H-8), 1.00*/1.04 (2 × d, 3H, *J* = 6.8 Hz, H-5), 1.29/1.31* (2 × s, 9H, H-1), 1.36–1.45 (m, 2H, H-6), 1.95/1.98* (2 × s, 3H, H-4), 2.33/2.47* (2 × d, 2H, H-2), 3.16*/3.32 (2 × m, 2H, H-3), 3.56/4.22* (2 × m, 1H, H-6). ^{13}C NMR (75 MHz, $CDCl_3$) δ = 11.3, 18.6*, 19.6, 22.3*, 22.4, 27.4*, 28.0*, 28.2, 34.8, 36.7, 36.9*, 40.2*, 51.7*, 55.7, 80.5, 81.3*, 170.4*, 170.6, 170.8*, 171.5. UPLC-MS gradient A, t_R = 1.68 min (>95%), *m/z* 244.2 ([M + H]$^+$, $C_{13}H_{26}NO_3$ calcd 244.3).

(*S*)-*tert*-butyl 3-(*N*-(1-(naphthalen-1-yl)ethyl)acetamido)-propanoate (5e). Yield: 205 mg (91%) as a yellow oil. ^{1}H NMR (300 MHz, $CDCl_3$) δ= 1.16*/1.85 (2 × m, 2H, H-2), 1.23 (s, 9H, H-1), 1.56/1.67* (2 × d, 3H, *J* = 6.9 Hz, H-6), 2.09/2.31* (2 × s, 3H, H-4), 3.17/3.35* (2 × m, 2H, H-3), 5.59*/6.56 (2 × q, 1H, *J* = 6.9 HZ, H-5), 7.38–7.93 (7H, H-*a*, H-*b*, H-*c*, H-*d*, H-*e*, H-*f*, H-*g*). ^{13}C NMR (75 MHz, $CDCl_3$) δ = 17.0, 19.1*, 22.2, 22.2*, 28.1 (3C), 34.5*, 36.0, 38.7*, 39.8, 47.8, 53.7*, 80.4*, 81.0, 122.6*, 123.8, 124.8*, 125.0, 125.2, 125.5*, 126.1*, 126.2, 127.0*, 127.1, 128.9, 129.1, 129.2*, 129.4*, 131.5*, 132.3, 133.8, 133.9*, 135.4*, 135.8, 170.3, 170.3, 170.7*, 171.2*. UPLC-MS gradient A, t_R = 2.10 min (>95%), *m/z* 342.3 ([M + H]$^+$, $C_{21}H_{28}NO_3^+$ calcd 342.4). $[\alpha]_{589.2}$: –63° (*c* = 1.3, 293 K, $CHCl_3$).

***tert*-Butyl 3-(*N*-(naphthalen-1-ylmethyl)acetamido)-propanoate (5f)**. Yield: 308 mg (59%). ^{1}H NMR (300 MHz, $CDCl_3$) δ = 1.41 (s, 9H, H-1), 2.07/2.25* (2 × s, 3H, H-4), 2.37*/2.62 (2 × t, 2H, *J* = 7.5*/7.0 Hz, H-2), 3.46*/3.71(2 × t, 2H, *J* = 7.0 Hz, H-3), 5.06*/5.10 (2 × s, 2H, H-5), 7.15–8.06 (7H, H-*a*, H-*b*, H-*c*, H-*d*, H-*e*, H-*f,* H-*g*). ^{13}C NMR (75 MHz, $CDCl_3$) δ = 21.8, 21.9*, 28.2*, 28.3, 34.4, 34.7*, 43.7*, 63.6, 45.9*, 51.0, 80.93, 81.6*, 122.3, 122.5, 124.0*, 125.5*, 125.8, 126.2*, 126.3, 126.7, 126.8*, 126.9*, 128.2, 128.7*, 128.8*, 129.8, 130.8*, 131.8*, 132.0, 132.4, 134.0, 134.1*, 170.6*, 170.7, 171.5, 172.0. UPLC-MS gradient A, t_R = 2.03 min (>95%), *m/z* 328.4 ([M + H]$^+$, $C_{20}H_{26}NO_3^+$ calcd 328.4).

***tert*-Butyl 3-(*N*-benzhydrylacetamido)propanoate (5g)**. Yield: 623 mg (93%) as a white solid. ^{1}H NMR (300 MHz, $CDCl_3$) δ = 1.25/1.27* (2 × s, 9H, H-1), 1.65*/1.81 (2 × t, 2H, *J* = 8.2 Hz, H-2), 2.13/2.20* (2 × s, 3H, H-4), 3.50–3.55 (m, 2H, H-4), 6.15/7.05* (2 × s, 1H, H-5), 7.11–7.30 (2 × m, 10H, H-*o*, H-*m*, H-*p*). ^{13}C NMR (75 MHz) δ = 22.1*, 22.5, 28.2 (3C), 33.8, 35.6*, 40.7, 42.2*, 60.8*, 66.2, 80,3, 81.1*, 127.8*, 128.2, 128.8* (2C), 128.8 (2C), 129.9 (2C), 129.0*(2C), 139.0, 139.5*, 170.3*, 171.0*, 171.1, 171.2. UPLC-MS gradient A, t_R = 2.16 min (>95%), *m/z* 354.4 ([M + H]$^+$, $C_{22}H_{28}NO_3^+$ calcd 354.5).

***tert*-Butyl 3-(*N*-phenylacetamido)propanoate (5h)**. Yield: 110 mg (46%) as an orange oil. ^{1}H-NMR (300 MHz) δ = 1.29 (s, 9H, H-1), 1.73 (s, 3H, H-4), 2.40 (t, 2H *J* = 7.4 Hz, H-2), 3.88 (t, 2H J = 7.4, H-3), 7.09–7.30 (2 × m, 5H, H-*o*-H-*m*, H-*p*). ^{13}C NMR (75 MHz, $CDCl_3$) δ: 22.9, 28.1, 34.1, 45.1, 80.8, 128.2, 128.3, 128.9, 142.8, 170.4, 170.8. UPLC-MS gradient A, t_R = 1.74 min (>95%), *m/z* 286.3 ([M + Na]$^+$, $C_{15}H_{21}NO_3Na^+$ calcd 286.3)

General procedure for preparation of morpholine containing monomers. 4-Acryloyl morpholine (1 equiv) were dissolved in MeOH and heated to 50 °C. The primary amine (1.2 equiv) were added and the reaction was stirred overnight. The solvent was removed *in vacuo*. The crude monomer (1 equiv) and pyridine (2 equiv) were dissolved in DMF (1–3 mL/mmol) and cooled to 0 °C. Acetyl chloride (2 equiv) was added dropwise. After being stirred for 1 hour at 0°C the reaction mixture was taken up in 1M HCl (aq) (50 mL) and extracted with ethyl acetate (2 × 50 mL). The organic phase was dried (Na_2SO_4), filtered, and evaporated to

dryness. The crude product was purified by VLC (3 × 6 cm column, CH_2Cl_2–MeOH, 0.2% gradient from 0→5%).

(*S*)-*N*-(3-morpholino-3-oxopropyl)-*N*-(1-phenylethyl)-acetamide (6a). Yield: 157 mg (17%) as a clear oil. ^{1}H NMR (300 MHz, $CDCl_3$) δ = 1.43*/1.58 (2 × d, 3H, *J* = 7.0 Hz, H-8), 1.68*/2.36 (2 × m, 2H, H-5), 2.10*/2.18(2 × s, 3H, H-7), 3.23/2.92* (2 × m, 2H, H-6), 3.38–3.57 (m, 8H, H-1, H-2, H-3, H-4), 5.02/6.02* (2 × q, 1H, *J* = 7.0* Hz, H-9), 7.18–7.32 (m, 5H, H-*o*, H-*m*, H-*p*). ^{13}C NMR (75 MHz, $CDCl_3$) δ = 16.4*, 18.3, 22.2*, 22.5, 32.59, 33.3*, 39.8, 40.4*, 41.9, 45.6*, 46.1, 50.7*, 66.6*, 66.9*, 67.0, 127.0, 127.8*, 128.1, 128.2*, 128.8*, 129.0, 140.2, 141.2*, 168.9*, 170.0, 170.8*, 171.0. UPLC-MS gradient A, t_R = 1.20 min (>95%), *m/z* 305.4 ([M + H]$^+$, $C_{17}H_{25}N_2O_3^+$ calcd 305.4). $[\alpha]_{589.2}$: –61° (*c* = 1.6, 293 K, $CHCl_3$).

(*S*)-*N*-(1-cyclohexylethyl)-*N*-(3-morpholino-3-oxopropyl)acetamide (6b). Yield: 35 mg (38%) as a clear oil. ^{1}H NMR (300 MHz, $CDCl_3$) δ = 0.70–0.88 (m, 2H, *c*-Hex), 1.06–1.16 (m, 2H, *c*-Hex), 1.07*/1.15 (m, d, 3H, *J* = 6.8 Hz, H-9), 1.35–1.41 (m, 2H, *c*-Hex), 1.58–1.74 (m, 5H, *c*-Hex), 2.02/2.04* (2 × s, 3H, H-7), 2.38/2.46 (m, 1H, H-5), 2.74–2.83 (m, 1H, H-5), 3.17–3.40 (2 × m, 2H, H-6), 3.42–3.62 (m, 9H, H-1, H-2, H-3, H-4, H-8). ^{13}C NMR (75 MHz, $CDCl_3$) δ = 17.3*, 17.6, 22.5, 26.0, 26.2, 26.3, 26.3*, 28.2*, 28.5*, 30.2*, 30.5*, 30.6, 30.7, 33.7*, 38.8, 40.9*, 41.5, 42.0, 45.8*, 46.2, 60.0, 67.0, 67.0, 169.0*, 170.2, 170.9*, 171.2, UPLC-MS gradient A: t_R = 1.52 min, *m/z* 311.4 ([M + H]$^+$, $C_{17}H_{31}N_2O_3^+$ calcd 311.4), Gradient C: >95%, $[\alpha]_{589.2}$: –2° (*c* = 1.4, 293 K, $CHCl_3$).

***N*-benzyl-*N*-(3-morpholino-3-oxopropyl)acetamide (6c)**. Yield: 56 mg (7%) as a clear oil. ^{1}H NMR (300 MHz, $CDCl_3$) δ = 2.08/2.19* (2 × s, 3H, H-7), 2.32*/2.61 (2 × t, 2H, *J* = 7.4 Hz, H-5), 3.18*/3.43 (2 × t, 2H, *J* = 5.5 Hz, H-6), 3.49–3.63 (m, 8H, H-1, H-2, H-3, H-4), 4.56*/4.60 (2 × s, 2H, H-8), 7.11–7.33 (5H, H-*o*, H-*m*, H-*p*). ^{13}C NMR (75 MHz, $CDCl_3$) δ = 21.8*, 22.04, 31.9, 31.9*, 42.1, 43.8, 44.6*, 45.8*, 46.2, 48.9*, 53.5, 66.6*, 66.9, 67.0*, 126.5, 127.6*, 127.8, 128.2*, 128.8*, 129.1, 137.1, 138.0*, 168.9*, 170.0, 171.0*, 171.6, UPLC-MS gradient A, t_R = 1.13 min (>95%), *m/z* 291.3 ([M + H]$^+$, $C_{16}H_{23}N_2O_3^+$ calcd 291.4).

***N*-(*sec*-butyl)-*N*-(3-morpholino-3-oxopropyl)acetamide (6d)**. Yield: 136 mg (20%) as a clear oil. ^{1}H NMR (300 MHz, $CDCl_3$) δ = 0.82 (t, 3H, *J* = 7.8 Hz, H-11), 1.06*/1.14 (2 × d, 3H, *J* = 6.9 Hz, H-8), 1.49 (m, 2H, H-10), 2.04/2.05* (2 × s, 2H, H-7), 2.45–2.72 (2 × m, 2H, H-5), 3.24–3.47 (2H, H-6), 3.55–3.68 (m, 9H, H-1, H-2, H-3, H-4, H-9). ^{13}C NMR (75 MHz, $CDCl_3$) δ = 11.4, 18.8*, 19.6, 22.3*, 22.4, 27.6*, 27.9, 32.9, 34.0*, 37.9, 40.2*, 42.0, 45.8*, 46.2, 52.5*, 56.0, 66.6*, 66.9*, 67.0, 67.1, 169.0*, 170.2, 170.9*, 171.1. UPLC-MS gradient A, t_R = 1.02 min (>95%), *m/z* 257.3 ([M + H]$^+$, $C_{13}H_{25}N_2O_3^+$ calcd 257.3)

(*S*)-*N*-(3-morpholino-3-oxopropyl)-*N*-(1-(naphthalen-1-yl)ethyl)acetamide (6e). Yield: 230 mg (24%) as a yellow oil. ^{1}H NMR (300 MHz, $CDCl_3$) δ = 0.82/1.36*/1.64 (3 × m, 3H, H-5), 1.34/1.70* (2 × d, 3H, *J* = 6.8 Hz, H-8), 2.10/2.36 (2 × s, 3H, H-7), 2.23/2.41/2.93 (3 × m, 2H, H-6), 2.90–3.51 (2 × m, 8H, H-1, H-2, H-3, H-4), 5.61*/6.60 (2 × q, 1H, *J* = 6.6 Hz, H-9), 7.38–7.97 (3 × m, 7H, H-*a*, H-*b*, H-*c*, H-*d*, H-*e*, H-*f*, H-*g*). ^{13}C NMR (75 MHz, $CDCl_3$) δ= 16.6, 19.0*, 22.2, 22.2*, 32.1* 32.6, 39.6*, 40.2, 41.7, 45.2, 45.8*, 47.8, 53.8, 66.3, 66.8, 66.9*, 122.7*, 124.1, 125.2, 125.3*, 125.5, 125.8*, 126.1*, 126.4, 127.0*, 127.4, 128.7, 128.9, 129.3*, 129.5*, 131.6*, 132.5, 133.9, 133.9*, 135.0*, 136.3, 168.8, 169.7*, 170.3, 170.9*. UPLC-MS gradient A, t_R = 1.45 min (>95%), *m/z* 355.6 ([M + H]$^+$, $C_{21}H_{27}N_2O_3^+$ calcd 355.4). $[\alpha]_{589.2}$: –49° (*c* = 2.3, 293 K, $CHCl_3$).

***N*-(3-morpholino-3-oxopropyl)-*N*-(naphthalen-1-ylmethyl)acetamide (6f)**. Yield: 308 mg (15%) as a clear oil. ^{1}H NMR (300 MHz, $CDCl_3$) δ = 2.09/2.25* (2 × s, 3H, H-7), 2.17*/2.74 (2 × t, 2H, *J* = 7.3 Hz, H-5), 2.98* (t, 1H, *J* = 5.0 Hz, H-6*), 3.43–3.74 (broad m, 9H, H-1, H-2, H-3, H-4, H-6), 5.09*/5.14 (2 × s, 2H, H-8), 7.19–8.07 (broad m, 7H, H-*a*, H-*b*, H-*c*, H-*d*, H-*e*, H-*f*, H-*g*). ^{13}C NMR (75 MHz) δ = 21.7, 21.9*, 31.8*, 31.9, 41.9*, 42.0, 44.0*, 44.3, 45.6*, 46.1, 46.9*, 51.4, 66.4*, 66.6*, 66.8, 66.9, 122.3, 122.5, 123.9*, 125.4*, 125.6, 126.2, 126.6, 126.8* 127.1* 128.2, 128.7*, 128.8*, 129.1, 130.7, 131.8*, 132.0, 133.0*, 133.9, 133.9*, 168.7*, 169.9, 170.7*, 172.3. UPLC-MS gradient A: t_R = 1.43 min (>95%), *m/z* 341.4 ([M + H]$^+$, $C_{20}H_{25}N_2O_3^+$ calcd 341.2).

***N*-benzhydryl-*N*-(3-morpholino-3-oxopropyl)acetamide (6g)**. Yield: 181 mg (18%) as a white solid. ^{1}H NMR (300 MHz, $CDCl_3$) δ = 1.58*/1.91 (2 × m, 2H, H-5), 2.22/2.28* (2 × s, 3H, H-7), 2.85*/3.23 (2 × t, 2H, *J* = 4.9 Hz, H-6), 3.45–3.75 (4 × m, 8H, H-1, H-2, H-3, H-4), 6.24*/7.18 (2 × s, 1H, H-8), 7.19–7.40 (2 × m, H-*o*, H-*m*, H-*p*). ^{13}C NMR (75 MHz, $CDCl_3$) δ = 21.8*, 22.3, 31.1, 32.2* 41.3, 41.5, 42.4*, 45.3*, 45.6, 60.2*, 65.9, 66.2*, 66.5, 66.6*, 66.7, 127.5*, 128.0, 128.5* (2C), 128.6, (2C), 128.8 (2C), 128.9* (2C), 138.6, 139.4*, 168.6*, 169.4, 170.8*, 171.3. UPLC-MS gradient A, t_R = 1.51 min (>95%), *m/z* 367.4 ([M + H]$^+$, $C_{22}H_{27}N_2O_3^+$ calcd 367.5).

***N*-(3-morpholino-3-oxopropyl)-*N*-phenylacetamide (6h)**. Yield: 154 mg (20%) as a red oil. ^{1}H-NMR (300 MHz,

$CDCl_3$) δ = 1.79 (s, 3H, H-7), 2.53 (t, 2H, *J* = 6.4 Hz, H-5), 2.93–4.17 (4 × t, 4 × 2H *J* = 4.8 Hz, H-1, H-2, H-3, H-4), 4.15 (t, 2H, *J* = 7.5 Hz, H-6), 6.95–7.12 (2 × m, 5H, H-*o*, H-*m*, H-*p*). ^{13}C NMR (75 MHz, $CDCl_3$) δ = 22.7, 31.4, 41.7, 46.0, 46.4, 66.6, 66.7, 127.8 (2C), 128.0, 129.7 (2C), 142.9, 169.2, 170.5. UPLC-MS gradient A, t_R = 1.06 min (>95%), *m/z* 277.3 ([M + H]$^+$, $C_{15}H_{21}N_2O_3^+$ calcd 277.3).

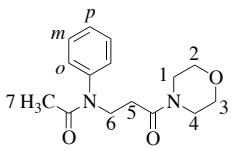

General procedure for trifluoroacetylation.

The monomer (**3a**, **3e**, **3f**, **4a**, **4e**, and **4f**) was dissolved in CH_2Cl_2 (3mL/mmol) and cooled to 0 °C. Then triethylamine (3 equiv) and trifluoroacetic anhydride (2 equiv) were added. After stirring for 4 h, the reaction was taken up in saturated aqueous sodiumhydrogen carbonate (50 mL), and extracted with ethyl acetate (3 × 100 mL). The combined organic phases were dried (Na_2SO_4), filtered and evaporated. The crude product was purified by VLC (3 × 6 cm column, hexane–EtOAc, 5% gradient).

(*S*)-*tert*-Butyl 3-(2,2,2-trifluoro-*N*-(1-phenylethyl)-acetamido)propanoate (7a). Yield: 383 mg (69%), as a clear oil. ^{1}H NMR (300 MHz, $CDCl_3$) δ = 1.37/1.39* (2 × s, 9H, H-1), 1.63*/ 1.67 (2 × s, 3H, *J* = 7.0Hz, H-4), 2.04/2.42 (2H, H-2), 3.35/3.55* (2H, H-3), 2.30/2.75* (2 × q, 1H, *J* = 6.9 Hz, H-5), 7.38 (m, 5H, H-*o*, H-*m*, H-*p*). ^{13}C NMR (75 MHz) δ= 16.5*, 17.6, 28.1 (3C), 33.4, 36.4*, 39.8, 54.8* 55.4, 81.0, 81.4*, 116.9 (q, $J_{C\text{-}F}$ = 287.0 Hz), 127.4 (2C), 127.9* (2C) 128.5*, 128.6, 129.0 (2C), 129.1 (2C), 137.9, 138.7*, 156.7 (q, $J_{C\text{-}O}$ = 35.9 Hz), 169.9*, 170.5. UPLC-MS gradient A, t_R = 2.36 min (>95%), *m/z* 368.2 ([M + Na]$^+$, $C_{17}H_{22}F_3NO_3Na^+$ calcd 368.4), $[\alpha]_{589.2}$: –43° (*c* = 2.3, 293 K, $CHCl_3$)

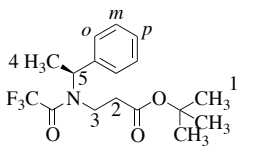

(*S*)-*tert*-Butyl-3-(2,2,2-trifluoro-*N*-(1-(naphthalen-1-yl)-ethyl)acetamido) propanoate (7e). Yield 252 mg (80%) as a clear oil. ^{1}H NMR (300 MHz, $CDCl_3$) δ = 1.18/2.00/2.25* (3 × m, 2H, H-2), 1.28 (s, 9H, H-1), 1.72/1.84* (2 × d, 3H, *J* = 6.9 Hz, H-4), 3.35 (m, 2H, H-3), 5.93*/6.53 (2 × q, 1H, *J* = 7.0 Hz, H-5), 7.48–7.91 (4 × m, 5H, H-*o*, H-*m*, H-*p*). ^{13}C NMR (75 MHz, $CDCl_3$) δ = 16.5, 19.8, 28.1 (3C), 33.4*, 35.6, 38.9, 40.5*, 50.7, 53.2*, 81.2, 116.8 (q, $J_{C\text{-}F}$ = 291.7 Hz), 122.5*, 122.9, 125.3, 125.6, 125.8*, 126.3*, 126.5, 127.3*, 127.7, 129.2, 129.5*, 129.9, 132.2, 133.4, 133.8, 157.3 (q, $J_{C\text{-}O}$ = 36.1 Hz), 169.7. UPLC-MS gradient A, t_R = 2.55 min (>95%), *m/z* 418.2 ([M + Na]$^+$, $C_{21}H_{24}F_3NO_3Na^+$ calcd 418.4). $[\alpha]_{589.2}$: –41° (*c* = 1.7, 293 K, $CHCl_3$).

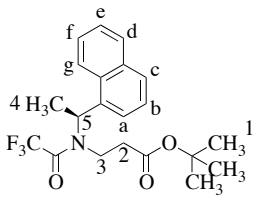

***tert*-Butyl 3-(2,2,2-trifluoro-*N*-(naphthalen-1-ylmethyl)-acetamido)propanoate (7f)**. Yield: 352 mg (77%) as a clear oil. ^{1}H NMR (300 MHz, $CDCl_3$) δ = 1.39*/1.42 (2 × s, 9H, H-1), 2.48*/2.61 (2 × t, 2H, *J* = 7.1 Hz, H-2), 3.63 (m, 2H, H-3), 5.16/5.23* (2 × s, 2H, H-4), 7.21–7.93 (7H, H-*a*, H-*b*, H-*c*, H-*d*, H-*e*, H-*f*, H-*g*). ^{13}C NMR (75 MHz, $CDCl_3$) δ = 27.9, 28.0*, 32.8, 34.6*, 42.1*, 44.1, 47.4, 49.4*, 81.2*, 81.5, 116.5*/116.7 (q, $J_{C\text{-}F}$ = 288.4 / 288.2 Hz), 121.9*, 122.9, 123.5*, 125.2, 125.4*, 126.2*, 126.2, 126.4, 126.7*, 129.9, 128.5*, 128.9, 129.1*, 129.1, 130.0, 130.5, 130.6*, 131.3*, 133.7* 133.9. UPLC-MS gradient A, t_R = 2.51 min (>95%), *m/z* 404.3 ([M + Na]$^+$, $C_{20}H_{22}F_3NO_3Na^+$ calcd 404.4).

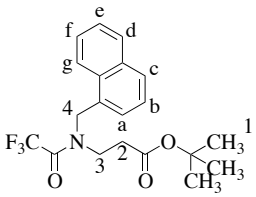

(*S*)-2,2,2-trifluoro-*N*-(3-morpholino-3-oxopropyl)-*N*-(1-phenylethyl)acetamide (8a). Yield: 242 mg (42%). ^{1}H NMR (300 MHz, $CDCl_3$) δ = 1.59*/1.72 (2 × d, 3H, *J* = 7.0*/7.0 Hz, H-9), 2.22*/2.46 (2 × m, 2H, H-5), 2.66/2.98* (2 × m, 2H, H6), 2.73*/2.85 (2 × s, 3H, H-7), 3.38–4.04* (2 × broad m, 8H, H-1, H-2, H-3, H-4), 5.57* (q, 1H, *J* = 6.9 Hz, H-8), 7.25–7.45 (broad m, 6H, H-8, H-*o*, H-*m*, H-*p*). ^{13}C NMR (75 MHz, $CDCl_3$) δ = 15.9*, 17.3*, 30.7, 33.2*, 39.8*, 40.5, 41.8, 45.3*, 54.7, 54.1*, 55.4, 66.3*, 66.5, 66.7*, 116.6 (q , $J_{C\text{-}F}$ = 288.9 Hz), 127.4, 128.1*, 128.3*, 128.5, 128.9*, 129.0, 137.7, 138.9*, 156.7 (q, $J_{C\text{-}O}$ = 35.2 Hz), 168.2*, 168.8. UPLC-MS gradient B, t_R = 1.95 min (>95%), *m/z* 359.2 ([M + H]$^+$, $C_{17}H_{22}F_3N_2O_3^+$ calcd 359.4), $[\alpha]_{589.2}$: –42° (*c* = 1.0, 293 K, $CHCl_3$).

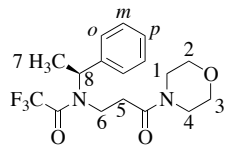

(*S*)-2,2,2-trifluoro-*N*-(3-morpholino-3-oxopropyl)-*N*-(1-(naphthalen-1-yl)ethyl) acetamide (8e). Yield 212 mg (43%) as a clear oil that can be crystallized from chloroform and hexane. ^{1}H NMR (300 MHz, $CDCl_3$) δ = 0.71/1.09*/1.72 (3 × m, 2H, H-5), 1.65/1.79 (2 × d, 3H, *J* = 6.8 Hz, H-7), 2.25/2.47/2.69*/2.88* (2H, H-6), 3.07–3.67 (broad m, 8H, H-1, H-2, H-3, H-4), 5.87*/6.52 (2 × q, 1H, *J* = 6.8 Hz, H-8), 7.41–7.97 (7H, H-*a*, H-*b*, H-*c*, H-*d*, H-*e*, H-*f*, H-*g*). ^{13}C NMR (75 MHz, $CDCl_3$) δ = 16.3, 19.7*, 30.7*, 32.7, 39.2, 41.3*, 41.7, 41.8*, 45.0. 45.5*, 50.4, 53.2*, 66.2, 66.5*, 66.8, 66.9*, 116.8 (q, $J_{C\text{-}F}$ = 287.2 Hz), 123.2, 125.6, 125.7*, 125.9, 126.3*, 126.7, 127.2*, 127.8, 128.9, 129.4*, 129.6, 130.0*, 132.4, 133.0*, 133.6, 133.9, 157.3/158.2 (2 × q, $J_{C\text{-}O}$ = 35.0 Hz), 168.2. UPLC-MS gradient B, t_R = 2.17 min (>95%), *m/z* 409.2 ([M + H]$^+$, $C_{21}H_{24}F_3N_2O_3^+$ calcd 409.4). $[\alpha]_{589.2}$: –49° (*c* = 11 , 293 K, $CHCl_3$).

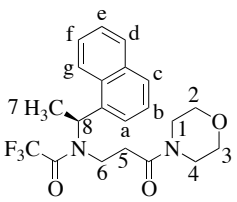

2,2,2-trifluoro-*N*-(3-morpholino-3-oxopropyl)-*N*-(naphthalen-1-ylmethyl) acetamide (8f). Yield: 195 mg (31%) as a clear oil. ^{1}H NMR (300 MHz, $CDCl_3$) δ = 2.33*/2.69 (m*/t, 2H, *J* = 6.9, H-5), 3.10*/ 3.42 (2 × t, 2H, *J* = 4.8*/4.6 Hz, H-6), 3.47–3.80 (broad m, 8 H, H-1, H-2, H-3, H-4), 5.18*/5.29 (2 × s, 2H, H-7), 7.22–7.95 (7H, H-*a*, H-*b*, H-*c*, H-*d*, H-*e*, H-*f*, H-*g*). ^{13}C

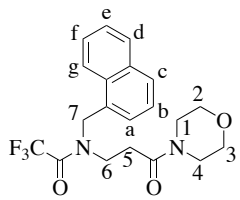

NMR (75 MHz, $CDCl_3$) δ = 30.5, 32.1*, 41.9*, 42.2, 43.0*, 44.8, 45.6*, 46.1, 48.4*, 49.8, 66.3* 66.6, 66.7*, 66.7, 116.5 / 116.7*(2 × q, $J_{C\text{-}F}$ = 288.0 / 288.0 Hz), 122.1, 123.1*, 123.8, 125.4*, 125.5, 126.3, 126.4*, 126.8*, 126.9, 127.1*, 128.7, 129.0*, 129.1, 129.3*, 130.4*/130.5, 130.8, 131.4*, 157.3/158.2 (2 × q, $J_{C\text{-}O}$ = 36.7/36.7 Hz), 168.2*, 169.3. UPLC-MS gradient A, t_R = 2.07 min (>95%), *m/z* 417.3 ([M + Na]$^+$, $C_{20}H_{21}F_3N_2O_3Na^+$ calcd 417.4).

General procedure for C-terminal thioamide formation. Lawesson's reagent (1.5 equiv) was dissolved in toluene 5mL/mmol) and heated to 110 °C under reflux. After the reagent was dissolved, the morpholine-containing monomer (**4a**, **e**, and **f**) was added and the reaction was heated at reflux for 3 hours. The solvent was removed *in vacuo*, and the crude product was purified by VLC (3 × 6 cm, CH_2Cl_2–MeOH, 0.2% gradient from 0→5%).

(*S*)-1-morpholino-3-((1-phenylethyl)amino)propane-1-thione (9a). Yield: 275 mg (45%) as a brown oil, UPLC-MS gradient B, t_R = 0.87min (50%), *m/z* 279.2 ([M + H]$^+$, $C_{15}H_{23}N_2OS^+$ calcd 279.4).

(*S*)-1-morpholino-3-((1-(naphthalen-1-yl)ethyl)amino)-propane-1-thione (9e). Yield: 453 mg (58%) as a brown oil, UPLC-MS gradient B, t_R = 1.10 min (83%), *m/z* 329.3 ([M + H]$^+$, $C_{19}H_{25}N_2OS^+$ calcd 329.5).

1-morpholino-3-((naphthalen-1-ylmethyl)amino)propane-1-thione (9f). Yield: 127 mg (21%) as a brown oil, UPLC-MS gradient B, t_R = 1.30min, *m/z* 315.2 ([M + H]$^+$, $C_{18}H_{23}N_2OS^+$ calcd 315.4).

General procedure for acetylation of C-terminal thioamides. The thioamide (1 equiv) was dissolved in CH_2Cl_2 (5 mL/mmol) and cooled to 0 °C. Then *i*-Pr_2NEt (2 equiv) and acetylchloride (2 equiv) were added and the reaction was stirred for 3 h at 0 °C. The solvent was evaporated, and the crude product purified by VLC (3 × 6 cm column, hexane–EtOAc, 5% gradient).

***(S)*-*N*-(3-morpholino-3-thioxopropyl)-*N*-(1-phenylethyl)-acetate (10a)**. Yield: 0.42 g (59 %) as a brown oil. ^{1}H NMR (300 MHz, $CDCl_3$) δ = 1.43*/1.65 (2 × d, 3H, *J* = 7.1 Hz, H-9), 2.24/2.24* (2 × s, 3H, H-7), 2.96–4.28 (7 × m, 12 H, H-1, H-2, H-3, H-4, H-5, H-6), 5.09/6.06* (2 × q, 1H, *J* = 7.0 Hz, H-8), 7.24–7.40 (m, 5H, H-*o*, H-*m*, H-*p*). ^{13}C NMR (75 MHz, $CDCl_3$) δ = 16.2*, 18.5, 22.2, 42.3*, 42.5, 43.0, 43.7*, 49.5*, 49.5, 50.9, 50.8*, 56.8, 66.4*, 66.9, 67.1, 126.7, 127.8*, 128.0, 128.4*, 128.7*, 129.0, 139.9, 171.2, 199.7. UPLC-MS gradient B, t_R = 1.71 min (>95%), *m/z* 321.2 ([M + H]$^+$, $C_{17}H_{25}N_2O_2S^+$ calcd 321.4), $[\alpha]_{589.2}$: –33° (*c* = 1.6 , 293 K, $CHCl_3$).

(*S*)-*N*-(3-morpholino-3-thioxopropyl)-*N*-(1-(naphthalen-1-yl)ethyl)acetamide (10e). Yield: 0.228 g (44%), as a clear oil. ^{1}H-NMR (300 MHz, $CDCl_3$) δ = 1.31/2.20* (m, 2H, H-5), 1.62/1.81* (2 × d, 2H, *J* = 6.8 Hz, H-7), 2.45/2.84* (2 × m, 2H, H-6), 2.28/2.40* (2 × s, 3H, H-7), 3.09–4.18 (broad m, 8H, H-1, H-2, H-3, H-4), 5.70*/6.65 (2 × q, 1H, *J* = 6.9 Hz, H-8), 7.54–7.89 (2 × broad m, 8H, H-*a*, H-*b*, H-*c*, H-*d*, H-*e*, H-*f*, H-*g*). ^{13}C NMR (75 MHz, $CDCl_3$) δ = 16.8, 23.3, 42.0, 43.7, 48.1, 49.3, 49.5, 66.3, 66.5, 124.2, 125.1, 125.3, 126.7, 127.0, 127.7, 128.7, 129.0, 129.5, 129.6, 170.9, 199.1. UPLC-MS gradient B: t_R = 2.00 min (>95%), *m/z* 371.2 ([M + H]$^+$, $C_{21}H_{26}N_2O_2S^+$ calcd 371.5). $[\alpha]_{589.2}$: –87° (*c* = 0.3 , 293 K, $CHCl_3$).

***N*-(3-morpholino-3-thioxopropyl)-*N*-(naphthalen-1-ylmethyl)acetamide (10f)**. Yield: 0.061 g (42%) as a clear oil. ^{1}H-NMR (300 MHz, DMSO-d_6) δ = 2.01*/2.19 (2 × s, 3H, H-7), 2.62*/3.51/3.63/3.85*/4.14 (m, 8H, H-1, H-2, H-3, H-4), 3.05 (m, 2H, H-5), 3.57 (m, 2H, H-6), 5.02/5.11* (2 × s, 2H, H-8), 7.22–8.05 (m, 7H, H-a, H-b, H-c, H-d, H-e, H-f, H-g). ^{13}C NMR (75 MHz, $CDCl_3$) δ = 21.6, 41.9, 46.7, 50.1, 50.7, 50.9, 66.6, 67.0, 122.1, 122.6, 125.6, 126.3, 126.8, 127.8, 128.4, 129.2, 130.7, 131.3, 169.4, 187.9. UPLC-MS gradient B: t_R = 1.95 min (>95%), *m/z* 357.2 ([M + H]$^+$, $C_{20}H_{25}N_2O_2S^+$ calcd 357.5).

General procedure for N-terminal thioacetyl formation. Lawesson's reagent (0.6 equiv) was dissolved in toluene 5mL/mmol) and heated to 110°C under reflux. After the solid was dissolved, the acetylated monomer (**5a**, **e**, and **f**) was added and the reaction was refluxed for 1 hour. The solvent was removed *in vacuo*. The crude product was purified by VLC (3 × 6 cm, hexane–EtOAc, 5% gradient).

(*S*)-*tert*-butyl 3-(*N*-(1-phenylethyl)ethanethioamido)-propanoate (11a). Yield: 145 mg (69%) as a yellow oil, UPLC-MS gradient B, t_R = 2.52 min (>95%), *m/z* 308.2 ([M + H]$^+$, $C_{17}H_{26}NO_2S^+$ calcd 308.4).

(*S*)-*tert*-butyl 3-(*N*-(1-(naphthalen-1-yl)ethyl)ethane-thioamido)propanoate (11e). Yield: 289 mg (74%) as a yellow oil, UPLC-MS gradient B, t_R = 2.47min (>95%), *m/z* 358.3 ([M + H]$^+$, $C_{21}H_{28}NO_2S^+$ calcd 358.5).

***tert*-butyl 3-(*N*-(naphthalen-1-ylmethyl)ethane-thioamido)propanoate (11f)**: Yield: 618 mg (70%) as a

yellow oil, UPLC-MS gradient B, t_R = 2.17min (>95%), *m/z* 344.3 ([M + H]$^+$, $C_{21}H_{28}NO_2S^+$ calcd 344.5).

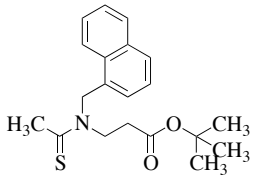

General procedure for morpholine amide formation in N-terminal thioamides.

The thioacetylated monomers (**11a**, **e**, and **f**) were dissolved in DMF (2mL/mmol) and hydrolyzed using 1M LiOH (4 eqiuv). After 2 hours the reaction mixture was taken up in 1M HCl and extracted with EtOAc (3 × 100 mL). The combined organic phases were dried (Na_2SO_4), filtered, and evaporated to dryness. The crude product, HBTU (2 equiv) and *i*-Pr_2NEt (2 equiv) were dissolved in CH_2Cl_2 (2 mL/mmol). After stirring for 10 min at room temperature, morpholine (2 equiv) was added. After stirring overnight, the solvent was evaporated and the crude product was purified by VLC (3 × 6 cm, CH_2Cl_2–MeOH, 0.2% gradient from 0→5%).

(*S*)-*N*-(3-morpholino-3-oxopropyl)-*N*-(1-phenylethyl)-ethanethioamide (12a). Yield: 91 mg (62%) as a clear oil.

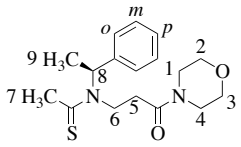

^{1}H NMR (300 MHz, $CDCl_3$) δ = 1.59*/1.72 (2 × d, 3H, *J* = 7.0 Hz, H-9), 2.22*/2.46 (2 × m, 2H, H-5), 2.66/2.98* (2 × m, 2H, H6), 2.73*/2.85 (2 × s, 3H, H-7), 3.38–4.04 (2 × broad m, 8H, H-1, H-2, H-3, H-4), 5.57* (q, 1H, *J* = 6.9 Hz, H-8), 7.25–7.45 (broad m, 6H, H-8, H-*o*, H-*m*, H-*p*). ^{13}C NMR (75 MHz, $CDCl_3$) δ = 30.2, 31.1* 32.7*, 32.9, 38.7, 41.8*, 42.0, 45.5*, 46.2, 47.2*, 51.3, 55.0, 66.2*, 66.6*, 66.7, 66.8, 122.1, 122.3, 123.6, 125.4*, 125.6, 126.3*, 126.3, 126.7*, 126.8, 127.0*, 128.4, 128.8*, 129.1, 130.0, 130.4, 131.0*, 131.6*, 133.8, 167.9*, 169.4, 201.2*, 201.9. UPLC-MS gradient A: t_R = 1.62 min (>95%), *m/z* 311.2 ([M + H]$^+$, $C_{17}H_{25}N_2O_2S^+$ calcd 321.4). $[\alpha]_{589.2}$: –133° (*c* = 0.8, 293 K, $CHCl_3$).

(*S*)-*N*-(3-morpholino-3-oxopropyl)-*N*-(1-(naphthalen-1-yl)ethyl)ethanethioamide (12e). Yield: 172 mg (57%) as a yellow oil.

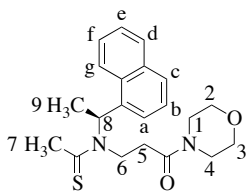

^{1}H-NMR (300 MHz, $CDCl_3$) δ = 0.80/1.75 (2 × m, 2H, H-5), 1.68/1.80* (2 × d, 2H, *J* = 6.7 Hz, H-9), 2.20/2.42 (2 × m, 2H, H-6), 2.68/3.03* (2 × s, 3H, H-7), 3.07–4.30 (8H, H-1, H-2, H-3, H-4), 6.00* (q, 1H, *J* = 6.7 Hz, H-8), 7.46–8.08 (broad m, 8H, H-8, H-*a*, H-*b*, H-*c*, H-*d*, H-*e*, H-*f,* H-*g*). ^{13}C NMR (75 MHz, $CDCl_3$) δ = 14.6, 17.2*, 17.6*, 18.6*, 29.6*, 31.4, 32.7, 32.82*, 41.6, 43.4, 44.9, 45.5*, 46.1*, 55.5*, 56.4, 57.6*, 66.0, 66.4*, 66.5, 66.6*, 122.1, 124.4, 125.5, 125.7, 126.2*, 126.4, 127.3*, 127.6, 128.5, 129.1, 129.3*, 129.7*, 131.7*, 132.8, 133.2, 133.2*, 133.5*, 135,2, 167.7, 168.9*, 199.3. UPLC-MS gradient B: t_R = 1.81 min (>95%), *m/z* 371.3 ([M + H]$^+$, $C_{21}H_{26}N_2O_2S^+$ calcd 371.5). $[\alpha]_{589.2}$: –309° (*c* = 2.8, 293 K, $CHCl_3$).

***N*-(3-morpholino-3-oxopropyl)-*N*-(naphthalen-1-ylmethyl)ethanethioamide (12f)**. Yield: 186 mg (56%) as a clear oil.

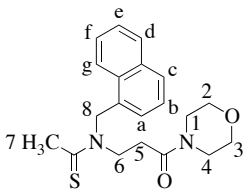

^{1}H NMR (300 MHz, $CDCl_3$) δ = 2.25*/3.01 (2 × t, 2H, *J* = 6.9 Hz, H-5), 2.65/2.84* (2 × s, 3H, H-7), 3.45–3.70 (8H, H-1, H-2, H-3, H-4), 3.87*/4.30 (2 × s, 2H, *J* = 6.8 Hz, H-6), 5.46/5.78* (2 × s, 2H, H-8), 7.10–8.03 (m, 7H, H-*a*, H-*b*, H-*c*, H-*d*, H-*e*, H-*f*, H-*g*). ^{13}C NMR (75 MHz, $CDCl_3$) δ = 30.2, 31.1* 32.7*, 32.9, 38.7, 41.8*, 42.0, 45.5*, 46.2, 47.2*, 51.3, 55.0, 66.2*, 66.6*, 66.7, 66.8, 122.1, 122.3, 123.6, 125.4*, 125.6, 126.26*, 126.3, 126.7*, 126.8, 127.0*, 128.4, 128.8*, 129.1, 130.0, 130.4, 131.0*, 131.6*, 133.8, 167.9*, 169.4, 201.2*, 201.9, UPLC-MS gradient B: t_R = 1.97min (>95%), *m/z* 357.1 ([M + H]$^+$, $C_{21}H_{26}N_2O_2S^+$ calcd 357.5).

(*S*)-*N*-(1-(naphthalen-1-yl)ethyl)-*N*-(2-oxo-2-(piperidin-1-yl)ethyl)acetamide (13). Yield: 53 mg as a pale yellow oil.

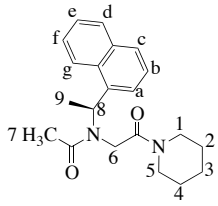

^{1}H NMR (300 MHz, $CDCl_3$) δ = 1.29-166 (broad m, 6H, H-2, H-3, H-4), 1.57/1.78* (2 × d, *J* = 7.0 Hz, 2H, H-9), 2.03/2.30* (2 × s, 3H, H-7), 2.86-3.79 (m, 6H, H-1, H-5, H-6), 5.79*/6.69 (2 × q, *J* = 7.1 Hz), 7.40-8.10 (m, 7H, H-a, H-b, H-c, H-d, H-e, H-f, H-g). ^{13}C NMR (75 MHz, $CDCl_3$) δ = 16.7, 19.9*, 21.8*, 22.3, 24.4, 24.6*, 25.6, 26.3*, 26.4, 43.5, 44.0*, 44.8, 45.4*, 45.8, 46.2*, 48.3, 49.8*, 54.0*, 54.5*, 122.6*, 124.1*, 124.4, 124.8, 124.9, 125.4*, 126.1*, 126.2, 126.9, 127.0*, 128.5, 128.8*, 128.9, 129.2*, 131.0*, 132.1, 133.9, 134.0*, 136.5, 137.2*, 166.1, 166.7*, 171.4*, 171.5. UPLC-MS gradient B: t_R = 1.92 (>95%). $[\alpha]_{589.2}$: –25° (*c* = 0.6, 293 K, CH_2Cl_2).

(*S*)-2,2,2-trifluoro-*N*-(1-(naphthalen-1-yl)ethyl)-*N*-(2-oxo-2-(piperidin-1-yl)ethyl)acetamide (14). Yield: 45 mg as a pale yellow oil.

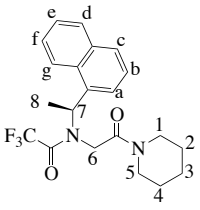

^{1}H NMR (300 MHz, $CDCl_3$) δ = 1.26-1.66 (broad m, 6H, H-2, H-3, H-4), 1.72/1.89 (2 × d, *J* = 6.8 Hz, 3H, H-8), 2.87-3.10/3.26-3.40/3.47-3.70 (4H, H-1, H-5), 3.52/3.90/4.24* (3 × d, *J* = 18.4 Hz, 2H, H-6), 6.04*/6.52 (2 × q, *J* = 6.9 Hz), 7.45-7.91 (7H, H-a, H-b, H-c, H-d, H-e, H-f, H-g). ^{13}C NMR (75 MHz, $CDCl_3$) δ = 15.1, 18.4*, 23.1, 24.2 (broad), 24.8 (broad), 29.7*, 36.0*, 36.8*, 37.3*, 37.4*, 42.5 (broad), 43.4 (broad), 43.5 (broad), 43.9*, 44.5 (broad), 49.5*, 50.4, 52.4*, 115.4 (q, $J_{C\text{-}F}$ = 288.3 Hz), 122.0, 123.6, 123.8*, 124.3, 125.0*, 125.1, 125.9*, 126.0, 127.6, 127.9*, 128.4, 130.6, 132.7, 132.9, 157.3 (q, $J_{C\text{-}O}$ = 35.0 Hz), 163.1*, 164.0. UPLC-MS gradient B: t_R = 2.36 (>95%). $[\alpha]_{589.2}$: –13° (*c* = 0.6, 293 K, CH_2Cl_2).

(*S*)-*N*-(1-(naphthalen-1-yl)ethyl)-*N*-(2-oxo-2-(piperidin-1-yl)ethyl)ethanethioamide (15). Yield: 52 mg as a white solid. ^{1}H NMR (300 MHz, $CDCl_3$) δ = 1.23-1.80 (m, 6H, H-

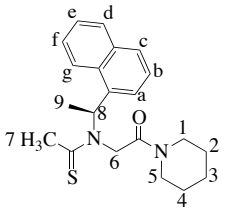

2, H-3, H-4), 1.70/1.91* (2 × d, *J* = 6.9 Hz, H-9), 2.60/2.94* (2 × s, H-7), 2.90-3.75 (m, 4H, H-1, H-5), 3.79*/3.80/3.93/5.24* (4 × d, *J* = 17.2 Hz, 2H, H-6), 6.13* (q, *J* = 7.0 Hz, H-8), 7.48-8.11 (m, 8H, H-8, H-a, H-b, H-c, H-d, H-e, H-f, H-g). ^{13}C NMR (75 MHz, $CDCl_3$) δ = 14.9, 19.1*, 22.5*, 22.7*, 24.4, 24.7*, 25.6, 25.7*, 26.2*, 26.4, 32.4*, 33.3, 43.5, 44.7*, 45.9, 46.6*, 48.0, 51.0*, 57.3, 58.5*, 122.4*, 124.4*, 124.9, 125.0, 125.5, 125.6*, 126.3*, 126.5, 127.3, 127.5*, 128.6, 129.3*, 129.4*, 129.5, 131.0*, 132.5, 133.9, 134.1*, 135.8*, 135.9, 164.0, 164.8*, 201.4*, 202.0. UPLC-MS gradient B: t_R = 2.24 (>95%). $[\alpha]_{589.2}$: –55° (*c* = 0.6, 293 K, CH_2Cl_2).

Table S1. High-resolution mass spectrometry (HRMS) Data.[a]

compd.	$[M+H]^+$	calcd.	found (*m*/*z*)	Δ*M* (ppm)
3a	$C_{15}H_{23}NO_2$	250.1802	250.1805	1.2
3b	$C_{15}H_{29}NO_2$	256.2271	256.2275	1.6
3c	$C_{14}H_{21}NO_2$	236.1645	236.1645	0.0
3e	$C_{19}H_{25}NO_2$	300.1958	300.1958	0.0
3f	$C_{18}H_{23}NO_2$	286.1802	286.1802	0.0
3h	$C_{13}H_{19}NO_2$	222.1489	222.1491	0.9
5a	$C_{17}H_{25}NO_3$	292.1907	292.1907	0.0
5b	$C_{17}H_{31}NO_3$	298.2377	298.2378	0.3
5c	$C_{16}H_{23}NO_3$	278.1751	278.175	0.4
5d	$C_{13}H_{25}NO_3$	244.1907	244.1905	0.8
5e	$C_{21}H_{27}NO_3$	342.2064	342.2068	1.2
5f	$C_{20}H_{25}NO_3$	328.1904	328.1908	1.2
5g	$C_{22}H_{27}NO_3$	354.2064	354.2069	1.4
5h	$C_{15}H_{21}NO_3$	264.1594	264.1596	0.6
6a	$C_{17}H_{24}N_2O_3$	305.1860	305.1859	0.3
6b	$C_{17}H_{30}N_2O_3$	311.2329	311.2331	0.6
6c	$C_{16}H_{22}N_2O_3$	291.1703	291.1706	1.0
6d	$C_{13}H_{24}N_2O_3$	257.1860	257.1861	0.4
6e	$C_{21}H_{26}N_2O_3$	355.2016	355.2017	0.3
6f	$C_{20}H_{24}N_2O_3$	341.1860	341.1862	0.6
6g	$C_{22}H_{26}N_2O_3$	367.2016	367.2021	1.4
6h	$C_{15}H_{20}N_2O_3$	277.1547	277.1551	1.4
7a	$C_{17}H_{22}F_3NO_3$	346.1625	346.1623	0.6
7e	$C_{21}H_{24}F_3NO_3$	396.1781	396.1779	0.5
7f	$C_{20}H_{22}F_3NO_3$	382.1625	382.1623	0.5
8a	$C_{17}H_{21}F_3N_2O_3$	359.1577	359.1579	0.6
8e	$C_{21}H_{23}F_3N_2O_3$	409.1734	409.1739	1.2
8f	$C_{20}H_{21}F_3N_2O_3$	395.1577	395.1583	1.5
10a	$C_{17}H_{24}N_2O_2S$	321.1631	321.1634	0.9
10e	$C_{21}H_{26}N_2O_2S$	371.1788	371.1790	0.5
10f	$C_{20}H_{24}N_2O_2S$	357.1631	357.1635	1.1
12a	$C_{17}H_{24}N_2O_2S$	321.1631	321.1641	3.1
12e	$C_{21}H_{26}N_2O_2S$	371.1788	371.1790	0.5
12f	$C_{20}H_{24}N_2O_2S$	357.1631	357.1640	2.5
14	$C_{21}H_{23}F_3N_2O_2$	393.1784	393.1788	1.1
15	$C_{21}H_{26}N_2OS$	355.1839	355.1840	0.3

[a]Determined by ESI-TOF HRMS on a maXis G3 quadrupole time-of-flight (TOF) mass spectrometer (Bruker Daltonics, Bremen, Germany) equipped with an electrospray (ESI) source.

Angewandte Communications

Foldamers

DOI: 10.1002/anie.201((will be filled in by the editorial staff))

Trianguler Prism-Shaped Helices—Synthesis and Structural Determination of β-Peptoid Oligomers**

*Jonas S. Laursen, Pernille Harris, and Christian A. Olsen**

Abstract: *"β-Peptoids" are N-alkylated β-aminopropionic acid residues (or N-alkyl-β-alanines). Here, we present the first examples of high-resolution structures of linear oligomeric constructs of this type of peptide mimic. We describe synthesis and characterization of oligomers up to the hexamer length containing two different types of N-alkyl side chains, and furthermore investigation of the effect of N-terminal trifluoroacetylation. Our X-ray crystallographic data reveal right-handed helical conformations with exactly three residues per turn and a helical pitch of 9.6–9.8 Å between turns in the solid state. These are the longest helical peptoid structures solved by X-ray crystallography to date.*

The ability to mimic or complement native protein and peptide folds using nonnatural oligomers endowed with resistance towards proteolysis holds promise for the design of chemotypes with valuable applications in medical and materials sciences. Oligomeric architectures able to adopt well-defined folding patterns have been coined "foldamers" ,[1] and several peptidomimetic designs have demonstrated this type of behavior,[2] including β-peptides[3, 4] and "peptoids" (N-alkylglycines).[5] The β-peptoids, first described as dimers and trimers by Hamper and coworkers,[6] combine the structural features of the two latter mentioned foldamers (Figure 1A), and have been suggested by theoretical methods to be able to adopt helical conformations.[7] However, CD-spectroscopical evaluation of oligomers containing β-peptoid units with α-chiral side chains have proven inconclusive,[8] and high-resolution structures have been lacking, except for head-to-tail cyclized species.[9] Nevertheless, β-peptoid units have been incorporated in oligomers showing non-hemolytic antimicrobial,[10, 11] antiplasmodial,[12] and cell-penetrating[13] activities as well as excellent stability towards proteolytic enzymes.[11] Inspired by studies performed with α-peptoid model systems,[14, 15] we and others have recently reported on tunability of the *cis–trans*-amide bond equilibria of the tertiary amide bonds in β-peptoids (Figure 1B).[16, 17] Building on these insights, we here report the first high-resolution structures of helical β-peptoid oligomers, which should enable a more informed and structure-based design of foldameric materials of this type in the future.

We planned to investigate oligomers up to the hexamer length. Since high-resolution structures of α-peptoids have been successfully obtained for oligomers of just 4–5 residues in length, we envisioned that a hexamer might be sufficient to acquire stabilized folding. Two different α-chiral side chains were chosen (Figure 1C), the *N*-(*S*)-1-phenylethyl (**1**–**5**), which has been studied in both α- and β-peptoids, and the *N*-(*S*)-1-(1-naphthyl)ethyl (**6**–**10**), which was applied in an α-peptoid tetramer structure solved by X-ray crystallography.[18]

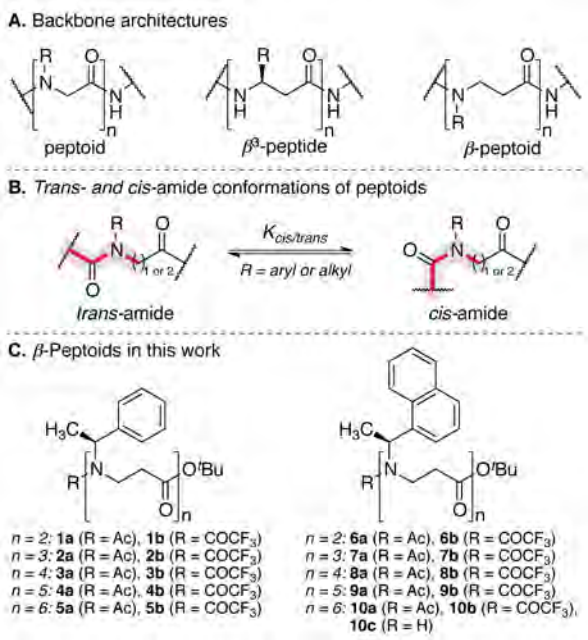

Figure 1. (A) Generic structures of the backbone architectures of peptoids (*i.e.*, α-peptoids), β^3-peptides (β^2- and disubstituted β-peptides are not shown), and β-peptoids. (B) Depiction of the equilibrium of *transoid* and *cisoid* amide conformations in peptoid residues. (C) β-Peptoid oligomers prepared for structural and spectroscopic evaluation in this study.

[*] M.Sc. J. S. Laursen, Prof. P. Harris, Prof. C. A. Olsen[+]
Department of Chemistry
Technical University of Denmark
Kemitorvet 207, DK-2800, Kongens Lyngby (Denmark)
Fax: (+45) 45933968
E-mail: cao@kemi.dtu.dk

[+] Note: Prof. Olsen's laboratory is moving to the Faculty of Health and Medical Sciences, University of Copenhagen, Jagtvej 162, DK-2100, Copenhagen (Denmark); Future correspondence should be directed there.

[**] We thank Ms. Anne Hector and Dr. Charlotte H. Gotfredsen for assistance with NMR spectroscopy, Ms. Tina Gustafsson for technical assistance with UPLC-MS, Ms. Lise Lotte Berring for assistance with X-ray data collection, and Novo Nordisk A/S for a generous donation of peptide-coupling reagents. We thank Dr. Søren W. Pedersen and Dr. Strømgaard (University of Copenhagen) for assistance with and access to a CD-spectrometer. This work was financially supported by DTU (PhD fellowship to J.S.L.), the Danish Independent Research Council | Natural Sciences (Steno Grant no. 10-080907, C.A.O.), and the Carlsberg Foundation (P.H.). C.A.O. is a Lundbeck Foundation Fellow.

Supporting information for this article is available on the WWW under http://dx.doi.org/10.1002/anie.201xxxxxx.

Table 1. Overall *Cis–Trans*-Amide Bond Ratios ($K_{cis–trans}$) Determined by NMR Spectroscopy.

N-(S)-1-Phenylethyl series										
Compound	**1a**	**1b**	**2a**	**2b**	**3a**	**3b**	**4a**	**4b**	**5a**	**5b**
CD_3CN	0.8	0.3	0.8	0.4	0.8	0.5	0.7	0.5	0.7	0.5
C_6D_6	0.6	0.3	0.6	0.3	0.6	0.3	0.5	0.3	0.4	0.3
N-(S)-1-(1-Naphthyl)ethyl series										
Compound	**6a**	**6b**	**7a**	**7b**	**8a**	**8b**	**9a**	**9b**	**10a**	**10b**
CD_3CN	5.2	5.4	5.2	6.0	5.9	7.3	_[a]	_[a]	_[a]	_[a]
C_6D_6	4.8	4.0	4.4	4.0	5.6	4.3	6.4	4.9	11.0	10.0

[a] Limited solubility of this compound did not allow for NMR analysis in acetonitrile-d_6.

The *N*-(*S*)-1-phenylethyl side chain, although shown to successfully induce helical conformations in α-peptoids,[19] does not induce significant control of the amide bond *cis–trans* equilibrium. It is therefore not entirely surprising that β-peptoid oligomers of this type have not previously been unambiguously shown to establish robust secondary structures. In recent monomer-based model systems, however, we found that the *trans*-amide conformation was preferred upon trifluoroacetylation of *N*-(*S*)-1-phenylethyl monomers.[17] The effect of this substitution was therefore included in the present investigation (**1b**–**5b**) along with the acetylated control compound series **1a**–**5a**. The second series contained the *N*-(*S*)-1-(1-naphthyl)ethyl side chain (**6a**–**10d**), which was first introduced in β-peptoids,[20] and later found to strongly induce *cis*-amide conformations in model systems[15, 17] as well as in helical[18] and ribbon-shaped[21] α-peptoids. All compounds were prepared by a subunit approach in solution, essentially as previously described[22] (see, the Supporting Information for details). For the considerably sterically congested naphthyl-containing compounds, in particular, we found the necessary reaction times to increase with the growing length of the oligomer. For future preparation of longer chains we therefore envision that a fragment-based strategy may be necessary.

^{1}H NMR spectra of the oligomers exhibited significant signal overlapping due to the identical side chains throughout each series as would be expected. We therefore focused on the shifts corresponding to the side chain methine protons to determine overall *cis–trans*-amide bond ratios (Table 1). NMR data showed no significant trend on the overall *cis–trans* ratios for the compounds in the *N*-(*S*)-1-phenylethyl series (**1**–**5**). In the *N*-(*S*)-1-(1-naphthyl)ethyl series (**6**–**10**), however, increases in $K_{cis–trans}$ values could be observed upon elongation of the oligomers, as particularly evident for the constants determined for the hexamers in benzene (Table 1). Unfortunately, the two highest oligomers were not sufficiently soluble in acetonitrile to obtain NMR spectra of sufficient quality, but especially for the trifluoroacetylated series, there appears to be a slight increase in $K_{cis–trans}$ from dimer to tetramer. Taken together, these values may indicate propensity for the oligomers to adopt length- as well as solvent-dependent secondary structures, although high-resolution measurements are required to determine whether this is the case.

Gratifyingly, we were able to crystallize compounds **10a**, **10b**, and **10c** by slow evaporation of MeOH–$CHCl_3$ or benzene solutions of the compounds. Diffraction quality crystals were obtained for **10a** and **10c** from MeOH–$CHCl_3$, and their structures were solved by X-ray crystallography at 1.05 Å and 1.00 Å resolution, respectively. The N-terminally non-acylated compound **10c** was solved first, and revealed a helical conformation of precisely three residues per turn and a pitch of ~9.6 Ångström with only the N-terminal naphthyl side chain twisted away from the helix (Figure 2A). The remaining naphthyl groups were highly organized along each of the three faces of the helix to give an equilateral triangle when viewed down the helical axis (Figure 2B,C). The main helix thus adopts a triangular prism shape, not taking the N-terminal side chain into consideration.

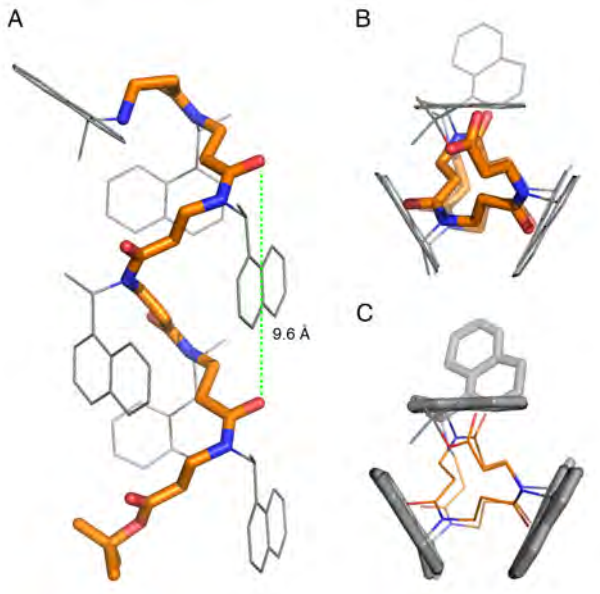

Figure 2. X-Ray crystal structure of compound **10c**. (A) Side view. (B and C) End views from the C-terminal. The backbone is shown in orange and hydrogen atoms are omitted for clarity. Representations of X-ray crystal structures were prepared using the PyMOL Molecular Graphics System, Schrödinger, LLC.

We envisioned, based on our monomer studies, that acetylation of the N-terminal would also force this amide into a *cisoid* configuration, and hoped that this would direct the final side chain to alignment along the third phase of the molecule. The X-ray crystal structure of compound **10a** indeed confirmed this (Figure 3), as this compound turned out to crystallize in the highly symmetric *R3* space group with only one -CH_2CON(1-(1-naphthyl)ethyl)CH_2- fragment in the asymmetric unit (see the CIF file in the Supporting Information for details). Thus, the crystal symmetry generates infinitely long, parallel chains, and this renders the *t*-butyl group

invisible, due to the 1:6 ratio of *t*-butyl to 1-(1-naphthyl)ethyl. This results in crystal packing where the helical segments are arranged in a head-to-tail manner to give highly regular elongated triangular threads (Figure 4) with a helical pitch of 9.8 Å (Figure 3A). To reveal the complete molecule, including the N-terminal-acetamido and C-terminal *t*-butyl ester groups, data sets were collected on several crystals and unsuccessful attempts were made to solve the structure in P1. This packing issue was not observed for compound **10c** due to the positioning of N-terminal side chain, and therefore enabled visualization of the full structure including the C-terminal *t*-butyl (Figure 4A).

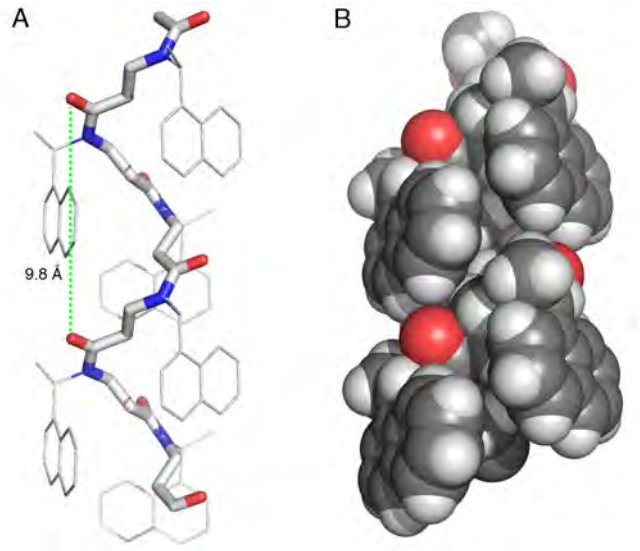

Figure 3. X-Ray crystal structure of compound **10a**. (A) Showing the backbone helical as sticks and side chains as lines (hydrogen atoms are omitted for clarity). (B) Spacefilling representation showing the packing of the naphthyl groups along the phases of the triangular prism-shaped conformation.

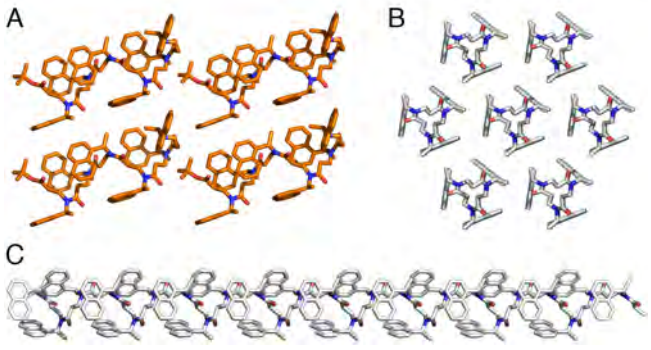

Figure 4. X-Ray crystal packing. (A) Compound **10c** viewed perpendicular to the helical axis with the N-terminal side chain pointing out of the plane. Additional representations of the packing are shown in Supplementary Figures S3 and S4. (B and C) Compound **10a**, viewed from the end and perpendicular to the helical axis, respectively. Hydrogen atoms are removed for clarity.

The torsion angles in the two helices are very similar (Table 2), and the extended structures compare reasonably well with one of the helical conformations previously suggested by density functional theory (DFT) calculations, albeit with a ~20 degree difference in the ω and θ angles (Supplementary Table S1).[7] To the best of our knowledge, however, the present work provides the first experimental demonstration of the existence of this helical type. Most previously determined helical conformations of a *β*-peptidic nature have been shown to contain stabilizing hydrogen bond networks,[4] and investigation of oligomers of homologated proline residues indicated *trans*-amide-containing conformations.[23] Our structures are thus unique to the field of foldamers. The highly ordered, tight packing of the side chains along the three phases of the helical axis (Figure 3B) combined with their strong *cis*-amide inducing properties,[17] it appears that this type of side chain provides a particularly strong stabilization of this novel secondary structure motif. Furthermore, intramolecular distances indicate CH–π interactions between backbone methylene group and side chain naphthyl groups, which may also contribute to stabilization and protection of the helical backbone from solvation (Supplementary Figure S4 and Table S2). This is quite different from the X-ray crystal structure reported for an α-peptoid tetramer containing the same side chains.[18] In agreement with that structure, however, as well as the findings from our previous monomer investigations, we did not see evidence for stabilizing $n\rightarrow\pi^*_{Ar}$ interactions in our crystal structure. On the other hand, our *cis*-amide conformations were in agreement with the recently described "bridged" effect.[24] In future work it will now be interesting to investigate the ratio of *N*-(*S*)-1-(1-naphthyl)ethyl side chains to other functionalities, which are required to adopt stable secondary structure.

Table 2. Torsion Angles in the Helical Structures.

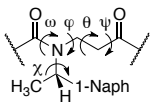

Compound **10a**[a]

φ	θ	ψ	ω	χ_1[b]	χ_2[c]
96.3	172.5	–175.3	–13.8	53.6	–80.4

Compound **10c**[a]

φ	θ	ψ	ω	χ_1[b]	χ_2[c]
97.4	166.0	–173.9	–13.4	56.3	–73.8

[a] Measured at residue 5 in the structure to give representative values for a residue within the helix. See Table S1 in the Supporting Information for dihedral angles of additional residues. [b] Measured by the naphthyl substituent. [b] Measured by the methyl substituent.

Finally, we evaluated the compounds by CD spectroscopy. The CD spectra of the acetylated *N*-(*S*)-1-phenylethyl series (Figure 5A–B) were similar to those previously reported for *β*-peptoids containing this side chain, whereas the *N*-(*S*)-1-(1-naphthyl)ethyl series (**6a**–**10a**) revealed a minimum at 224–228 nm and a maximum at 215–218 nm (Figure 5C). At first glance, we were surprised that these Cotton effects decreased with increasing length of the oligomer. However, both the minimum and the maximum were present in the CD spectrum of an acetyled monomer and not of a non-acetylated monomer (Supplementary Figure S5), which indicates that these signals are not indicative of secondary structure formation but rather a signature of the amide motif itself. Starting at the tetramer length (**8a**), on the other hand, a positive signal started to appear near 232 nm. This signal intensified with growing length of the oligomers, suggesting that this peak may be indicative of length-dependent secondary structure formation.

We also obtained CD spectra of the trifluoroacetylated oligomers, which exhibited the same overall spectral shapes (Figure 5D). Notably, six residues were necessary to obtain a positive signal

at 232 nm in this series, suggesting that trifluoroacetylation has a negative effect on secondary structure formation in acetonitrile. In our monomer study, we observed stabilization of the *cis*-amide conformation upon trifluoroacetylation compared to acetylation, but this apparently does not translate into a stabilizing effect on oligomer secondary structure. This may be explained by a steric clash between the bulkier trifluoroacetyl group and the first backbone methylene group at the N-terminal.

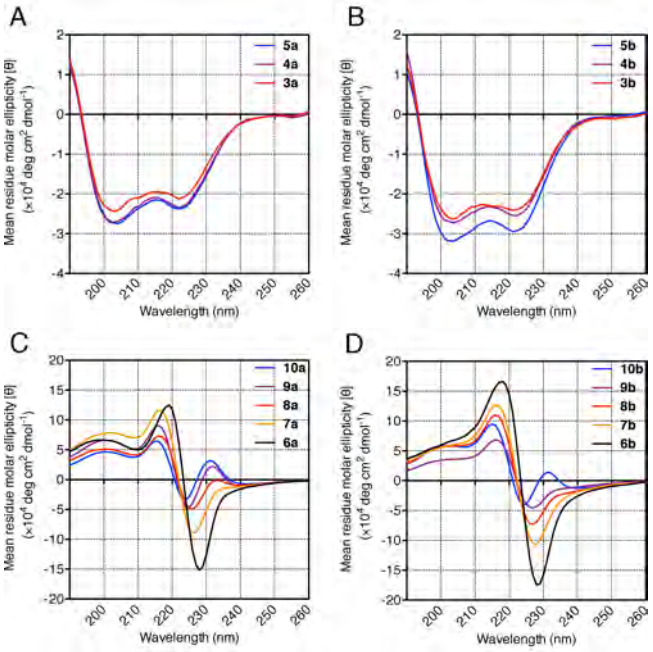

Figure 5. CD spectra of compounds **3a–5a** (A), **3b–5b** (B), **6a–10a** (C), and **6b–10b** (D) in acetonitrile (~60 μM).

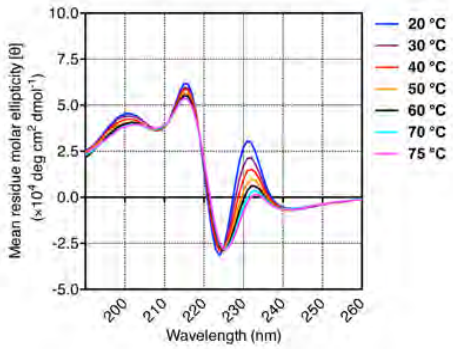

Figure 6. CD spectra of compound **10a** at varying temperatures in acetonitrile (~60 μM).

To assess whether the positive signal at 232 nm is indicative of folding, we also collected CD spectra at temperatures in the range 20–75 °C (Figure 6). The gradual decrease in signal intensity at 232 nm upon heating is indeed indicative of temperature-mediated denaturation. Importantly, the remaining spectral shape was not affected significantly, which is in accordance with our hypothesis that this is not related to secondary structure. Furthermore, spectra recorded upon cooling were identical to those obtained before heating, indicating refolding of the structure (Supplementary Figure S6). However, CD spectroscopy of peptide analogues is not sufficient to derive specific secondary structures,[25] and although we find it likely that our oligomers may adopt some degree of helical conformation in solution based on our collective results, we stress that this is be no means proven by our current level of NMR and CD data.

In summary, we report the first examples of high-resolution structures of linear oligomeric β-peptoids, which are also the longest structures of any peptoid oligomer determined by X-ray crystallography to date. These novel helical structures definitively show that the β-peptoids qualify as a valid addition to the already rich ensemble of foldamer designs. Our crystal structures revealed highly regular equilateral triangular prism-shaped conformations in the solid state, which was achieved by synthesis of homomeric hexamers containing the highly *cis*-amide-inducing side chain, (*S*)-1-(1-naphthyl)ethylamine. Furthermore, ^{1}H NMR- and CD spectroscopic data supported the existence of length-and temperature-dependent secondary structures in solution in organic solvents, although the determination of high-resolution solution structures will be an important future challenge. Taken together we demonstrate control of β-peptoid folding for the first time, which now opens the possibility of taking advantage of β-peptoids in design of novel structurally well-defined biomimetic materials. We are therefore currently investigating various strategies to introduce alternative functionalities while retaining the structural integrity of these novel scaffolds.

Received: ((will be filled in by the editorial staff))
Published online on ((will be filled in by the editorial staff))

Keywords: Foldamers • peptidomimetics • peptide folding • biomimicry • β-peptoids

[1] S. H. Gellman, *Acc. Chem. Res.* **1998**, *31*, 173.
[2] (a) C. M. Goodman, S. Choi, S. Shandler, W. F. DeGrado, *Nat. Chem. Biol.* **2007**, *3*, 252; (b) W. S. Horne, S. H. Gellman, *Acc. Chem. Res.* **2008**, *41*, 1399; (c) C. A. Olsen, *ChemBioChem* **2010**, *11*, 152; (d) W. S. Horne, *Expert Opin. Drug Discov.* **2011**, *6*, 1247.
[3] (a) R. P. Cheng, S. H. Gellman, W. F. DeGrado, *Chem. Rev.* **2001**, *101*, 3219; (b) D. Seebach, J. Gardiner, *Acc. Chem. Res.* **2008**, *41*, 1366.
[4] D. Seebach, A. K. Beck, D. J. Bierbaum, *Chem. Biodivers.* **2004**, *1*, 1111.
[5] (a) R. J. Simon, R. S. Kania, R. N. Zuckermann, V. D. Huebner, D. A. Jewell, S. Banville, S. Ng, L. Wang, S. Rosenberg, et al., *Proc. Natl. Acad. Sci. U. S. A.* **1992**, *89*, 9367; (b) G. L. Butterfoss, P. D. Renfrew, B. Kuhlman, K. Kirshenbaum, R. Bonneau, *J. Am. Chem. Soc.* **2009**, *131*, 16798.
[6] B. C. Hamper, S. A. Kolodziej, A. M. Scates, R. G. Smith, E. Cortez, *J. Org. Chem.* **1998**, *63*, 708.
[7] C. Baldauf, R. Guenther, H.-J. Hofmann, *Phys. Biol.* **2006**, *3*, S1.
[8] (a) A. S. Norgren, S. Zhang, P. I. Arvidsson, *Org. Lett.* **2006**, *8*, 4533; (b) C. A. Olsen, M. Lambert, M. Witt, H. Franzyk, J. W. Jaroszewski, *Amino Acids* **2008**, *34*, 465.
[9] O. Roy, S. Faure, V. Thery, C. Didierjean, C. Taillefumier, *Org. Lett.* **2008**, *10*, 921.
[10] (a) S. W. Shuey, W. J. Delaney, M. C. Shah, M. A. Scialdone, *Bioorg. Med. Chem. Lett.* **2006**, *16*, 1245; (b) C. A. Olsen, G. Bonke, L. Vedel, A. Adsersen, M. Witt, H. Franzyk, J. W. Jaroszewski, *Org. Lett.* **2007**, *9*, 1549; (c) R. D. Jahnsen, N. Frimodt-Moller, H. Franzyk, *J. Med. Chem.* **2012**, *55*, 7253.
[11] C. A. Olsen, H. L. Ziegler, H. M. Nielsen, N. Frimodt-Møller, J. W. Jaroszewski, H. Franzyk, *ChemBioChem* **2010**, *11*, 1356.
[12] L. Vedel, G. Bonke, C. Foged, H. Ziegler, H. Franzyk, J. W. Jaroszewski, C. A. Olsen, *ChemBioChem* **2007**, *8*, 1781.

[13] C. Foged, H. Franzyk, S. Bahrami, S. Frokjaer, J. W. Jaroszewski, H. M. Nielsen, C. A. Olsen, *Biochim. Biophys. Acta, Biomembr.* **2008**, *1778*, 2487.
[14] B. C. Gorske, B. L. Bastian, G. D. Geske, H. E. Blackwell, *J. Am. Chem. Soc.* **2007**, *129*, 8928.
[15] B. C. Gorske, J. R. Stringer, B. L. Bastian, S. A. Fowler, H. E. Blackwell, *J. Am. Chem. Soc.* **2009**, *131*, 16555.
[16] C. Caumes, O. Roy, S. Faure, C. Taillefumier, *J. Am. Chem. Soc.* **2012**, *134*, 9553.
[17] J. S. Laursen, J. Engel-Andreasen, P. Fristrup, P. Harris, C. A. Olsen, *J. Am. Chem. Soc.* **2013**, *135*, 2835.
[18] J. R. Stringer, J. A. Crapster, I. A. Guzei, H. E. Blackwell, *J. Am. Chem. Soc.* **2011**, *133*, 15559.
[19] (a) P. Armand, K. Kirshenbaum, R. A. Goldsmith, S. Farr-Jones, A. E. Barron, K. T. V. Truong, K. A. Dill, D. F. Mierke, F. E. Cohen, R. N. Zuckermann, E. K. Bradley, *Proc. Natl. Acad. Sci. U. S. A.* **1998**, *95*, 4309; (b) K. Kirshenbaum, A. E. Barron, R. A. Goldsmith, P. Armand, E. K. Bradley, K. T. V. Truong, K. A. Dill, F. E. Cohen, R. N. Zuckermann, *Proc. Natl. Acad. Sci. U. S. A.* **1998**, *95*, 4303; (c) C. W. Wu, T. J. Sanborn, K. Huang, R. N. Zuckermann, A. E. Barron, *J. Am. Chem. Soc.* **2001**, *123*, 6778; (d) C. W. Wu, T. J. Sanborn, R. N. Zuckermann, A. E. Barron, *J. Am. Chem. Soc.* **2001**, *123*, 2958.
[20] G. Bonke, L. Vedel, M. Witt, J. W. Jaroszewski, C. A. Olsen, H. Franzyk, *Synthesis-Stuttgart* **2008**, 2381.
[21] J. A. Crapster, I. A. Guzei, H. E. Blackwell, *Angew. Chem., Int. Ed.* **2013**, *52*, 5079.
[22] T. Hjelmgaard, S. Faure, C. Caumes, E. De Santis, A. A. Edwards, C. Taillefumier, *Org. Lett.* **2009**, *11*, 4100.
[23] S. Abele, K. Vogtli, D. Seebach, *Helv Chim Acta* **1999**, *82*, 1539.
[24] B. C. Gorske, R. C. Nelson, Z. S. Bowden, T. A. Kufe, A. M. Childs, *J. Org. Chem.* **2013**, *78*, 11172.
[25] A. Glattli, X. Daura, D. Seebach, W. F. van Gunsteren, *J. Am. Chem. Soc.* **2002**, *124*, 12972.

Entry for the Table of Contents (Please choose one layout)

Layout 2:

Foldamers

J. S. Laursen, P. Harris, C. A. Olsen*

_____ Page – Page

Trianguler Prism-Shaped Helices—Synthesis and Structural Determination of β-Peptoid Oligomers

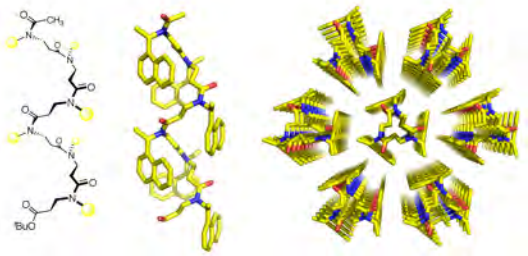

The first examples of high-resolution structures of linear oligomeric β-peptoids are presented. We describe synthesis and characterization of oligomers up to the hexamer length containing two different types of N-alkyl side chains, and furthermore investigation of the effect of N-terminal trifluoroacetylation. Our X-ray crystallographic data reveal right-handed helical conformations of the longest solid-state helical peptoid structures solved to date.

Supporting Information

Contents

Figures and Schemes

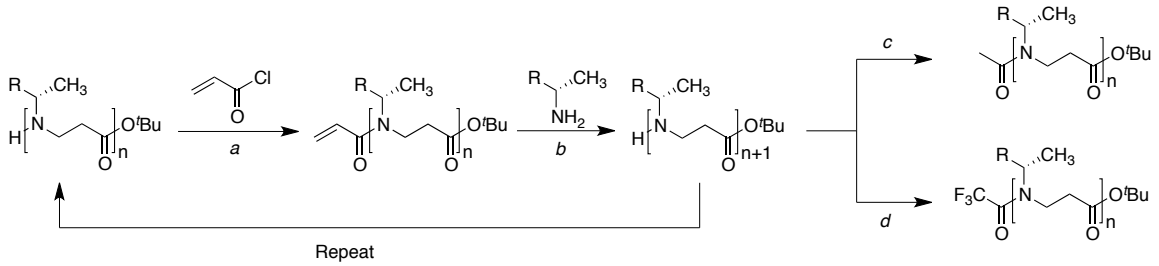

Scheme S1. Oligomerization and N-terminal functionalization of *β*-peptoids. a) NEt_3, THF, 0 °C. *b*) MeOH, 50. *c*) AcCl, NEt_3, 0 °C. *d*) $(CF_3CO)_2O$, NEt_3, CH_2Cl_2, 0 °C→20 °C .

Figure S1. The asymmetric unit in crystal **10c**. Left: seen perpendicular to the helix axis. Right: Seen along the helix axis. The figure was prepared using the Mercury software.[2]

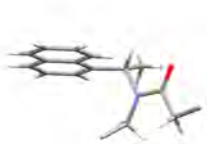

Figure S2. The asymmetric unit in crystal **10a**. The figure was prepared using the Mercury software.[2]

A

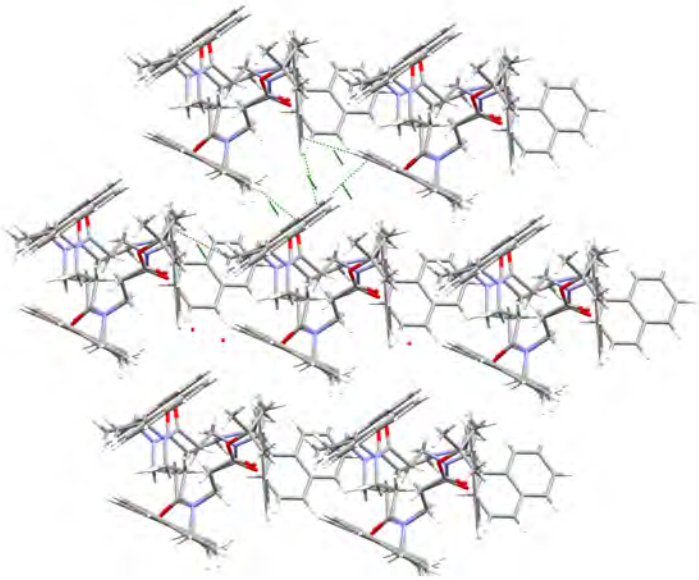

B

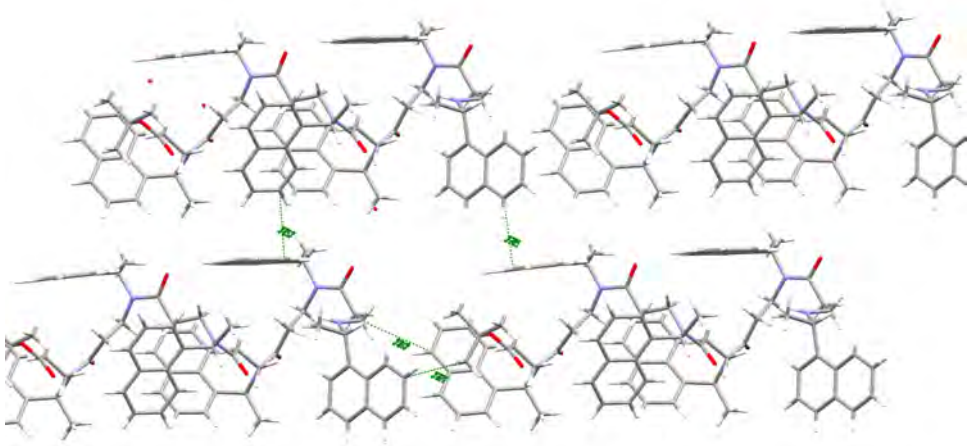

Figure S3: Crystal packing of **10c**. (A) Viewed along the helical axis. The helices arrange in a pseudo-trigonal manner. (B) Perpendicular to the helical axis. The figure was prepared using the Mercury software.[2]

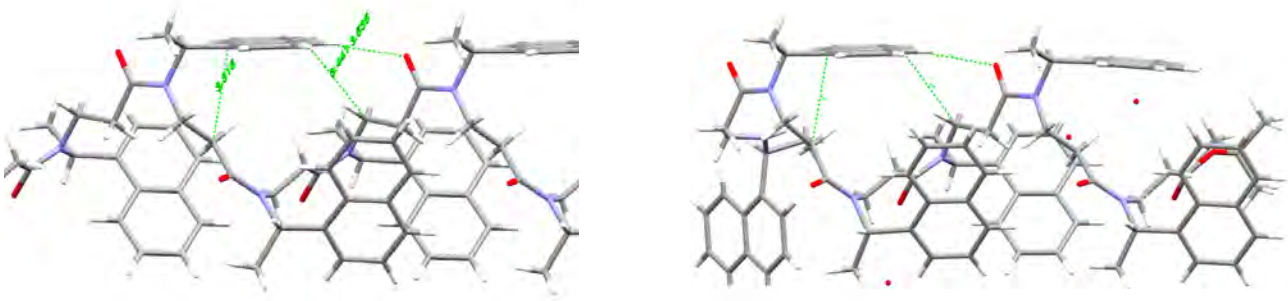

A **B**

Figure S4. (A) Naphthyl-backbone interactions in cpd **10a**. (B) Naphthyl-backbone interactions in cpd **10c**.

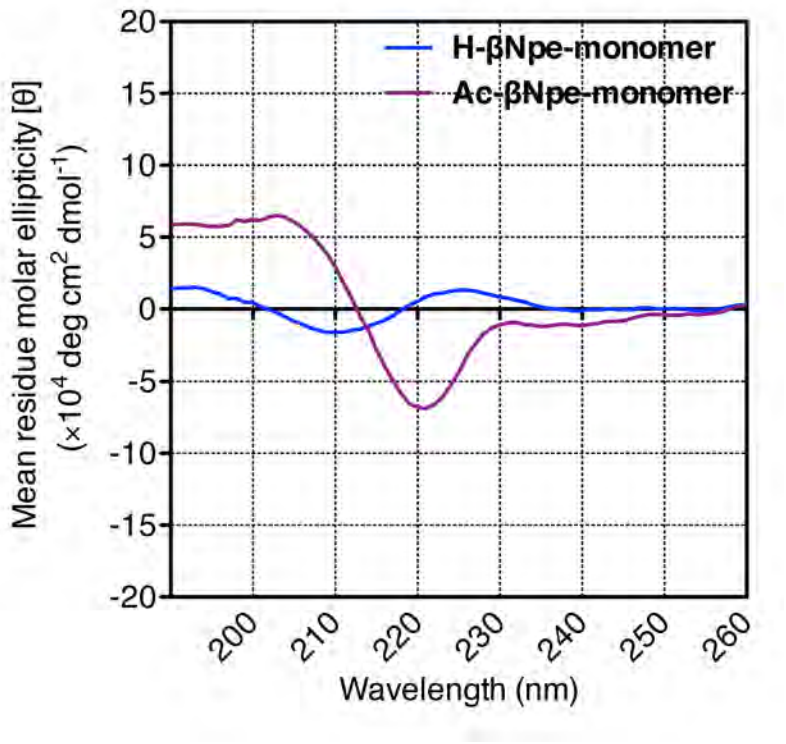

Figure S5. CD spectra of acylated and non-acylated *(S)*-1-(1-naphthyl)ethyl-containing monomers.

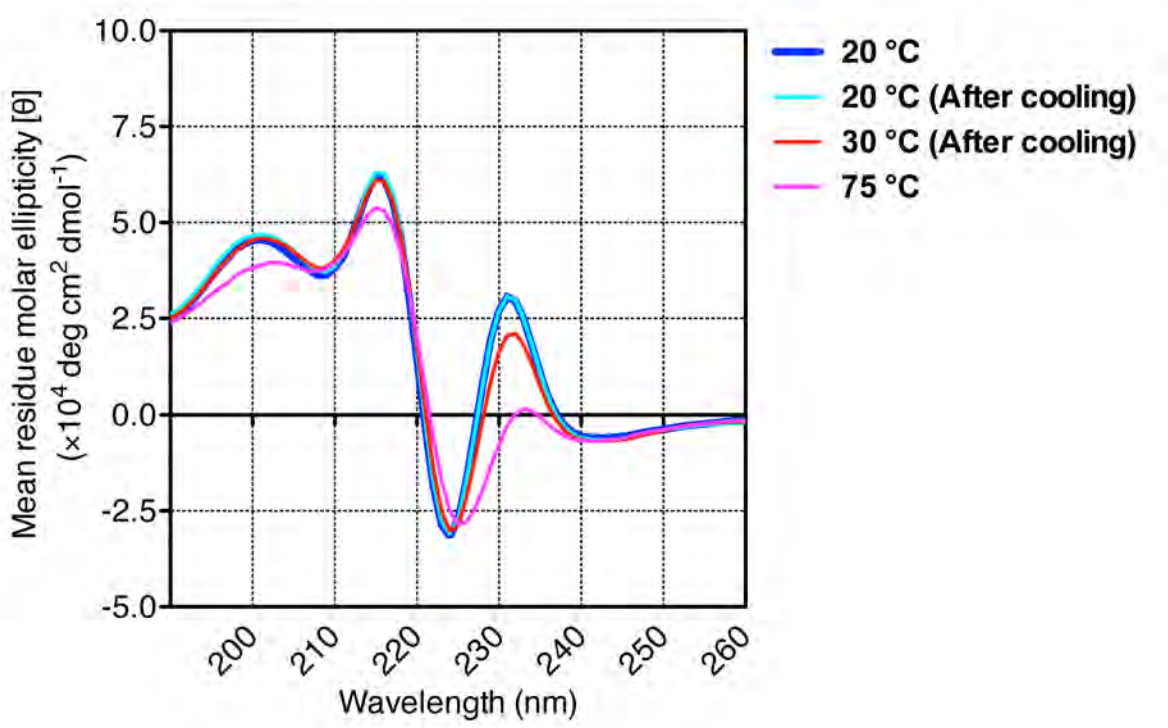

Figure S6. CD spectra of compound **10a** recorded at varying temperatures upon cooling the sample back down to room temperature.

Table S1. Torsion Angles for Additional Residues

Compound **10a**						
	φ	θ	ψ	ω	χ_1	χ_2
	96.2	172.5	–175.3	–13.7	53.6	–80.5
Compound **10c**						
Residue	φ	θ	ψ	ω	χ_1	χ_2
3	96.9	166.4	–179.9	–19.4	66.7	–61.5
4	94.3	168	–178.8	–9.5	54.4	–74.2
5	97.4	166	–173.9	–13.4	56.3	–73.8
From DFT calculations previously published (Hofmann et al.)[3]						
	95.8	–179.6	–178.2	8.6	n.a.	n.a.

Table S2. Examples of Naphthyl-Backbone Interactions (shown in green in Figure S4)

Compound **10a**	Distance (Å)	Compound **10c**	Distance (Å)
C1–C6	3.31(2)	C22–C62	3.35(2)
C3–C15	3.44(2)	C14–C152	3.40(2)
O1–C15	3.54(1)	C152–O14	3.53(2)

Table S3. Characterization Data for Compounds **1a–10b**

Comp.	Formula	Yield[a] (%)	MS: *m/z* for $[M+H]^+$ (calcd./obs.)	HRMS: *m/z* for $[M+H]^+$ [calcd./obs. (ΔM)]	HPLC (t_R/min)	HPLC (% Purity)[b]
1a	$C_{28}H_{38}N_2O_4$	21	467.3/467.3	467.2904/467.2920 (3.4)	12.50	96
1b	$C_{28}H_{35}N_2O_4$	30	521.3/521.2	521.2622/521.2630 (1.6)	14.11	95
2a	$C_{39}H_{51}N_3O_5$	35	642.4/642.5	642.3901/642.3901 (0.0)	13.32	95
2b	$C_{39}H_{48}F_3N_3O_5$	25	696.4/696.4	696.3619/696.3625 (0.9)	15.10	98
3a	$C_{50}H_{64}N_4O_6$	34	817.5/817.5	839.4718/839.4737[c] (2.3)	14.24	93
3b	$C_{50}H_{61}F_3N_4O_6$	45	871.5/871.5	871.4616/871.4658 (4.8)	16.06	95
4a	$C_{61}H_{77}N_5O_7$	22	992.6/992.8	992.5896/992.5935 (4.0)	15.00	97
4b	$C_{61}H_{74}F_3N_5O_7$	34	1046.6/1046.7	1046.5613/1046.5646 (3.1)	16.83	95
5a	$C_{72}H_{90}N_6O_8$	44	1167.9/1167.8	1189.6712/1189.6737[c] (2.1)	16.23	98
5b	$C_{72}H_{87}F_3N_6O_8$	43	1221.7/1221.7	1243.6430/1243.6429[c] (0.1)	18.42	97
6a	$C_{36}H_{42}N_2O_4$	38	567.3/567.4	567.3218/567.3242 (4.3)	14.05	96
6b	$C_{36}H_{39}F_3N_2O_4$	36	621.3/621.2	621.2935/621.2959 (3.8)	16.14	99
7a	$C_{51}H_{57}N_3O_5$	39	792.4/792.4	792.4371/792.4396 (3.1)	18.40	95
7b	$C_{51}H_{54}F_3N_3O_5$	16	846.4/846.3	846.4089/846.4114 (3.3)	19.41	98
8a	$C_{66}H_{72}N_4O_6$	30	1017.6/1017.5	1017.5526/1017.5566 (3.9)	20.34	99
8b	$C_{66}H_{69}F_3N_4O_6$	32	1071.5/1071.5	1071.5242/1071.5287 (4.2)	23.17	97
9a	$C_{81}H_{87}N_5O_7$	34	1242.7/1242.6	1264.6498/1264.6537[c] (3.2)	24.31	96
9b	$C_{81}H_{84}F_3N_5O_7$	6	1296.6/1296.4	n.a.	22.14	97
10a	$C_{96}H_{102}N_6O_8$	53	1468.9/1468.7	734.8969/734.8985[d] (2.1)	28.66	96
10b	$C_{96}H_{99}F_3N_6O_8$	54	1522.9/1522.4	761.8828/761.8832[d] (0.5)	30.06	95

[a]Isolated yields for addition of one residue and subsequent acylation (3 steps). [b]The HPLC purities are reported at 230 nm. [c]The values correspond to $[M+Na]^+$. [d]The values correspond to $[M+2H]^{2+}$

Materials and Methods

General. All chemicals and solvents were analytical grade and used without further purification. Vacuum liquid chromatography (VLC) was performed on silica gel 60 (particle size 0.015–0.040 mm). UPLC–MS analyses were performed on a Phenomenex Kinetex column (1.7 μm, 50 × 2.10 mm) using a Waters Acquity ultra high-performance liquid chromatography system. A gradient with eluent I (0.1% HCOOH in water) and eluent II (0.1% HCOOH in acetonitrile) rising linearly from 0% to 95% of II during t = 0.00–5.20 min was applied at a flow rate of 1 mL/min. Preparative HPLC purification was performed on a C18 Phenomenex Luna column (5 μm, 100 Å, 250 mm × 20 mm) using an Agilent 1260 LC system equipped with a diode array UV detector and an evaporative light scattering detector (ELSD). A gradient with eluent III (water–MeCN–TFA, 95:5:0.1) and eluent IV (0.1% TFA in acetonitrile) rising linearly from 45% to 95% of IV during t = 5–35 min, and isocratically at 95% from t = 35–55 min was applied at a flow rate of 20 mL/min. Analytical HPLC was performed on a C18 phenomenex Luna column (3 μm, 100 Å, 150 mm × 4.60 mm) using an Agilent 1100 series system equipped with a diode array UV detector. A gradient using eluent III and eluent IV rising linearly from 0% to 80% of IV during t = 2–10 min, then from 80% to 95% during t = 10–27 min, and finally isocratically at 95% IV from t = 27–33 min was applied at a flow rate of 1 mL/min. High-resolution LC-DAD-MS was performed on an Agilent 1100 system equipped with a photodiode array detector (DAD) and coupled to a LCT orthogonal time-of-flight mass spectrometer (Waters-Micromass, Manchester, UK) with Z-spray electrospray ionisation (ESI). 2D NMR spectra were recorded on a Bruker Ascend 400 MHz at 400 MHz for ^{1}H and 100 MHz for ^{13}C. All spectra were recorded at 298 K. Heteronuclear single quantum coherence (HSQC) spectra were recorded with a relaxation delay of 1.5 sec before each scan, a spectral width of 4800 × 16600, collecting 4 FIDs and 1k × 256 datapoints. All spectra were recorded at 298 K. Chemical shifts are reported in ppm relative to deuterated solvent peaks as internal standards (δH, C_6D_6 7.16 ppm; δC, C_6D_6 128.06 ppm, δH, CD_3CN 1.94 ppm; δC, CD_3CN 1.32 ppm).

Oligomerization of β-peptoids. The β-peptoids were oligomerized using a procedure closely resembling that of Taillefumier and co-workers.[1] Briefly, the β-peptoid (1.0 equiv) and NEt_3 (1.2 equiv) were dissolved in THF (0.05 M) and cooled to 0 °C. Then acryloyl chloride (1.4 equiv) was added and the reaction was stirred for 1 h. The reaction mixture was filtered and the solids were washed with EtOAc. The combined filtrates were concentrated *in vacuo* yielding crude acrylamide. The crude acrylamide was dissolved in MeOH (0.1 M), the desired primary amine (2.0 eqiuv) was added, and the reaction was stirred for 18 h at room temperature. In case of the penta- and hexamer of compounds containing *N*-(*S*)-1-(1-naphthyl)ethyl side chains, additional amine (2.0 equiv) and stirring for 72 h were needed for the reaction to go to completion. Furthermore, the acrylamide of the *N*-(*S*)-1-(1-naphthyl)ethyl-containing pentamer was poorly soluble in MeOH, therefore MeOH–

CH_2Cl_2 (1:3, 0.015 M) was used for the final aza-Michael step. Purification was performed using Vacuum liquid silica gel chromatography, applying a gradient of MeOH in CH_2Cl_2 from 0→5%.

N-terminal functionalization of *β*-peptoid oligomers. Acetylation of *β*-peptoid oligomers was achieved by dissolving the *β*-peptoid oligomer (1.0 eqiuv) in CH_2Cl_2 (0.02 M) at 0 °C, then adding NEt_3 (1.4 equiv) and acetyl chloride (1.2 equiv) under stirring for 1h. Trifluoroacetylation of *β*-peptoid oligomers required addition of NEt_3 (4.0 equiv) and trifluoroacetic anhydride (5.0 equiv) to the *β*-peptoid solution, which was stirred for 1 h at 0 °C, followed by ambient temperature for 18h. For both acetylated and trifluoroacetylated compounds, purification could be achieved by evaporation of the solvent *in vacuo* followed by preparative reversed-phase HPLC.

Vacuum liquid silica gel chromatographic (VLC) purification of compounds **6a–10b** applying a gradient of 0.2% MeOH in CH_2Cl_2 from 0→5% was unsuccessful. However, crude **10a** and **10b** could be redisolved in DMF, and precipitated upon addition of water. The solid product contained only minor impurities, which could be removed using VLC with the mentioned gradient.

CD spectroscopy. Spectra were acquired with an Olis DSM 10 CD spectrophotometer (Olis Inc., Bogart, GA, USA), equipped with a Quantum Systems temperature control module, using 1 mm quartz cuvettes at 25 °C. Samples (60 μM) were prepared in CH_3CN. Compound concentrations (60 μM) were determined using dry weight of the lyophilized material. The data are averages of 3 successive accumulations. Spectra were recorded in millidegree units, corrected for solvent contributions, and normalized to mean residue ellipticity $[\theta] = 100\psi/lcn$, where ψ is the signal in millidegrees, l is the path length (0.1 cm), c is the concentration in mM, and n is the number of peptoid amide bonds.

Crystallization. Selected peptoid hexamers (~30 mg) were dissolved in a minimum amount of $CHCl_3$ and MeOH was added until precipitation could be observed, then sufficint $CHCl_3$ was added to give clear solutions. The solutions were left slow evaporation at room temperature, and crystrals were generally formed within a week. The crystals could be removed from the solvent and washed using MeOH. The hexamers (30 mg) also crystalized upon slow evaporation from benzene, however, these specimens were of insufficient quality for X-ray diffraction.

X-ray crystallography.

Data collection. Several crystals of each compound were tested before suitable crystals were found. Measurements were performed at room temperature as cryo cooling turned out to destroy the crystals. Data collection was performed on an Agilent Supernova Diffractometer using CuK_α radiation. For crystal **10a** data was included to 1.00 Å resolution and for crystal **10c** data to 1.05 Å resolution were included. Data were processed and scaled using the *CrysAlisPro* software (Agilent Technologies). Details of the data collection are found in the supplementay cif-files.

Structural determination and refinement. Compound **10c** crystallized in space group *P1* with one molecule in the asymmetric unit. The structure was solved using SHELXS and refined using SHELXL (Sheldrick, 2008).[3] Due to the rather low resolution, it turned out, however, that geometric restraints had to be included in the refinement. All naphthyl groups were imposed with FLAT and DELU restraints. The N-terminal naphthyl group had rather large thermal parameters and was restrained further using RIGU and ISOR restraints. Furthermore, the *tert*-butyl group was restrained using DELU, and all 6 residues were restrained to be similar using a SAME command. In the rather large voids between the helices we observed disordered electron density. The three largest peaks were modeled as oxygen with occupancy of 0.5. Compound **10a**, on the other hand, crystallized in space group *R3* with one peptoid residue in the asymmetric unit. The structure was solved using SHELXS and refined in SHELXL (Sheldrick, 2008).[4] Also here geometric restraints had to be included in the refinement and the naphthyl group was imposed with FLAT and DELU restraints. The peptoid oligomer reveals when crystallographic symmetry is imposed. However, the crystal structure generates infinitely long chains and the *tert*-butyl group was invisible, although for every sixth naphthyl group a *tert*-butyl group must be present. Hydrogen atoms were included on ideal positions using riding coordinates for both crystals. The data quality did not allow for determination of the absolute configurations, which were imposed in accordance with the stereochemistry of the building blocks used in the synthesis.

Supporting References.

(1) T. Hjelmgaard, S. Faure, C. Caumes, E. De Santis, A. A. Edwards, C. Taillefumier, C. *Org. Lett*. **2009**, *11*, 4100.

(2) C. F. Macrae, I. J. Bruno, J. A. Chisholm, P. R. Edgington, P. McCabe, E. Pidcock, L. Rodriguez-Monge, R. Taylor, J. van de Streek, P. A. Wood *J. Appl. Crystallogr*. **2008**, *41*, 466.

(3) C. Baldauf, R. Guenther, H.-J. Hofmann, *Phys. Biol*. **2006**, *3*, S1.

(4) G. M. Sheldrick *Acta Crystallogr*. **2008**, *A64*, 112.

Parts of the HSQC 2D NMR spectra showing the side chain methyne cross peaks.

1a, MeCN

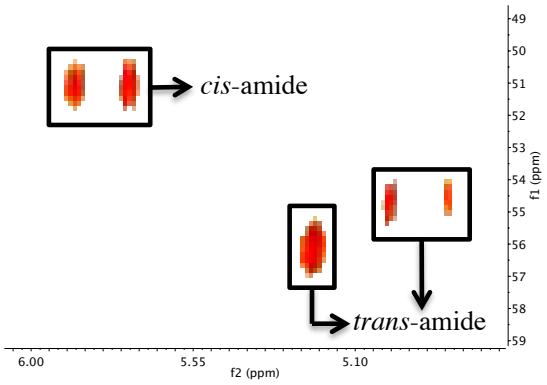

1a, benzene

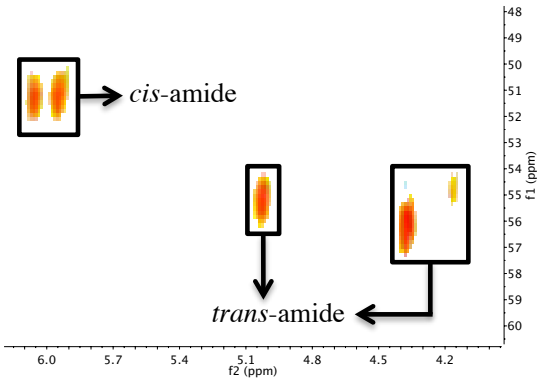

1b, MeCN

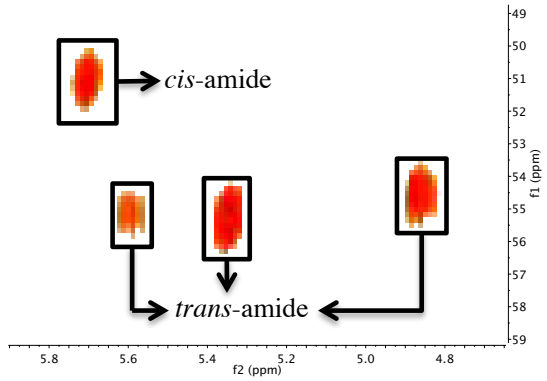

1b, benzene

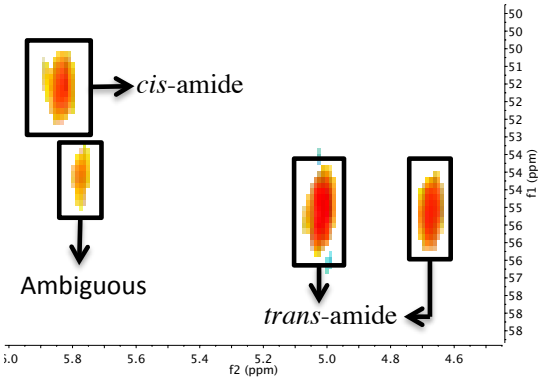

2a, MeCN

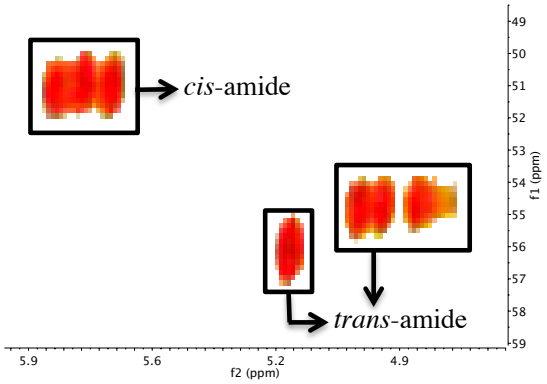

2a, benzene

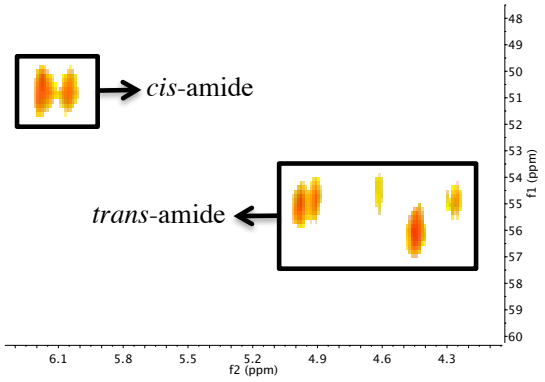

2b, MeCN

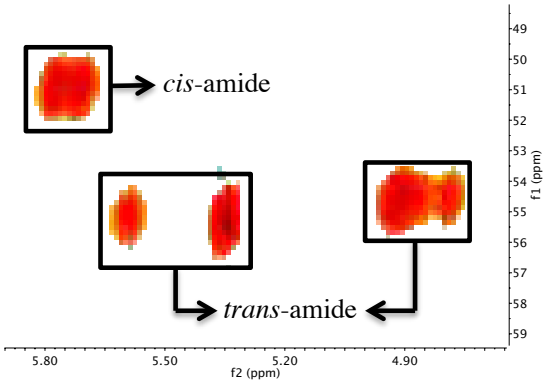

2b, benzene

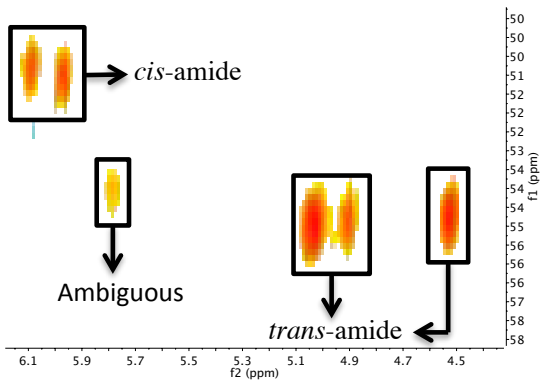

3a, MeCN

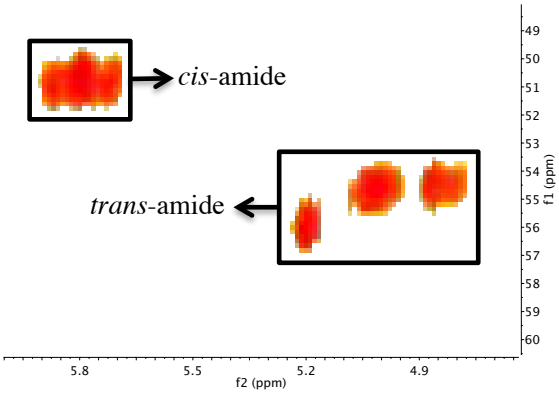

3a, benzene

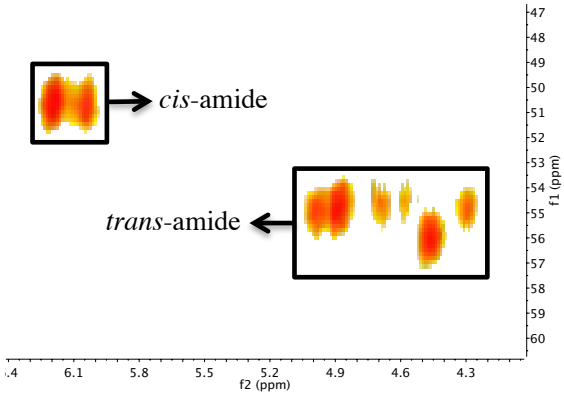

3b, MeCN

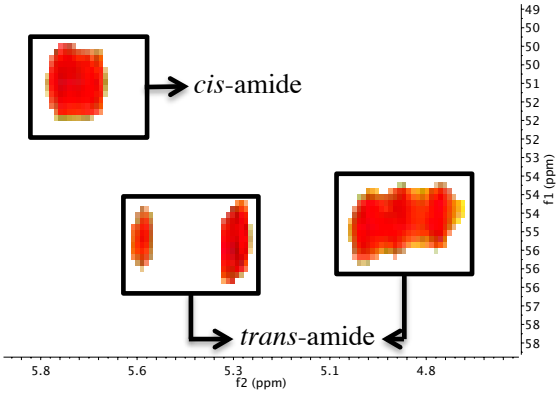

3b, benzene

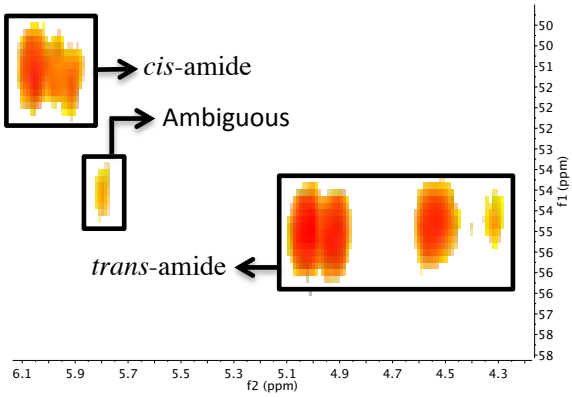

4a, MeCN

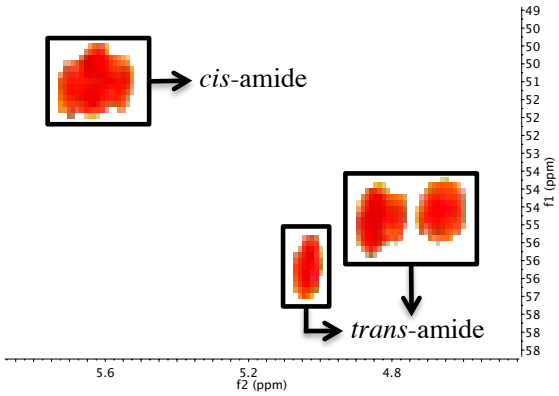

4a, benzene

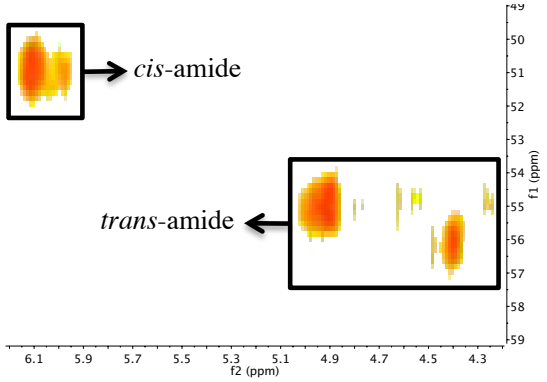

4b, MeCN

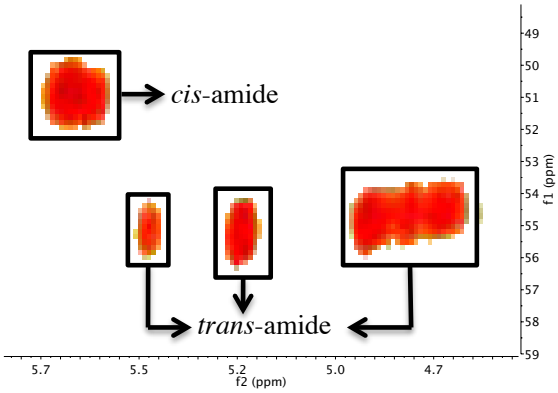

4b, benzene

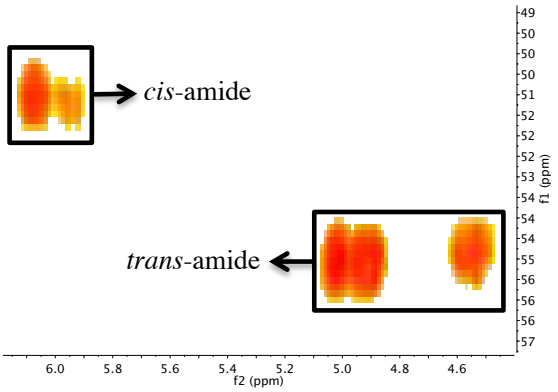

5a, MeCN

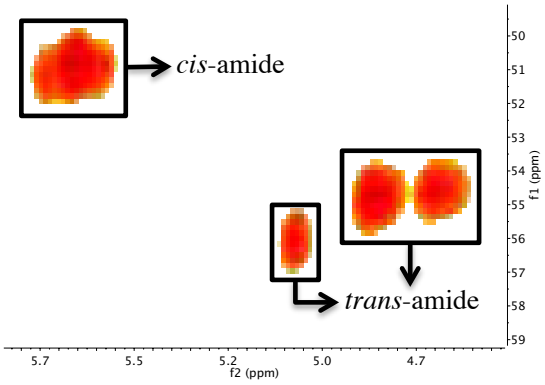

5a, benzene

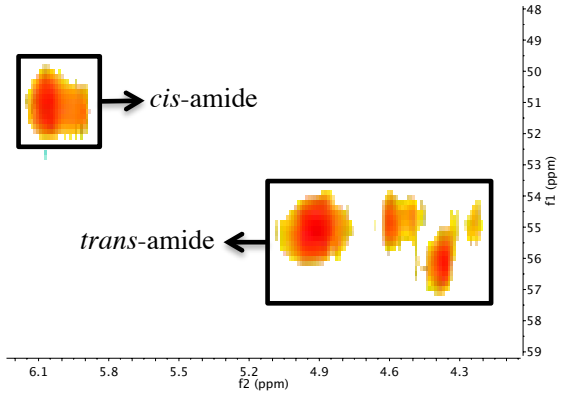

5b, MeCN

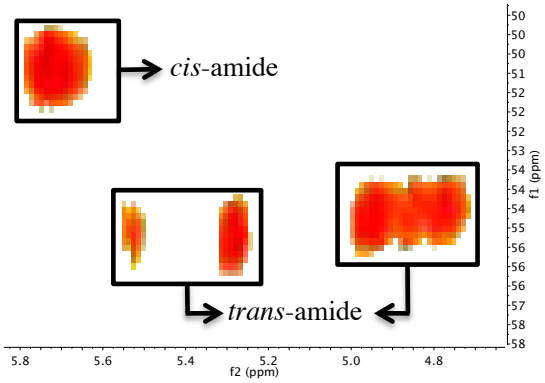

5b, benzene

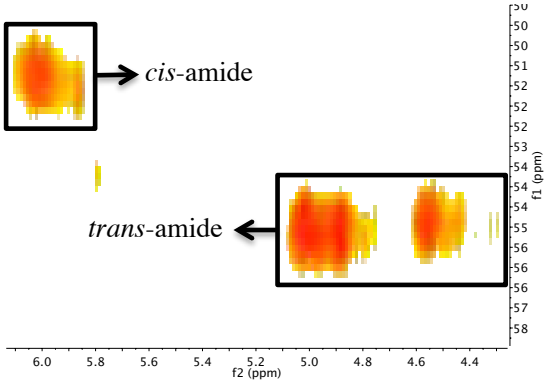

6a, MeCN

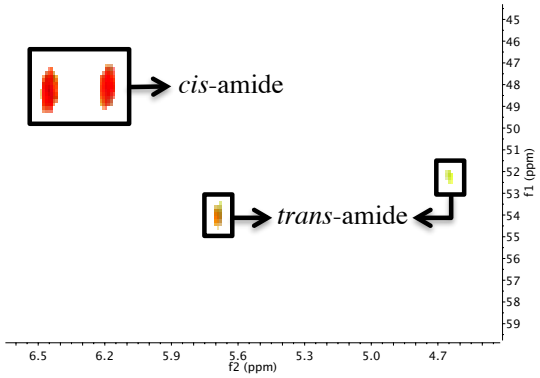

6a, benzene

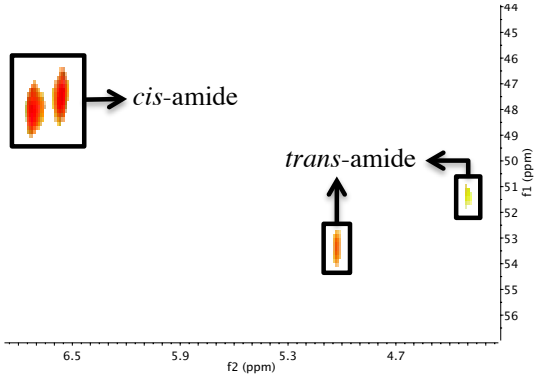

6b, MeCN

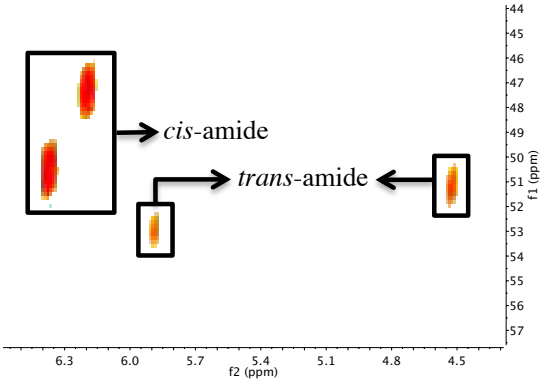

6b, benzene

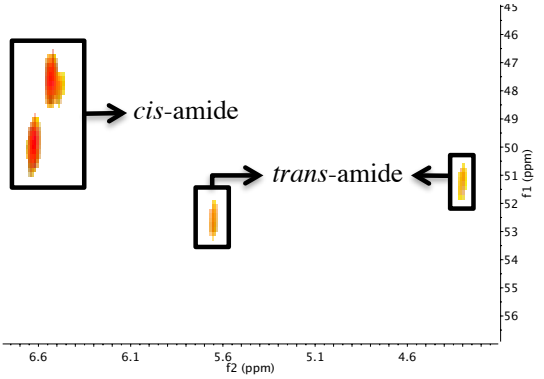

7a, MeCN

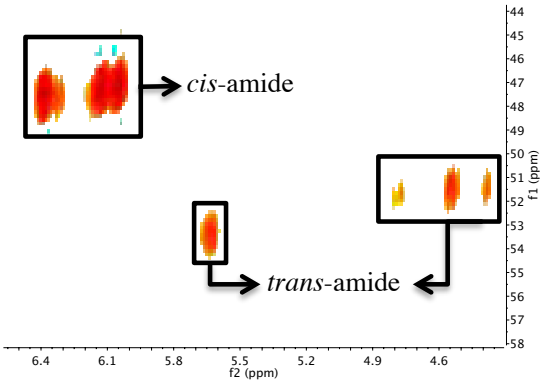

7a, benzene

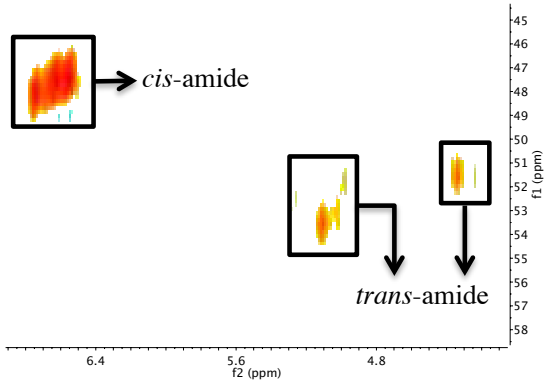

7b, MeCN

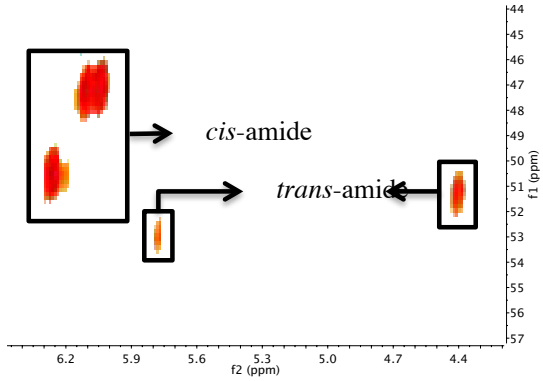

7b, benzene

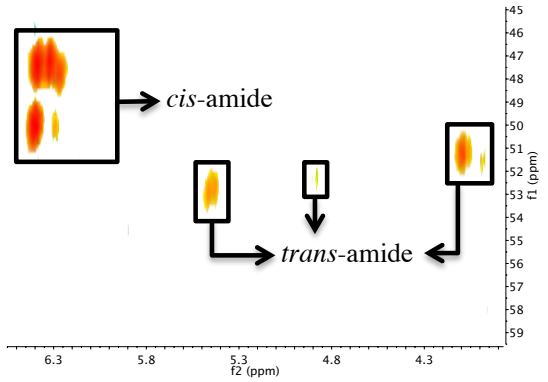

8a, MeCN

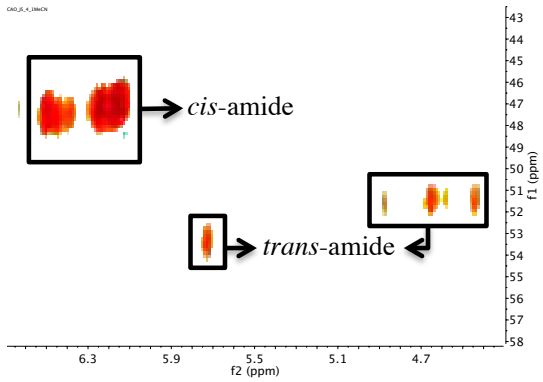

8a, benzene

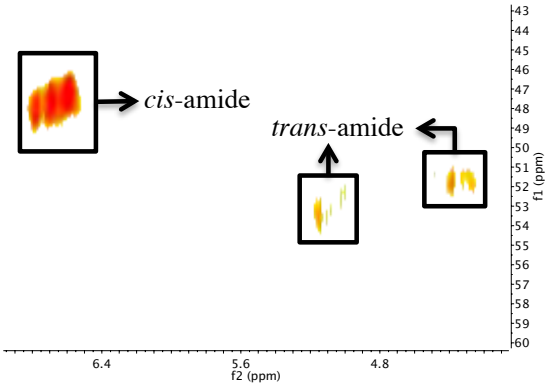

8a, MeCN

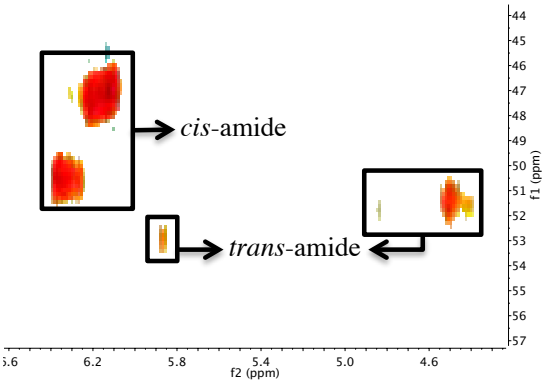

8a, benzene

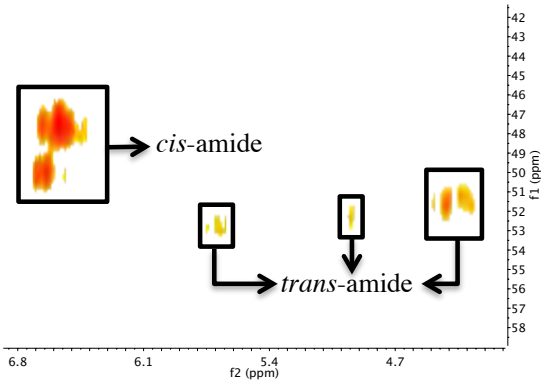

9a, benzene

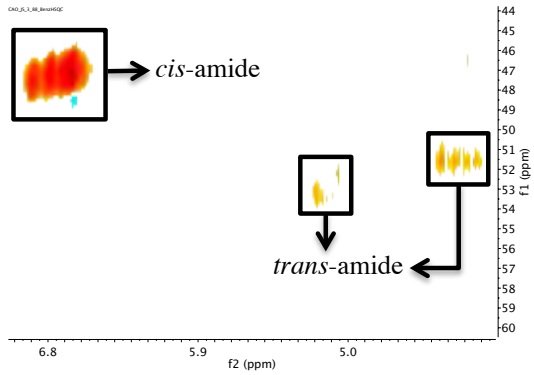

9b, benzene

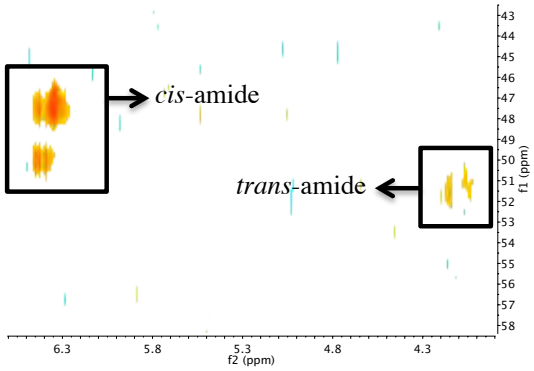

10a, benzene

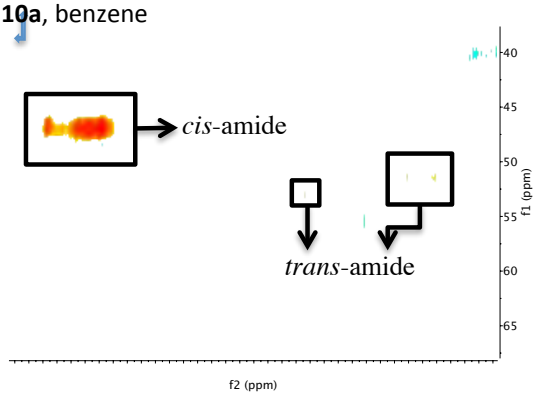

10b, benzene

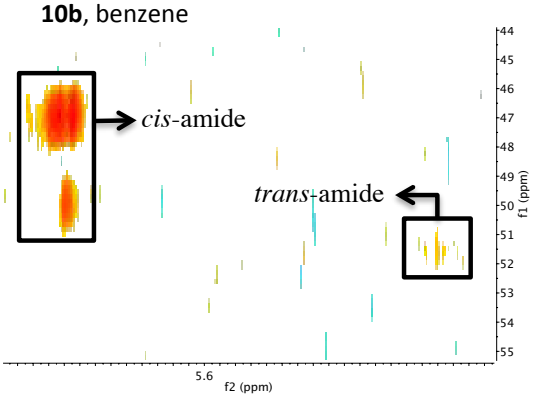

^{1}H NMR Spectra.

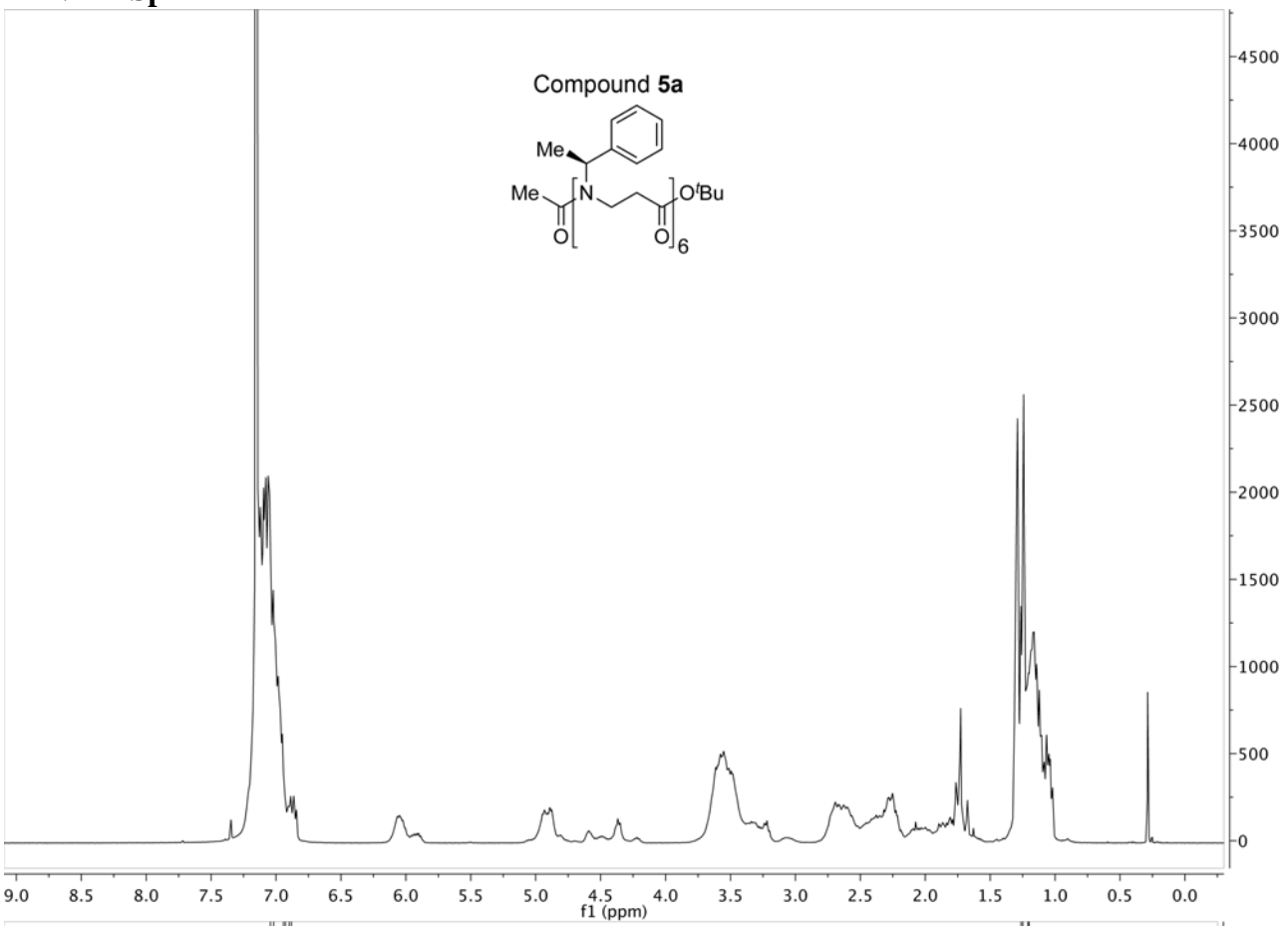

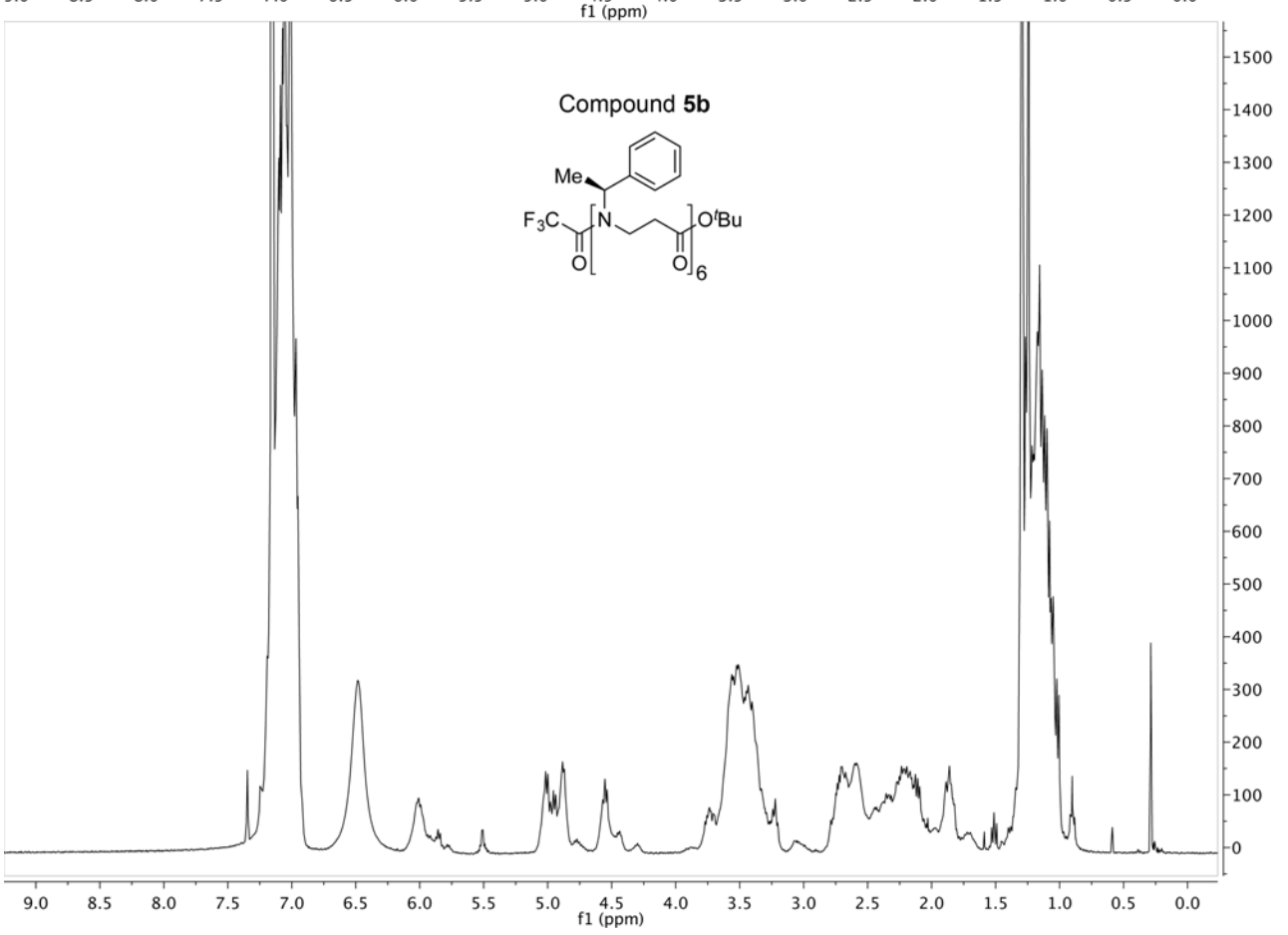

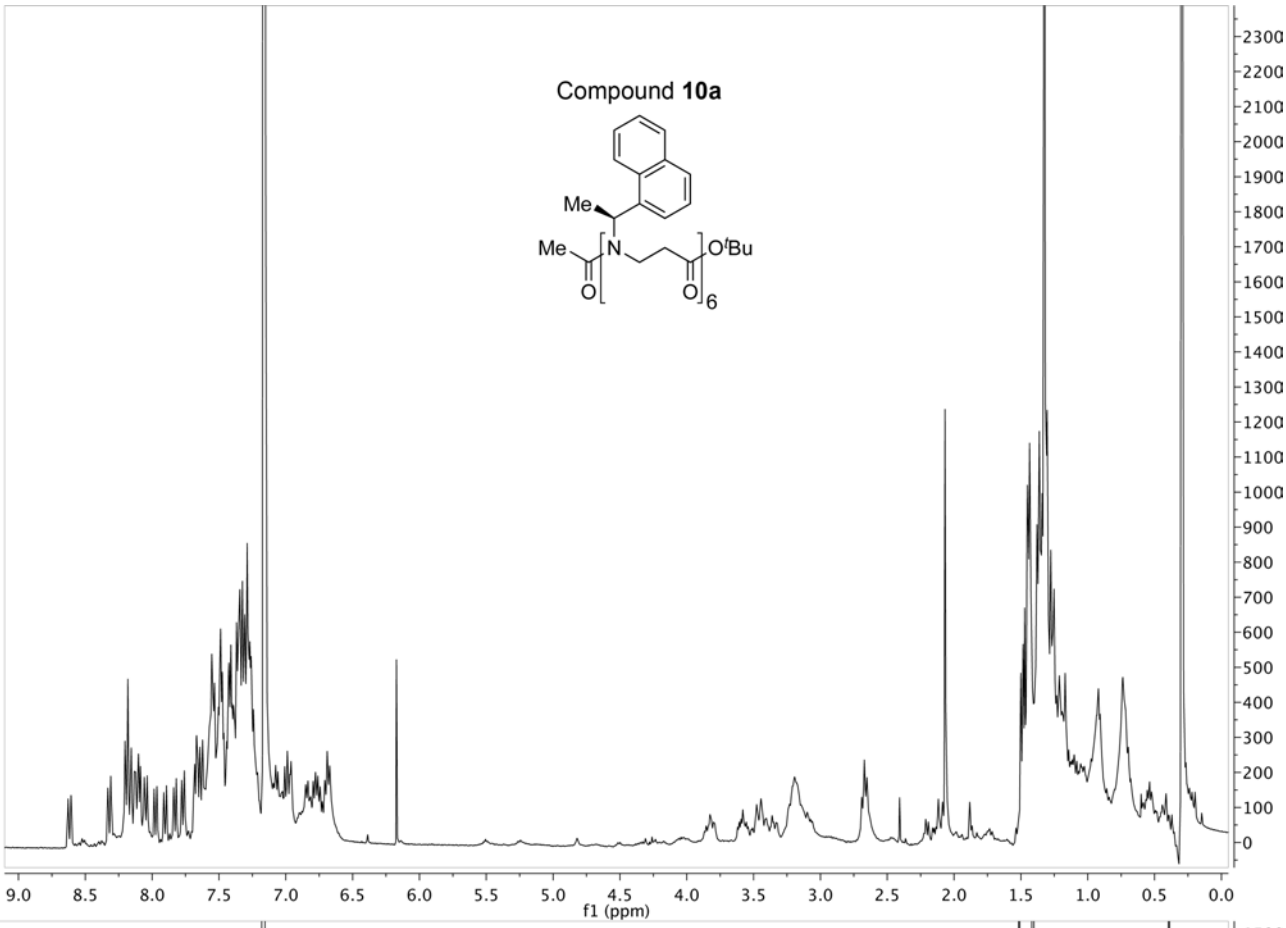
Compound 10a
Me
Me
N
O
O
O
O
6
tBu
9.0 8.5 8.0 7.5 7.0 6.5 6.0 5.5 5.0 4.5 4.0 3.5 3.0 2.5 2.0 1.5 1.0 0.5 0.0
f1 (ppm)

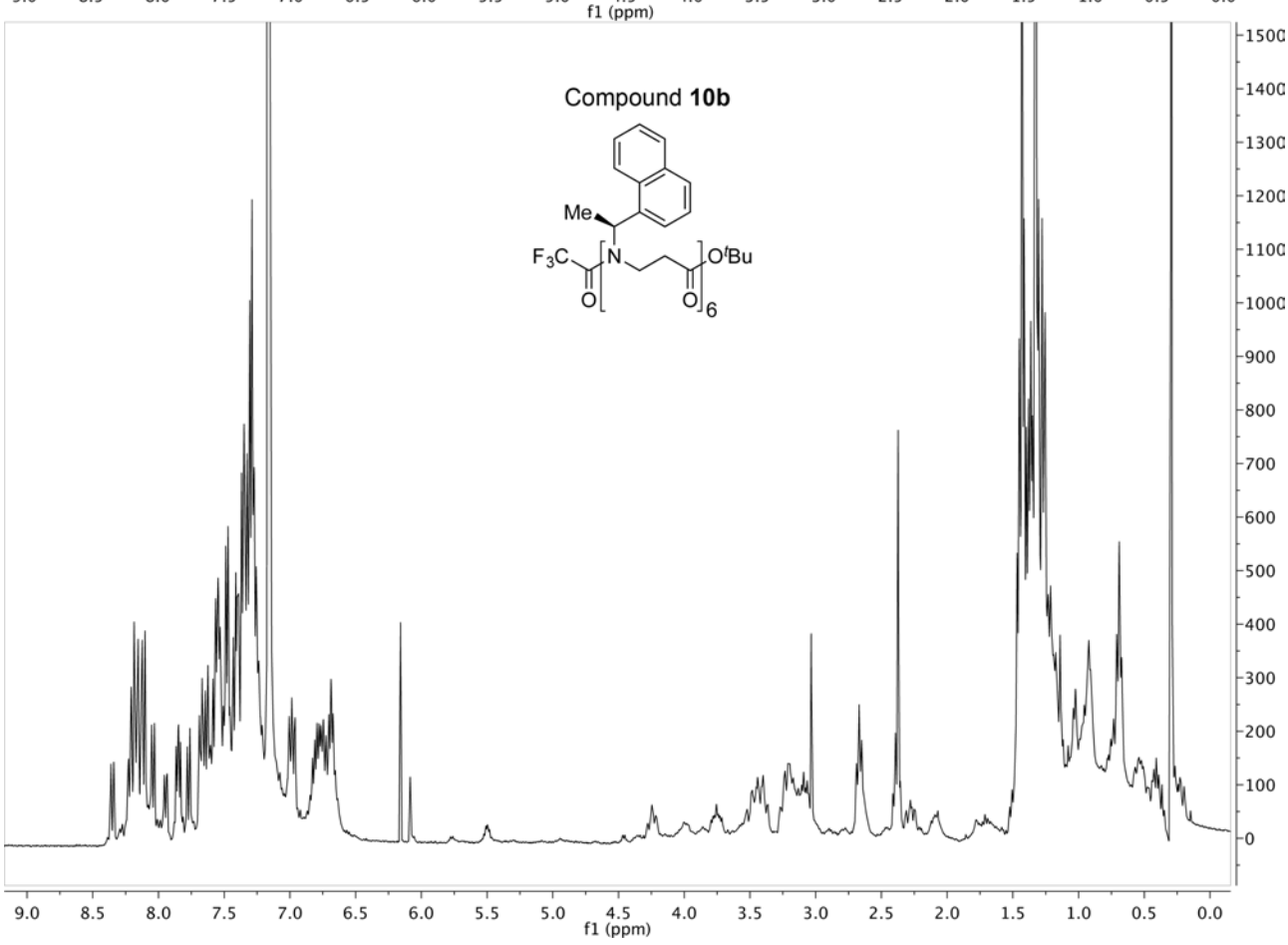
Compound 10b
Me
F3C
N
O
O
O
O
6
tBu
9.0 8.5 8.0 7.5 7.0 6.5 6.0 5.5 5.0 4.5 4.0 3.5 3.0 2.5 2.0 1.5 1.0 0.5 0.0
f1 (ppm)

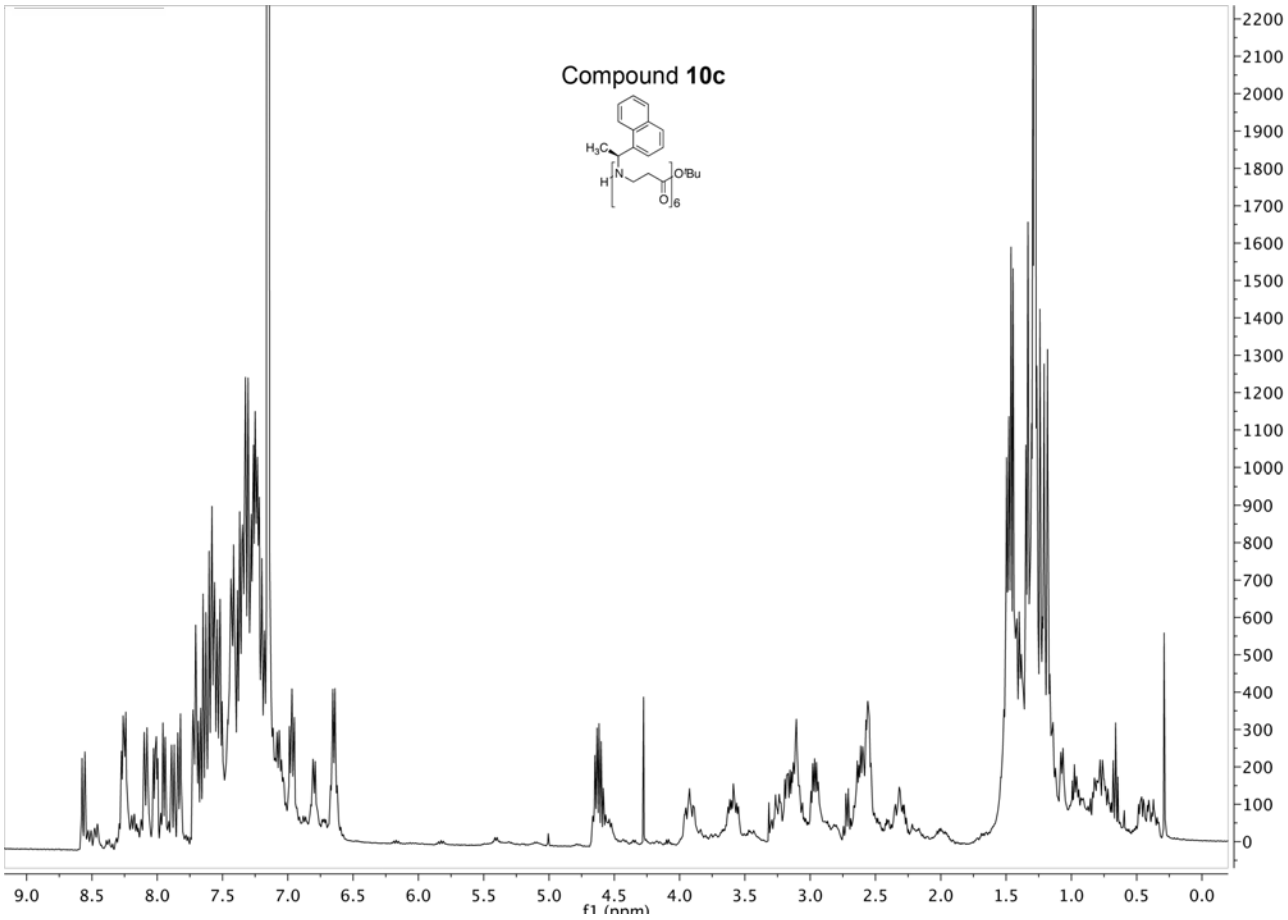
Compound 10c
H3C
N
H
O
OtBu
6
2200
2100
2000
1900
1800
1700
1600
1500
1400
1300
1200
1100
1000
900
800
700
600
500
400
300
200
100
0
9.0
8.5
8.0
7.5
7.0
6.5
6.0
5.5
5.0
4.5
4.0
3.5
3.0
2.5
2.0
1.5
1.0
0.5
0.0
f1 (ppm)

Analytical HPLC traces.

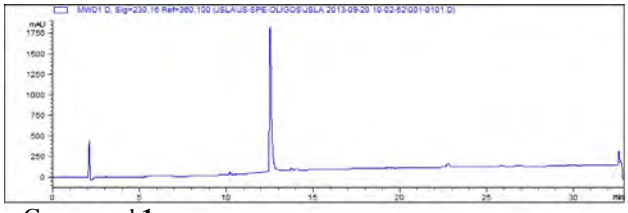

Compound **1a**

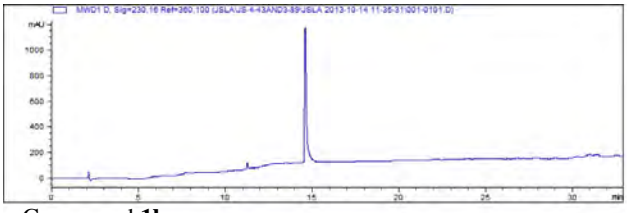

Compound **1b**

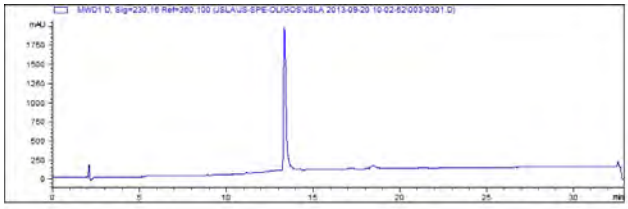

Compound **2a**

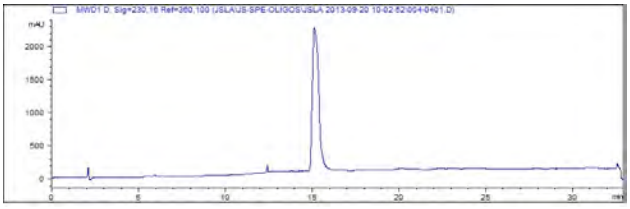

Compound **2b**

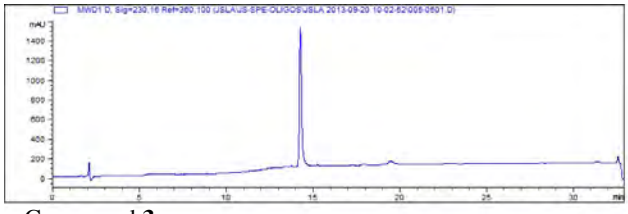

Compound **3a**

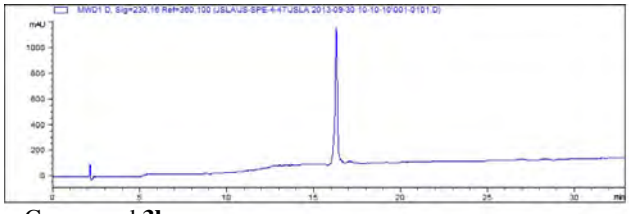

Compound **3b**

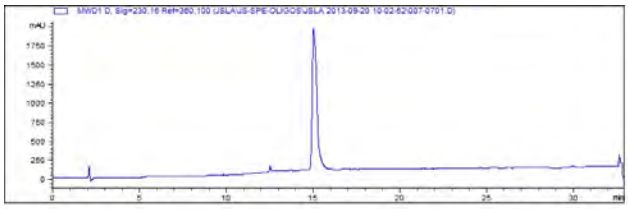

Compound **4a**

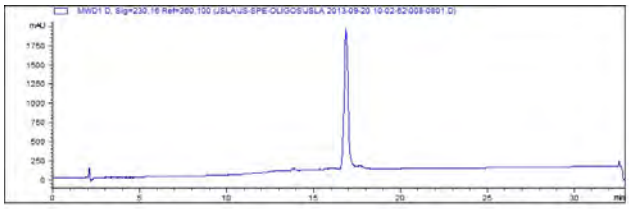

Compound **4b**

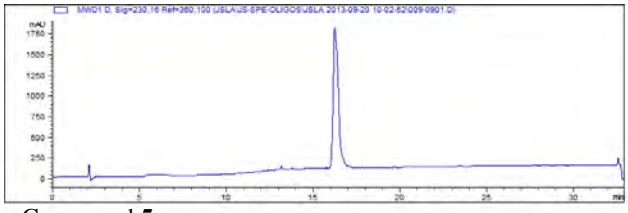

Compound **5a**

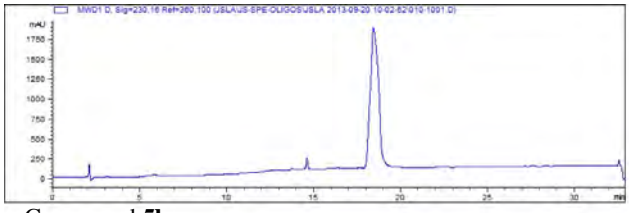

Compound **5b**

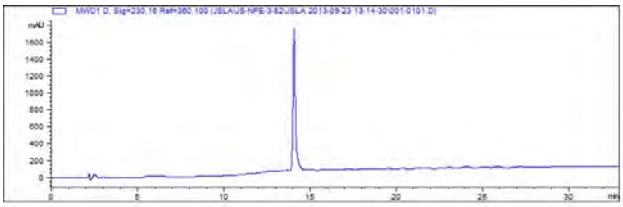

Compound **6a**

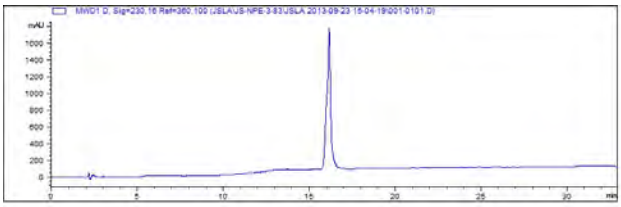

Compound **6b**

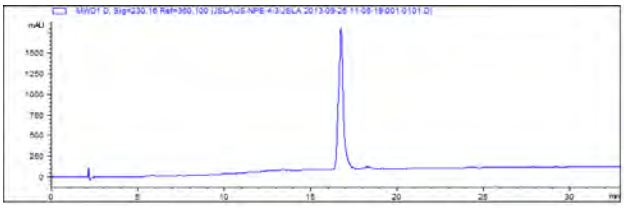

Compound **7a**

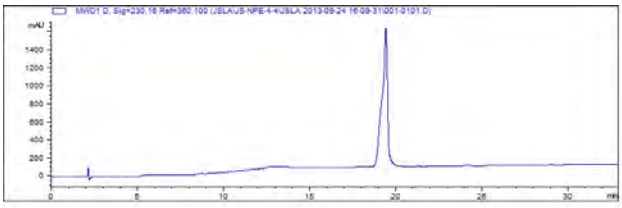

Compound **7b**

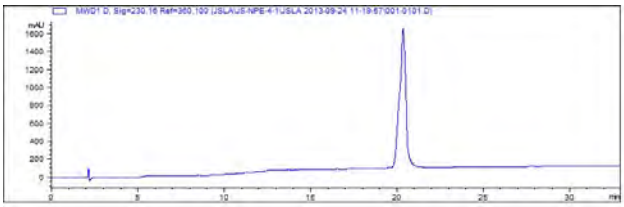

Compound **8a**

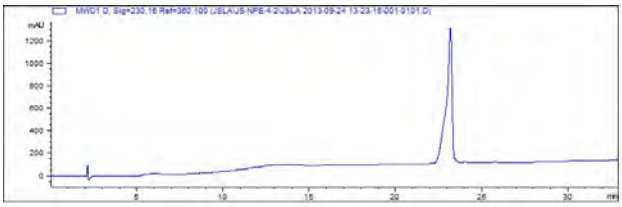

Compound **8b**

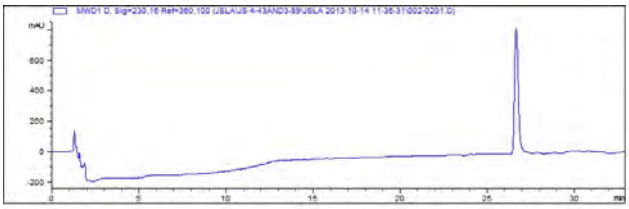

Compound **9a**

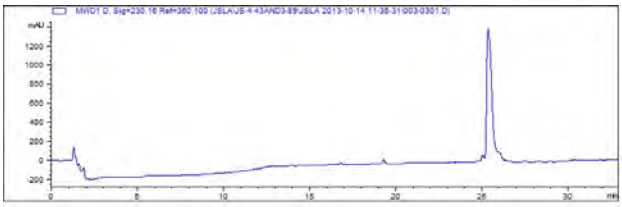

Compound **9b**

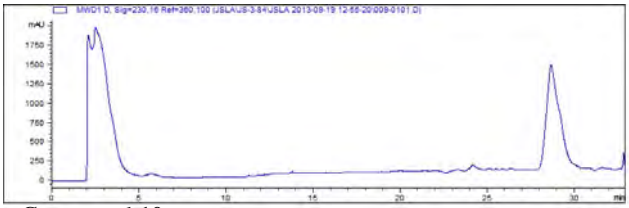

Compound **10a**

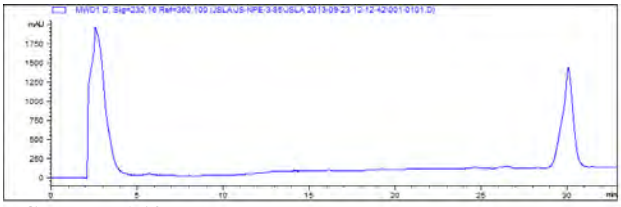

Compound **10b**

Guanidino Groups Greatly Enhance the Action of Antimicrobial Peptidomimetics Against Lipid Monolayers Mimicking Gram-positive Bacteria Membranes.

Konstantin Andreev[a #], Christopher Bianchi[a #], Jonas S. Laursen[b], Line Hein-Kristensen[c], Lone Gram[c], Ivan Kuzmenko[d], Christian A. Olsen[b], David Gidalevitz[a] *

[a]Center for Molecular Study of Condensed Soft Matter (μCoSM), Pritzker Institute of Biomedical Science and Engineering and Department of Physics, Illinois Institute of Technology, 3440 S. Dearborn St., Chicago, IL 60616 (USA)
[b]Department of Chemistry, Technical University of Denmark, Kemitorvet 207, DK-2800 Kgs. Lyngby (Denmark)
[c]Division of Industrial Food Research, National Food Institute, Technical University of Denmark, Søltofts Plads 221, DK-2800, Kgs Lyngby (Denmark)
[d]Advanced Photon Source, Argonne National Laboratory, 9700 S. Cass Ave., Lemont, IL 60439 (USA)

*Corresponding author:
David Gidalevitz
Center for Molecular Study of Condensed Soft Matter (μCoSM)
Pritzker Institute of Biomedical Science and Engineering
Department of Physics
Illinois Institute of Technology
3440 S. Dearborn St., Chicago, IL 60616 (USA)
Tel: (+1) 312-567-3534
Fax: (+1) 312-567-8856
E-mail: gidalevitz@iit.edu

Abstract:

A promising class of potential new antibiotics are the antimicrobial peptides or their synthetic mimics. Herein we assess the effect of the type of cationic side chain (i.e., guanidino vs. amino groups) on the membrane perturbing mechanism of antimicrobial *α*-peptide–*β*-peptoid chimeras. Two separate Langmuir monolayers composed of 1,2-dipalmitoyl-*sn*-glycero-3-phosphatidylglycerol (DPPG) and lipopolysaccharide Kdo2-lipid A were applied to model the outer membranes of Gram-positive and Gram-negative bacteria, respectively. We report the results of the measurements using an array of techniques, including high-resolution synchrotron surface X-ray scattering, epifluorescence microscopy, and *in vitro* antimicrobial activity to study the molecular mechanisms of peptidomimetic interaction with bacterial membranes. We found guanidino group-containing chimeras to exhibit greater disruptive activity on DPPG monolayers than the amino group-containing analogues. However, this effect was not observed for lipopolysaccharide monolayers where the difference was negligible. Furthermore, the addition of the nitrobenzoxadiazole fluorophore did not reduce the activity of these antimicrobials, which may be useful for future cellular localization studies.

Keywords: antimicrobial peptidomimetics; peptide–peptoid chimeras; guanidino cation; bacterial membrane; X-Ray scattering

1. Introduction

Antimicrobial peptides (AMPs) are ubiquitous in Nature; present in virtually all organisms they serve as endogenous antibiotics through the innate immune response.[1, 2] Members of this class of compounds have been studied extensively due to their potential as promising alternative antibiotics to treat disease caused by the growing number of resistant pathogenic microbes.[1-4] It is generally believed that AMPs exert their direct killing of invading pathogens by selectively interacting with the negatively charged bacterial surfaces over the globally neutral (zwitterionic) eukaryotic cell membranes. The mechanism by which the membranes are permeated is not completely understood, and several models have been proposed based on studies conducted with various peptidic structures.[1] Moreover, recent studies have shown that some of these chemotypes are endowed with additional intracellular modes of action such as interference with cell wall biosynthesis or immunomodulatory effects.[5-9] These findings complicate the understanding of this class of compounds even further and have called for the use of a perhaps more appropriate class designation, host-defense peptides (HDPs).[3]

Despite their diversity in amino acid sequence, lipophilicity and secondary structure,[10] most HDPs share common features includig positive net charge and generally amphipathic nature, separating hydrophilic and hydrophobic residues to the opposite faces of the molecule.[11-13] Typically, positive net charge of naturally occurring peptides is contributed by the guanidino groups of the arginine (Arg)[14, 15] and/or amino groups of the lysine (Lys) residues.[16-18] Both Arg and Lys side chains are generally thought to promote the initial long range electrostatic attractive forces that guide antimicrobials towards the negatively charged bacterial membranes.[19] However, guanidino groups have higher acid dissociation constant (pK_a) due to efficient resonance stabilization of the charged protonated state together with efficient solvation in water, which makes them stronger bases and, thus, better suited for stable electrostatic interactions with the negatively charged phosphodiester and phosphomonoester groups of phospholipids.[20-24] Examples of naturally occuring AMPs containing arginine rather than lysine residues include several members of the cathelicidin family, such as indolicidin and tritrpticin.[25, 26] Also, Muhle and Tam[28] found that Arg-to-Lys substitution in a cyclic disulfide-stabilized peptide decreased activity against Gram-negative bacteria. Nakase *et al.* demonstrated improved membrane permeability of antimicrobial peptide (RLA) with lysine substituted by arginine.[29] Other studies have shown that for lactoferricin B and bactenecin 5, which have no hemolytic activity, the replacement of arginine for lysine reduced antibacterial activity.[30] So, the incorporation of guanidino groups into the peptide side chains may have its appeal in drug design.[31-33]

However, there are concerns related to the use of α-peptides in a clinical setting due to their high cost of manufacturing[34] and inherent susceptibility to proteases,[35] which has led to numerous studies aimed at mimicry of peptides using non-natural compounds. Thus, a variety of classes such as β-peptides,[36-38] oligoureas,[39] arylamides,[40, 41] *N*-substituted oligoglycines (peptoids),[42-44] cyclic D,L-α-peptides,[45-47] hybrid peptidomimetics,[33, 48-50] and polymers[51-53] have been designed to mimic the function of AMPs.

α-peptide–β-peptoid chimeras represent a distinct class of peptidomimetics with backbone composed of alternating peptide and β-peptoid residues. In the present, study we elucidate the role of the cation type on the antimicrobial properties of this type of synthetic AMP mimics using two α-peptide–β-peptoid chimeras (**1** and **2**),[33, 50, 60-62] which differ from each

other solely in the identity of cationic functionality [amine (lysine) vs. guanidino group (homoarginine)]. In addition, because fluorophore-labeled analogues of AMPs, which retain antimicrobial activity, constitute powerful tools for studying mechanisms of action and cellular localization, we also prepared and evaluated nitrobenzoxadiazole (NBD)-labeled oligomers **1a** and **2a** (*Fig. 1A*).

Regardless of whether the primary mode of action is of a membrane-disrupting nature or entails perturbation of intracellular targets, the initial interaction between antimicrobial and bacteria involves the cell surface. A fundamental understanding of these lipid–antimicrobial interactions is therefore important for the future design of improved antibiotics for potential clinical use. Since cell membranes have a complex structure and are currently not applicable for highly sensitive surface X-ray scattering methods, the model systems are generally employed to undertake detailed mechanistic studies of membrane-associated processes.[63-67] Previously, the membrane-destabilizing effects of the *α*-peptide–*β*-peptoid chimeras have only been investigated in model liposomes prepared from phosphatidylcholine (PC), a phospholipid found predominantly in eukaryotic cells.[61] However, PC-containing systems do not adequately represent bacterial envelope, and furthermore, these compounds have not been investigated using sensitive X-ray methods before.

In order to model the outer surface of Gram-positive and Gram-negative bacteria we have employed insertion assay experiments on two separate Langmuir monolayers composed of 1,2-dipalmitoyl-sn-glycero-3-phosphatidylglycerol (DPPG) and truncated lipopolysaccharide (LPS) Kdo2-Lipid A, respectively (Fig. 1B). The reason behind this choice of lipids is that Kdo-2 lipid A constitutes the hydrophobic core of LPS envelope in most Gram-negative bacteria, while PGs are predominat phospholipid species within cytoplasmic membranes of Gram-positive strains. This approach has been successfully used in conjunction with liquid surface X-ray scattering to study bacterial membrane lysis by human antimicrobial peptide LL-37,[66] protegrin-1,[63, 68] gramicidin,[69] and SMAP-29[67] antimicrobial peptides as well as by peptide mimics.[44, 65, 70, 71]

2. Experimental Section

2.1 Monolayer construction

Both DPPG and Kdo2-Lipid A were purchased from Avanti Polar Lipids (Alabaster, AL) and were used without further purification. To form the monolayer systems both DPPG and Kdo2-Lipid A were first dissolved in chloroform–methanol (65:25) at a concentration of 0.2 mg/mL. Using a microliter syringe (Hamilton) the solutions were then spread on the surface of a Dulbecco's phosphate buffered saline (DPBS) (Invitrogen, Carlsbad, Ca) void of calcium and magnesium ions contained in a single barrier Langmuir trough. Over 15 minutes the organic solvents evaporated to form a self-assembled monolayer. The monolayer was then compressed to a biologically relevant packing density of 30 mN × m^{-1}, which was monitored by a Wilhelmy

plate. This surface pressure and a temperature of 22 ± 0.5 ^{o}C were maintained throughout the experiment. As a result, if changes in the surface pressure occur, the barrier will have to move in order to maintain the set surface pressure. Such change in barrier position then allows for change in area/lipid molecule or area/LPS molecule ΔA to be calculated. Once the monolayer was compressed the chamber containing the Langmuir trough was sealed and purged with helium to lower the oxygen levels in the chamber, which minimizes background X-ray scattering during the X-ray experiments[64, 72].

2.2 X-ray reflectivity (XR)

XR gives the information about electron density gradient along the plane perpendicular to the surface of monolayer as well as about the film thickness. [73-75] A slab-model, also known as a box model, was used to analyze XR data. This model is based on the Parratt recursive method[76] that describes the interface as a stack of slabs with distinct electron densities (ρ), and thicknesses (l).[77-81] The final fit was achieved by minimizing the χ2-square value while ensuring that parameters obtained were physically relevant. The software used to fit experimental XR data was RFit2000.[82-84] In addition to model-dependent fits, model-independent fits where the electron density profile of the film versus the vertical position along film perpendicular was generated using the software StochFit.[85]

2.3 Grazing-incidence X-ray diffraction (GIXD)

Grazing incidence X-ray diffraction measurements were performed to monitor the effect of compound insertion on the molecular packing of the lipid monolayers.[86] Lipid films spread at the air-water interface may be described by a large number of two-dimensional crystalline domains of ordered hydrocarbon chains randomly oriented around the surface normal.[87] In a GIXD experiment, the momentum transfer has a horizontal and vertical component, Q_{xy} and Q_z.[88] The Q_{xy} positions of the observed Bragg peaks yield the repeat distances, $d_{hk} = 2\pi/q_{hk}$ for the 2D lattice, from which specific parameters (a, b, γ) of the crystal system can be extracted. From the full-width half-maximum (FWHM) values of Bragg peaks, the in-plane coherence length, L_{xy} was calculated using the Scherrer formula, $L_{xy} = 0.9 \times 2\pi/\text{FWHM}$. The intensity distribution along the Bragg rod was measured at Bragg peak positions to evaluate the tilt of acyl chains.

All X-ray measurements were done at sector 9-ID at the Advanced Photon Source (APS) of Argonne National Labs (Chicago IL) with an X-ray wavelength of 0.9202 Å. After XR and GIXD were performed on a given monolayer system α-peptide–β-peptoid hybrids were introduced into the system using a bent needle syringe (Hamilton). The needle is placed underneath the barrier and the compounds were injected underneath the monolayer to mimic the approach of the compound from the extracellular fluid to the outer leaflet of the membrane. After injection both XR and GIXD measurements were taken for comparison.

2.4 Real-time epifluorescence microscopy (EFM) imaging

Morphological changes of DPPG films were studied on a microscopic level before and after the introduction of α-peptide–β-peptoid chimeras according to protocols previously described.[89, 90] Briefly, the Langmuir trough setup and procedures used in the formation of the lipid monolayers were essentially the same, except that a 0.1 mol % of lipid-linked Texas

Red dye [TR-DHPE (Molecular Probes, Eugene, OR)] was premixed with stock DPPG solution. A heated glass-plate was placed over the trough to reduce contamination and evaporation of the subphase during the experiment.

2.5 Chemical synthesis

Fmoc-Lys(Dde)-β*N*spe-OH (8). Fmoc-Lys-β*N*spe-OH (**7**) (1.61 g, 2.96 mmol) and *i*Pr$_2$NEt (1.4 mL, 8.0 mmol) were dissolved in DMF (30 mL), and added acetyl dimedone (913 mg, 5.0 mmol). After stirring for 18 h, the solvent was evaporated *in vacuo* and the crude product redissolved in EtOAc (100 mL). The solution was washed with 1 M HCl (aq) (2 × 100 mL) and water (2 × 100 mL), dried (Na_2SO_4), filtered, and evaporated *in vacuo* to give 1.22 g (82%) of the desired product as a white solid. ^{1}H NMR (300 MHz, CD_3OD) δ 1.48 (m, 2H, H-7), 1.66/1.56* (2 × d, 3H, J = 7.0 Hz, H-4), 1.68–1.82 (broad m, 4H, H-6, H-8), 2.17/2.51 (3 × m, 2H, H-1), 2.27*/2.28/2.51*/2.52 (4 × m, 6H, H-11, H-12) 3.19/3.38 (2 × m, 2H, H-2), 3.48 (m, 5H, H-9, H-10), 4.17 (m, 1H, H-15), 4.27–4.43 (broad m, 2H, H-14), 4.52*/4.81 (2 × m, 2H, H-5) 5.42/5.81* (2 × q, 1H, J = 7.0 Hz, H-3), 7.23–7.41 (broad m, 9H, Ph, Fmoc ArH), 7.66 (m, 2H, Fmoc ArH) 7.79 (d, 2H, J = 7.5 Hz, Fmoc Ar). [α]$_{589.2}$: –46° (c = 1.0, 293 K, $CHCl_3$). UPLC-MS gradient A, t_R = 2.20 min (>95), MS: (*m/z*) $[M + H]^+$ calcd. for $C_{32}H_{38}N_3O_5^+$: 708.9, found: 708.6. HRMS: (*m/z*) $[M + H]^+$ calcd. for $C_{32}H_{38}N_3O_5^+$: 708.3643, found: 708.3649 (ΔM = 0.8 ppm).

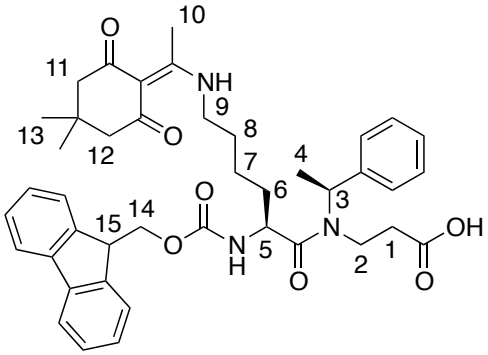

Solid-phase synthesis of 9. Fmoc-protected Rink amide resin (590 mg, 0.25 mmol) was treated with piperidine–DMF (1:4, 5 mL, 2 × 20 min), and washed with DMF, MeOH, and CH_2Cl_2 (3 × 5 mL). Oligomerization was performed with a mixture of Fmoc-Lys(Dde)-β*N*spe-OH (**8**) (750 mg, 1.1 mmol, 4.5 equiv), HBTU (417 mg, 1.1 mmol, 4.5 equiv), and *i*Pr$_2$NEt (0.38 mL, 2.2 mmol, 9 equiv) in DMF (5 mL), which were preincubated for 10 min before being added to the Rink amide resin and shaken for 18 h. After each coupling the resin was washed with MeOH, DMF and CH_2Cl_2 (3 × 5 mL). Fmoc deprotection was achieved with piperidine–DMF (1:4, 5 mL, 2 × 20 min) followed by DBU–piperidine–DMF (2:2:96, 5 mL, 2 × 20 min), after each deprotection step the resin was washed using the same procedure as above. This three-step coupling/deprotection sequence was performed 6 times to give the resin-bound oligomer.

Ac-(Lys-β*N*spe)$_6$-NH$_2$ (1). The terminal amino groups of (**9**) (100 mg, 0.024 mmol) were capped with a mixture of Ac_2O–*i*Pr$_2$NEt–DMF (1:2:3, 2 mL, 2 h) and the resin was washed with DMF, MeOH, and CH_2Cl_2 (3 × 2 mL). The side chains were deprotected using 2% hydrazine in DMF (2 × 2 mL, 45 min). The crude product was cleaved from the support with 50% TFA–CH_2Cl_2 (2 mL, 2 × 1 h). The TFA was co-evaporated with toluene (3 × 30 mL), toluene–CH_2Cl_2 (3 × 30 mL), and CH_2Cl_2 (3 × 3 mL). The residue was purified by preparative RP-HPLC (gradient C) and fractions were lyophilized to give compound **1** as white fluffy material [12.3 mg, 15% (90% per step)]. HPLC gradient D, t_R = 10.47 (>95%). HRMS: *m/z* $[M+3H]^{3+}$ calcd for $C_{104}H_{158}N_{19}O_{13}^{3+}$: 627.07567, found: 627.07553 (ΔM: 0.22 ppm).[50]

Ac-(hArg-β*N*spe)$_6$-NH$_2$ (2). The terminal amino group of (**9**) (75 mg, 0.024 mmol) was capped with a mixture of Ac_2O–*i*Pr_2NEt–DMF (1:2:3, 2 mL, 2 h) and the resin was washed with DMF, MeOH, and CH_2Cl_2 (3 × 2 mL). The side chains were deprotected using 2% hydrazine in DMF (2 × 2 mL, 2 × 45 min), and washed as above. Boc-protected guanidino groups were introduced by addition of a mixture of *N,N'*-bis(*tert*-butoxycarbonyl)-1H-pyrazole-1-carboxamidine (**11**) (285 mg, 0.92 mmol) and *i*Pr_2NEt (0.32 mL, 1.84 mmol) in DMF for 18 h, followed by the above washing procedure. The crude guanidinium-containing product was simultaneously deprotected and cleaved from the support with TFA–CH_2Cl_2 (1:1, 2 mL, 2 × 1 h). The TFA was co-evaporated with toluene (3 × 30 mL), toluene–CH_2Cl_2 (3 × 30 mL) and CH_2Cl_2 (3 × 30 mL). The residue was purified by preparative RP-HPLC (gradient C) and fractions were lyophilized to give compound **2** as white fluffy material [12.9 mg, 20% (90% per step)]. HPLC gradient D, t_R = 10.39 (>95%). HRMS: *m*/*z* $[M+3H]^{3+}$ calcd for $C_{110}H_{170}N_{31}O_{13}^{3+}$: 711.1193, found: 711.1190 (ΔM: 0.35 ppm).[50]

NBD-(Lys-β*N*spe)$_6$-NH$_2$ (1a). A Rink amide resin-bound oligomer with Boc protected lysine side chains (150 mg, 0.039 mmol) was prepared as described for **9** using the Fmoc-Lys(Boc)-b*N*spe-OH[59] building block. The N-terminal was then functionalized with a mixture of *N*-NBD-6-aminohexanoic acid (73 mg, 0.25 mmol), *i*Pr_2NEt (87 μL, 0.5 mmol), and PyBOP (156 mg, 0.3 mmol) in DMF (2 mL). After shaking for 18 h, the resin was washed with DMF, MeOH, and CH_2Cl_2 (3 × 2 mL), and the compound was cleaved from the support using TFA–CH_2Cl_2 (1:1, 2 mL, 2 × 1 h). Trifluoroacetic acid was co-evaporated with toluene (3 × 30 mL), toluene–CH_2Cl_2 (3 × 30 mL), CH_2Cl_2 (3 × 3 mL), and the residue was purified by preparative RP-HPLC (gradient C). Lyophilization of the fractions containing the titel compound furnished a yellow fluffy material [12.5 mg, 15% (88% per step)]. HPLC gradient D, t_R = 10.29 (>95%). HRMS: *m*/*z* $[M+3H]^{3+}$ calcd. for $C_{114}H_{168}N_{23}O_{16}^{3+}$: 705.4352, found: 705.4361 (ΔM: 1.3 ppm), and *m*/*z* $[M+4H]^{4+}$ calcd. for $C_{114}H_{169}N_{23}O_{16}^{4+}$: 529.3252, found: 529.3261 (ΔM: 1.7 ppm).

NBD-(hArg-β*N*spe)$_6$-NH$_2$ (2a). Crude NBD-(Lys-β*N*spe)$_6$-NH_2 **(1a)** (30 mg, 0.014 mmol) and *i*Pr_2NEt (29 μL, 0.16 mmol) were dissolved in DMF (2 mL), followed by addition of *N,N'*-bis(*tert*-butoxycarbonyl)-1H-pyrazole-1-carboxamidine (40 mg, 0.13 mmol). After stirring for 3 h, the solvent was evaporated *in vacuo*, and excess reagent removed by vacuum silica gel chromatography [2 × 6 cm, CH_2Cl_2–MeOH 0.5% gradient 0→10% (containing 1% concentrated aqueous NH_3)]. The product was then deprotected with TFA–CH_2Cl_2 (1:1, 2 mL, 2 × 1 h) and TFA was removed by co-evaporation with toluene (3 × 30 mL), toluene–CH_2Cl_2 (3 × 30 mL), and CH_2Cl_2 (3 × 3 mL). The compound was purified by preparative RP-HPLC (gradient C) to give **2a** as a yellow fluffy material (5 mg, 15%). HPLC gradient D, t_R = 11.05 (>95%). HRMS: *m*/*z* $[M+4H]^{4+}$ calcd. for $C_{120}H_{181}N_{35}O_{16}^{4+}$: 592.5609, found: 592.5603 (ΔM: 1 ppm).

Details of synthetic procedures, charaterization data, as well as ^1H and ^{13}C NMR spectra for all new compounds are presented in Supporting Information.

2.6 Bacterial strains and culture conditions

Activity experiments were carried out with five bacterial species representing common laboratory strains and clinical strains derived from both food-borne and nosocomial infections. Stock cultures were stored at –80 °C in 4% (w/v) glycerol, 0.5% (w/v) glucose, 2% (w/v)

skimmed milk powder, and 3% (w/v) tryptone soy powder. All experiments were carried out with bacteria incubated for one night (approximately 18 hours) at 37 ^{o}C. Experiments were performed in cation-adjusted Mueller Hinton II broth [MHB (Becton Dickinson 212322)] adjusted to pH 7.4. Brain Heart Infusion (CM1135) with 1.5% agar (VWR 20768.292) as gelling agent was used throughout for colony plating.

2.7 Antimicrobial activity assay

MIC was determined using the micro-dilution method according to guidelines of the Clinical and Laboratory Standards Institute (CLSI). Two-fold serial dilutions of the peptidomimetic hybrids were prepared from 1024 μg/mL stock solutions in Milli-Q water to give a final range of 512–0.5 μg/mL in the wells; compound **3** containing only the fluorophore and the spacer was included but due to solubility issues this stock was 258 μg/mL, thus giving a final range of 128–0.125 μg/mL in the wells. Colonies grown on BHI agar for approximately 18 hours were suspended in 0.9% saline to give a turbidity of 0.13 at OD_{546} (approximately 1×10^8 CFU/mL), and then diluted in MHB pH 7.4 to a final concentration of 5×10^5 CFU/mL in each well. Polypropylene plates (Nunc 442587) were used to minimize peptide binding, and the incubation time was 18–20 hours at 37 ^{o}C. MIC values, i.e., the lowest concentration of the peptide analogue at which no visible growth was observed, were determined in duplicate. Activity is expressed in μg/mL and μM.

3. Results

3.1 Synthesis

The syntheses of **1**–**2a** were achieved by preparation of dimeric building blocks followed by oligomerization on solid support using variations of previously described methods.[50, 59, 91] In order to enable an on-resin functionalization of the lysine ε-amino groups we installed an orthogonal 1-(4,4-dimethyl-2,6-dioxacyclohexylidene)ethyl (Dde) group[92, 93] on the lysine side chain functionality to give building block **8** (*Scheme 1*).

For the standard Fmoc solid-phase peptide synthesis (SPPS) oligomerization, a ChemMatrix® resin was chosen due to its excellent swelling properties in a variety of solvents. After six rounds of coupling/deprotection (**9**), the N-terminal was acetylated and the Dde group was removed to give **10**, which upon cleavage afforded compound **1** (*Scheme 2*). Functionalization of the free amines in **10** by guanidinylation,[94] followed by simultaneous deprotection and cleavage furnished compound **2**. Unfortunately, introduction of the fluorophore proved incompatible with our new protecting group strategy, most likely due to sensitivity towards hydrazine during the Dde deprotection step. For the syntheses of labeled analogues **1a** and **2a**, a different strategy involving guanidinylation in solution was therefore adopted as shown in Supplementary *Scheme S1* and *Scheme S2*.

3.2 Antimicrobial activities

Previously, fluorescein-labelled versions of these *α*-peptide–*β*-peptoid oligomers have been prepared to investigate their potential as cell-penetrating peptides,[60, 61] and subsequent antimicrobial testing of these showed a severe decrease in potency when introducing the fluorescein label.[33] The compounds were therefore tested for their antimicrobial activity against a selection of pathogens to determine if the novel fluorescent-labeled analogues could inhibit bacterial growth. The NBD-labeled compounds exhibited minimum inhibitory concentrations (MICs) that were comparable to the parent compounds with a maximum difference of 4-fold in MIC values (*Table 1*).

Interestingly, however, the labeled compound gave rise to lower MIC values than the parent in about half of the cases in the amino series, while this trend was opposite in the guanidino series. To determine whether the fluorophore itself was responsible for any antimicrobial activity, compound **3** containing the fluorophore and the spacer was synthesized and evaluated as well, and no effect was recorded against the tested strains. Since the fluorescent-labeled compounds retained activity within acceptable range of the parent compounds, we decided to include the NDB-labeled compounds in the model study along with **1** and **2**.

3.3 Epifluorescence microscopy

EFM images of the DPPG monolayer at 30 mN × m^{-1} displays an array of branched dark domains of condensed phase ~25–50 μm in diameter separated from each other by brightly colored "fluid" (disordered) areas. *Fig. 2* shows the dynamics of surface morphology changes in lipid film after injection of **1** and **2** into the subphase. Both compounds caused a decrease in the size of condensed-phase domains starting from 4^{th} min and followed by their complete elimination with transition of the majority of the film to a liquid-disordered phase after 15–20 min. Structurally ordered regions in this case might be either fully destroyed or reduced in size to become smaller than the microscope resolution (<1 μm). This points out to a crystallinity-disruptive behavior of the studied *α*-peptide–*β*-peptoid chimeras against DPPG monolayers regardless of the identity of the cations they contain, at least on micrometer scale.

3.4 Specular X-ray reflectivity

Fig. 3 shows electron density profiles along the surface normal extracted from reflectivity data by model-independent stochastic fitting. The graphs are combined in such a way as to allow visual comparison of amino- and guanidino-containing compounds. For the lipid monomolecular films, the electron density is zero at the air-water interface, then rises sharply through the hydrocarbon tail region, and comes to a plateau reaching its maximum values for the head groups (at a distance of ~20–25 Å from the air side of the film) before slightly decaying to the subphase electron density. In addition, model-dependent analyses were performed on XR data. Pure DPPG monolayers were modeled as two slabs, with the first slab corresponding to the phospholipid acyl chains, and the second reperesenting the lipid head groups. XR analysis yielded the thickness of the slab related to acyl chains to be 16.5 Å with an electron density of 0.312 $e^{-}/Å^3$. The thickness of the slab used to model the head groups was found to be 8.3 Å with an electron density of 0.477 $e^{-}/Å^3$. Two-slab model-dependent fitting of Kdo-2 Lipid A data yielded 12.0 Å long upper hydrocarbon chain region with electron density of 0.31 $e^{-}/Å^3$. The second slab corresponding to the complex of head moieties and the outer layer of carbohydrate

3-deoxy-D-mannooctulosonic acid known as Kdo has the thickness of 12.8 Å and an electron density of 0.485 $e^{-}/Å^3$. Insertion of antimicrobials into the membrane mimic results in extra electrons per lipid molecule in each slab and is calculated using formula (1). Here, l_{slab} and ρ_{slab} are thickness and electron density of the slab, respectively; $A_{lipid} + \Delta A_{lipid}$ is the area per lipid molecule upon insertion and $N_{initial}\ e^{-}_{slab}$ minus the number of electrons in the slab in the original untreated monolayer.

$$N_{extra}\ e^{-}_{slab} = l_{slab} \times \rho_{slab} \times (A_{lipid} + \Delta A_{lipid}) - N_{initial}\ e^{-}_{slab} \quad \text{(eq. 1)}$$

Preliminary information about the mode of antimicrobial interaction with membane mimics can be obtained directly from the electron density profiles (*Fig.3A*). Compounds **1** and **2** displayed a drastic difference in their mode of action against DPPG monolayers. Following injection of **1** the first minimum of reflectivity curve shifted from $q_z \approx 0.24\ Å^{-1}$ to a higher q_z value with the peak of electron density moved towards the air–water interface. This indicates a decrease in thickness of the film as a result of its insertion. However, compound **2** instead of thinning DPPG monolayer, led to appearance of two minima on the reflectivity profile at $q_z \approx 0.21\ Å^{-1}$ and $0.35\ Å^{-1}$ and a notable bump of the electron density curve within the range of 20–40 Å away from air-water interface. This might be due to an additional layer of distinct electron density higher than the electron density of subphase present underneath the head group region. These data are corroborated by the model-dependent analysis and are summarized in Supplementary *Table S1*. Injection of **1** into DPPG resulted in an experimental XR curve, which was again best fit with two layers. However, an additional box was required to fit XR data upon introduction of compound **2**. The lower increase in area per lipid molecule observed upon insertion of compound **2** as compared with **1** could possibly be explained by partial dimerization or aggregation of **2** on the outer surface of lipid monolayer. According to the number of extra electrons contributed by incorporated antimicrobials, both **1** and **2** readily insert into the polar moieties of DPPG and Kdo-2 Lipid A resulting in reduced electron density of bottom slab, but they are both unable to penetrate deeply into overlying hydrophobic core of lipid monolayers. The more substantial decrease in electron density of the DPPG head group region, along with three times more additional electrons present upon introduction of **2** points to a higher Gram-positive membrane disruptive potential of guanidino-containing oligomer versus its amino-containing counterpart. The same trend was observed for the NBD-tagged hybrids. Here compound **2a** permeated the entire depth of DPPG film including hydrophobic acyl chains, whereas **1a** was found only in the hydrophilic outer shell of the lipid monolayer. Furthermore, the introduction of **2a** led to a greater contribution of additional electrons *in toto*, as well as to a four-fold larger increase in area per single DPPG molecule (ΔA_{lipid}) indicating a favorable effect of arginine residues on the antimicrobial insertion.

In contrast to DPPG, the reflectivity curves of Kdo-2 Lipid A monolayer after introduction of **1** and **2** look nearly identical (*Fig. 3B*). For model-dependent analysis two boxes were sufficient to fit experimental XR data and revealed very similar mechanism of action utilized by guanidino- and amino-containing hybrid oligomers against Gram-negative bacteria LPS. This consistency in mode of action between **1** and **2,** as well as between **1a** and **2a** was confirmed by similar changes in thickness of respective slabs within Kdo-2 Lipid A monolayer and by similar number of contributed extra electrons.The area increase per lipid molecule in both pairs of compounds was also about the same.

Additionally, the effect of NBD-fluorophore was investigated by comparing **1** and **2** to their NBD-tagged fluorescent analogues **1a** and **2a** respectively. According to the results of XR analysis, functionalization of *α*-peptide–*β*-peptoid chimeras by NBD does not reduce their capability to interact with bacterial membranes. Moreover, fluorophore-carrying chimeras have provided even greater contribution of additional electrons to the lipid head-groups. This implies a higher number of chimeras to be inserted into the lipid films.

3.5 Grazing-incidence X-ray diffraction.

GIXD data for DPPG monolayer before and after injection of antimicrobials are presented in *Fig. 4*. The corresponding values of unit cell dimensions, *d*-spacings and sizes of crystallized domains are presented in *Table 2*. At the surface pressure of 30 mN × m^{-1} pure DPPG yields two distinct Bragg peaks at Q_{xy} = 1.39 $Å^{-1}$ and Q_{xy} = 1.47 $Å^{-1}$ corresponding to *d*-spacings of 4.51 and 4.26 Å, respectively. This indicates the presence of ordered structure with the centered rectangular packing ($a \neq b$, $\gamma = 90^{o}$) having unit cell dimensions a = 5.32 Å and b = 8.54 Å and an area of 45.5 $Å^2$ per single DPPG molecule. For Kdo2-Lipid A, on the other hand, no Bragg peak was observed. This means that there were no diffractable 2D crystalline regions within the monolayer, which does not allow a detailed analysis of the surface morphology. According to GIXD data, guanidino group-containing compounds **2** and **2a** fully destroy the lateral crystallinity of DPPG monolayers evidenced by complete disappearance of Bragg peaks. Conversely, both **1** and **1a**, instead of disordering, caused structural rearrangement of the crystal lattice from a centered rectangular crystal packing to a hexagonal ($a = b$, $\gamma = 120^{o}$) resulting in appearance of a single Bragg peak. The coherence length was also reduced, which might explain the disappearance of ordered regions upon introduction of compound **1** observed by EFM. Furthermore, fluorophore-labelled **1a** was shown to decrease the size of crystallized domains as well as the order of their crystallinity to a greater extent than its non-labelled counterpart, even though the main parameters of crystal lattice didn't change much. This supports the hypothesis that labelling of antimicrobials with NBD may enhance their membrane-disruptive potential without drastically changing the primary mechanism of action.

4. Discussion

Overall, our data provide solid mechanistic evidence of higher membrane activity against Gram-positive strains displayed by guanidino-containing *α*-peptide–*β*-peptoid chimeras as compared to their amino-substituted counterparts. Guanidino groups were shown to considerably improve the capability of these antimicrobial peptidomimetics to compromise the integrity of DPPG monolayers mimicking the external leaflet of Gram-positive bacteria cell membranes. Surprisingly, this favorable effect of guanidinium cations on their insertion properties was not observed for lipopolysaccharide (Kdo-2 Lipid A) monolayers, which model the outer membrane of Gram-negative bacteria. These XR data are in excellent agreement with the previously published results obtained from biological assays on a larger array of *α*-peptide–*β*-peptoid oligomers, especially at higher oligomer lengths.[33, 62] The increased potency of guanidino-containing chimera **2** over its amino-containing counterpart **1** on Gram-negative strains *in vitro*

(Table 1) might thus arise from other mechanisms of action in addition to direct membrane permeabilization. A full explanation of this finding, however, would require extensive experiments beyond the scope of this work. A schematic cartoon illustrating the proposed mechanism of membrane interaction of the antimicrobials is represented in *Fig. 5*.

As both types of cation are fully protonated at physiological pH we hypothesize that the ability of the guanidino group to form a more stable bidentate electrostatic interaction with negatively charged phosphodiester moieties affects the DPPG lipids to a greater extent than the more structurally rigid Kdo-2 Lipid A. These findings thus provide fundamental insights that should be useful in the future design of optimized synthetic peptidomimetics with selective antibiotic effects.

Finally, addition of the NBD fluorophore did not reduce the insertion activity of the tested chimeras that also correlate with their retained antimicrobial potency against bacteria *in vitro*. Moreover, the NBD-labeled compounds demonstrated even greater ability to destroy both DPPG and Kdo-2 Lipid A monolayers, than their non-tagged analogues. It is assumed that this is a result of increased lipophilicity of modified molecules due to incorporation of the hydrophobic benzofurazan ring of NBD. The resulting amphiphilic properties may reduce the energy penalties associated with penetration of antimicrobials into hydrophobic core and, thus, favor the disruption of membrane structure. The use of fluorescently tagged AMP mimics might facilitate future cellular localization studies aimed at the elucidation of the mechanism of action of oligomeric AMPs in general.

Notes

The authors declare no competing financial interest.
[#] These authors contributed equally to the work.

Acknowledgements

We thank Dr. Andrey Ivankin for assistance with synchrotron X-ray scattering experiments, Ms. Anne Hector and Dr. Charlotte H. Gotfredsen for assistance with NMR spectroscopy, and Ms. Tina Gustafsson for technical assistance with UPLC-MS and HRMS. The National Center for Antimicrobials & Infection Control, Statens Serum Institut, Denmark is acknowledged for providing the Danish clinical sample of ESBL-producing *E. coli*.

This work was supported by funds from NIH (R01 AI073892, D.G.), DARPA (W911NF-09-1-378, D.G.), the Danish Research Council for Technology and Production (09-065902 and 09-066098), the Danish Independent Research Council | Natural Sciences (Steno Grant no. 10-080907, C.A.O.), and the Technical University of Denmark. Use of the APS was supported by DOE under contract no. W-31-109-Eng-38. C.A.O. is a Lundbeck Foundation.

References

[1] M. Zasloff, Antimicrobial peptides of multicellular organisms, Nature, 415 (2002) 389-395.
[2] R.E.W. Hancock, H.G. Sahl, Antimicrobial and host-defense peptides as new anti-infective therapeutic strategies, Nature Biotechnology, 24 (2006) 1551-1557.
[3] A.T.Y. Yeung, S.L. Gellatly, R.E.W. Hancock, Multifunctional cationic host defence peptides and their clinical applications, Cell Mol Life Sci, 68 (2011) 2161-2176.
[4] J.L. Fox, Antimicrobial peptides stage a comeback, Nature Biotechnology, 31 (2013) 379-382.
[5] E. Breukink, I. Wiedemann, C. van Kraaij, O.P. Kuipers, H.G. Sahl, B. de Kruijff, Use of the cell wall precursor lipid II by a pore-forming peptide antibiotic, Science, 286 (1999) 2361-2364.
[6] T. Schneider, T. Kruse, R. Wimmer, I. Wiedemann, V. Sass, U. Pag, A. Jansen, A.K. Nielsen, P.H. Mygind, D.S. Ravents, S. Neve, B. Ravn, A.M.J.J. Bonvin, L. De Maria, A.S. Andersen, L.K. Gammelgaard, H.G. Sahl, H.H. Kristensen, Plectasin, a Fungal Defensin, Targets the Bacterial Cell Wall Precursor Lipid II, Science, 328 (2010) 1168-1172.
[7] S. Sandgren, A. Wittrup, F. Cheng, M. Jonsson, E. Eklund, S. Busch, M. Belting, The human antimicrobial peptide LL-37 transfers extracellular DNA plasmid to the nuclear compartment of mammalian cells via lipid rafts and proteoglycan-dependent endocytosis, Journal of Biological Chemistry, 279 (2004) 17951-17956.
[8] K.A. Brogden, Antimicrobial peptides: Pore formers or metabolic inhibitors in bacteria?, Nat Rev Microbiol, 3 (2005) 238-250.
[9] M.G. Scott, E. Dullaghan, N. Mookherjee, N. Glavas, M. Waldbrook, A. Thompson, A.K. Wang, K. Lee, S. Doria, P. Hamill, J.J. Yu, Y.X. Li, O. Donini, M.M. Guarna, B.B. Finlay, J.R. North, R.E.W. Hancock, An anti-infective peptide that selectively modulates the innate immune response, Nature Biotechnology, 25 (2007) 465-472.
[10] C.D. Fjell, J.A. Hiss, R.E.W. Hancock, G. Schneider, Designing antimicrobial peptides: form follows function, Nat Rev Drug Discov, 11 (2012) 37-51.
[11] Z. Oren, Y. Shai, Mode of action of linear amphipathic alpha-helical antimicrobial peptides, Biopolymers, 47 (1998) 451-463.
[12] R.E. Hancock, Host defence (cationic) peptides: what is their future clinical potential?, Drugs, 57 (1999) 469-473.
[13] Z. Jiang, A.I. Vasil, J.D. Hale, R.E. Hancock, M.L. Vasil, R.S. Hodges, Effects of net charge and the number of positively charged residues on the biological activity of amphipathic alpha-helical cationic antimicrobial peptides, Biopolymers, 90 (2008) 369-383.
[14] D.A. Steinberg, M.A. Hurst, C.A. Fujii, A.H.C. Kung, J.F. Ho, F.C. Cheng, D.J. Loury, J.C. Fiddes, Protegrin-1: A broad-spectrum, rapidly microbicidal peptide with in vivo activity, Antimicrob Agents Ch, 41 (1997) 1738-1742.
[15] M.H. Wu, R.E.W. Hancock, Interaction of the cyclic antimicrobial cationic peptide bactenecin with the outer and cytoplasmic membrane, Journal of Biological Chemistry, 274 (1999) 29-35.
[16] M. Zasloff, Magainins, a class of antimicrobial peptides from Xenopus skin: isolation, characterization of two active forms, and partial cDNA sequence of a precursor, Proc Natl Acad Sci U S A, 84 (1987) 5449-5453.

[17] Y. Ge, D.L. MacDonald, K.J. Holroyd, C. Thornsberry, H. Wexler, M. Zasloff, In vitro antibacterial properties of pexiganan, an analog of magainin, Antimicrob Agents Chemother, 43 (1999) 782-788.
[18] D. Savoia, R. Guerrini, E. Marzola, S. Salvadori, Synthesis and antimicrobial activity of dermaseptin S1 analogues, Bioorganic & Medicinal Chemistry, 16 (2008) 8205-8209.
[19] T. Hessa, H. Kim, K. Bihlmaier, C. Lundin, J. Boekel, H. Andersson, I. Nilsson, S.H. White, G. von Heijne, Recognition of transmembrane helices by the endoplasmic reticulum translocon, Nature, 433 (2005) 377-381.
[20] Y.C. Su, T. Doherty, A.J. Waring, P. Puchala, M. Hong, Roles of Arginine and Lysine Residues in the Translocation of a Cell-Penetrating Peptide from C-13, P-31, and F-19 Solid-State NMR, Biochemistry, 48 (2009) 4587-4595.
[21] M. Hong, Y.C. Su, Structure and dynamics of cationic membrane peptides and proteins: Insights from solid-state NMR, Protein Sci, 20 (2011) 641-655.
[22] P.A. Gale, Special issue: Anion coordination chemistry II - Preface, Coordin Chem Rev, 250 (2006) 2917-2917.
[23] J. Mavri, H.J. Vogel, Ion pair formation of phosphorylated amino acids and lysine and arginine side chains: a theoretical study, Proteins, 24 (1996) 495-501.
[24] A.S. Woods, S. Ferre, Amazing stability of the arginine-phosphate electrostatic interaction, Journal of proteome research, 4 (2005) 1397-1402.
[25] L.T. Nguyen, L. de Boer, S.A. Zaat, H.J. Vogel, Investigating the cationic side chains of the antimicrobial peptide tritrpticin: hydrogen bonding properties govern its membrane-disruptive activities, Biochimica et biophysica acta, 1808 (2011) 2297-2303.
[26] S.T. Yang, S.Y. Shin, C.W. Lee, Y.C. Kim, K.S. Hahm, J.I. Kim, Selective cytotoxicity following Arg-to-Lys substitution in tritrpticin adopting a unique amphipathic turn structure, FEBS letters, 540 (2003) 229-233.
[27] R.A. Llenado, C.S. Weeks, M.J. Cocco, A.J. Ouellette, Electropositive Charge in alpha-Defensin Bactericidal Activity: Functional Effects of Lys-for-Arg Substitutions Vary with the Peptide Primary Structure, Infect Immun, 77 (2009) 5035-5043.
[28] S.A. Muhle, J.P. Tam, Design of Gram-negative selective antimicrobial peptides, Biochemistry, 40 (2001) 5777-5785.
[29] I. Nakase, S. Okumura, S. Katayama, H. Hirose, S. Pujals, H. Yamaguchi, S. Arakawa, S. Shimizu, S. Futaki, Transformation of an antimicrobial peptide into a plasma membrane-permeable, mitochondria-targeted peptide via the substitution of lysine with arginine, Chem Commun (Camb), 48 (2012) 11097-11099.
[30] Y. Tokunaga, T. Niidome, T. Hatakeyama, H. Aoyagi, Antibacterial activity of bactenecin 5 fragments and their interaction with phospholipid membranes, Journal of peptide science : an official publication of the European Peptide Society, 7 (2001) 297-304.
[31] F. Saczewski, L. Balewski, Biological activities of guanidine compounds, Expert opinion on therapeutic patents, 19 (2009) 1417-1448.
[32] B. Findlay, P. Szelemej, G.G. Zhanel, F. Schweizer, Guanidylation and tail effects in cationic antimicrobial lipopeptoids, PloS one, 7 (2012) e41141.
[33] C.A. Olsen, H.L. Ziegler, H.M. Nielsen, N. Frimodt-Moller, J.W. Jaroszewski, H. Franzyk, Antimicrobial, hemolytic, and cytotoxic activities of beta-peptoid-peptide hybrid oligomers: improved properties compared to natural AMPs, Chembiochem : a European journal of chemical biology, 11 (2010) 1356-1360.

[34] A. Giuliani, G. Pirri, S.F. Nicoletto, Antimicrobial peptides: an overview of a promising class of therapeutics, Cent Eur J Biol, 2 (2007) 1-33.
[35] S.M. Miller, R.J. Simon, S. Ng, R.N. Zuckermann, J.M. Kerr, W.H. Moos, Proteolytic Studies of Homologous Peptide and N-Substituted Glycine Peptoid Oligomers, Bioorganic & Medicinal Chemistry Letters, 4 (1994) 2657-2662.
[36] Y. Hamuro, J.P. Schneider, W.F. DeGrado, De Novo design of antibacterial Œ≤-peptides, J. Am. Chem. Soc., 121 (1999) 12200-12201.
[37] E.A. Porter, X. Wang, H.S. Lee, B. Weisblum, S.H. Gellman, Non-haemolytic beta-amino-acid oligomers, Nature, 404 (2000) 565.
[38] P.I. Arvidsson, J. Frackenpohl, N.S. Ryder, B. Liechty, F. Petersen, H. Zimmermann, G.P. Camenisch, R. Woessner, D. Seebach, On the antimicrobial and hemolytic activities of amphiphilic beta-peptides, Chembiochem, 2 (2001) 771-773.
[39] A. Violette, S. Fournel, K. Lamour, O. Chaloin, B. Frisch, J.P. Briand, H. Monteil, G. Guichard, Mimicking helical antibacterial peptides with nonpeptidic folding oligomers, Chem Biol, 13 (2006) 531-538.
[40] G.N. Tew, D. Liu, B. Chen, R.J. Doerksen, J. Kaplan, P.J. Carroll, M.L. Klein, W.F. DeGrado, De novo design of biomimetic antimicrobial polymers, Proceedings of the National Academy of Sciences of the United States of America, 99 (2002) 5110-5114.
[41] S. Choi, A. Isaacs, D. Clements, D. Liu, H. Kim, R.W. Scott, J.D. Winkler, W.F. DeGrado, De novo design and in vivo activity of conformationally restrained antimicrobial arylamide foldamers, Proceedings of the National Academy of Sciences of the United States of America, 106 (2009) 6968-6973.
[42] B. Goodson, A. Ehrhardt, S. Ng, J. Nuss, K. Johnson, M. Giedlin, R. Yamamoto, W.H. Moos, A. Krebber, M. Ladner, M.B. Giacona, C. Vitt, J. Winter, Characterization of novel antimicrobial peptoids, Antimicrob Agents Chemother, 43 (1999) 1429-1434.
[43] J.A. Patch, A.E. Barron, Helical peptoid mimics of magainin-2 amide, J Am Chem Soc, 125 (2003) 12092-12093.
[44] N.P. Chongsiriwatana, J.A. Patch, A.M. Czyzewski, M.T. Dohm, A. Ivankin, D. Gidalevitz, R.N. Zuckermann, A.E. Barron, Peptoids that mimic the structure, function, and mechanism of helical antimicrobial peptides, Proceedings of the National Academy of Sciences of the United States of America, 105 (2008) 2794-2799.
[45] S. Fernandez-Lopez, H.S. Kim, E.C. Choi, M. Delgado, J.R. Granja, A. Khasanov, K. Kraehenbuehl, G. Long, D.A. Weinberger, K.M. Wilcoxen, M.R. Ghadiri, Antibacterial agents based on the cyclic D,L-alpha-peptide architecture, Nature, 412 (2001) 452-455.
[46] V. Dartois, J. Sanchez-Quesada, E. Cabezas, E. Chi, C. Dubbelde, C. Dunn, J. Granja, C. Gritzen, D. Weinberger, M.R. Ghadiri, T.R. Parr, Jr., Systemic antibacterial activity of novel synthetic cyclic peptides, Antimicrob Agents Chemother, 49 (2005) 3302-3310.
[47] L. Motiei, S. Rahimipour, D.A. Thayer, C.H. Wong, M.R. Ghadiri, Antibacterial cyclic D,L-alpha-glycopeptides, Chem Commun (Camb), (2009) 3693-3695.
[48] I.S. Radzishevsky, S. Rotem, D. Bourdetsky, S. Navon-Venezia, Y. Carmeli, A. Mor, Improved antimicrobial peptides based on acyl-lysine oligomers, Nat Biotechnol, 25 (2007) 657-659.
[49] F. Zaknoon, H. Sarig, S. Rotem, L. Livne, A. Ivankin, D. Gidalevitz, A. Mor, Antibacterial Properties and Mode of Action of a Short Acyl-Lysyl Oligomer, Antimicrob Agents Ch, 53 (2009) 3422-3429.

[50] C.A. Olsen, G. Bonke, L. Vedel, A. Adsersen, M. Witt, H. Franzyk, J.W. Jaroszewski, Alpha-peptide/beta-peptoid chimeras, Org Lett, 9 (2007) 1549-1552.
[51] K. Kuroda, W.F. DeGrado, Amphiphilic polymethacrylate derivatives as antimicrobial agents, J Am Chem Soc, 127 (2005) 4128-4129.
[52] B.P. Mowery, S.E. Lee, D.A. Kissounko, R.F. Epand, R.M. Epand, B. Weisblum, S.S. Stahl, S.H. Gellman, Mimicry of antimicrobial host-defense peptides by random copolymers, J Am Chem Soc, 129 (2007) 15474-15476.
[53] F. Nederberg, Y. Zhang, J.P.K. Tan, K.J. Xu, H.Y. Wang, C. Yang, S.J. Gao, X.D. Guo, K. Fukushima, L.J. Li, J.L. Hedrick, Y.Y. Yang, Biodegradable nanostructures with selective lysis of microbial membranes, Nat Chem, 3 (2011) 409-414.
[54] R.N. Zuckermann, J.M. Kerr, S.B.H. Kent, W.H. Moos, Efficient Method for the Preparation of Peptoids [Oligo(N-Substituted Glycines)] by Submonomer Solid-Phase Synthesis, J Am Chem Soc, 114 (1992) 10646-10647.
[55] R.N. Zuckermann, Peptoid origins, Biopolymers, 96 (2011) 545-555.
[56] M.T. Dohm, R. Kapoor, A.E. Barron, Peptoids: bio-inspired polymers as potential pharmaceuticals, Current pharmaceutical design, 17 (2011) 2732-2747.
[57] M. Wetzler, A.E. Barron, Progress in the de novo design of structured peptoid protein mimics, Biopolymers, 96 (2011) 556-560.
[58] R.J. Simon, R.S. Kania, R.N. Zuckermann, V.D. Huebner, D.A. Jewell, S. Banville, S. Ng, L. Wang, S. Rosenberg, C.K. Marlowe, et al., Peptoids: a modular approach to drug discovery, Proceedings of the National Academy of Sciences of the United States of America, 89 (1992) 9367-9371.
[59] G. Bonke, L. Vedel, M. Witt, J.W. Jaroszewski, C.A. Olsen, H. Franzyk, Dimeric building blocks for solid-phase synthesis of alpha-peptide-beta-peptoid chimeras, Synthesis-Stuttgart, (2008) 2381-2390.
[60] L. Vedel, G. Bonke, C. Foged, H. Ziegler, H. Franzyk, J.W. Jaroszewski, C.A. Olsen, Antiplasmodial and prehemolytic activities of alpha-peptide-beta-peptoid chimeras, ChemBioChem, 8 (2007) 1781-1784.
[61] C. Foged, H. Franzyk, S. Bahrami, S. Frokjaer, J.W. Jaroszewski, H.M. Nielsen, C.A. Olsen, Cellular uptake and membrane-destabilizing properties of alpha -peptide/beta -peptoid chimeras: lessons for the design of new cell-penetrating peptides, Biochim. Biophys. Acta, Biomembr., 1778 (2008) 2487-2495.
[62] L. Hein-Kristensen, K.M. Knapp, H. Franzyk, L. Gram, Bacterial membrane activity of alpha-peptide/beta-peptoid chimeras: influence of amino acid composition and chain length on the activity against different bacterial strains, BMC Microbiol, 11 (2011) 144.
[63] D. Gidalevitz, Y. Ishitsuka, A.S. Muresan, O. Konovalov, A.J. Waring, R.I. Lehrer, K.Y. Lee, Interaction of antimicrobial peptide protegrin with biomembranes, Proceedings of the National Academy of Sciences of the United States of America, 100 (2003) 6302-6307.
[64] A. Ivankin, B. Apellaniz, D. Gidalevitz, J.L. Nieva, Mechanism of membrane perturbation by the HIV-1 gp41 membrane-proximal external region and its modulation by cholesterol, Biochimica et biophysica acta, 1818 (2012) 2521-2528.
[65] A. Ivankin, L. Livne, A. Mor, G.A. Caputo, W.F. Degrado, M. Meron, B. Lin, D. Gidalevitz, Role of the conformational rigidity in the design of biomimetic antimicrobial compounds, Angew Chem Int Ed Engl, 49 (2010) 8462-8465.

[66] F. Neville, M. Cahuzac, O. Konovalov, Y. Ishitsuka, K.Y. Lee, I. Kuzmenko, G.M. Kale, D. Gidalevitz, Lipid headgroup discrimination by antimicrobial peptide LL-37: insight into mechanism of action, Biophys J, 90 (2006) 1275-1287.
[67] F. Neville, A. Ivankin, O. Konovalov, D. Gidalevitz, A comparative study on the interactions of SMAP-29 with lipid monolayers, Biochimica et biophysica acta, 1798 (2010) 851-860.
[68] F. Neville, Y. Ishitsuka, C.S. Hodges, O. Konovalov, A.J. Waring, R. Lehrer, K.Y. Lee, D. Gidalevitz, Protegrin interaction with lipid monolayers: Grazing incidence X-ray diffraction and X-ray reflectivity study, Soft matter, 4 (2008) 1665-1674.
[69] C. Whitehouse, D. Gidalevitz, M. Cahuzac, R.E. Koeppe Ii, A. Nelson, Interaction of gramicidin derivatives with phospholipid monolayers, Langmuir : the ACS journal of surfaces and colloids, 20 (2004) 9291-9298.
[70] H. Sarig, L. Livne, V. Held-Kuznetsov, F. Zaknoon, A. Ivankin, D. Gidalevitz, A. Mor, A miniature mimic of host defense peptides with systemic antibacterial efficacy, FASEB journal : official publication of the Federation of American Societies for Experimental Biology, 24 (2010) 1904-1913.
[71] F. Zaknoon, H. Sarig, S. Rotem, L. Livne, A. Ivankin, D. Gidalevitz, A. Mor, Antibacterial properties and mode of action of a short acyl-lysyl oligomer, Antimicrobial agents and chemotherapy, 53 (2009) 3422-3429.
[72] A. Ivankin, I. Kuzmenko, D. Gidalevitz, Cholesterol-phospholipid interactions: new insights from surface x-ray scattering data, Physical review letters, 104 (2010) 108101.
[73] M. Losche, Surface-sensitive X-ray and neutron scattering characterization of planar lipid model membranes and lipid/peptide interactions, Curr Top Membr, 52 (2002) 117-+.
[74] M. Schalke, M. Losche, Structural models of lipid surface monolayers from X-ray and neutron reflectivity measurements, Adv Colloid Interface Sci, 88 (2000) 243-274.
[75] T.R. Jensen, K. Balashev, T. Bjornholm, K. Kjaer, Novel methods for studying lipids and lipases and their mutual interaction at interfaces. Part II. Surface sensitive synchrotron X-ray scattering, Biochimie, 83 (2001) 399-408.
[76] L.G. Parratt, Surface studies of solids by total reflection of x-rays, Physical Review, 95 (1954) 359.
[77] K. Kjaer, Some Simple Ideas on X-Ray Reflection and Grazing-Incidence Diffraction from Thin Surfactant Films, Physica B, 198 (1994) 100-109.
[78] K. Kjaer, J. Alsnielsen, C.A. Helm, P. Tippmankrayer, H. Mohwald, Synchrotron X-Ray-Diffraction and Reflection Studies of Arachidic Acid Monolayers at the Air-Water-Interface, J Phys Chem-Us, 93 (1989) 3200-3206.
[79] J.S. Pedersen, I.W. Hamley, Analysis of Neutron and X-Ray Reflectivity Data by Constrained Least-Squares Methods, Physica B, 198 (1994) 16-23.
[80] H. Mohwald, Phospholipid and Phospholipid-Protein Monolayers at the Air/Water Interface, Annu Rev Phys Chem, 41 (1990) 441-476.
[81] M. Thoma, M. Schwendler, H. Baltes, C.A. Helm, T. Pfohl, H. Riegler, H. Mohwald, Ellipsometry and X-ray reflectivity studies on monolayers of phosphatidylethanolamine and phosphatidylcholine in contact with n-dodecane, n-hexadecane, and bicyclohexyl, Langmuir, 12 (1996) 1722-1728.

[82] O.V. Konovalov, L.A. Feigin, B.M. Shchedrin, Statistical evaluation of the accuracy of structure parameter determination from x-ray and neutron reflectivity data, Kristallografiya+, 41 (1996) 640-643.
[83] O.V. Konovalov, L.A. Feigin, B.M. Shchedrin, Allowance for apparatus distortions in modeling the structure of Langmuir-Blodgett films from reflectivity data, Kristallografiya+, 41 (1996) 629-634.
[84] I.I. Samoilenko, O.V. Konovalov, L.A. Feigin, B.M. Shchedrin, L.G. Yanusova, Processing of experimental reflectivity data within the REFLAN software package, Crystallogr Rep+, 44 (1999) 310-318.
[85] S.M. Danauskas, D. Li, M. Meron, B. Lin, K.Y.C. Lee, Stochastic fitting of specular X-ray reflectivity data using StochFit, Journal of Applied Crystallography, 41 (2008) 1187-1193.
[86] T.R. Jensen, K. Kjaer, Structural properties and interactions of thin films at the air-liquid interface explored by synchrotron X-ray scattering, Studies in Interface Science, 11 (2001) 205-254.
[87] J. Als-Nielsen, D. Jacquemain, K. Kjaer, F. Leveiller, M. Lahav, L. Leiserowitz, Principles and Applications of Grazing-Incidence X-Ray and Neutron-Scattering from Ordered Molecular Monolayers at the Air-Water-Interface, Phys Rep, 246 (1994) 252-313.
[88] D. Jacquemain, S.G. Wolf, F. Leveiller, M. Deutsch, K. Kjaer, J. Als□Nielsen, M. Lahav, L. Leiserowitz, Two□Dimensional Crystallography of Amphiphilic Molecules at the Air–Water Interface, Angewandte Chemie International Edition in English, 31 (1992) 130-152.
[89] H. Sarig, L. Livne, V. Held-Kuznetsov, F. Zaknoon, A. Ivankin, D. Gidalevitz, A. Mor, A miniature mimic of host defense peptides with systemic antibacterial efficacy, Faseb J, 24 (2010) 1904-1913.
[90] H. Brockman, Lipid monolayers: why use half a membrane to characterize protein-membrane interactions?, Curr Opin Struc Biol, 9 (1999) 438-443.
[91] J.S. Laursen, J. Engel-Andreasen, P. Fristrup, P. Harris, C.A. Olsen, Cis-Trans Amide Bond Rotamers in beta-Peptoids and Peptoids: Evaluation of Stereoelectronic Effects in Backbone and Side Chains, Journal of the American Chemical Society, 135 (2013) 2835-2844.
[92] J.J. Diaz-Mochon, L. Bialy, M. Bradley, Full orthogonality between Dde and Fmoc: the direct synthesis of PNA--peptide conjugates, Org Lett, 6 (2004) 1127-1129.
[93] W.C. Chan, B.W. Bycroft, D.J. Evans, P.D. White, A Novel 4-Aminobenzyl Ester-Based Carboxy-Protecting Group for Synthesis of Atypical Peptides by Fmoc-Bu(T) Solid-Phase Chemistry, J Chem Soc Chem Comm, (1995) 2209-2210.
[94] M.S. Bernatowicz, Y.L. Wu, G.R. Matsueda, Urethane Protected Derivatives of 1-Guanylpyrazole for the Mild and Efficient Preparation of Guanidines, Tetrahedron Letters, 34 (1993) 3389-3392.

Figure legends

Figure 1. Molecular structures of the tested compounds (A) and lipids used for modeling bacterial cell membranes (B).

Figure 2. Epifluorescence images of DPPG monolayers after injection of compound 1 (A) and 2 (B) at concentrations corresponding to 20% of their MIC values observed against *S. aureus* respectively. Lipid-linked Texas Red-DHPE fluorescence probe (1 mol %) was added to the phospholipid solutions for EFM experiments. Because of steric hindrance, the dye is located in the liquid-disordered phase, rendering it bright whereas the liquid-ordered phase remains dark.

Figure 3. Electron density profiles and corresponding Fresnel-divided reflectivity curves against the scattering vector (q) in the z direction (q_z) for DPPG (A) and Kdo2-Lipid A (B) monolayers at 30 mN × m^{-1}. Electron density profiles were normalized to the electron density of the subphase buffer. On the XR graphs, the scatter plots are experimental values and solid lines are the best fits of the models to the experimental data. Fresnel reflectivity is the reflectivity from ideal smooth surface.

Figure 4. Bragg peaks plot of scattering vector Q_{xy} as a function of intensity.

Figure 5. Cartoon schematic of possible interactions of compounds 1 and 2 with (A) DPPG and (B) Kdo-2 Lipid A monolayers at 30 mN × m^{-1}. Chimeras carrying amino groups are solely located in the polar head-moieties of DPPG accompanied with considerable thinning of the entire monolayer, whereas their guanidino-substituted analogues form an extra layer on the surface of lipid film resulting in more compact distribution of inserted molecules within the model membrane. Unlike DPPG, the mechanisms of antimicrobial insertion into Kdo-2 Lipid A model look nearly identical.

Scheme 1. Synthesis of Dimeric Building Block **8**. Reagents and conditions: (*a*) Fmoc-Lys(Boc)-OH (1.7 equiv), HBTU (1.7 equiv), *i*Pr_2NEt (4 equiv), DMF, 18 h. (*b*) TFA–CH_2Cl_2 (4:6), 2 h. (*c*) Acetyl dimedone (1.7 equiv), *i*Pr_2NEt (2.7 equiv), DMF, 18 h.

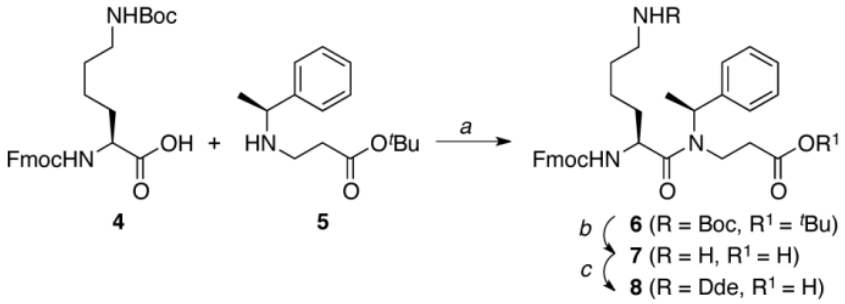

Scheme 2. Solid Supported Oligomerization of Building Block **8**. Reagents and conditions: (*a*) **8** (4.5 equiv), HBTU (4.5 equiv), *i*Pr$_2$NEt (9 equiv), DMF, 18 h. (*b)* Piperidine–DMF (1:4), 2 × 10 min. (*c*) DBU–piperidine–DMF (2:2:96), 20 min. (*d*) Ac$_2$O–*i*Pr$_2$NEt–DMF (1:2:3), 2 h. (*e*) Hydrazine–DMF (2:98), 2 × 45 min. (*f*) 50% TFA–CH_2Cl_2, 2 × 1 h. (*g*) *N,N'*-Bis(*tert*-butoxycarbonyl)-1H-pyrazole-1-carboxamidine (**11**, 36 equiv), *i*Pr$_2$NEt (72 equiv), DMF, 18 h. HBTU = *O*-(Benzotriazol-1-yl)-*N,N,N',N'*-tetramethyluronium hexafluorophosphate.

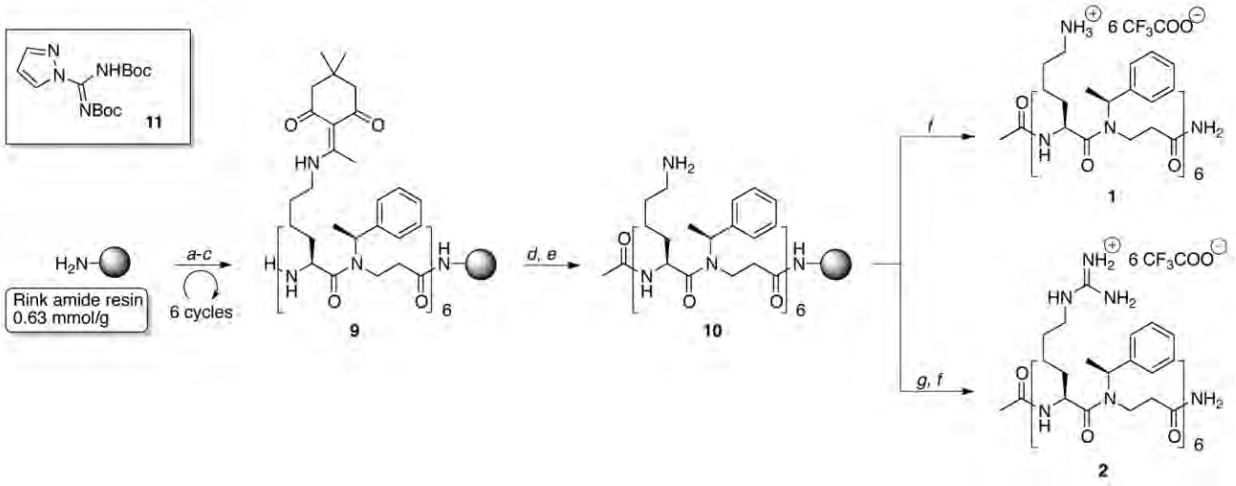

Table 1. Antimicrobial Activities of α-Peptide–β-Peptoid Chimeras

	MIC measurements for selected pathogens (μg × mL^{-1} / μM)[a]				
	Gram-negative				Gram-positive
	E. coli[b]	E. coli[c]	K. pneumoniae[d]	V. vulnificus[e]	S. aureus[f]
1	128/50	128/50	256-512/100-200	64/25	64-128/25-50
1a	32/11	32/11	128/44	64/22	32/11
2	8/3	16/3	16-32/3-6	8/3	4/1.5
2a	16/5	32/10	64/20	16/5	16/5
3	>128/>436	>128/>436	>128/>436	>128/>436	>128/>436

[a] MIC = Minimum Inhibitory Concentration: lowest concentration without visible growth. The values are based on two individual experiments conducted in duplicate. [b]*Escherichia coli* ATCC 25922. [c]*Escherichia coli* AAS-EC-009 [Extended Spectrum Beta-Lactamase (ESBL)-producing clinical sample isolated from a Danish patient in 2007]. [d]*K. pneumoniae* = *Klebsiella pneumoniae* ATCC 13883. [e]*V. vulnificus* = *Vibrio vulnificus* ATCC 27562. [f]*S. aureus* = *Staphylococcus aureus* 8325-4.

Table 2. Structural Parameters of Crystal Monolayer Lattice

Sample	Peak position ($Å^{-1}$)	D-spacing (Å)	Unit cell parameters	L_{xy} [a] (Å)	Area unit cell ($Å^2$)
DPPG	$Q_{xy\ 1}$=1.39, $Q_{xy\ 2}$=1.47	d_{11}=4.51, d_{02}=4.26[b]	a = 5.32 Å b = 8.54 Å γ = 90° θ =27°	L_{11}=93 L_{02}=196	44.51
DPPG-**1**	1.48	4.25	a = 6.93 Å γ = 120° θ =0°	156	41.62
DPPG-**1a**	1.48	4.25	a = 6.94 Å γ = 120°, θ =0°	85	41.69
DPPG–**2** and DPPG–**2a** displayed no visible GIXD peaks					

Fig. 1

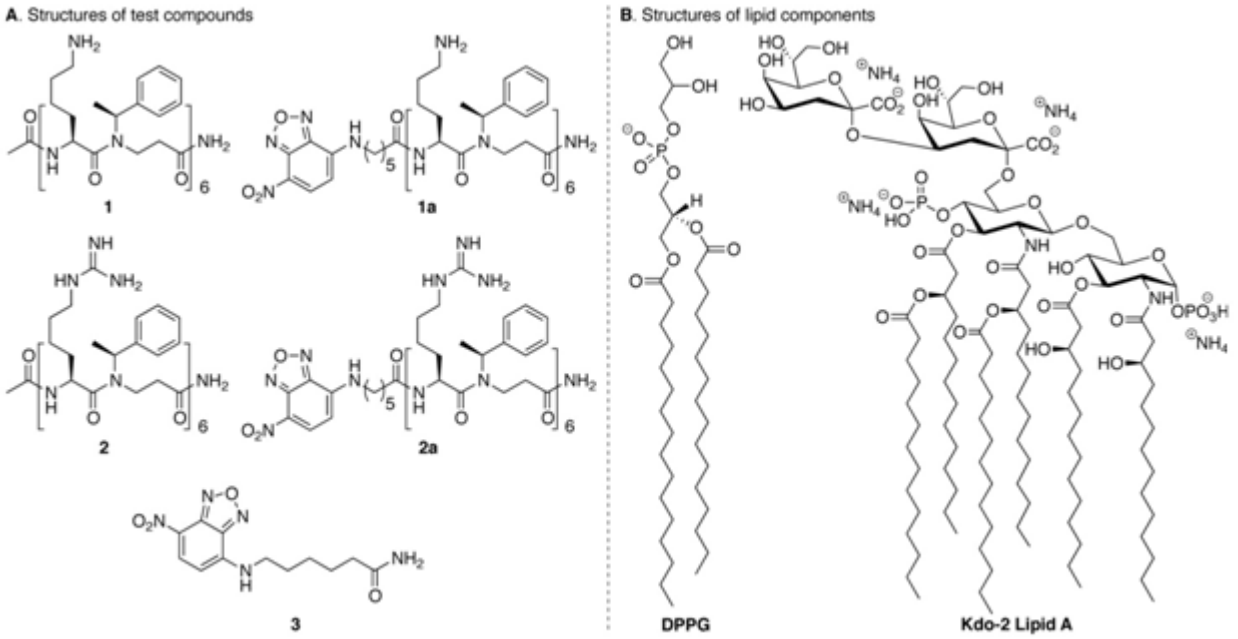
A. Structures of test compounds
1
1a
2
2a
3
B. Structures of lipid components
DPPG
Kdo-2 Lipid A

Fig. 2

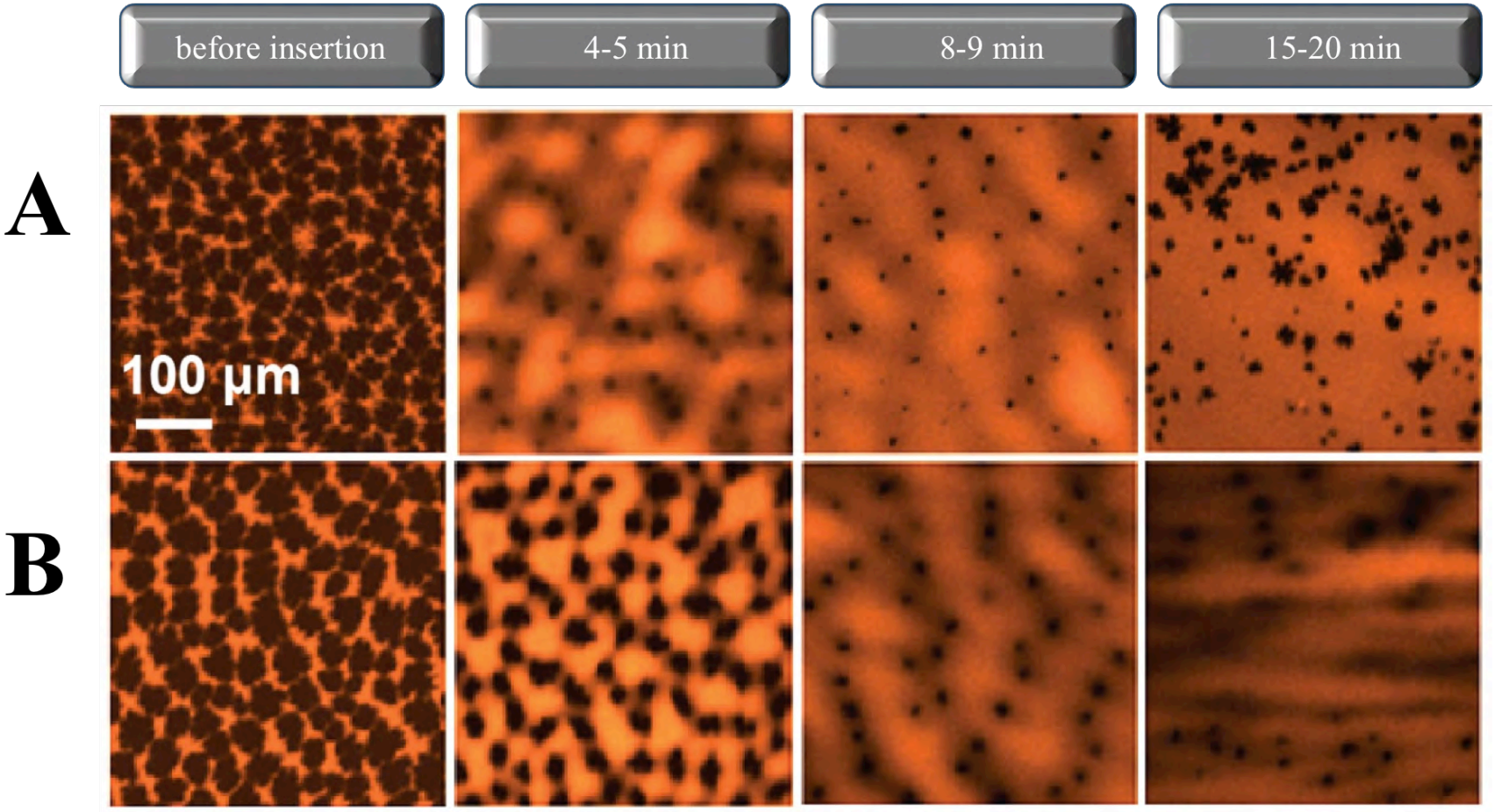

Fig. 3

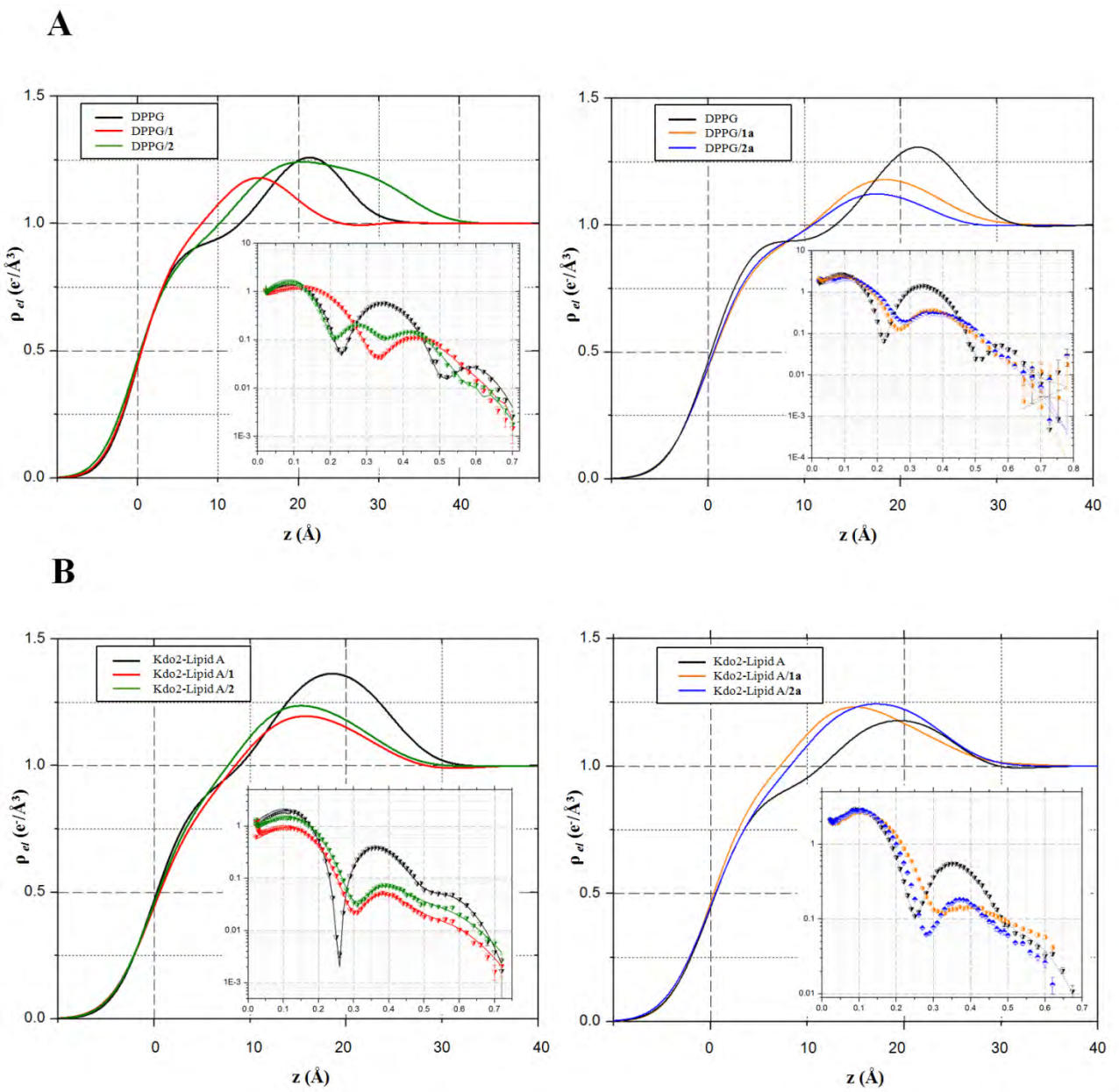
A
DPPG
DPPG/1
DPPG/2
DPPG/1a
DPPG/2a
B
Kdo2-Lipid A
Kdo2-Lipid A/1
Kdo2-Lipid A/2
Kdo2-Lipid A/1a
Kdo2-Lipid A/2a
ρ el (e⁻/Å³)
z (Å)

Fig. 4

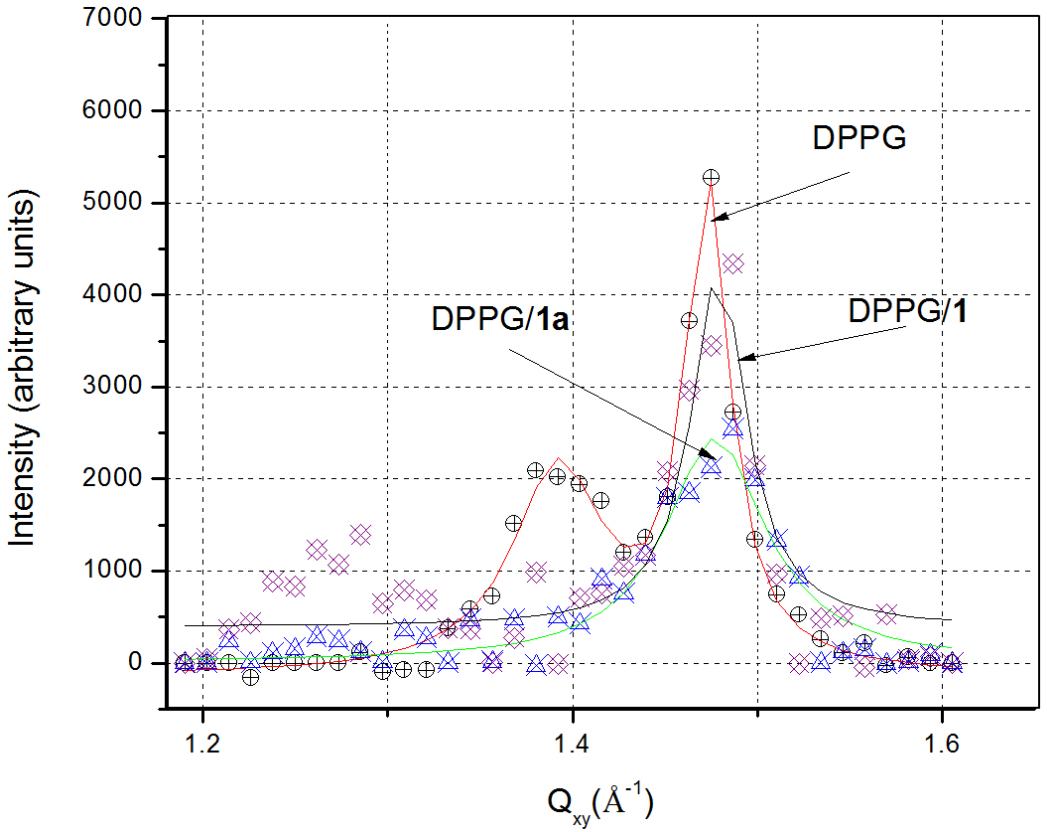
7000
6000
5000
4000
3000
2000
1000
0
Intensity (arbitrary units)
DPPG
DPPG/1a
DPPG/1
1.2
1.4
1.6
Q_xy(Å^-1)

Fig. 5

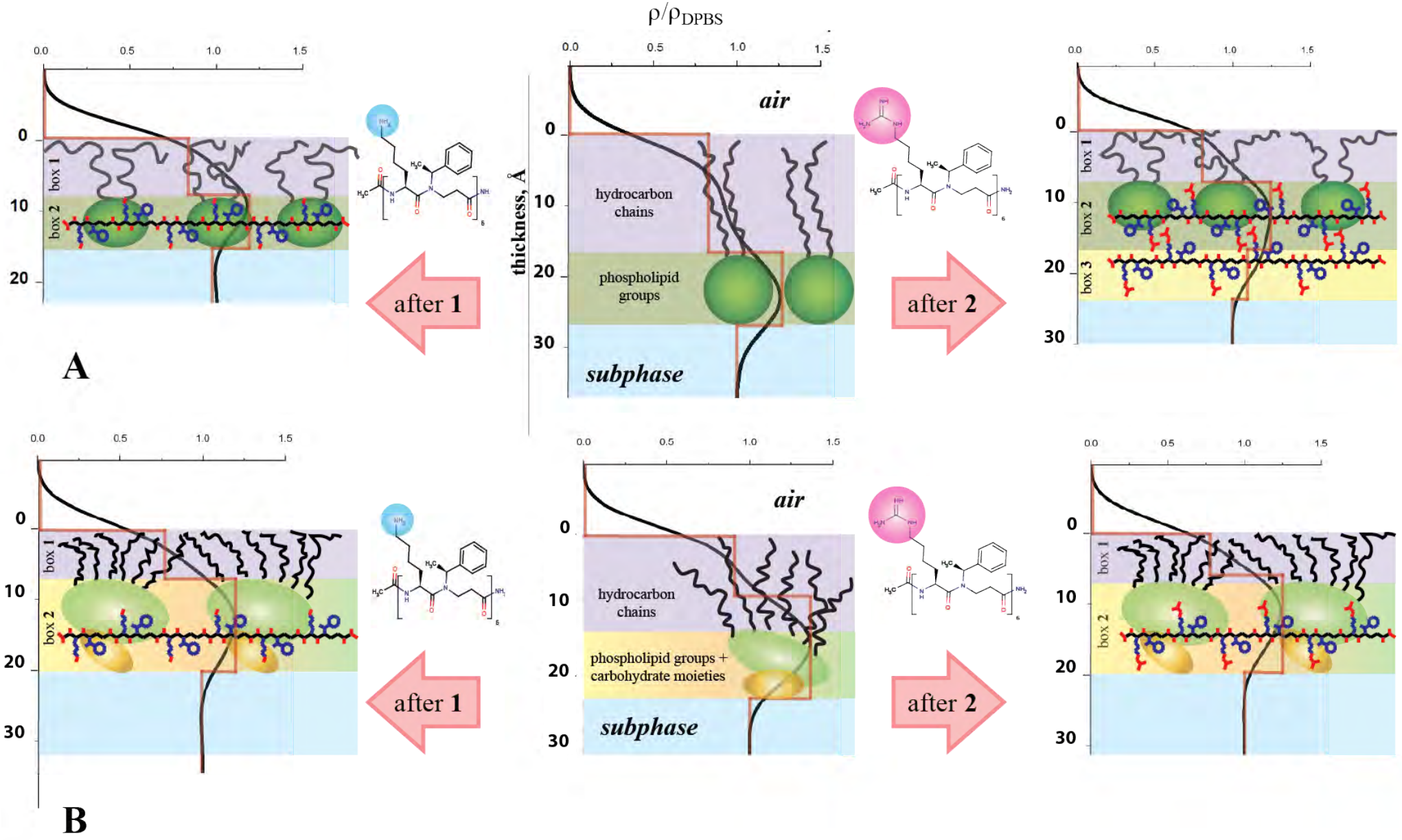
ρ/ρDPBS
thickness, Å
air
hydrocarbon chains
phospholipid groups
subphase
box 1
box 2
box 3
after 1
after 2
A
phospholipid groups + carbohydrate moieties
B

SUPPORTING INFORMATION

Guanidino Groups Greatly Enhance the Action of Antimicrobial Peptidomimetics Against Gram-positive Bacteria Membranes.

Konstantin Andreev,[†,#] Christopher Bianchi,[†,#] Jonas S. Laursen,[‡] Line Hein-Kristensen,[Δ] Lone Gram,[Δ] Ivan Kuzmenko,[○] Christian A. Olsen,[‡] and David Gidalevitz[†]*

[†]Department of Physics, Center for Molecular Study of Condensed Soft Matter, Pritzker Institute of Biomedical Science and Engineering, Illinois Institute of Technology, 3440 S. Dearborn St., Chicago, Illinois 60616, United States.

[‡]Department of Chemistry, Technical University of Denmark, Kemitorvet 207, DK-2800, Denmark.

[Δ]Division of Industrial Food Research, National Food Institute, Technical University of Denmark, Søltofts Plads 221, DK-2800, Kongens Lyngby, Denmark.

[○]Advanced Photon Source, Argonne National Laboratory, 9700 S. Cass Ave., Lemont, Illinois.

Table of Contents

Supplementary Figures and Schemes

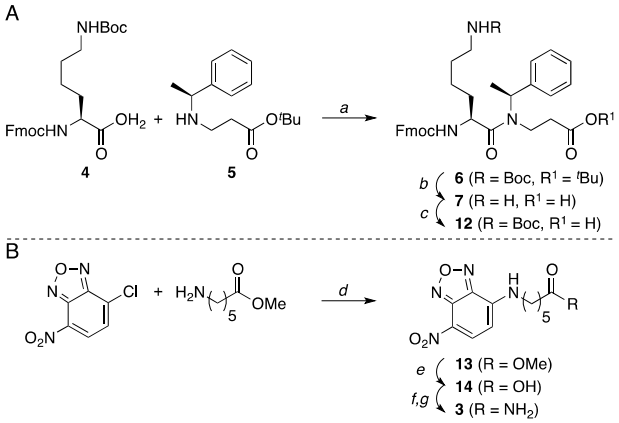

Scheme S1. Building block syntheses. (**A**) (*a*) Fmoc-Lys(Boc)-OH (1.7 equiv), HBTU (1.7 equiv), *i*Pr_2NEt (4 equiv), DMF, 18 h. (*b*) TFA–CH_2Cl (4:6), 2 h. (*c*) Boc_2O (1.5 equiv), *i*Pr_2NEt (2 equiv), DMF, 0 °C for 1 h then rt 2 h. (**B**) (*d*) NBD-Cl (1 equiv), Methyl 6-aminohexanoate (1 equiv), NEt_3 (1.1 equiv), DMF, 18h. (*e*) 1 M LiOH (aq) (28 equiv, MeOH, 3h. (*f*) **14** (4 equiv), Rink amide Chem-Matrix® (1 equiv), PyBOP (4 equiv), *i*Pr_2NEt (4 equiv), DMF, 18h. (*g*) TFA–CH_2Cl_2 (1:1), 2 × 1 h.

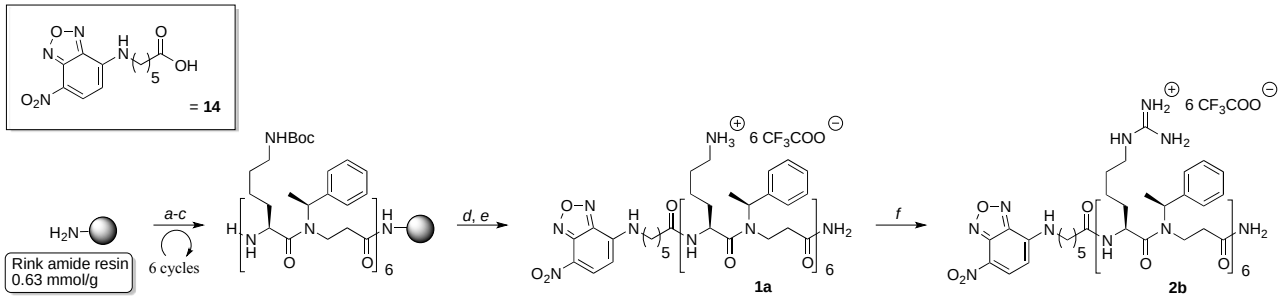

Scheme S2. Solid supported oligomerization of building block **12**. (*a*) **12** (4.5 equiv), HBTU (4.5 equiv), *i*Pr_2NEt (9 equiv), DMF, 18 h. (*b)* piperidine–DMF (1:4), 2 × 10 min. (*c*) DBU–piperidine–DMF (2:2:96), 20 min. (*d*) **14** (6.5 equiv), PyBOP (7.5 equiv), *i*Pr_2NEt (13 equiv), DMF, 18 h. (*e*) TFA–CH_2Cl_2 (1:1), 2 × 1 h. (*f*) *N,N'*-Bis(*tert*-butoxycarbonyl)-1H-pyrazole-1-carboxamidine (**11**, 36 equiv), *i*Pr_2NEt (72 equiv), DMF, 18 h.

Materials and Methods

General. All chemicals and solvents were analytical grade and used without further purification. Vacuum liquid chromatography (VLC) was performed on silica gel 60 (particle size 0.015−0.040 mm). UPLC−MS analyses were performed on a Phenomenex Kinetex column (1.7 μm, 50 × 2.10 mm) using a Waters Acquity ultra high-performance liquid chromatography system. A gradient with eluent I (0.1% HCOOH in water) and eluent II (0.1% HCOOH in acetonitrile) rising linearly from 0% to 95% of II during t = 0.00–2.50 min was applied at a flow rate of 1 mL/min (gradient A) or during t = 0.00–5.20 min (gradient B). Preparative HPLC purification was performed on a C18 Phenomenex Luna column (5 μm, 100 Å, 250 mm × 20 mm) using an Agilent 1260 LC system equipped with a diode array UV detector and an evaporative light scattering detector (ELSD). A gradient with eluent III (water−MeCN−TFA, 95:5:0.1) and eluent IV (0.1% TFA in acetonitrile) rising linearly from 0% to 95% of IV during t = 5−45 min was applied at a flow rate of 20 mL/min (gradient C). High-resolution LC-DAD-MS was performed on an Agilent 1100 system equipped with a photodiode array detector (DAD) and coupled to a LCT orthogonal time-of-flight mass spectrometer (Waters-Micromass, Manchester, UK) with Z-spray electrospray ionisation (ESI). Analytic HPLC was performed on a C18 phenomenex Luna column (3 μm, 100Å, 150mm × 4.60mm) using an Agilent 1100 series system equipped with a diode array UV detector. A gradient with eluent V (0.1% TFA in water) and eluent IV (0.1% TFA in acetonitrile) rising linearly from 0% to 95% of IV during t = 5−26 min was applied at a flow rate of 1 mL/min (gradient D). ^{1}H NMR and ^{13}C NMR spectra were recorded on a Varian Mercury 300 instrument at 300 and 75 MHz, respectively. 2D NMR spectra were recorded on a Bruker Ascend 400 MHz instrument. All spectra were recorded at 298 K. Correlation spectroscopy (COSY) spectra was recorded with a relaxation delay of 1.5 sec before each scan, a spectral width of 6k × 6k, collecting 8 FIDs and 1k × 512 data points. Chemical shifts are reported in ppm relative to deuterated solvent peaks as internal standards (δH, CD_3OD 3.31 ppm; δC, CD_3OD 49.00 ppm, δH, $CDCl_3$ 7.26 ppm; δC, $CDCl_3$ 77.16 ppm. Coupling constants (J) are given in hertz (Hz). Multiplicities of 1H NMR signals are reported as follows: s, singlet; d, doublet; t, triplet; q, quartet; m, multiplet. Signals marked with an asterisk (*) correspond to peaks assigned to the minor rotamer conformation.

(*S*)-*tert*-Butyl 3-((1-phenylethyl)amino)propanoate (5).[1] *t*-Butyl acrylate (6.0 mL, 41 mmol) was dissolved in MeOH and heated to 50 °C on an oil bath, followed by addition of (*S*)-1-phenylethylamine (6.25 mL, 48 mmol). After stirring for 18 h, the solvent was evaporated *in vacuo* and the crude product was purified by vacuum liquid chromatography (6 × 6 cm, heptane–EtOAc 0→12%) to give 8.78 g (86%) as a colorless oil. ^{1}H NMR (300 MHz, $CDCl_3$) δ 1.34 (d, 3H, J = 6.6 Hz, H-6), 1.44 (s, 9H, H-1), 1.70 (s, 1H, H-4), 2.38 (t, 2H, J = 6.3 Hz, H-2), 2.60–2.75 (m, 2H, H-3), 3.77 (q, 1H, J = 6.6 Hz, H-5),

7.20–7.27 (m, 1H, H-*p*), 7.20–7.35 (m, 4H, H-*o*, H-*m*). ^{13}C NMR (75 MHz, $CDCl_3$) δ 24.7, 28.3, 36.1, 43.4, 58.4, 80.7, 126.8, 127.1, 128.6, 145.8, 172.52. UPLC-MS gradient A, t_R = 0.96 min (>95%), MS: (*m/z*) $[M + H]^+$ calcd. for $C_{15}H_{24}NO_2^+$: 250.4, found 250.3. $[\alpha]_{589.2}$: –29° (*c* = 2.2 , 293 K, $CHCl_3$).

Fmoc-Lys(Boc)-β*N*spe-O^{t}Bu (6).[2] Fmoc-Lys(Boc)-OH (3.75 g, 7.95 mmol), HBTU (3.02 g, 8.0 mmol) and *i*Pr_2NEt (3.45 ml, 19.8 mmol) were dissolved in DMF (50 mL), and preincubated for 10 min at room temperature, followed by addition of the β*N*spe peptoid (**15**) (1.70 g, 4.8 mmol). The reaction mixture was stirred at room temperature for 18 h. The reaction mixture was diluted with EtOAc (300 mL), and washed with water (3 × 100 mL), 1 M HCl (aq.) (2 × 100 ml), sat aq. $NaHCO_3$ (2 × 100 mL) and brine (2 × 100 mL). The organic phase was dried (Na_2SO_4), filtered and evaporated *in vacuo* to give the crude product, which was purified by VLC (6 × 6 cm, heptane–EtOAc 0→16%) to give 2.65 g (78%) as colorless solid. UPLC-MS gradient B, t_R = 2.79 min (>90%), MS: (*m/z*) $[M + H]^+$ calcd. for $C_{32}H_{38}N_3O_5^+$: 700.9, found: 700.5.

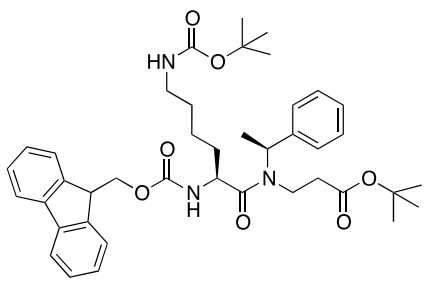

Fmoc-Lys-β*N*spe-OH (7).[2] Fmoc-Lys(Boc)-β*N*spe-O^{t}Bu (**6**) (2.90 g, 4.3 mmol) was dissolved in 40% solution of trifluoroacedic acid in CH_2Cl_2 (30 mL). After stirring for 2 h at room temperature, the solvent was evaporated *in vacuo*. The residual trifluoroacetic acid was co-evaporated with toluene (3 × 100 mL), toluene–CH_2Cl_2 (3 × 100 mL, 1:1, v/v) and CH_2Cl_2 (3 × 100 mL) to give 2.33 g (82%) of the desired product as a colorless oil. UPLC-MS gradient B, t_R = 1.61 min, MS: (*m/z*) $[M + H]^+$ calcd. for $C_{41}H_{54}N_3O_7^+$: 544.7, found: 544.3.

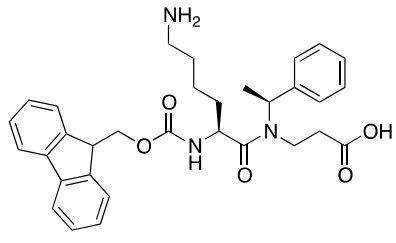

Fmoc-Lys(Boc)-β*N*spe-OH (12).[2] Fmoc-Lys-β*N*spe-OH (**7**) (3.65 g, 5.2 mmol) and *i*Pr_2NEt (2.04 mL, 11.7 mmol) were dissolved in DMF (25 mL) and cooled to 0 °C, followed by addition of Boc_2O (1.70 g, 7.8 mmol). After stirring for 1 h the reaction was allowed to warm to ambient temperature and was stirred for 2 h. The reaction mixture was poured into EtOAc (200 mL) and extracted with 1 M HCl (aq) (3 × 100 mL), water (2 × 100 mL) and brine (2 × 100 mL). The organic phase was dried (Na_2SO_4), filtered, and evaporated. The crude product was purified by VLC (6 × 6 cm, CH_2Cl_2–MeOH, 0.5% grad from 0→5%), to give 2.44 g (72%) of the product as a white solid. ^{1}H NMR (300 MHz, CD_3OD) δ 1.41 (s, 9H, H-10), 1.53*/1.67 (2 × d, 3H, *J* = 6.9 Hz, H-4), 1.61–1.80 (broad m, 2H, H-6), 2.17/2.62 (3 × m, 2H, H-1), 3.04/3.47* (2 × m, 2H, H-9), 3.10–4.42 (3 ×

m, 2H, H-2), 4.18 (m, 1H, H-12), 4.27–4.35 (m, 2H, H-11), 4.52*/4.81 (2 × m, H, H-5) 5.42/5.81* (2 × q, 1H, J = 6.9 Hz, H-3), 7.22–7.42 (broad m, 9H, Ph, Fmoc ArH), 7.67 (m, 2H, Fmoc ArH) 7.80 (d, 2H, J = 7.5 Hz, Fmoc Ar). ^{13}C NMR (100 MHz, CD_3OD) δ 17.1*, 18.1, 23.0*, 23.7, 24.0, 24.2*, 28.8, 30.5*, 30.6, 33.1, 40.8*, 40.9, 41.0, 41.1*, 45.7, 48.4, 52.9, 53.3*, 53.5*, 56.1, 68.0, 79.5, 79.8*, 120.9, 126.3, 128.2, 128.2*, 128.4, 128.8, 129.7, 141.0, 141.9*, 142.6, 145.2*, 145.3, 158.5, 158,5, 174.2, 175,1. UPLC-MS gradient B, t_R = 2.53 min (>95), MS: *m/z* $[M + H]^+$ calcd. for $C_{32}H_{38}N_3O_5^+$: 644.8, found: 644.4. $[\alpha]_{589.2}$: -49° (c = 3.2, 293 K, $CHCl_3$)

Methyl 6-((7-nitrobenzo[*c*][1,2,5]oxadiazol-4-yl)amino)hexanoate (13).[3] Methyl 6-aminohexanoate (460 mg, 2.5 mmol) and NEt_3 (38 µL, 2.75 mmol) were dissolved in DMF (5 mL). 4-Chloro-7-nitrobenzofurazan (0.5 g, 2.5 mmol) was dissolved in DMF (4 mL) and added dropwise to the methyl 6-aminohexanoate solution. After stirring for 18 h, the reaction mixture was poured into water (100 mL) and extracted with CH_2Cl_2 (3 × 100 mL). The combined organic phases were dried ($MgSO_4$), filtered and evaporated *in vacuo*. The crude product was purified by VLC (2 × 6 cm, hexane–EtOAc, 5% gradient) to give 315 mg (41%) of the desired product as a red solid. ^{1}H NMR (300 MHz, $CDCl_3$) δ 1.52 (m, 2H, H-4), 1.73 (m, 2H, H-3), 1.84 (m, 2H, H-5), 2.37 (t, 2H, J = 7.3 Hz, H-2), 3.51 (q, 2H, J = 6.9 Hz, H-6), 3.60 (s, 3H, H-1), 6.17 (d, 1H, J = 8.8 Hz, H-8) 6.23 (broad s, 2H, H-7) 8.50 (d, 1H, J = 8.8 Hz, H-9). ^{13}C NMR (100 MHz, DMSO-d_6) δ 24.1, 25.9, 27.3, 33.2, 43.2, 51.2, 99.1, 120.5, 138.0, 144.2, 144.4, 145.2, 173.3. UPLC-MS gradient A, t_R = 1.62 min (>95%), MS: *m/z* $[M+H]^+$ calcd. for $C_{13}H_{17}N_4O_5^+$: 309.3, found: 309.3.

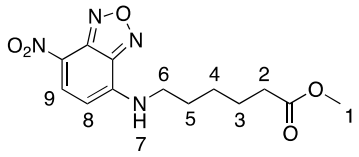

6-((7-Nitrobenzo[*c*][1,2,5]oxadiazol-4-yl)amino)hexanoic acid (14).[3] Methyl 6-((7 nitrobenzo[*c*][1,2,5]oxadiazol-4-yl)amino)hexanoate (**16**) (110 mg, 0.35 mmol) was dissolved in MeOH (20 mL) and 1 M LiOH (aq) (10 mL, 10 mmol) was added. After stirring for 3 h at room temperature, the reaction was taken up in 1 M HCl (aq.) (100 mL) and extracted with CH_2Cl_2 (3 × 100 mL). The organic phase was dried (Na_2SO_4), filtered, and evaporated *in vacuo* to give the desired product as a red solid. UPLC-MS gradient A, t_R = 1.31 min, MS: *m/z* $[M+H]^+$ calcd. for $C_{12}H_{16}N_5O_4^+$: 295.3, found: 295.2.

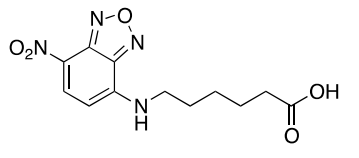

6-((7-Nitrobenzo[*c*][1,2,5]oxadiazol-4-yl)amino)hexanamide (3). 6-((7-Nitrobenzo[*c*] [1,2,5]oxadiazol-4-yl)amino)hexanoic acid (**14**) (205 mg, 0.66 mmol), HBTU (250 mg, 0.66 mmol) and iPr$_2$NEt (115 µL, 0.66 mmol) in DMF (2 mL) were preincubated for 10 min at room temperature. The activated acid was then added to a Rink amide resin (370 mg, 16.6 mmol)

and shaken for 18 h. The compound was cleaved from the solid support using 50% TFA in CH_2Cl_2 (2 × 2 mL) for 30 min. The resin was washed with MeOH and CH_2Cl_2 (2 × 2 mL each), the washings were collected and evaporated *in vacuo*. The crude was purified by preparative HPLC to give the desired product as a red solid (56 mg, 29% two steps). ^{1}H NMR (300 MHz, CD_3OD) δ 1.49 (m, 2H, H-4), 1.69 (m, 2H, H-3), 1.80 (m, 2H, H-5), 2.23 (t, 2H, J = 7.6 Hz, H-2), 3.54 (m, 2H, H-6), 6.34 (d, 1H, J = 8.7 Hz, H-8) , 8.52 (d, 1H, J = 8.7 Hz, H-9). ^{13}C NMR (100 MHz, DMSO-d_6) δ 24.7, 26.1, 27.7, 35.0, 43.3, 99.1, 120.5, 138.0, 144.2, 144.5, 145.2, 174.2. UPLC-MS gradient B, t_R = 1.17 min (>95%), MS: *m/z* $[M+H]^+$ calcd. for $C_{12}H_{16}N_5O_4^+$: 294.1, found: 294.1. HRMS: (*m/z*) $[M + H]^+$ calcd. for $C_{12}H_{16}N_5O_4^+$: 294.1197 found: 294.1206 (ΔM = 3.0 ppm).

Supplementary References

1. Laursen, J. S.; Engel-Andreasen, J.; Fristrup, P.; Harris, P.; Olsen, C. A. *J. Am. Chem. Soc.* **2013**, *135*, 2835-2844.
2. Bonke, G.; Vedel, L.; Witt, M.; Jaroszewski, J. W.; Olsen, C. A.; Franzyk, H. *Synthesis-Stuttgart* **2008**, 2381-2390
3. Wender, P. A.; Baryza, J. L., Identification of a tunable site in bryostatin analogs: C20 bryologs through late stage diversification. *Org. Lett.* **2005,** *7* (6), 1177-1180.

NMR Spectra

12

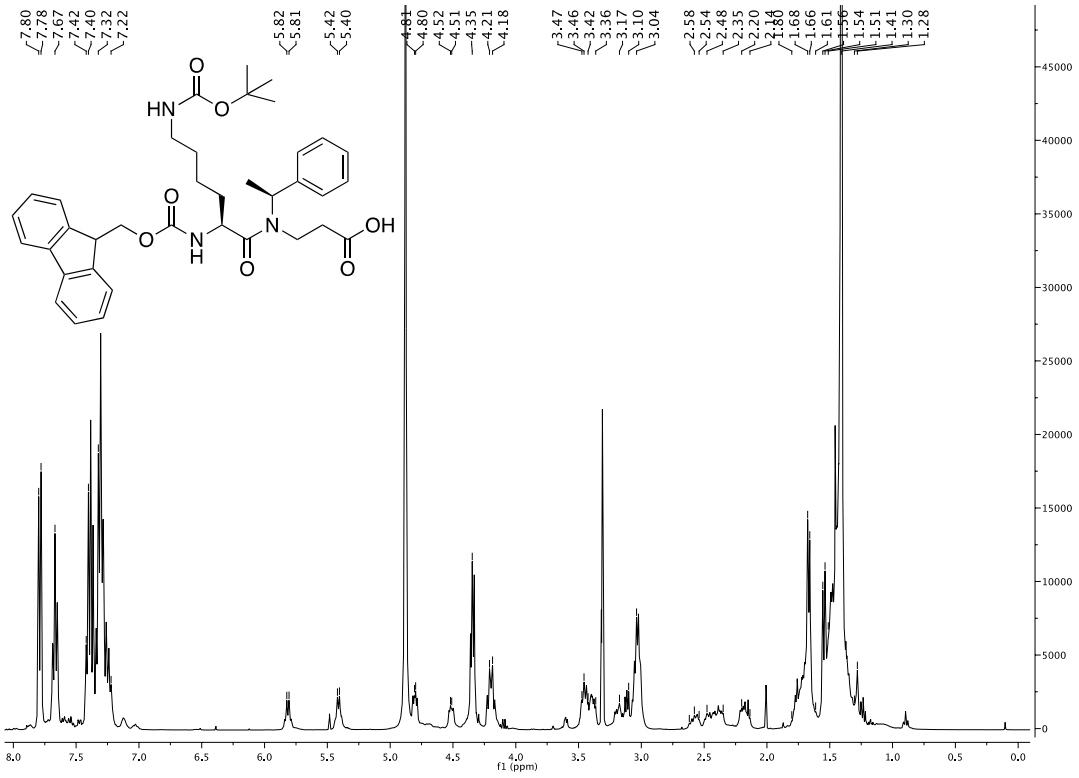

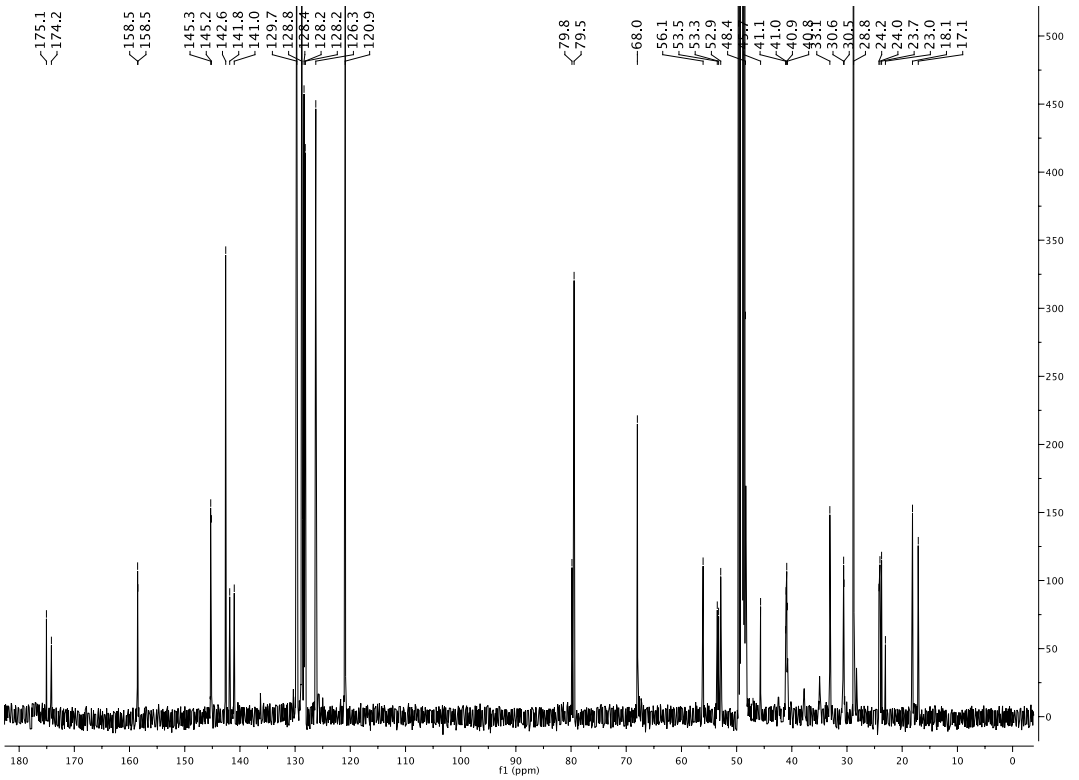

16

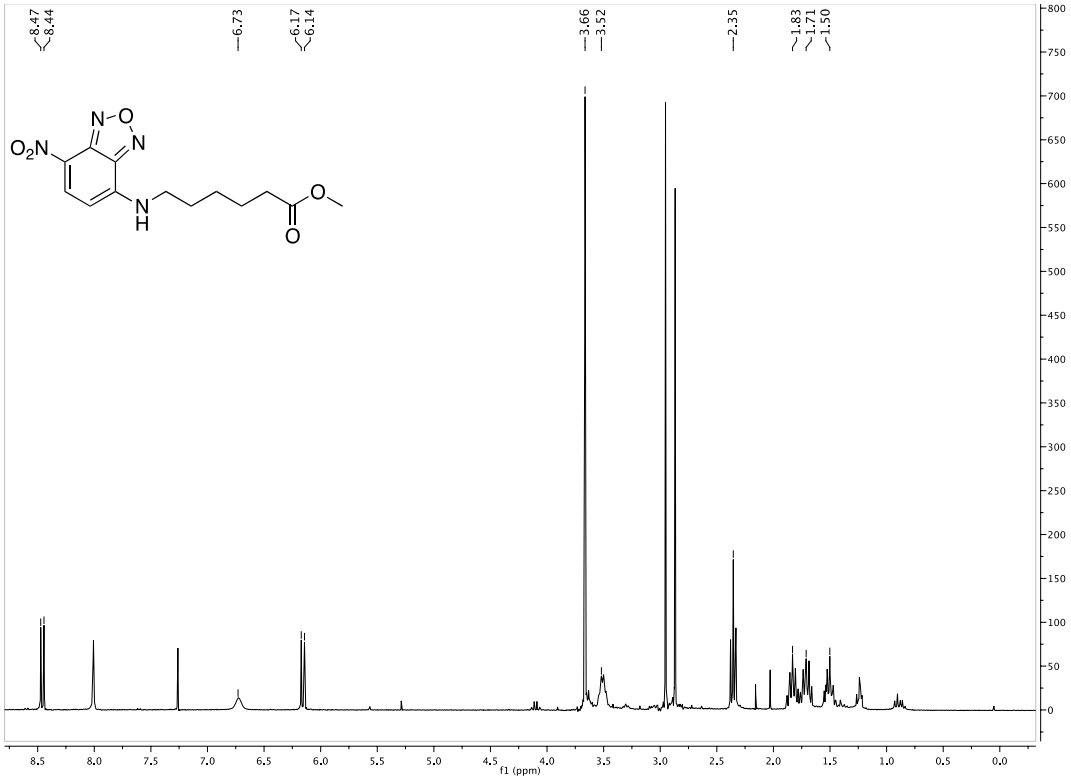
8.47
8.44
6.73
6.17
6.14
3.66
3.52
2.35
1.83
1.71
1.50
f1 (ppm)

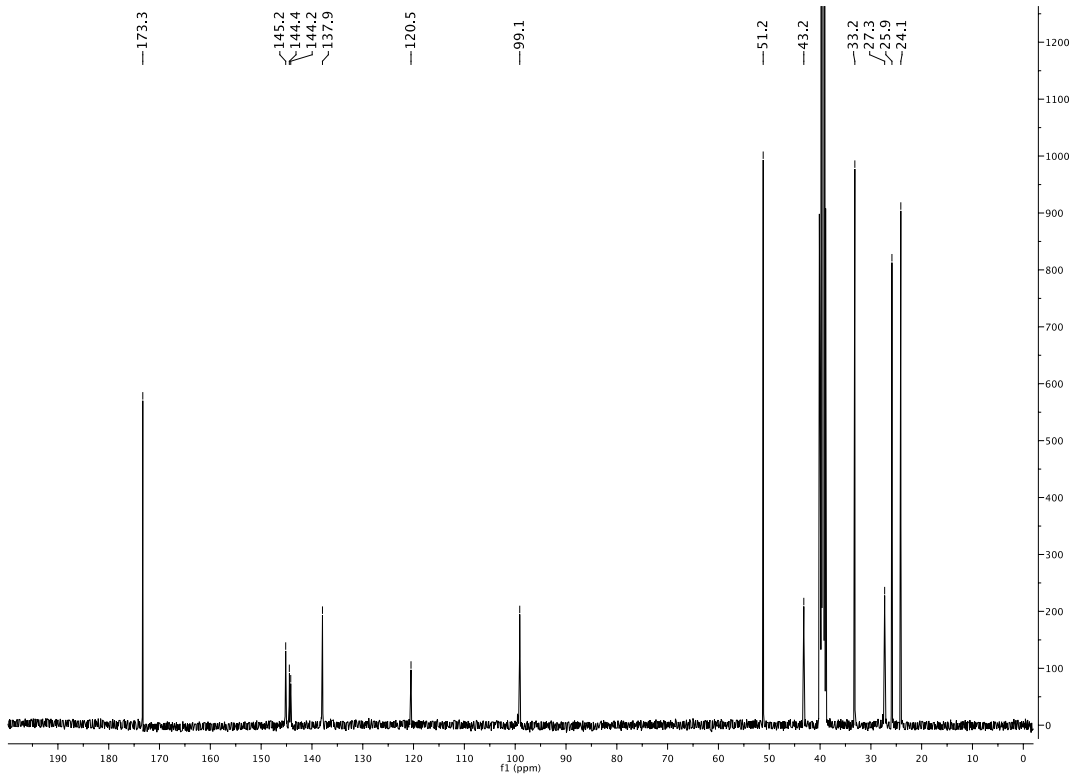
173.3
145.2
144.4
144.2
137.9
120.5
99.1
51.2
43.2
33.2
27.3
25.9
24.1
f1 (ppm)

3

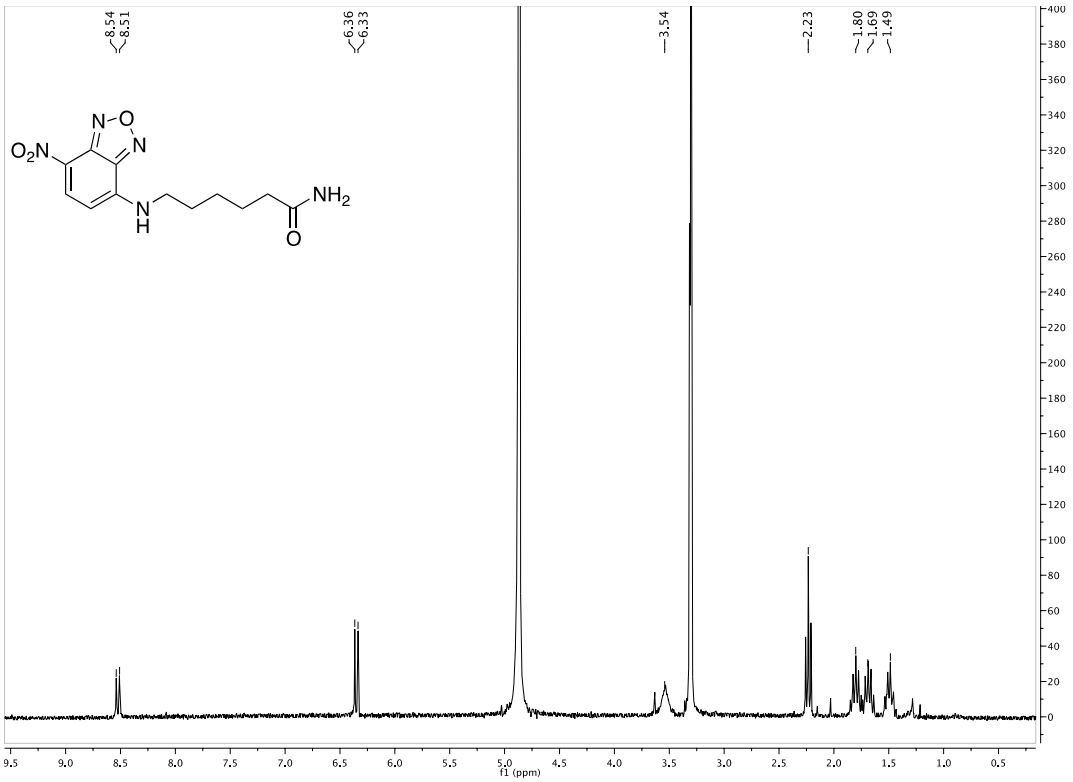
8.54
8.51
6.36
6.33
3.54
2.23
1.80
1.69
1.49
O2N
N
O
N
NH2
H
O
f1 (ppm)

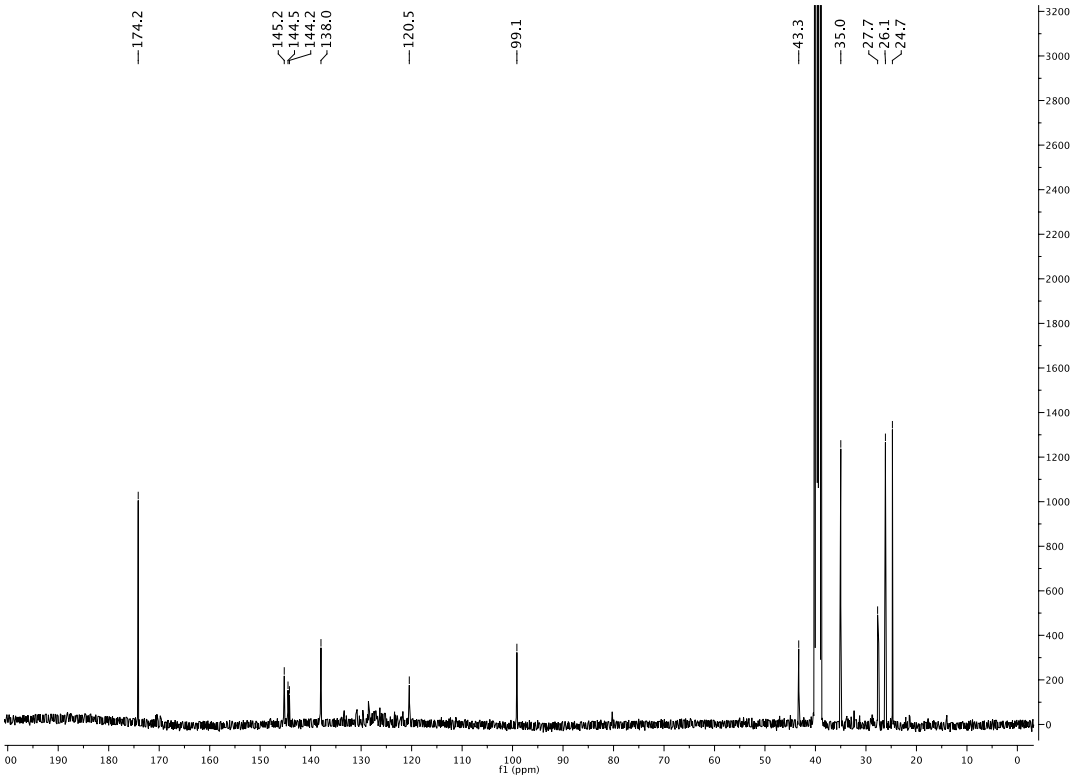
174.2
145.2
144.5
144.2
138.0
120.5
99.1
43.3
35.0
27.7
26.1
24.7
f1 (ppm)

8

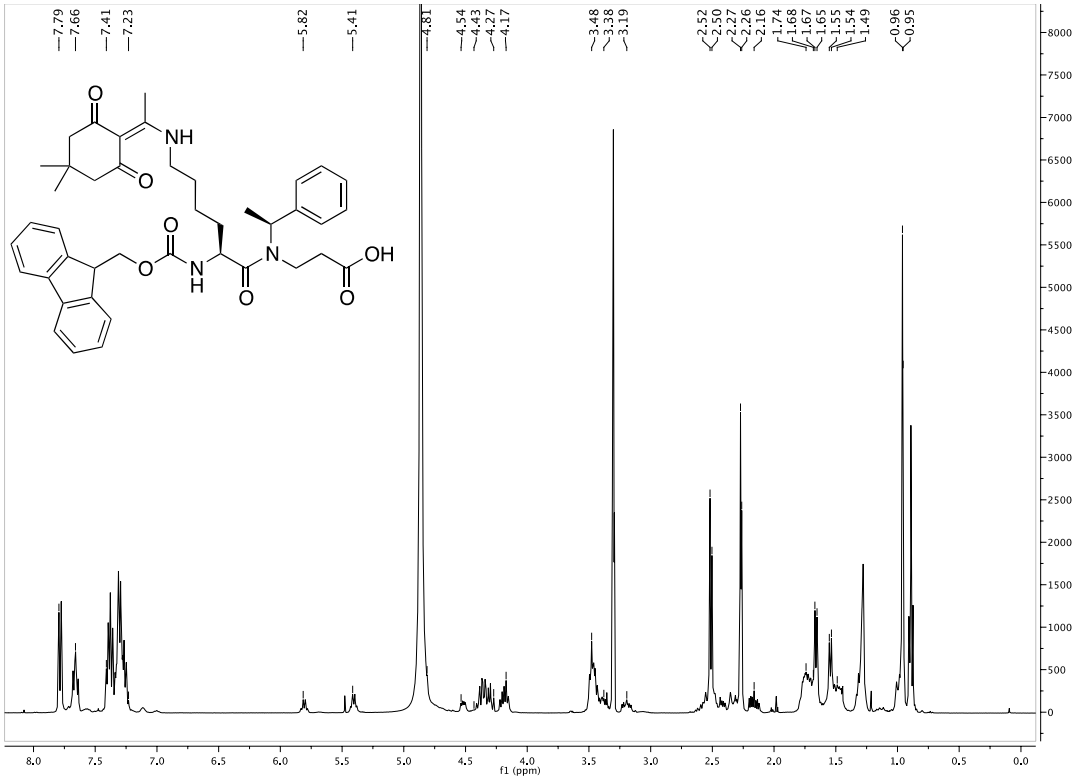
7.79
7.66
7.41
7.23
5.82
5.41
4.81
4.54
4.43
4.27
4.17
3.48
3.38
3.19
2.52
2.50
2.27
2.26
2.16
1.74
1.68
1.67
1.65
1.55
1.54
1.49
0.96
0.95
NH
O
N
OH
f1 (ppm)

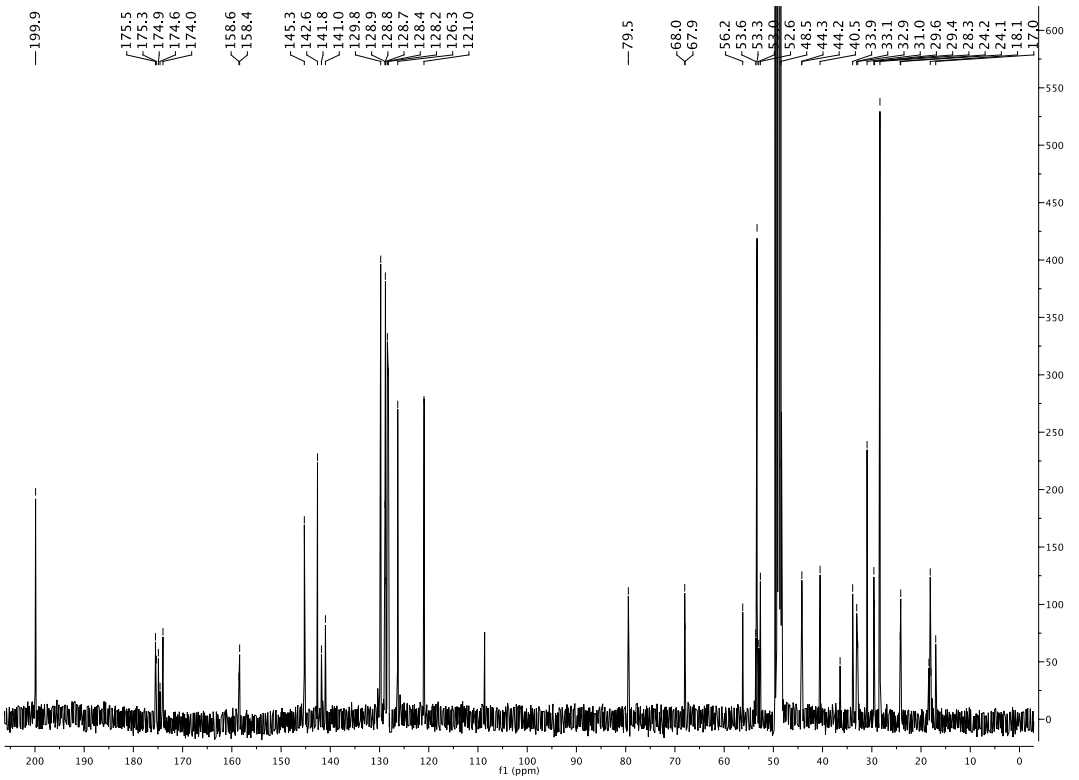
199.9
175.5
175.3
174.9
174.6
174.0
158.6
158.4
145.3
142.6
141.8
141.0
129.8
128.9
128.8
128.7
128.4
128.2
126.3
121.0
79.5
68.0
67.9
56.2
53.6
53.3
52.6
48.5
44.3
44.2
40.5
33.9
33.1
32.9
31.0
29.6
29.4
28.3
24.2
24.1
18.1
17.0
f1 (ppm)